THE STABILITY OF CUTS IN FRIARS FORMATION
AN INVESTIGATION OF THE LONG-TERM STABILITY OF SLOPES IN STIFF, FISSURED CLAYS AND SHALES

by

Athanasios D. Platis

A report prepared in partial fulfillment of the requirements for the Master of Engineering degree in the graduate division of the University of California, Berkeley.

March 1980

TABLE OF CONTENTS

1. DESCRIPTION OF THE PROBLEM AND SCOPE 1

2. FRIARS FORMATION 5

2.1 General Information and Geologic Description . . . 5
2.2 Previous Investigations in Friars Formation 7
2.3 Summary 20

3. THE LONG-TERM STABILITY OF SLOPES IN STIFF, FISSURED CLAYS AND SHALES 21

3.1 General 21
3.2 Peak Strength of O.C. Clays 23
3.3 Residual Strength 26
3.4 Progressive Failure 33
3.5 "Fully Softened" and Critical State Strengths . . .65
3.6 Summary 71

4. APPROACH TO THE PROBLEM 74

4.1 General 74
4.2 The "Stress Path" Approach 75
4.3 Summary 81

5. FINITE ELEMENT ANALYSIS OF THE STRESS CHANGES INDUCED BY AN EXCAVATION BEHIND A SLOPE 83

5.1 General 83
5.2 Presentation of the Analysis 83
5.3 Summary 137

6. TESTING PROGRAM 138

6.1 General 138
6.2 Sample Preparation 140
6.3 "Stress Path" Tests 155
a. Estimating the Stress Path 155
b. Description of Apparatus & Testing Procedure 171
c. Results 188
6.4 Testing Techniques for Measuring the Residual Strength in the Laboratory. 203
a. Direct Shear Test 203
b. Multiple Reversal Direct Shear Test 206
c. Ring Shear Apparatus Test 207
d. Triaxial Test 209
e. Direct Shear Test Using Composite Specimens . 211
6.5 Residual Strength Measurements. 212
a. Description of Apparatus & Testing Procedure. 213
b. Results 219
6.6 Summary 232

7. CONCLUSIONS AND RECOMMENDATIONS 234

8. REFERENCES 239

9. LIST OF SYMBOLS AND ABBREVIATIONS 246

10. APPENDICES

    1. Results of Finite Element Analysis

    2. Settlement vs. Log (Time) Curves from the Consolidation of the Slurry

    3. Corrections for Filter and Membrane Effects and Estimation of True Area of Contact in Triaxial Drained Tests, on Precut Samples, for Residual Strength Measurements

1. DESCRIPTION OF THE PROBLEM AND SCOPE

During the last few winters there have been heavy rainfalls in Southern California and many landslides have occurred, especially in the Rancho Bernardo-Poway Province and Santee-Fletcher Hills Province. The dominant formation within which most of the slides have occurred is the Friars Formation (refer to geologic description). Many of these were construction slides, while others occurred in older slopes which at the time were considered to be safe. One thing that drew the attention of the engineers was the fact that the back-calculated soil strengths were found to be lower (sometimes considerably lower) than the strengths that had originally been measured in the laboratory and which had been used for the design of the slopes.

Subsequent investigations revealed the "bedding plane faults" (remolded clay seams along the bedding planes; refer to the geologic description of the Friars Formation) as the source of many landslides. The "bedding plane faults" are usually dipping from 0° to 10°, but the strength of the remolded clay along the contact has been found to be as low as the residual strength so that sliding can easily occur along these planes. However, slides have also occurred within the claystone beds of this formation, in places where no "bedding plane faults" seemed to exist. Even in these cases, the back-calculated strengths were

again found to be lower than the ones measured in the laboratory.

There are a few things that should be mentioned here, the importance of which will become evident later. First, the ground water table is normally very deep. However, in periods of heavy rainfalls it rises to very shallow depths. In addition, the majority of the landslides have occurred during the rainy periods. Second, in designing the slopes in the Friars Formation, the effect of surface cracks and fissures, which extend to a depth of a few feet and which are filled with water during the rainy periods, has not generally been taken into account. Finally, the claystone is in general highly fissured, at least down to the depth that excavations are normally made.

It was decided by the engineers designing the slopes that the residual strength would be the appropriate design strength in places where "bedding plane faults" were found to exist. However, there were several problems associated with such a decision. First, the "bedding plane faults" were difficult to locate in many cases (at least before a slide had occurred), as was the depth to which they extended laterally behind the slope. Second, even if a "bedding plane fault" were located behind a slope, an efficient, reliable and economic laboratory test would have to be found for the determination of the residual strength.

It should be pointed out here that the determination

of the residual strength would be a useful thing to do even if no "bedding plane faults" existed, since that strength could be used as a lower limit for design purposes and also as the strength to be considered for the stability of slopes where previous slides or large ground movements had occurred. However, the use of the residual strength for design would be rather conservative in places where no "bedding plane faults" existed. Hence, the question that still remained unanswered was what should be the design strength in places where no "bedding plane faults" existed and how could this strength be measured in the laboratory.

This being the situation, the scope of this project is:

—Examine an alternative approach to laboratory testing and analysis for slope stability problems other than the conventional one. This alternative approach should more closely approximate the field conditions and could probably lead to some useful conclusions about the stability of cuts in highly overconsolidated stiff, fissured clays and shales, in general, and in the Friars Formation in particular.

—Investigate the problem of the long-term stability of cuts in stiff, fissured clays and shales, with special reference to the operative strength of such soils for first-time slides. Also investigate what is the mechanism of the development of such a strength.

—Find an efficient, economic and reliable laboratory test to determine the residual strength of a soil; determine the residual strength of samples from the Friars Formation.

In the following sections information from previous investigations of the Friars Formation is first presented, along with other work pertinent to an understanding of the stability of cuts and slopes in highly overconsolidated stiff, fissured clays and shales. Then some basic concepts which are used extensively in the present work are discussed. From these concepts a theoretical and experimental approach to the present problem is developed. Finally, the results of the investigation are presented and discussed, and several significant conclusions are drawn.

2. FRIARS FORMATION

2.1 General Information and Geologic Description

The Friars Formation extends over a significant area of the northern and eastern portions of the city of San Diego and the adjoining communities. The study area is situated within the erosional surface known as the "Area of High Terraces," extending from El Cajon to Escondido. It is estimated that 15,700 acres of land is affected by this formation and that approximately 40% of this area has been developed to date. The topography is generally one of rolling hills and requires significant cutting and filling to develop. The main areas of slope stability problems are the Rancho Bernardo-Poway and Santee-Fletcher Hills (El Cajon) Provinces.

The Rancho Bernardo-Poway Province and the Santee-Fletcher Hills Province have a common geology and geomorphology, and hence, type, cause, general appearance, and age of landsliding. In brief, the area is underlain by the essentially flat-lying Middle to Late Eocene Friars Formation and Stadium Conglomerate. Extensive folding has occurred within the general Friars Formation area, but tight folds and other related structures common to thicker sedimentary basins in Southern California are absent.

In the landslide areas, the Friars Formation is

composed of thin to massive beds of brown, red, and green mudstones and claystones, alternating with fine to medium grained sandstones. This formation typically makes up the lower slopes of canyon walls, while the overlying Stadium Conglomerate occupies the upper slopes. The Stadium Conglomerate consists of a massive cobble conglomerate with a dark-yellowish-brown, coarse-grained sandstone matrix. The conglomerate contains dispersed lenses of fossiliferous crossbedded sandstone.

Most landslides are initiated at or near the contact between conglomerate and mudstone or claystone formations as a result of erosional oversteeping created by the more resistant nature of the Stadium Conglomerate. The rupture typically occurs within a claystone bed or along a sloping interbed contact. It has also been suggested (Pickney and Lee) that "bedding plane faults" may have a significant influence on landslides, as they constitute planes of weakness within the formation along which sliding can easily occur.

The "bedding plane faults" are remolded seams of clay occurring along bedding planes throughout the sedimentary formations in the San Diego area. They typically range from a fraction of an inch to seyeral inches in thickness and they generally consist of firm to stiff fine sandy to silty clay with water contents at or near the plastic limit. The remolded clay seams are generally found within the more

argillaceous sections where there has been extensive faulting and folding and at the contact between a relatively weak clay bed and an overlying stronger material in areas of relatively nominal flexing. The frequency of occurrence of remolded clayey seams along the bedding appears to be related to the intensity of folding or faulting within the general area. Laboratory tests on samples from "bedding plane faults" have been performed by Woodward-Clyde Consultants, San Diego and the results indicate low values of strength, namely close to the residual strength. The photographs in Fig. 2.1.1 and 2.1.2 show a slide in the Friars Formation and an exposure of a "bedding plane fault."

2.2 Previous Investigations in the Friars Formation

There have been several investigations made in Friars Formation recently, both by geotechnical firms and researchers. One of the most significant investigations has been done by C. J. Pinckney and L. J. Lee of Woodward-Clyde Consultants, who have tried to determine the influence of "bedding plane faults" on the stability of natural slopes and cuts in the Friars Formation. Their conclusion is that "bedding plane faults" are responsible for most of the slides occurring in the Friars Formation. In addition, "bedding plane faults" form a predetermined failure plane, along which sliding is most likely to occur. Their investigation has revealed that the frequency of occurrence of "bedding plane faults" varies from

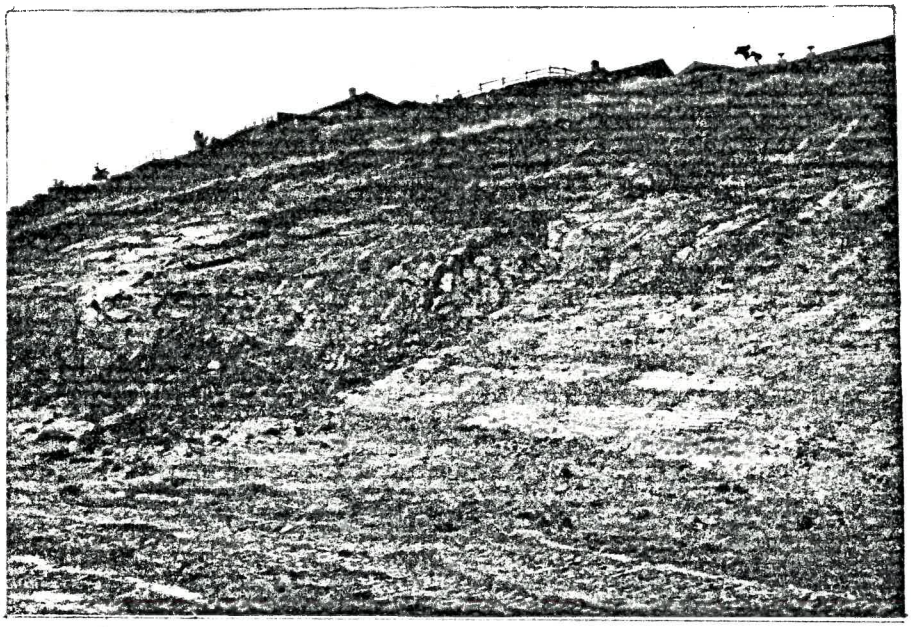


Fig. 2.1.1 A landslide in the Friars Formation.

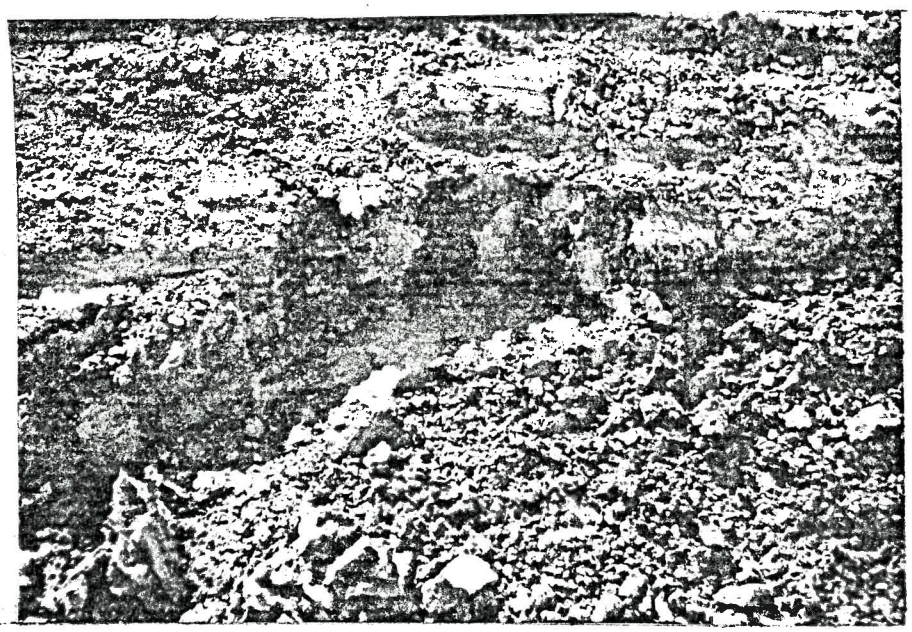


Fig. 2.1.2 Exposure of a "bedding plane fault."

place to place and as it was mentioned in the previous section, it seems to be related to the intensity of folding or faulting within the general area. For example, in the Ardath Formation in the Mountain Soledad area, west of the Rose Canyon fault, it is not uncommon to find 3 to 6 clay seams within a particular 100-foot stratigraphic section. In the eastern portion of the area, for example in the Friars Formation near Fletcher Hills, it is rare to encounter more than two seams within any 100-foot interval. The lateral extent of the clay seams is difficult to determine. Pickney and Lee, however, report that particular seams or series of seams have been followed continuously for several thousand feet. In other areas, by utilizing lithologic correlations, they have identified clay seams on either side of some of the larger canyons in the Clairmont and Encinitas areas. Pickney and Lee have performed laboratory tests on numerous samples of clay seams from various depths within the sedimentary formations throughout the county, and their results indicate that these seams have typically low strength, which is equal or near to the residual strength of the intact claystone. Measured values of residual friction angle range from approximately 6° to 15°. These values appear to be consistent with field observations where strengths have been back-figured for cases where actual movements have been observed.

Another investigation, by Woodward-Clyde Consultants, was initiated in 1978 in the Friars Formation. Their studies also show that the "bedding plane faults" are responsible, in most cases, for the landslides (see also Fig. 2.2.1), while in some cases there have been landslides within the intact formation. Their analyses show that the claystone is mainly composed of montmorillonite and kaolinite. Summarized results of their classification tests are shown in Fig. 2.2.2 (grain size distribution curves) and Fig. 2.2.3 (Atterberg limits and indices). Typical strength data from a number of tests performed on the various soil types comprising the Friars Formation are shown in Table 2.2.1. Among other things, they have tried to determine the residual strength of the Friars Formation claystone and of the "bedding plane fault" material, by using the multiple reversal direct shear tests. The number of reversals they have used in these tests is 6 to 8, and the values of residual friction angle they have obtained range from 6° to 10°.

While the above investigation was still in progress, a compositional analysis on samples from the Friars Formation was carried out at the University of California, Berkeley, during the Fall of 1978, by Caldwell, Deere, Lawton and Platis, in an effort to supplement the above laboratory test data and to also relate the strength and deformation behavior of the soils comprising the Friars

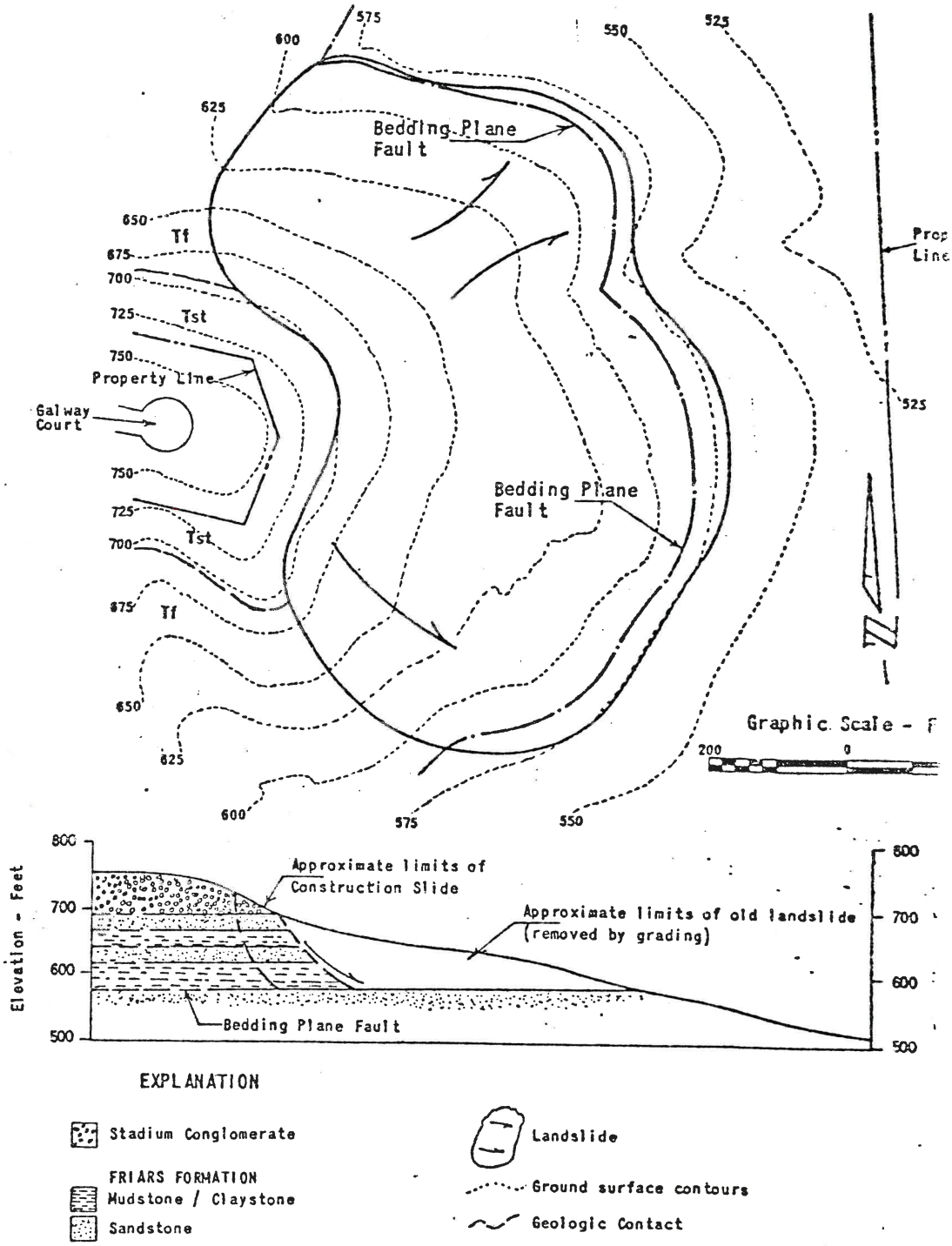


Fig. 2.2.1 Typical landslide caused by the presence of a "bedding plane fault" (from Woodward-Clyde Consultants, San Diego, 1978).

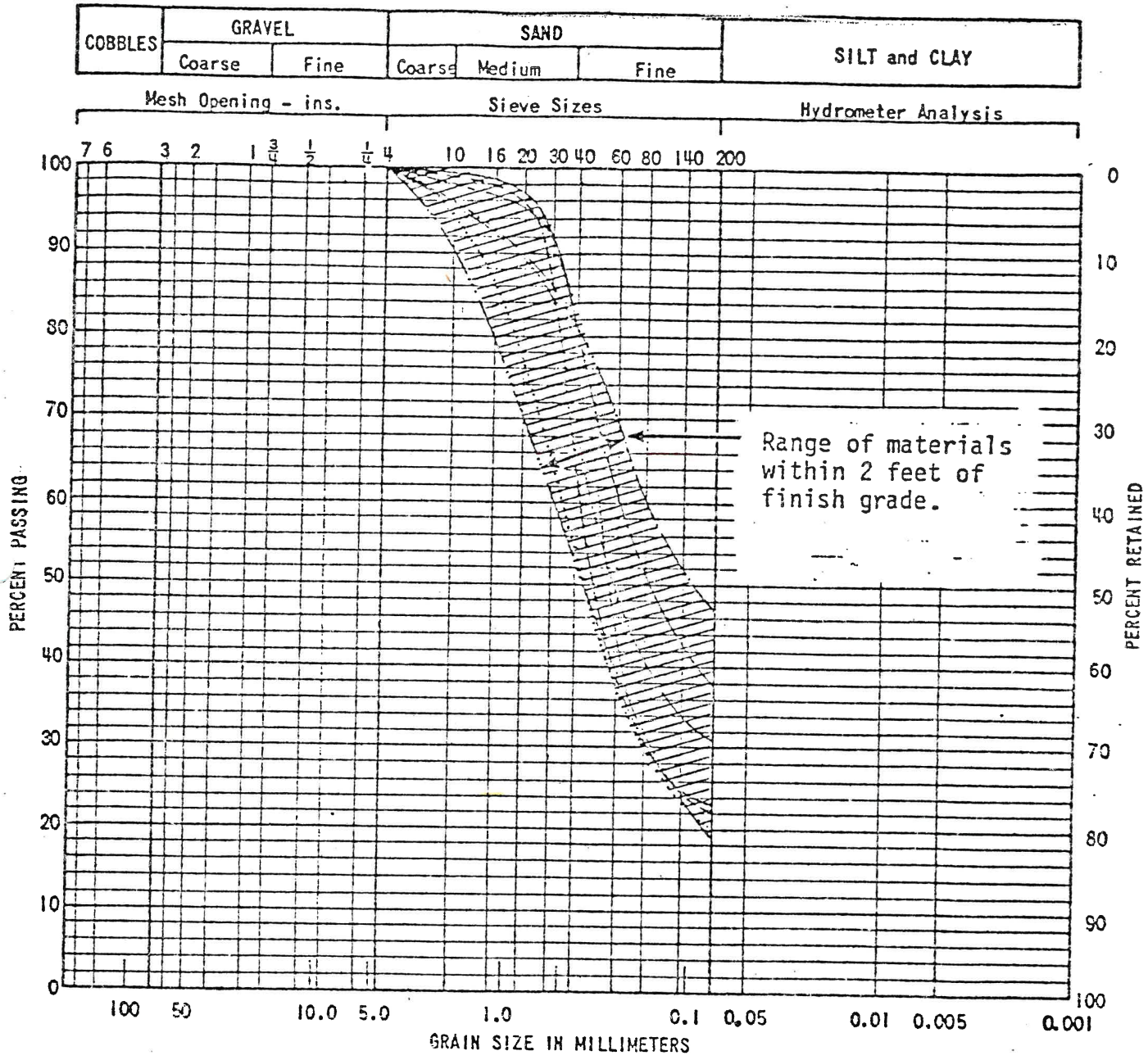
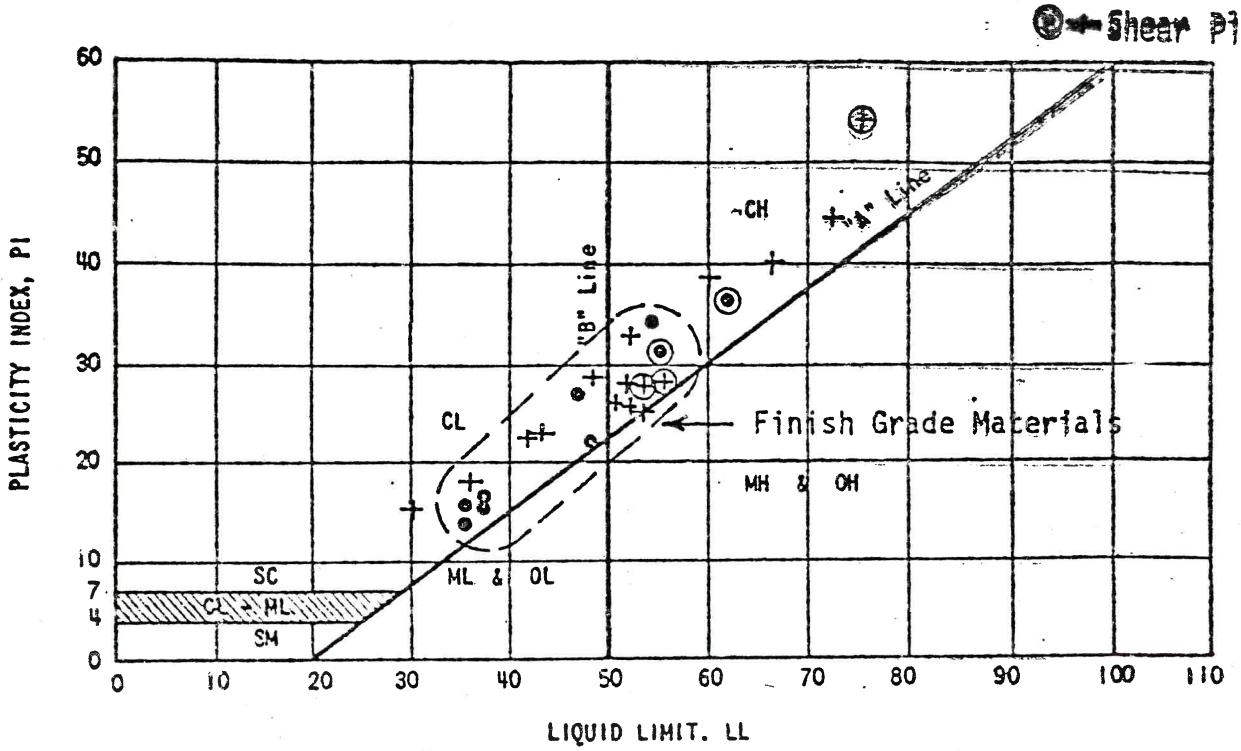


Fig. 2.2.2 Typical grain size distribution curves of soils comprising Friars Formation (from Woodward-Clyde Consultants, San Diego, 1978).



PLASTICITY CHART
For Classification of Fine - Grained Soils in Unified System

Legend	
CL	Inorganic clay of low to medium plasticity.
CH	Inorganic clay of high plasticity.
ML	Inorganic silt of low plasticity.
MH	Inorganic soil of high plasticity.
OL	Organic silt or clay of low plasticity.
OH	Organic clay of high plasticity.
SM	Silty sand.
SC	Clayey sand.

- ⊙ Tested for Preliminary Investigation
- ◎ Tested for Preliminary Investigation - Shear Test on sample
- \+ Tested during Grading
- ⊕ Tested during Grading - Shear Test on sample

Fig. 2.2.3 Atterberg limits and indices of soils comprising the Friars Formation (from Woodward-Clyde Consulting, San Diego, 1978).

Table 2.2.1

Typical Strength Data from the Friars Formation

(from Woodward-Clyde Consultants, San Diego, 1978)

Soil Type	Unit Weight (pcf)	Angle of Friction ϕ (degrees)	Cohesion c (psf)
Undisturbed Formational (Clayey Sandstone)	125	31	300
Recompacted Fill (SC-CC)	125	27	600
Fractured Formational (Claystone)	120	24	0
Residual Slide Plane (CH)	125	10	100

Table 2.2.2

A Summary of a Compositional Analysis

on Samples from Friars Formation and Ardath Shale

(from Caldwell, Deere, Lawton, Platis, 1978)

Sample	Fault Material	Graben Material	Slide Plane	Ardath Shale
Clay Minerals in Order of Abundance	Smectite Kaolinte Illite	Smectite Kaolinite Illite	Smectite Mix-layered	Smectite Illite Kaolinite
Non-clay Minerals and other Constituents in Order of Abundance	Quartz Feldspar Calcite Mica Organics	Feldspar Quartz Organics	Quartz Feldspar Organics ?	Quartz Feldspar Organics
Liquid Limit	60	61	77	80
Plastic Limit	32	38	25	32
PI	28	23	52	48
Activity	1.2	0.6	1.1	0.7
% Clay Size	28%	46%	53%	71%
pH	7.9	7.5	4.4	6.8
TDS $\frac{\text{gm.salt}}{\text{gm. soil}}$	0.00083	0.011	0.0029	0.004
% Sodium	71%	67%	100%	71%

Formation to their mineral composition and pore water chemistry (a summary of the results of this compositional analysis is presented in Table 2.2.2).

During the early part of 1979, a series of in situ direct shear tests was carried out by the California State University, Long Beach (under the direction of Professor B. Yen) on an exposure of the Friars Formation at Rancho Bernardo, in order to determine the peak and residual strength characteristics of the fissured claystone. Two of these tests were also attended by the writer and an undisturbed box sample was obtained from that same area together with some bag samples for later testing. The location which the box sample was obtained from is schematically shown in Fig. 2.2.4. Two interesting features of these field tests were the use of an accoustic emission sensor and of a microwave moisture meter. The accoustic emission sensor was used in order to correlate accoustic emission intensity to stress level around the failure plane. The microwave moisture meter was used for measuring the relative moisture of the soil close to the failure plane. Fig. 2.2.5 (a) and (b) shows a schematic design of the shear testing set up and it also schematically shows the kinds of measurements that were made during the tests. Unfortunately, the results of these tests were not available at the time this report was written.

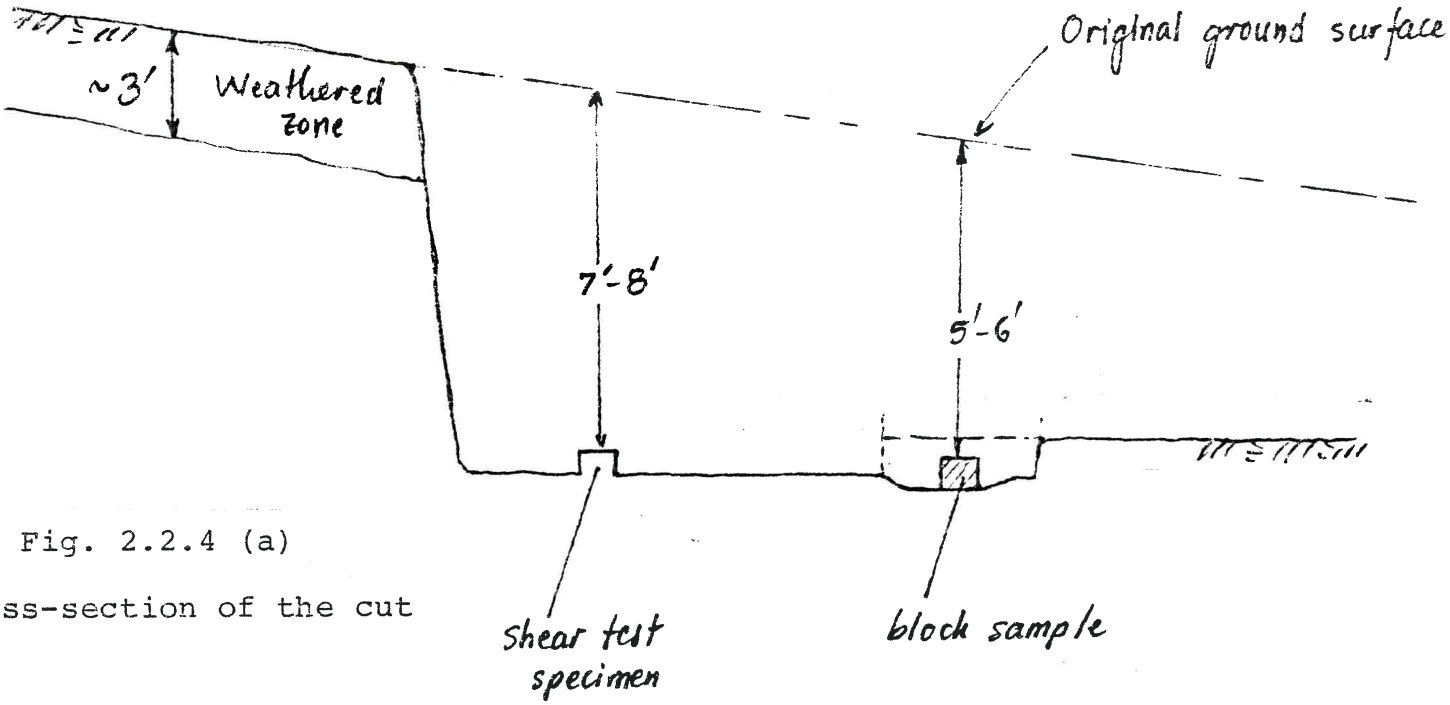


Fig. 2.2.4 (a)

Cross-section of the cut

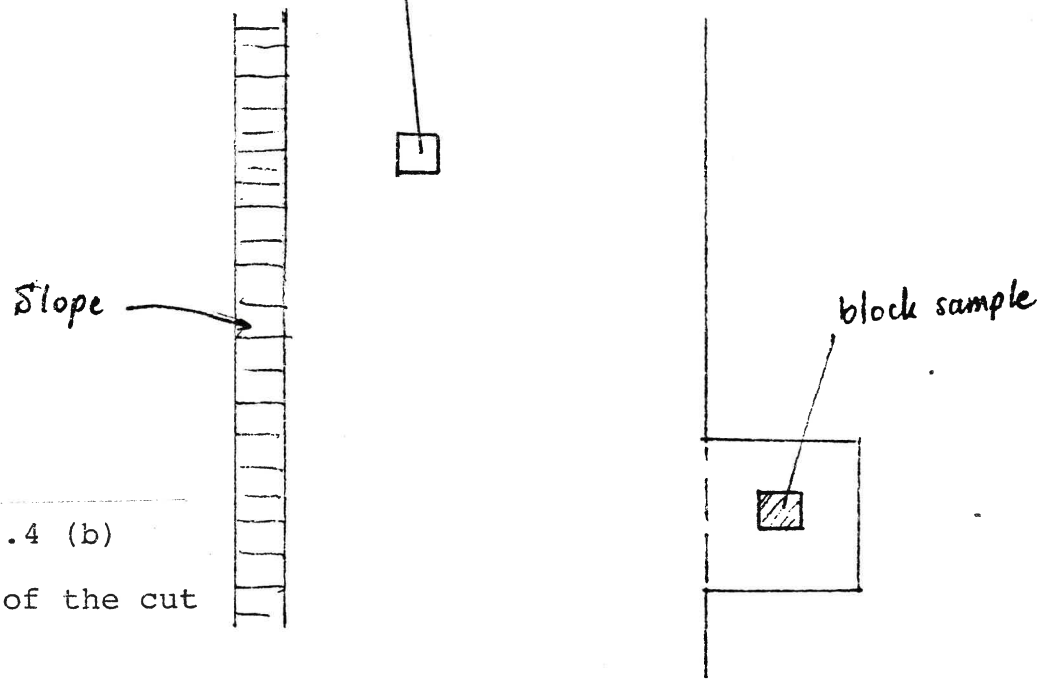


Fig. 2.2.4 (b)

Plan view of the cut

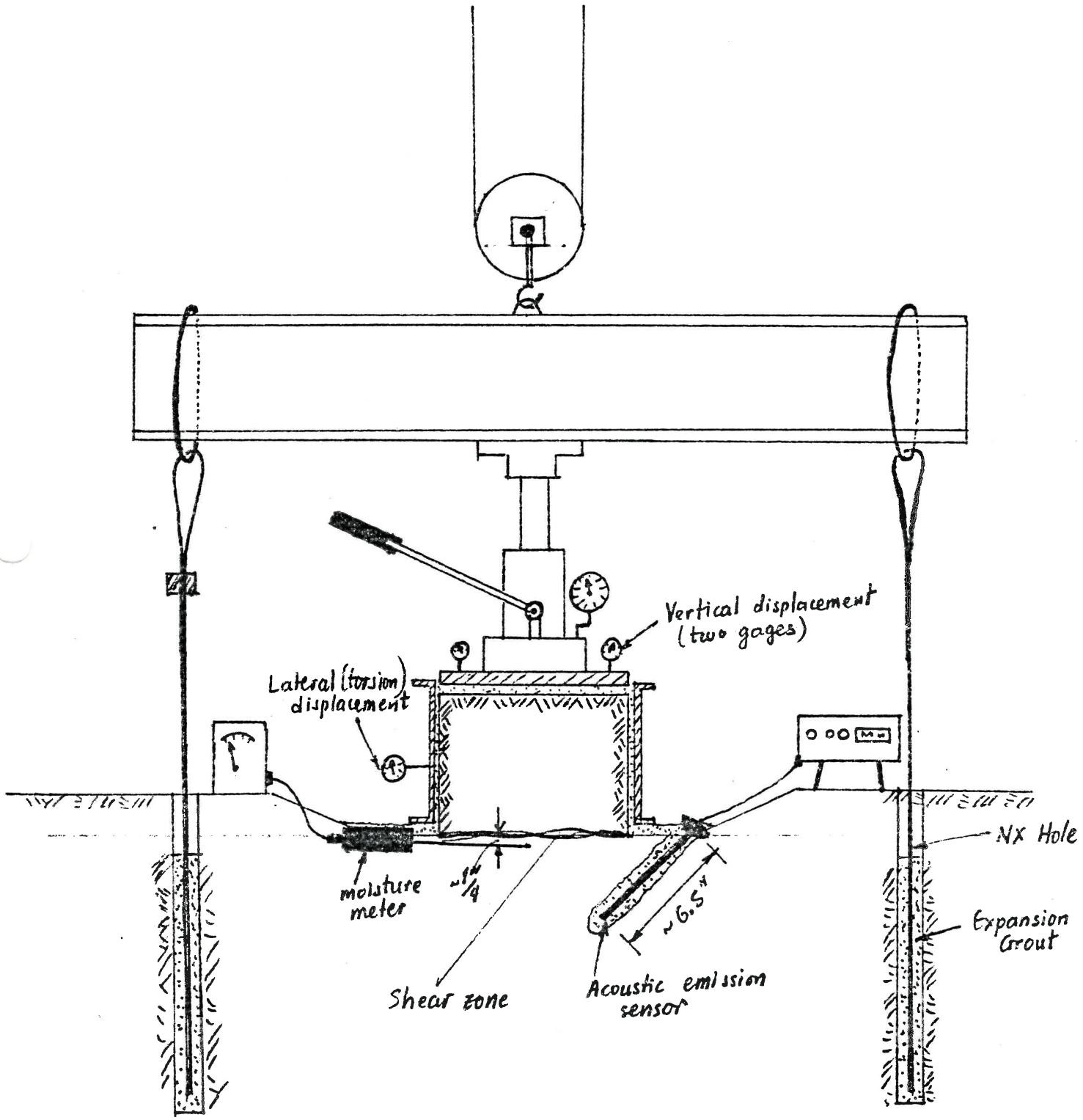


Fig. 2.2.5 (a) Schematic design of shear testing set up

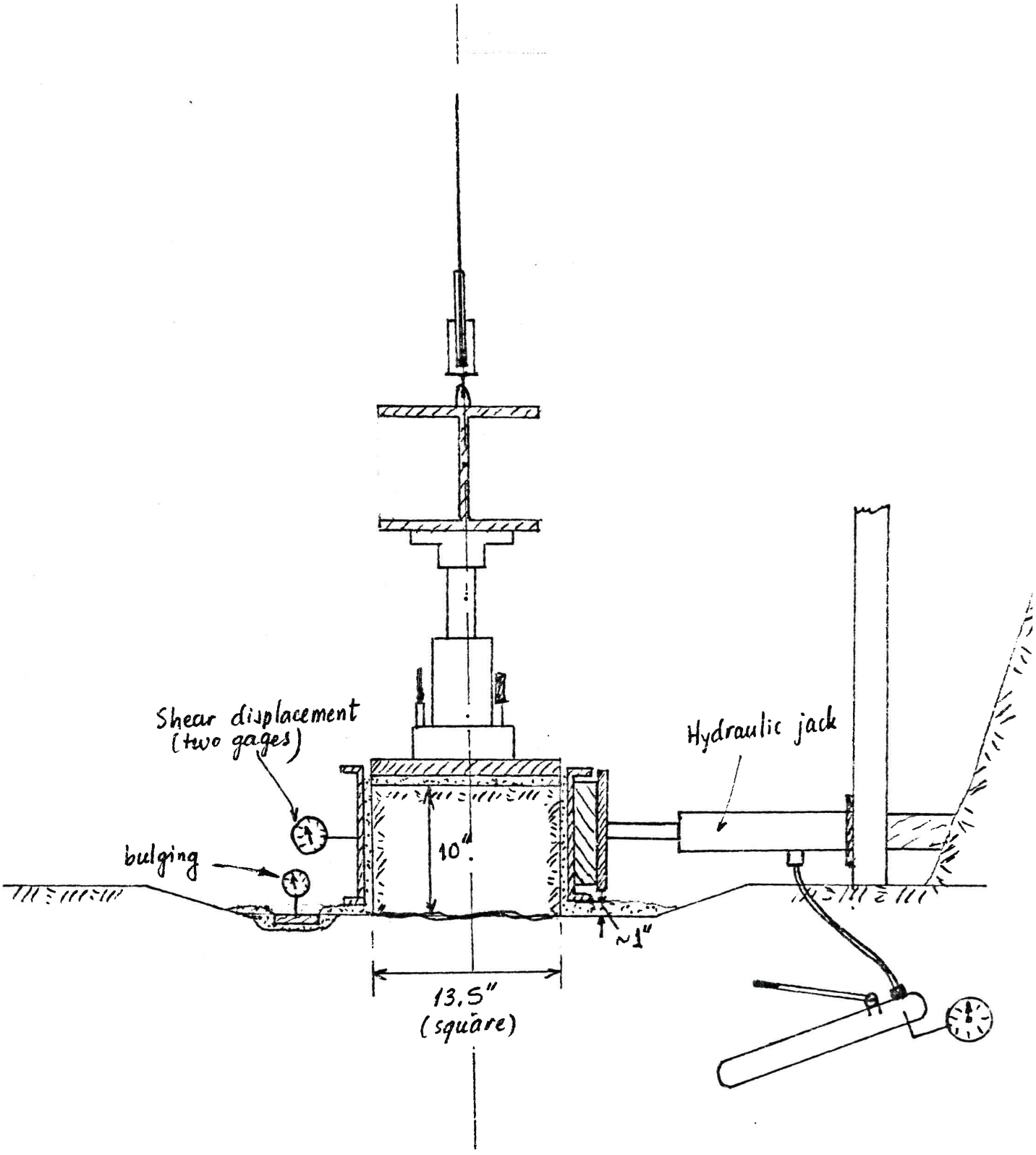


Fig. 2.2.5 (b) Schematic design of shear testing set up

2.3 Summary

The Friars Formation consists of alternating beds of claystones and sandstones. Most of the landslides in the Friars Formation are initiated at or near the contact between conglomerate and claystone beds. The rupture typically occurs within a claystone bed or along a sloping interbed contact. "Bedding plane faults" are believed to be responsible for the majority of the landslides in the Friars Formation. The strength along these weakness planes has been measured to be as low as the residual.

Other investigations that have been previously conducted at the Friars Formation are:

—By Pickney and Lee, who examined the importance of the "bedding plane faults" in the evaluation of landslides in the Friars Formation.

—By Woodward-Clyde Consultants, who determined classification and strength parameters for the soils comprising the Friars Formation.

—By Caldwell, Deere, Lawton and Platis, who performed compositional analyses on samples from the Friars Formation and Ardath Shale.

—By B. Yen of the California State University, Long Beach, who performed in situ, drained direct shear tests for the determination of the peak and residual strengths of the Friars Formation claystone.

3. THE LONG-TERM STABILITY OF SLOPES IN STIFF, FISSURED CLAYS AND SHALES

3.1 General

The problem of the stability of slopes in stiff, fissured clays and shales has been a subject of extensive research and discussion for many years because in many respects, the behavior of this class of soils is very difficult to predict. One of the very important questions usually raised by the design engineer, and one that is difficult to answer, is what strength parameters should be used for design in these materials. Except for places where extensive research has been done in the past or there is extensive local experience with a particular soil (as for example the London clay), for which practical design parameters have been established, there is really no general approach to the problem of directly measuring or even indirectly obtaining, with some degree of accuracy, the parameters that should be used for design. An engineer can only establish upper and lower bounds for the strength parameters as for example the peak and residual strengths, which can be measured with a fair degree of accuracy in the laboratory and which will be defined and discussed in sections 3.2 and 3.3. He must then take into account the degree of fissuring and jointing of the clay, the presence of pre-existing shear zones (as for example tectonic

shear zones or old landslides), the presence of surface cracks, the ground water conditions, the degree of strength anisotropy of the clay, the stress-strain behavior and swelling characteristics of the clay and, based on empirical correlations and on his engineering judgment, he can establish approximate strength parameters for design. The reasons that such difficulties exist in determining the operative strength in stiff, fissured clays and shales are:

—It is very difficult to quantitatively determine how large is the effect of all the aforementioned factors on the stress-strain-strength behavior of stiff, fissured clays and shales.

—Progressive failure is believed to cause a significant lowering in strength of stiff, fissured clays and shales. However, at the moment, there is no analytical approach which can take progressive failure fully into account. The only analysis which may make some consideration of the progressive failure mechanism is based on the method of finite elements applied to a strain-softening material (i.e., a material whose strength decreases with increasing strain, after the peak strength has been reached) (Lo and Lee, 1973). We will define progressive failure and discuss the subject in more detail in Section 3.4.

Chapter 3 will be closed with what Skempton (1970, 1977, 1978) has called "fully softened strength" (Section 3.5) and which he has determined to be the operative strength for first-time slides in stiff, fissured clays and shales.

3.2 Peak Strength of Stiff, Fissured Clays and Shales

The peak strength of the stiff, fissured clays and shales is a parameter which depends on many factors and which can vary, for the same soil, over a wide range. Such factors are:

—Degree of overconsolidation. In general the more overconsolidated the clay is the higher its peak strength is.

—Structure. Morgenstern (1967) distinguishes between macrostructure (fissures, joints, slickensides, etc.) and microstructure (e.g., microscopic discontinuous shear planes). Not much is known about the origin of fissures, but it is generally accepted that they have a weakening effect on stiff clays. In some cases the structure may entirely dominate the behavior and strength of the clay, as for example in the case of large continuous joints. The structure influences not only the strength, but also the general behavior of the stiff clay (e.g., permeability and drainage may heavily depend on the number and opening of

fissures (Ward, 1967)).

—Degree of weathering. In general the more weathered the clay is, the lower its strength.

—Strength of diagenetic bonds. The diagenetic bonds are bonds formed due to chemical and physical alterations in the clay over long periods of time. They are described in more detail in Section 3.4. In general, the stronger the diagenetic bond, the higher the peak strength of the clay.

—Sample size. This is related to the degree of fissuring and it is a factor which of course affects not the actual, but the measured peak strength; the smaller the sample is, the less the amount of fissures and consequently the higher the measured peak strength. In the extreme case, if the sample is smaller than the average fissure spacing, no fissures may be encountered in the sample tested, in which case the measured peak strength is maximum and it corresponds to the strength of the intact (unfissured) clay. Morgenstern (1967) reports that the sample size effect is more pronounced for the undrained strength of the stiff, fissured clays, while this effect is rather small on the peak strength in terms of effective stresses.

A characteristic feature of the peak shear strength parameters (c', ϕ') of stiff, fissured clays is the reported decrease of the cohesion intercept in terms of effective stresses, with time. This long-term decrease of cohesion may be associated with weathering, progressive failure or softening resulting from dilatancy and increase in water content in the shear zone (Chandler and Skempton, 1974). The cohesion intercept c' corresponding to the peak strength of unweathered clays and clay shales with diagenetic bonds is comparatively large. However, fissures and/or brecciation may reduce c' considerably. Chandler and Skempton (1974) for example report that fissures in blue London clay reduce the cohesion intercept, as measured from tests on 98mm diameter triaxial specimens, to about one-quarter of the value measured on small (38mm) laboratory specimens. In contrast to c', the angle of internal friction in terms of effective stresses, ϕ', doesn't seem to change appreciably with time.

However, progressive failure can lead to a decrease in ϕ', as will be described in Section 3.4, but that is due to the strain softening behavior of the stiff clays (i.e., the process of progressive failure takes the clay locally past its peak strength to a lower strength, but it does not lead to an actual lowering of the peak strength).

An important aspect of the behavior of overconsolidated, stiff clays is the fact that they dilate when sheared. This

leads to an increase in water content during drained shear, which results in a decrease in strength with deformation after the peak. Under undrained shearing, the overconsolidated, stiff clays tend to dilate, which leads in a decrease of the pore pressure. This is especially important in the case of excavations in such clays, since the undrained increase in shear stresses caused by the excavation leads to a decrease of pore pressures and in a corresponding increase of effective stresses. However, as the pore pressures increase with time due to water flow towards the zones of high shear stresses (for pore pressure equilibrium to be attained), the effective stresses drop and failure may eventually occur. Consequently, the long-term stability is in general more critical than the short-term stability for slopes excavated in stiff, fissured clays. In cases where the permeability is very low, this pore pressure equilibrium may take several decades and failure may be delayed for as long as 40 to 50 years (Skempton, 1977) or even longer.

3.3 Residual Strength

The residual strength of a soil is defined as the strength exhibited at very large strains, under drained conditions, provided it is given sufficient time to consolidate or swell. Deformation at the residual strength is a constant volume process (Fig. 3.3.1).

The residual strength does not depend on such factors as original structure, stress history, strain rate, sample size, initial void ratio and in general factors which dominate the path dependent properties of soils. However, it does depend on the amount and composition of the clay present in the soil (Fig. 3.3.2; Kenney, 1967, 1977), Atterberg limits (which also depend on type of clay) (Voight, 1973; Kanji, 1974, 1977; see also Fig. 3.3.3), adsorbed cations for a given type of clay (most important for sensitive clays), salt concentration in the pore fluid (most important for Na-Montmorillonite; Fig. 3.3.2; Kenney, 1967, 1977) and stress level (Kenny, 1967; Bishop et al., 1971; Chattopadhyay, 1972; see also Fig. 3.3.4, 3.3.5).

The nature of residual strength is frictional. Basal plane slip is the dominant mechanism of deformation at large strain for clay minerals and layered silicates. It involves continuous rupturing and making of bonds along the cleavage planes at the solid interparticle contacts in the shear zone. The number of bonds at any solid contact probably depends on the true effective stress (apparent effective stress-repulsive forces, assuming negligible long-range attractions) transmitted at the contact. The types of bonds that could exist between the mineral cleavage planes are the secondary valence, the exchangeable ion-linkage and the hydrogen bonds. For Na-Montmorillonite for which the

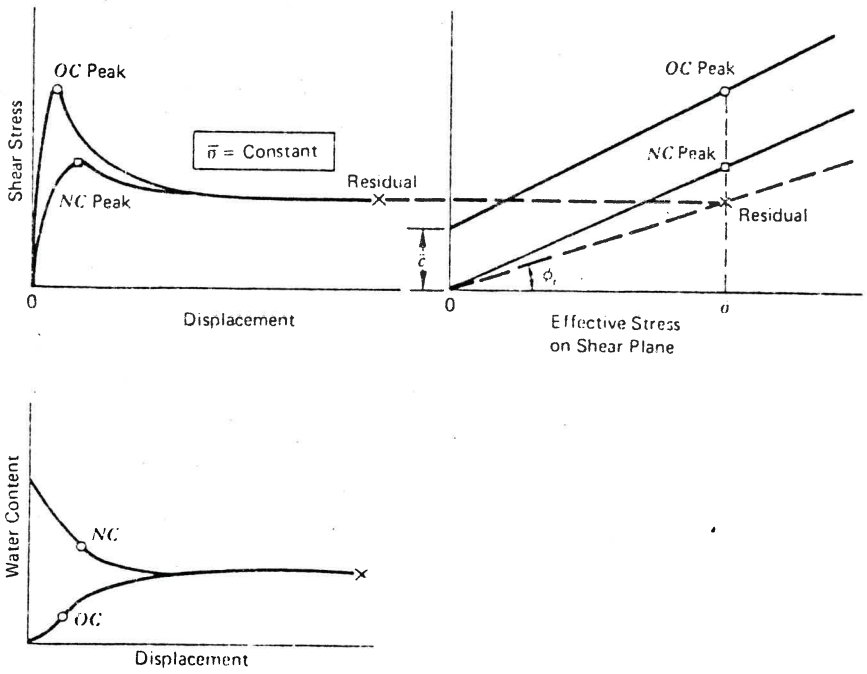


Fig. 3.3.1 Shear characteristics of clays under fully drained conditions (from Mitchell, 1976).

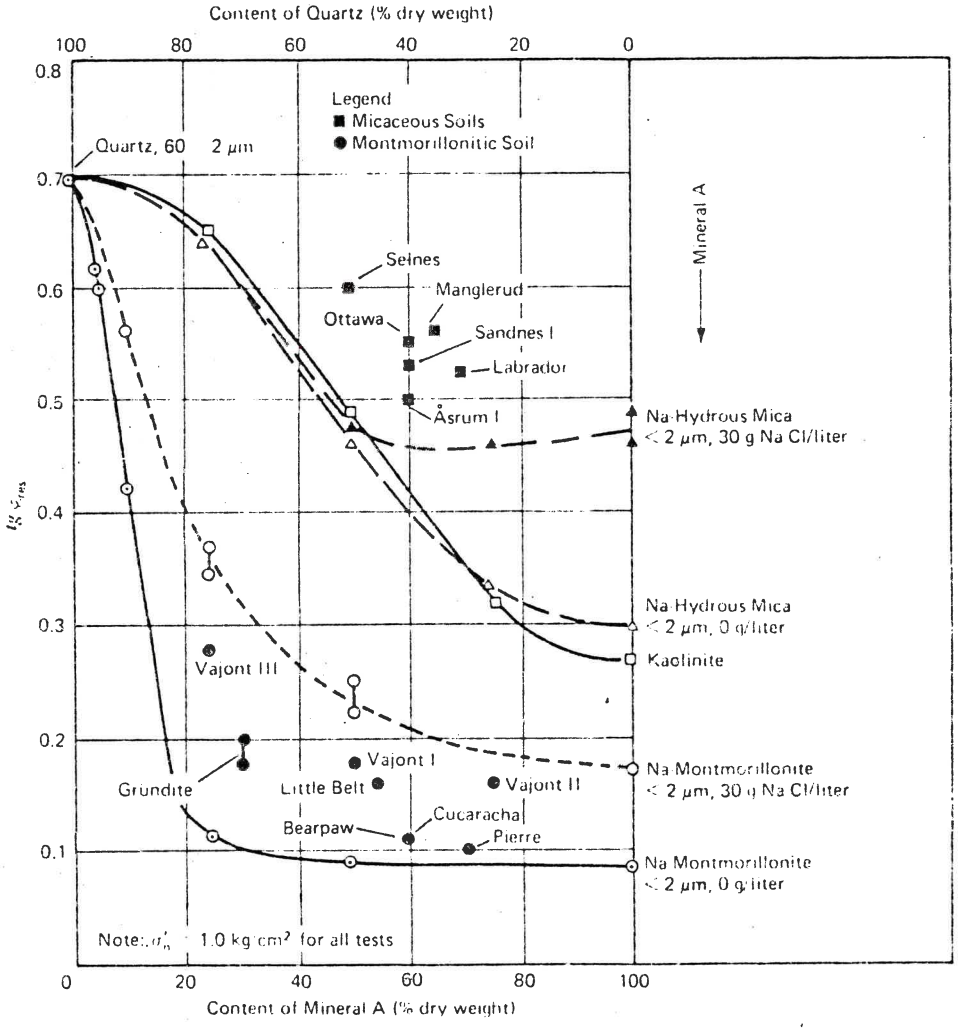


Fig. 3.3.2 Residual friction angles for clay-quartz mixtures and natural soils (Kenney, 1967).

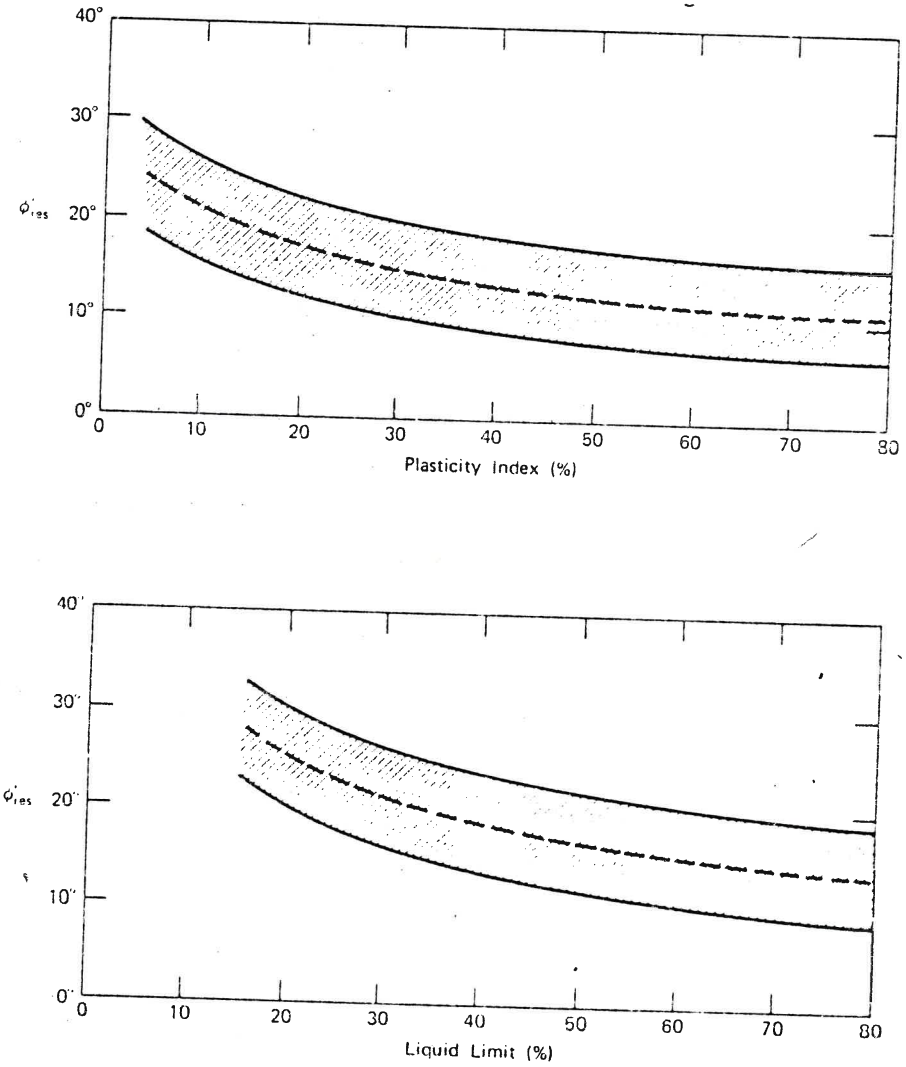
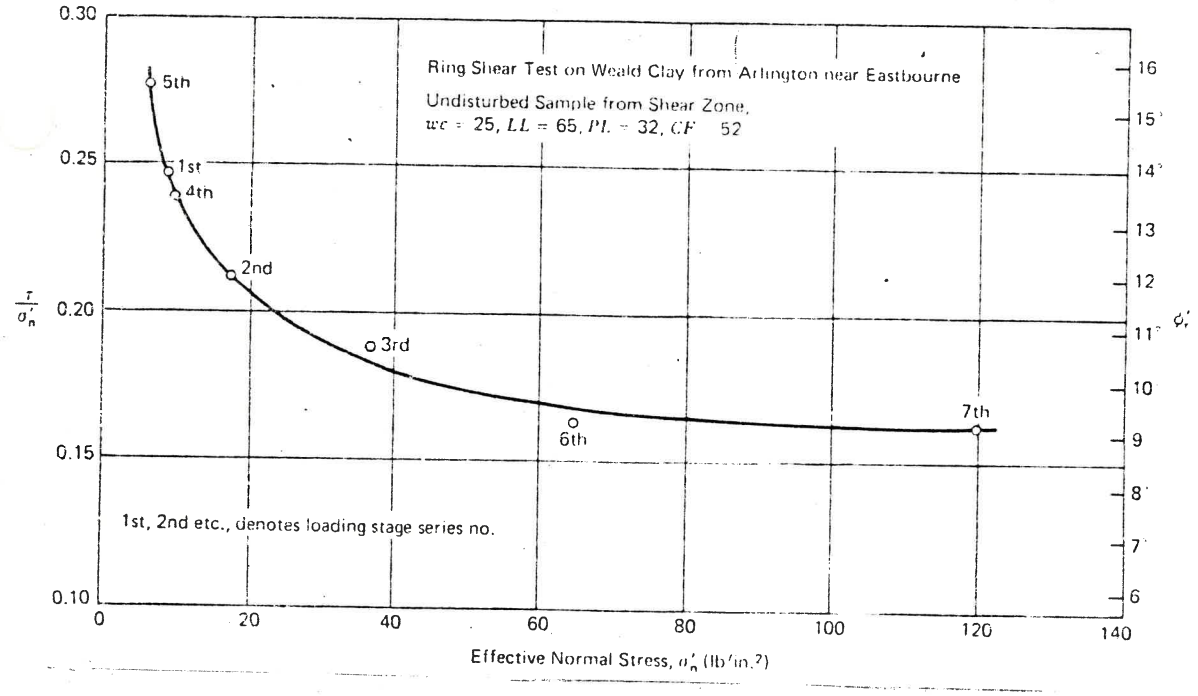
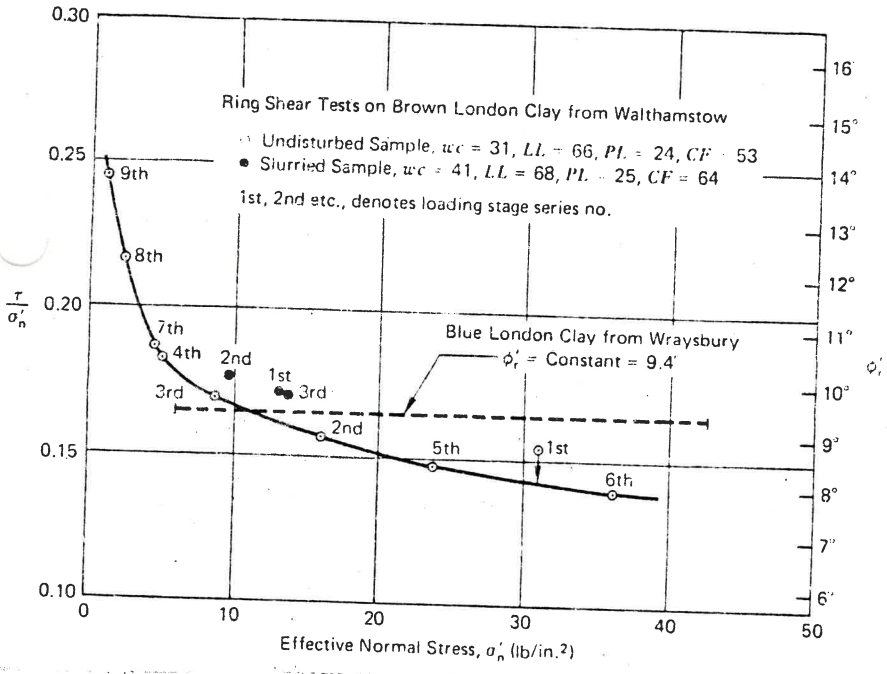


Fig. 3.3.3 Relationship between residual friction angle and Atterberg limits (from Mitchell, 1976).



(a)



(b)

Fig. 3.3.4

Variation of residual strength with stress level (Bishop et al., 1971).

(a) Brown London clay.
(b) Weald clay.

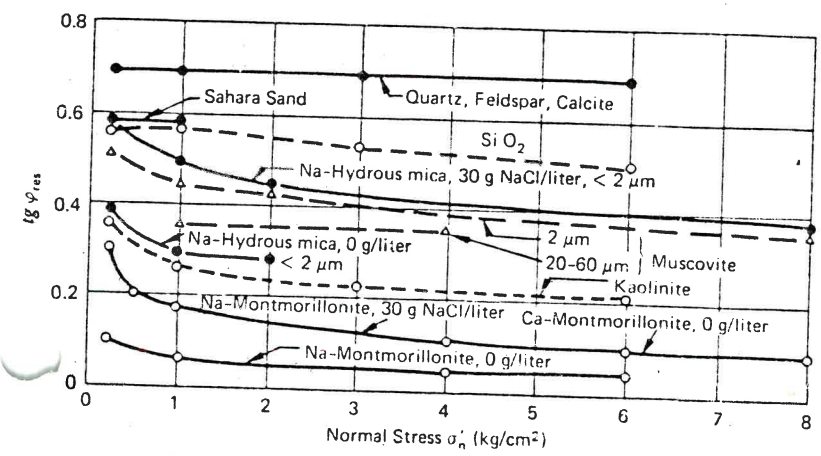


Fig. 3.3.5

Relationship between residua friction angle and normal stress for different mineral (Kenney, 1967).

repulsive forces may equal the apparent effective stress (no interparticle contacts; e.g., when salt concentration in pore fluid is low), no bonds of the type previously described can be established and consequently its residual strength must be low. In fact, very low values for φ'_{res} have been reported (2° - 3°; Kenney, 1967) for Na-Montmorillonite at low salt environments and this supports the previous statement.

φ'_{res} depends on the effective stress only at low stress levels and it decreases with increasing normal stress until it becomes constant (Fig. 3.3.4, 3.3.5). There are two hypotheses available to explain this stress-dependency of φ'_{res}:

—Under low normal stresses, less work would be required to shear the clay without imposing perfect particle orientation than would be required by imposing perfect particle orientation. Under higher normal stresses, however, less work is expended if perfect particle reorientations develop during shear displacement (Mitchell, 1976).

—The second hypothesis is based on the elastic junction theory, according to which the area of true contact between two particles (at the asperities) is proportional to $(\text{load})^{2/3}$ at low stress levels, this leading to:

$$\tan \varphi'_r = (\text{const.}) \times (\sigma')^{-1/3}$$ (Chattopadhyay, 1972).

Skempton (1964, 1971) reports that the residual strength controls the movements of slopes on pre-existing slip planes. Such pre-existing slip planes may have been formed due to a previous slip or due to tectonic movements (Skempton, 1966). He also reports that displacements as large as 1-2 meters are required, along a first-time formed slip surface, for the mobilized strength to drop to the residual value (Skempton, 1977). The residual strength is associated with strong particle orientation. Skempton (1964) reports that the zone of perfect particle orientation is only in the order of microns (e.g., 20μ); this very thin zone of residual strength mobilization is located within a larger shear zone of moderate particle orientation, with thicknesses in the order of 1 to 2 inches.

3.4 Progressive Failure

The term progressive failure, as it was originally defined by Terzaghi and Peck (1943), indicates the spreading of the failure over a potential surface of sliding from a point towards the boundaries of the surface. This is due to non-uniform stresses and strains along a potential failure surface (Taylor, 1948). Because of this mechanism the strength which is operative at each point along a potential failure surface is not necessarily the peak, but a value lower than that if the stress at the point has already

exceeded the peak shear strength. This statement holds true for strain-softening materials (for example stiff clays), which exhibit a drop in strength for displacements past that corresponding to the peak strength. If the displacements at a point are large enough, the strength can eventually drop to a limiting value, the residual strength, which has already been discussed in detail in Section 3.3. From the above it is evident that in the extreme case of a slope at the point of limiting equilibrium, the operative strength along a potential failure surface could vary from the residual at the point where progressive failure first started, to the peak strength at the point which will potentially fail last.

Two questions arise at this point. The first is, how large a displacement along the potential failure surface is required for the progressive failure mechanism to develop and how big is this effect on the computed factor of safety using a uniform mobilization of peak shear strength along the failure surface at the point of limiting equilibrium? The second question is, where is the point of progressive failure initiation located behind a slope and what factors does this point depend on? An attempt will be made to answer these questions based upon both analytical work that has been done in the past, as well as on field observations of slopes that have failed.

The answer to the first question is very much dependent upon the post peak behavior of the soil; i.e., it depends on how big the drop from the peak to the residual strength is and how fast it occurs (in terms of displacement). If the drop in strength after the peak is very abrupt and significant in magnitude, then--once the stresses have reached the peak strength at a point behind a slope--it takes only a very small displacement for the strength to drop very low at that point. This small displacement could be caused by a variety of reasons, for example, by a small rise in the ground water table or even by expansion of the clay caused by weathering as will be described later. Since the strength drops at the point where failure is initiated, the excess load which can no longer be carried by the soil at that point will have to be carried by the rest of the soil which has not failed, along a potential failure surface. This will cause an increase in stress in all unfailed points which will result in a certain shear deformation along the potential failure surfaces. Two things will happen because of this. First the strength will drop further at the point where failure first started, as a result of the shear deformation along the potential failure surface, thus bringing this material closer to the residual state. Second, the peak strength may be reached at some other point(s) in the slope because of the increase in stresses and some drop in

strength may also occur there if the overall displacement is sufficient to cause that. Since a drop in strength occurs at this stage, at the point of failure initiation and possibly at some other point(s), the process of stress redistribution along a potential failure surface, described previously, will be repeated. One of two things will eventually happen. The process described above will either come to an end because there is a limit on how low the strength can drop (residual strength) or it will eventually lead to complete failure of the slope once the stresses have reached or have come over the peak everywhere along the failure surface. Clearly, the previously described mechanism is a continuous one although it was described as a step process. From the previous discussion it becomes evident that the faster and lower the strength drops after the peak, the smaller the displacement required to initiate the progressive failure mechanism. It is rather difficult, however, to give a quantitative estimation of the necessary magnitude of this displacement. Skempton (1977) has observed that a relative displacement of 1 to 2 meters is usually necessary in the field for the strength to drop to the residual for London clay (a highly overconsolidated fissured clay). Bishop (1971), on the other hand, notes that a relative displacement of one foot is usually necessary in the laboratory for the strength to drop to the residual when performing ring shear tests on undisturbed

samples. It should be pointed out here, however, that only a small fraction of the aforementioned total displacement required for the strength to drop to the residual is enough for most of the drop in strength to take place.

As far as the factor of safety is concerned, a significant error can be involved in the design if the conventional assumption is made that the stresses at the point of limiting equilibrium are the same everywhere along a potential failure surface and equal to the peak strength. As was shown earlier, progressive failure results in a redistribution of the strength along the failure surface which can vary from the peak, at the point(s) which fails last, down to a value between the peak and the residual, and depending on the type of soil and amount of displacement even down to the residual strength, at the point which fails first. This means that the average mobilized strength along the failure surface is lower than the peak strength and consequently the actual factor of safety is also lower than the factor of safety which is computed assuming that the average mobilized strength along the failure surface is the peak.

From the foregoing discussion it has become evident that those soils which exhibit a very significant and abrupt drop in strength after the peak are the ones which are more susceptible to progressive failure and for which the average

mobilized strength along the failure surface can be drastically lower than the peak. Such soils are called brittle and a typical stress-strain curve for a brittle soil is shown in Fig. 3.4.1. The overconsolidated (O.C.) clays of high plasticity and the clay shales belong in this category. They are usually referred to as stiff-fissured clays and shales. They are stiff because they have been subjected to very high effective overburden pressures in the past for long periods of time and due to physical and chemical alterations (diagenesis) strong bonds (diagenetic bonds; Bjerrum, 1966) have been formed. Not much is known about the nature of diagenetic bonds. It seems, however, that they are related to recrystallization occurring under high pressures at the contact points between clay particles, resulting in molecular bonds, and on the precipitation of cementing agents at the zones of contact over long periods (Bjerrum, 1966). The strength of the diagenetic bonds depends on the consolidation pressure and on the minerals, pore fluid, temperature and time and it can vary from clay to clay. Whatever their nature is, however, they contribute to the strength and stiffness of an overconsolidated clay. In addition, they are responsible for the limited amount of rebound of these clays during unloading (due to erosion for example). Because the clay is prevented from swelling as much as it would tend to if no bonds existed, there is strain energy locked into this type of

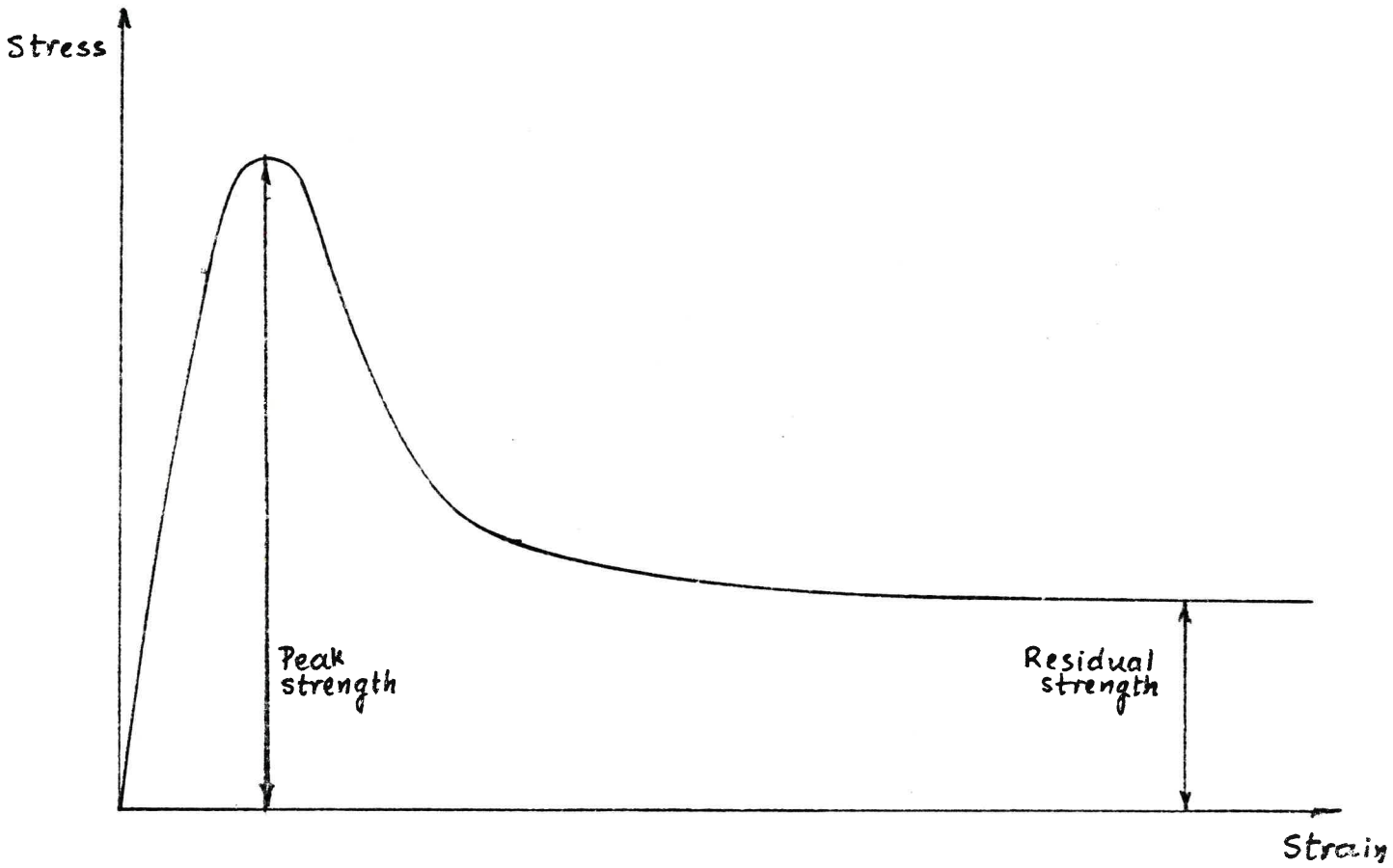


Fig. 3.4.1 Typical stress-strain curve of brittle soils.

clays. This strain energy is recoverable, however, upon deterioration of these bonds for some reason (e.g., weathering). In general, the more plastic the clay is (e.g., because of high content of active clay minerals), the greater the recoverable strain energy is. The importance of diagenetic bonds and of recoverable strain energy will become clear later, when a model of progressive failure, which has been proposed by Bjerrum (1966), will be described.

It was mentioned previously that the O.C. clays of high plasticity are usually referred to as stiff-fissured clays and it was subsequently explained why they are stiff. It should be mentioned here, however, that not all of them are fissured. The degree of fissuring of O.C., plastic clays is associated with their brittleness, their depth and their degree of weathering (the latter is related also to depth). In general the more brittle, shallow and weathered the clay is, the higher its degree of fissuring.

In order to determine the point of progressive failure initiation, the distribution of stresses behind an excavated slope will have to be considered. For a homogeneous soil deposit, this distribution will mainly depend on the initial stresses (before excavation), the geometry of the slope and the ground water conditions (depth of ground water table). The problem of finding the stresses behind an excavated slope has been treated in the past using

the finite differences and relaxation method (Bishop, 1952, 1967) and the finite element method (Brown and King, 1966; Duncan and Bishop, 1966; Dunlop and Duncan, 1970). In the process of the present work, a linearly elastic, plane strain, finite element analysis of the stresses behind an excavated slope has also been performed and it is presented in Chapter 5. Fig. 3.4.2 and 3.4.3 show contours of $\tau_{max}/\gamma H$ obtained from the analysis for a 1.5:1 slope and for two different values of the coefficient of total earth pressure at rest* (K = 0.875, K = 1.88). Notice that, depending on the drainage conditions in the field at the time of failure, τ/σ_n' or τ_{max} will be the relevant measure of strength for drained or undrained conditions respectively. In the above, τ and σ_n' are the shear and effective normal stresses on the plane of failure along a potential failure surface, while τ_{max} is the maximum shear stress along a potential failure surface. Fig. 3.4.4 (a) and (b) presents the distribution of τ/σ_n' along a potential failure surface, which is shown on Fig. 3.4.2 and 3.4.3, for the two cases of K = 0.875 and K = 1.88. Fig. 3.4.5 (a) and (b) presents the distribution of $\tau_{max}/\gamma H$ along the same potential failure surfaces. The potential failure surface that has

---

*The coefficient of total earth pressure at rest is defined as the ratio of the total horizontal stress over the total vertical stress, for conditions of no lateral strain.

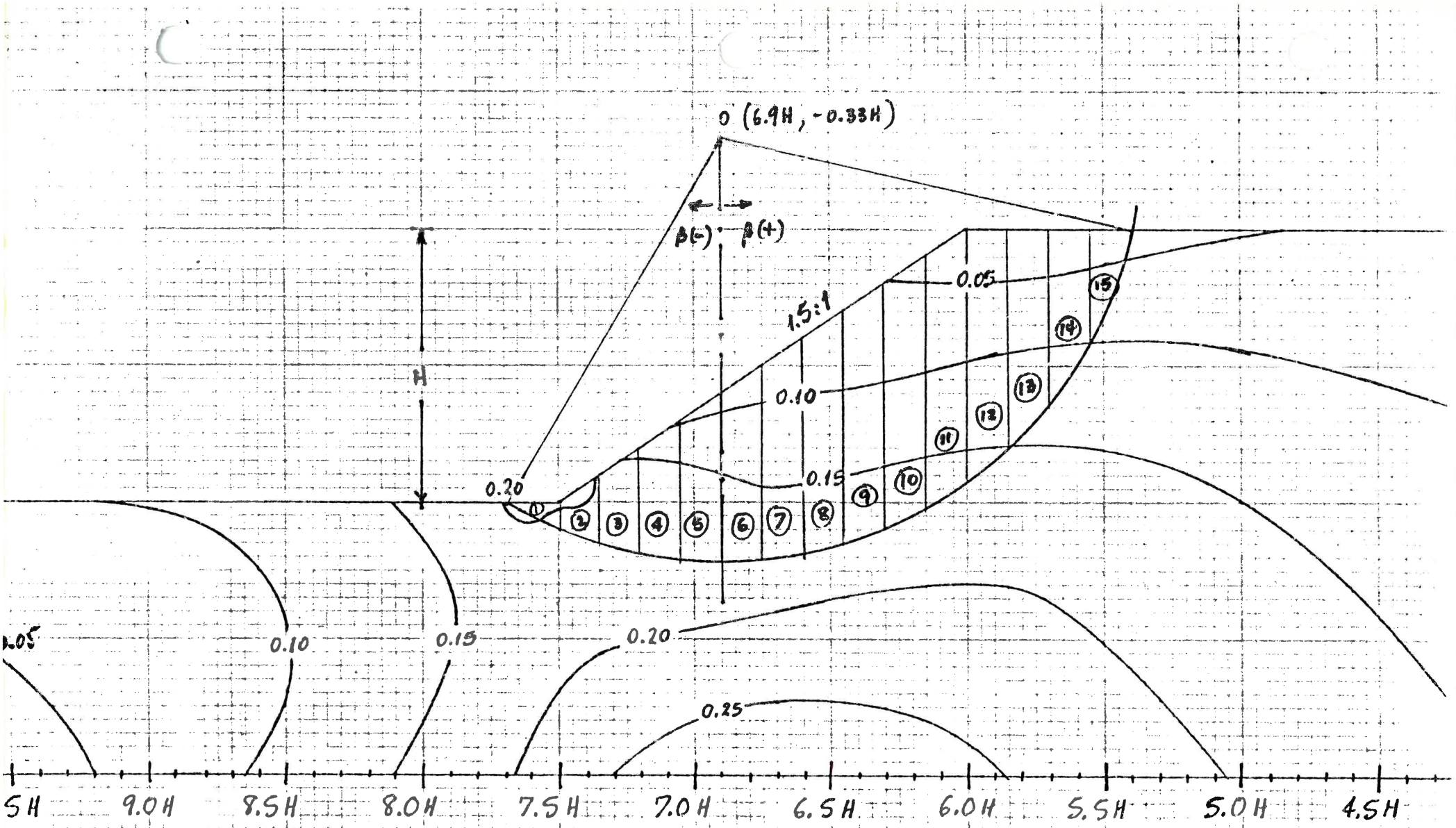


Fig. 3.4.2 Contours of $\tau_{max}/\gamma H$ for K = 0.875.

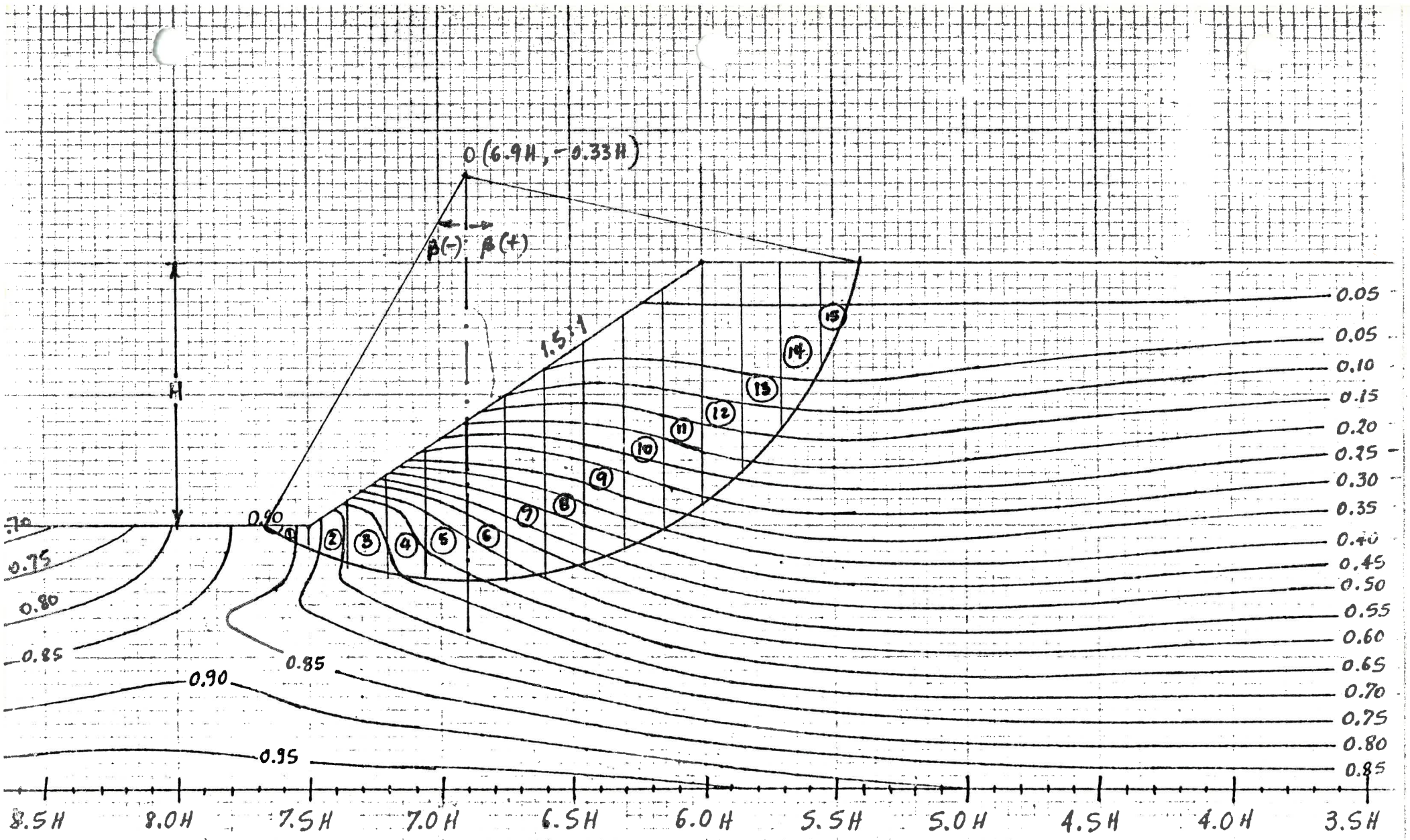


Fig. 3.4.3 Contours of $\tau_{max}/\gamma H$ for $K = 1.88$.

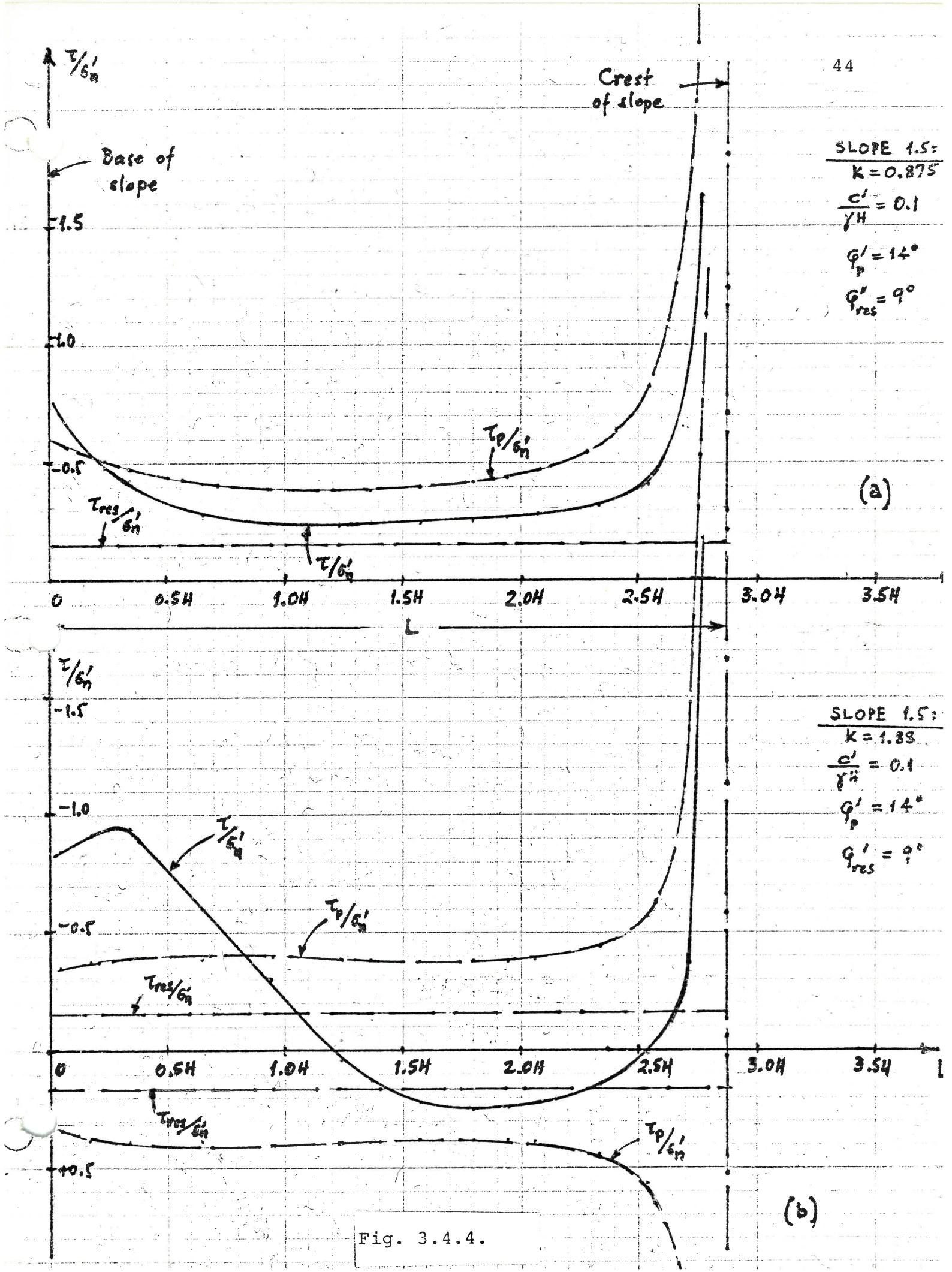

τ/σn'
Crest of slope
Base of slope
SLOPE 1.5:
K = 0.875
c'/γH = 0.1
φp' = 14°
φres' = 9°
1.5
1.0
0.5
τp/σn'
τres/σn'
τ/σn'
(a)
0
0.5H
1.0H
1.5H
2.0H
2.5H
3.0H
3.5H
L
τ/σn'
SLOPE 1.5:
K = 1.33
c'/γH = 0.1
φp' = 14°
φres' = 9°
1.5
1.0
0.5
τ/σn'
τp/σn'
τres/σn'
0
0.5H
1.0H
1.5H
2.0H
2.5H
3.0H
3.5H
L
τres/σn'
τp/σn'
0.5
(b)

Fig. 3.4.4.

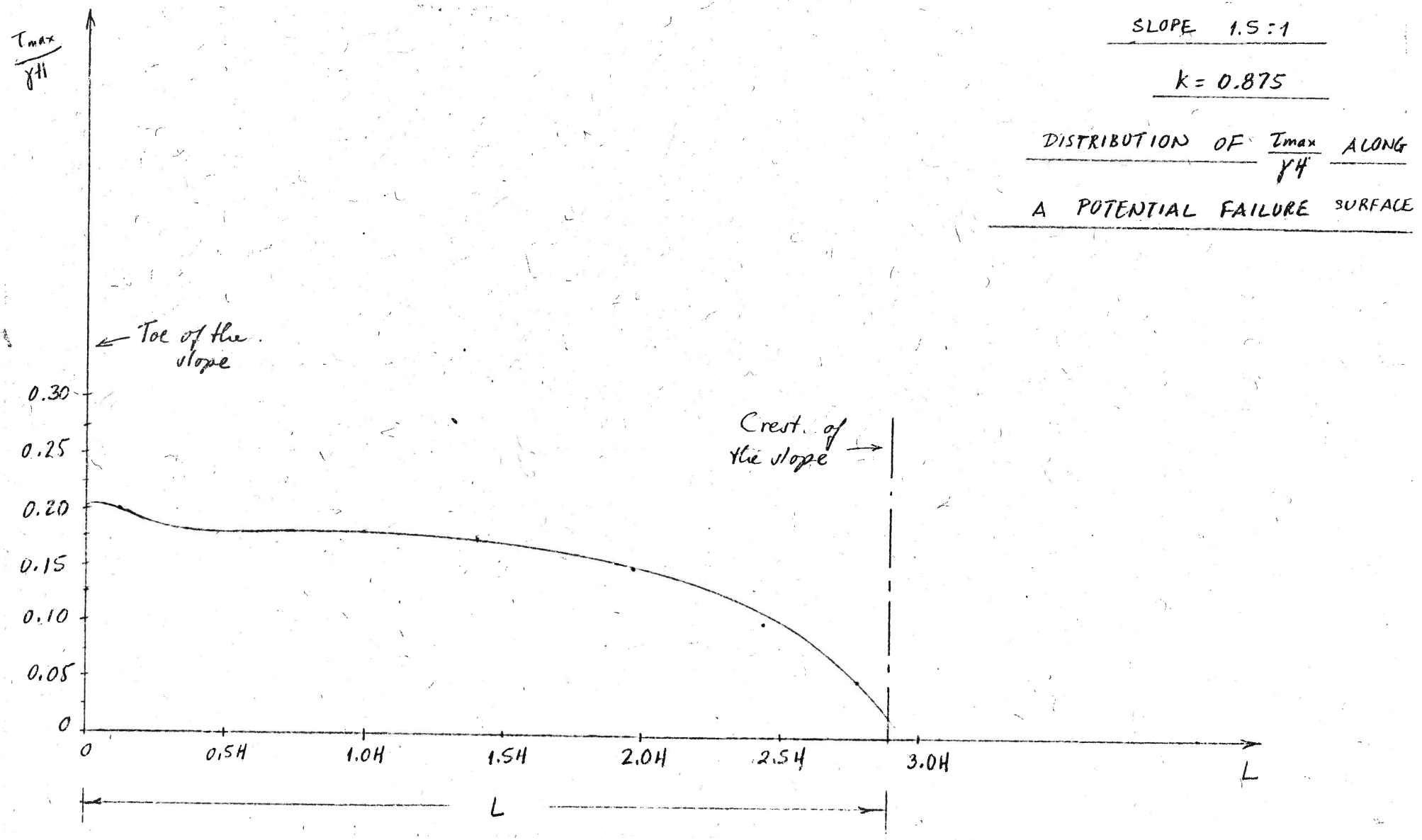


Fig. 3.4.5 (a) Distribution of $\tau_{max}/\gamma H$ along a potential failure surface.

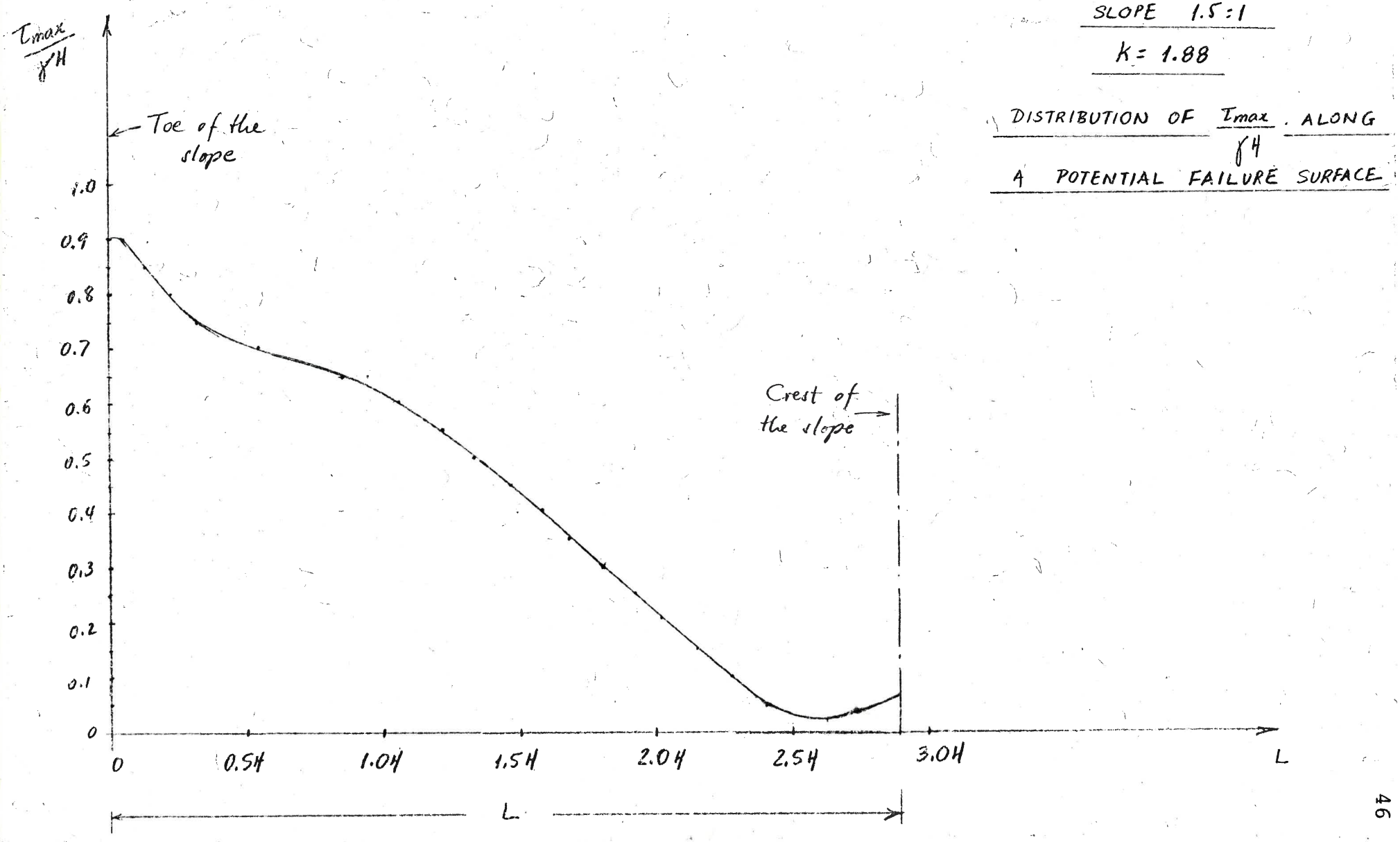


Fig. 3.4.5 (b) Distribution of $\tau_{max}/\gamma H$ along a potential failure surface.

been picked corresponds to a circular arc and it is not necessarily a critical one. Whether it is a critical one or not will depend on the strength of the soil and the ground water conditions. The selected surface serves nevertheless the purpose of this example. If some strength parameters for the soil are now picked, the ratios τ_p/σ'_n and τ_{res}/σ'_n can be plotted on the same graph, where τ_p and τ_{res} are the peak and residual shear strengths for the soil selected and σ'_n is the effective normal stress on the potential failure surface. The following strength and geometric parameters have been used in this example:

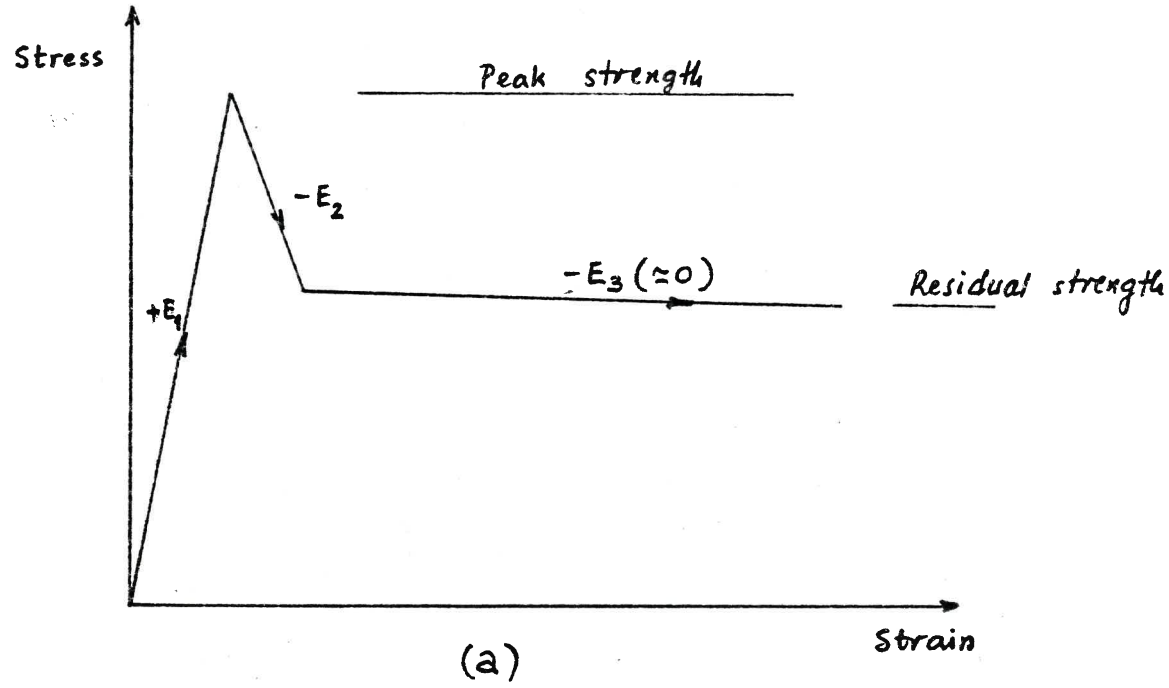
$\varphi'_p = 14°$

$\varphi'_{res} = 9°$

$\frac{c'}{\gamma H} = 0.1$ (γ is the unit weight of the soil; H is the height of the excavation).

The ground water table has also been assumed to be deep and doesn't affect the stability of the slope. Fig. 3.4.4 (a) and (b) shows the distribution of τ_p/σ'_n and τ_{res}/σ'_n along the above-selected circular arc. Two things can be immediately observed. First, the stress ratio τ/σ'_n has a much more intensive variation along the circular arc for the K = 1.88 case (which corresponds to a rather highly O.C. clay) than for the K = 0.875 case (which corresponds to a rather lightly O.C. clay); for the latter case, the τ_p/σ'_n distribution is almost constant, except for the upper portion of the arc. Second, the shear stress (τ/σ'_n) and peak shear strength (τ_p/σ'_n) distributions are almost parallel for

the K = 0.875 case. This means that the peak shear strength will be mobilized almost simultaneously along the failure surface at the point of limiting equilibrium in this case. For the K = 1.88 case, however, the shear stresses (τ / σ'_n) at the region of the toe of the slope are considerably higher than the peak shear strength (τ_p / σ'_n). This means that the soil will come over the peak at the region of the toe of the slope for as long a length along the arc as 9.825H, or 29% of the total length of the arc. This is more than enough to initiate the progressive failure mechanism, described earlier. However, with the present information in hand, we cannot really tell whether the progressive failure in this case will lead to complete failure of the slope or to an equilibrium condition. To be able to answer this question, one would have to perform a finite element analysis of the stress distribution in a strain-softening material (Bishop, 1971). Such analyses have been performed by Lo and Lee (1973), who have developed an iterative process of stress release and transfer and have assumed a stress-strain curve for strain softening materials like the one shown in Fig. 3.4.6 (a), which consists of three linear portions. Dunlop and Duncan (1970) have also analyzed the problem of the development of failure around excavated slopes, using a finite element program which is capable of handling bilinear materials with stress-



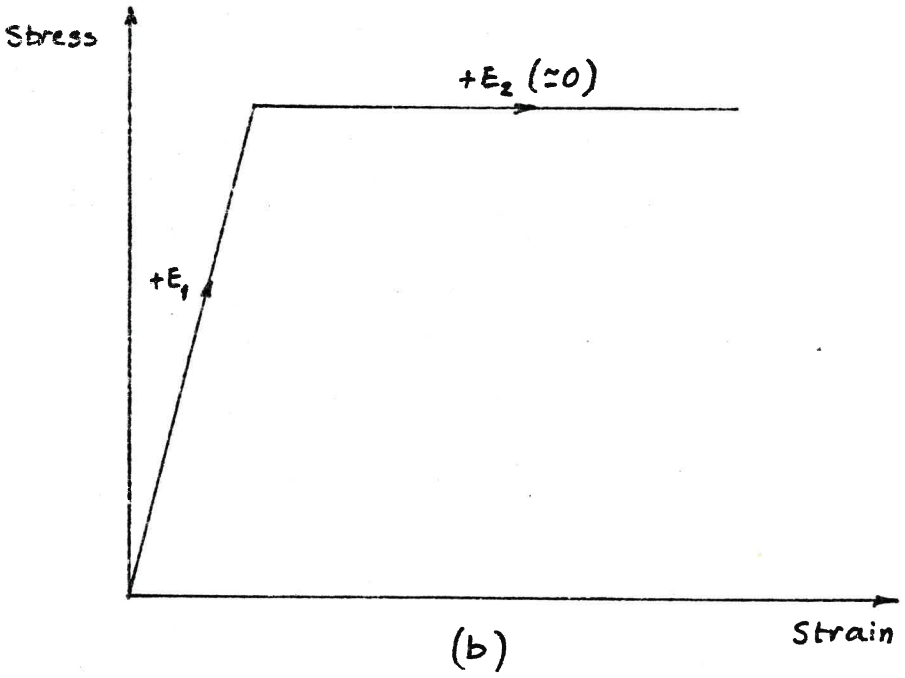


Fig. 3.4.6 Analytical models for soils: (a) Strain-softening material; (b) Elastoplastic material.

strain curves like the one shown in Fig. 3.4.6 (b). Whatever the case, this example shows clearly that the potential for progressive failure increases with increasing overconsolidation ratio (OCR) of the clay and also that progressive failure is more likely to start near the toe of the slope, for drained conditions. Notice that if the geometry of the slope, ground water conditions or strength of the clay had been different, the picture would have changed considerably for the same initial stress conditions in the ground before excavation. In general, the steeper and higher the slope and the shallower the ground water table, the higher the potential of the progressive failure mechanism to lead to complete failure of the slope. It is a matter of interest to note that a stability analysis was made for the aforementioned circular arc, using Bishop's modified method of slices. This analysis gave a factor of safety (F.S.) of 1.34. The strength parameters used were the ones mentioned previously ($\varphi'_p = 14°$, $c'/\gamma H = 0.10$). This result stresses further the point made earlier, namely that progressive failure leads to an actual factor of safety which is lower than the one calculated based on the assumption that the peak strength is reached simultaneously at every point along the failure surface (i.e., that the average operative strength at the point of limiting equilibrium is the peak). Indeed, although the computed factor

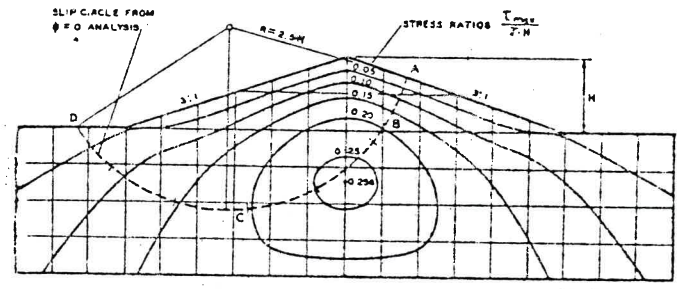
of safety is 1.34, 29% of the length of the potential failure surface, for the K = 1.88 case, will come over the peak, this leading to progressive failure, which will result either to complete failure of the slope, or to a considerable lowering of the average operative strength (and of the actual factor of safety) along this surface.

The above conclusions were drawn for the case of drained conditions for which the comparison of τ_p / σ'_n to τ / σ'_n is relevant. For the case of a short-term failure, as for example an end of construction slide, where undrained conditions prevail, we would have to compare the undrained shear strength (S_u) of the clay against τ_{max}, which has been plotted in Fig. 3.4.5 (a) and (b) for the two cases of K = 0.875 and K = 1.88. From this figure we can see again that the zone of overstress is at the region of the toe of the slope for the K = 1.88 case. Notice however that, for highly overconsolidated clays, the long-term stability is more critical than the short-term, as the pore pressure changes that develop during excavation are negative.

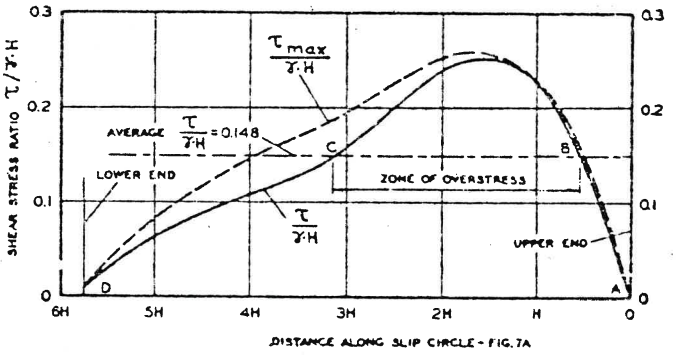
An analysis similar to the above has been performed by Bishop (1967) for the case of an embankment, using the finite differences and relaxation method. He concludes that in the case of an embankment, progressive failure is more likely to start both at the lower and upper ends of

a potential failure surface and then progress towards the middle, for drained conditions. His conclusion for undrained conditions is that progressive failure would most likely start at the middle of the potential failure surface and then progress towards the boundaries. Fig. 3.4.7 and 3.4.8 show Bishop's results for the cases of drained and undrained conditions respectively.

Lo and Lee (1973) have performed a finite element analysis of the stresses behind a slope for a strain-softening material, as mentioned previously. They conclude that for O.C. clays failure starts at the toe of the slope and propagates towards the interior and upslope. They also conclude that for given ground water conditions and strength parameters, the size of the post-peak zone increases with slope height, slope angle and the value of the coefficient of earth pressure at rest (K_o). Three examples of their analysis are shown in Fig. 3.4.9. The soil properties, elastic constants, slope geometry, and ground water conditions they have used in their analyses are shown on the same figure. The shear stress level, λ, is defined as the ratio of shear stress to peak shear strength for elements in which the peak strength is not exceeded, and it is the ratio of shear stress to residual shear strength for elements which have failed. The fact that no contours with λ greater than 1.0 are shown on Fig. 3.4.9 indicates that the second linear



(a)



(b)

Fig. 3.4.7 (a) Contours of maximum shear stresses in a uniform embankment and foundation (after Bishop, 1967).

(b) Shear stresses along a slip circle in an embankment (after Bishop, 1967).

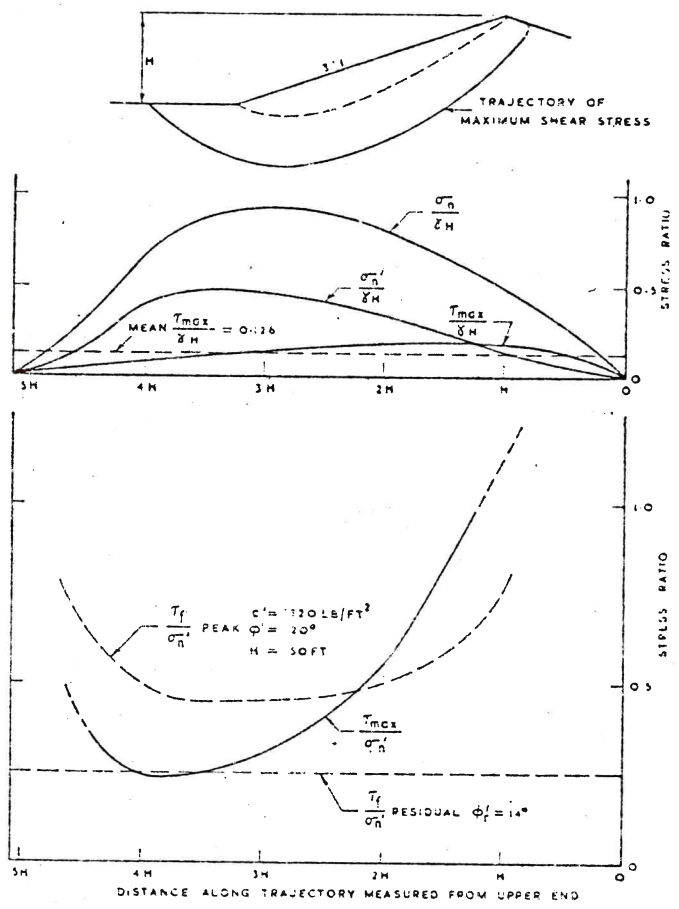
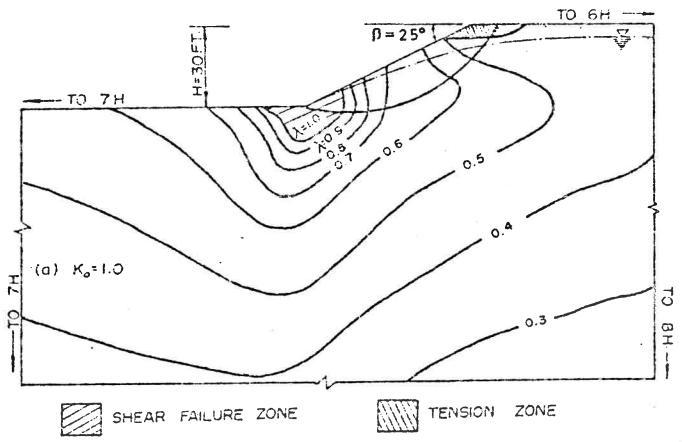
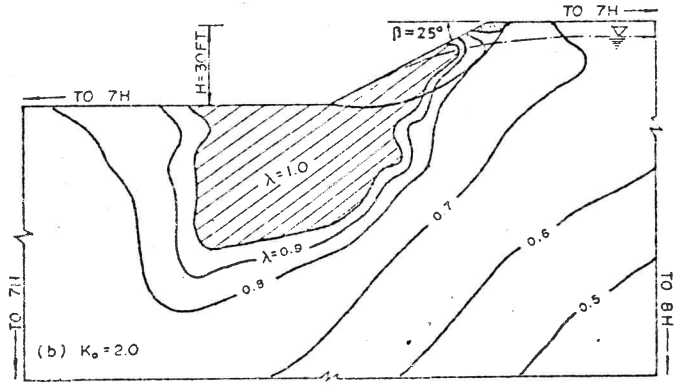


Fig. 3.4.8 Distribution of stresses and stress ratios along a trajectory of maximum shear stress for a pore pressure ratio r_u (= $u/\gamma h$) of 0.5 (from relaxation solution by A. W. Bishop, 1952).





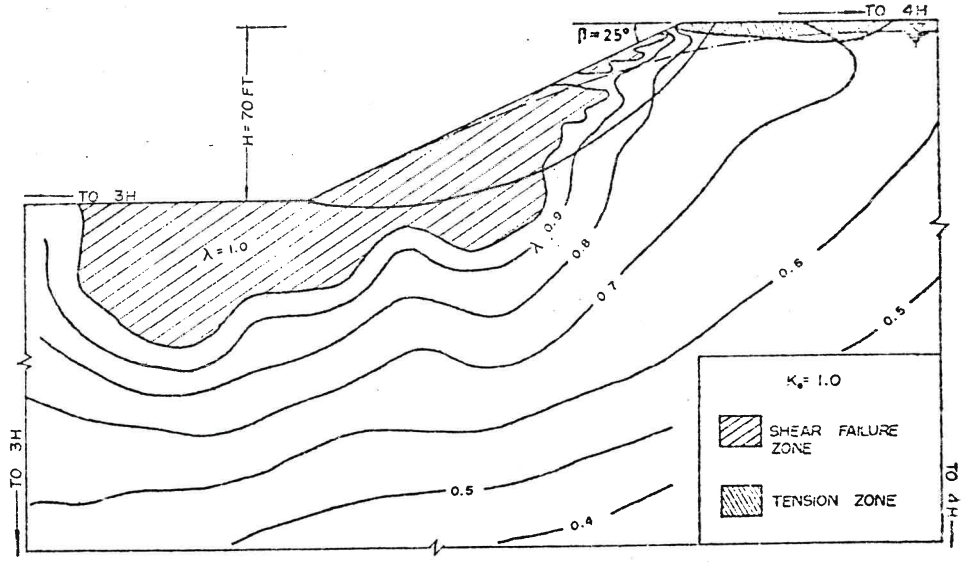


Fig. 3.4.9 Contours of stress level, λ, from a finite element analysis applied on strain-softening materials (from Lo & Lee, 1973).

portion of the stress-strain curve that they have used for their analysis (refer also to Fig. 3.4.6 (a)) has been taken to be practically vertical, i.e., they assume that the strength drops immediately from the peak to the residual.

All of the foregoing discussion, which is related to the area of progressive failure initiation, leads to the conclusion that progressive failure starts from the toe of a slope and progresses inwards and upslope for highly overconslidated clays. Bjerrum (1966) has proposed a somewhat different progressive failure mechanism, which is based on the recoverable strain energy of the highly O.C., plastic clays and clay shales, and which will be briefly described below. He has also illustrated the type of non-uniformity of stress and strain to be expected at the toe of a cut due to expansion as a consequence of high lateral stresses in the ground and he has also indicated that progressive failure starts at the toe and progresses inwards behind the slope.

According to Bjerrum (1966), it can be taken for granted that, under certain conditions, slides in O.C. plastic clays and clay shales are preceded by the development of a continuous failure surface by a mechanism of progressive failure. He has postulated a possible mechanism, which can explain how progressive failure can occur and how it can lead to the development of a continous sliding

surface. To illustrate in a brief and general way the principles of this mechanism, consider the stability of a small section of a uniform stable slope of inclination α, as shown in Fig. 3.4.10 (a). Further, consider the equilibrium of a section OAA'O'. The shear stress along OA due to the gravity force is:

$$\tau = \frac{[(\gamma z).[(OA).\cos\alpha]].\sin\alpha}{(OA)} = \gamma z \sin\alpha.\cos\alpha \quad (1)$$

where z is the depth of surface OA from the ground surface. If we assume that the boundary O'O has been formed by excavation, then the removal of the lateral support of block OAA'O' on O'O by excavation produces a redistribution of the internal stresses within this block. Provided that AA' is so far from OO' that the lateral stress on AA' has remained unaltered, the equilibrium of the block can only be maintained if the shear force along OA increases by the amount E, the total lateral earth pressure that acted on OO' before excavation:

$$E = \int_0^A \tau_E . dl \quad (2)$$

where τ_E is the shear stress distribution along OA due to the removal, by excavation, of the lateral support of block OAA'O' on OO'. This distribution is non-uniform, it will have its maximum at point O and it is approximately shown in Fig. 3.4.10 (b). The shear stress at point O now becomes:

$$\tau_o = \gamma z . \sin\alpha . \cos\alpha + (\tau_E)_{max} \quad (3)$$

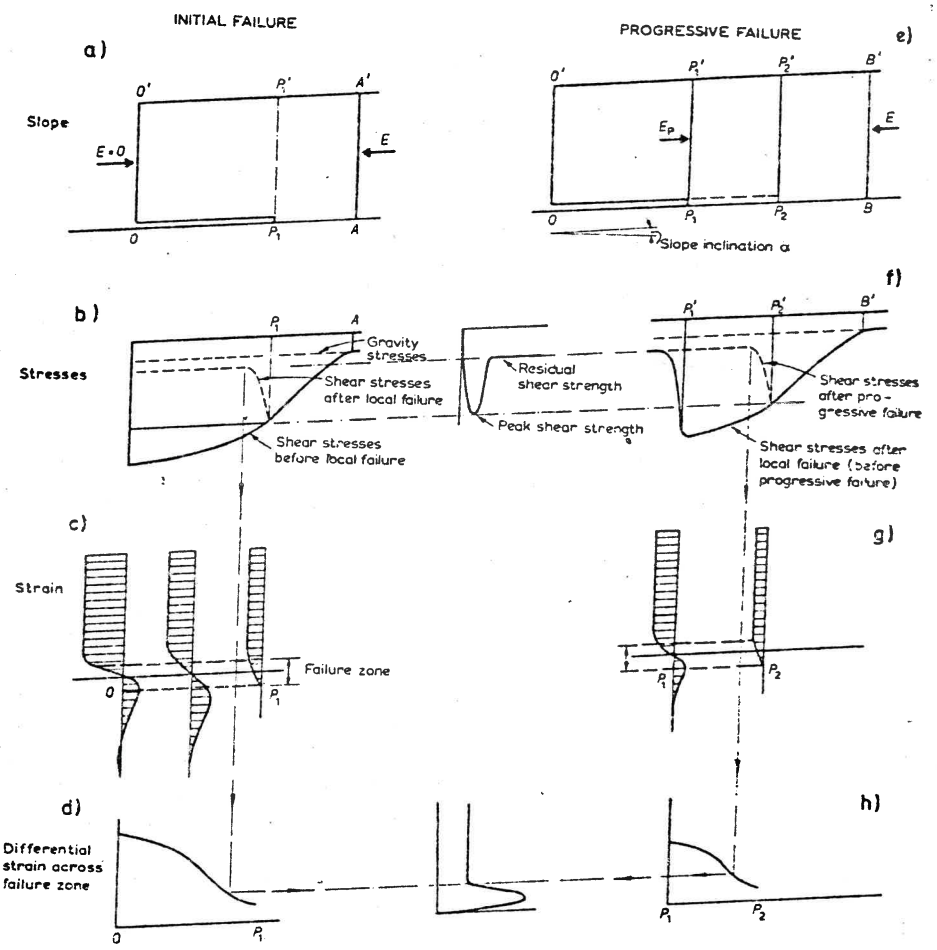


Fig. 3.4.10 Principle of development of continuous sliding surface by progressive failure (from Bjerrum, 1966).

If τ_o is greater than the peak strength of the clay, then local shear failure will occur. It will start at point O and it will proceed as far as the shear stresses exceed the peak strength. In Fig. 3.4.10 (b), for instance, the local failure will occur as far as P_1. Note that $(\tau_E)_{max}$ is proportional to E, i.e., the higher the internal lateral pressure E the higher the value of $(\tau_E)_{max}$ and consequently the further local failure will occur. The occurrence of a shear failure at the base of the block $OO'P'_1P_1$ will in the first place mean a reduction of the shear stresses on OP_1 from the theoretical value expressed above to the peak shear strength. Correspondingly, the internal lateral stresses in the block of clay $OO'P'_1P_1$ will decrease. Due to the elastic behavior of the clay, this lateral unloading will cause the clay to expand towards the excavation by sliding on the newly formed failure plane OP_1 (Fig. 3.4.10 (c)). The resulting differential strain (Fig. 3.4.10 (b)) across the failure zone is governed by the recoverable strain energy of the clay, and if this is large enough, the strain will be sufficient to reduce the shear strength from the peak to the residual value. This will cause a large reduction of the shear stresses along OP_1 and a corresponding increase of the shear stresses on the surface to the right of P_1. Next we consider the equilibrium of the block $P_1BB'P'_1$, where section BB' is so far from $P_1P'_1$ that the lateral stresses on BB' are unaffected by what has happened

to the left of point P_1 (Fig. 3.4.10 (e)). With considerations similar to the ones made previously, it is concluded that the maximum shear stress will now be at P_1 and it will be equal to:

$$\tau_{P_1} = \gamma z.\cos\alpha \cdot \sin\alpha + (\tau_{E-E_P})_{max} \quad (4)$$

where $(\tau_{E-E_P})_{max}$ is the maximum value of the new shear stress distribution produced to the right of P_1 in order to resist the lateral force $(E-E_p)$, where E is as defined previously (it now acts on BB') and E_P is the value that the lateral force E has reduced to on $P_1P'_1$ after failure occurred along OP_1. Obviously, the larger and more abrupt the drop in strength from peak to residual, the lower the value of E_P will be and consequently the larger the value of $(E-E_P)$ and, as $(\tau_{E-E_P})_{max}$ is proportional to $(E-E_P)$, the larger the value of $(\tau_{E-E_P})_{max}$ will be. If the value of τ_{P_1}, as defined by (4), is higher than the peak shear strength of the clay, local failure will occur along a certain distance to the right of P_1 and progressive failure will continue upslope as described previously. Depending on the inclination of the slope and on the relative magnitude of E and E_P in each step, the process will either lead to the formation of a continuous failure surface and eventual sliding of the slope or the value of E_P will eventually be large enough that progressive failure will come to a halt.

Based on the above mechanism, Bjerrum (1966) has specified some requisite conditions for progressive failure:

—Firstly, in order to start a progressive failure leading to the development of a continuous failure surface, there must be a discontinuity somewhere in the clay mass, or at its boundary, where failure can be initiated and the deformations required for a further development can be produced. This discontinuity may be a steep erosion slope or a cut at the toe of a slope, or it might be a soft spot somewhere in a slope.

—The development of a continuous failure surface by progressive failure is only possible if there exist, or can develop, local shear stresses exceeding the peak shear strength of the clay. All other conditions being equal, the danger of local shear failure will increase with the ratio of the lateral internal stress to the peak shear strength.

—The advance of a failure surface must be accompanied by local differential strain in the zone of shear failure sufficient to strain the clay beyond failure. The ratio of the lateral strain, due to stored recoverable strain energy in the clay, to the failure strain is a measure of the degree to which the former will

exceed the latter, when the lateral stresses are reduced.

—The clay must show a large and rapid decrease in shear strength with strain after the failure strength has been mobilized, so that the shear resistance in the failure zone will not obstruct the movement required to obtain the differential strain and thus to move the zone of stress concentration into the neighboring zone of unfailed clay. The ratio of peak to residual shear strength expresses the degree of strain softening of the clay.

The previously described model of progressive failure, although it is rather general and there is no proof of its validity, provides an approximate but consistent picture of the possible occurrence of progressive failure, adequate for an understanding of the problem involved and for an evaluation of the governing factors such as the soil properties.

It should be pointed out here that the model relies very much upon the recoverable strain energy of the highly O.C. plastic clays, which is released by weathering due to deterioration of the diagenetic bonds and which is responsible for bringing the clay from the peak to the residual strength. As noted early in this section, the relative displacements necessary to bring the clay from

the peak to the residual strength are of the order of 1 to 2 meters (Skempton, 1977), and it is questionable whether the above process could lead to such displacements. It can, however, lead to a considerable drop in strength from the peak to a value somewhat higher than the residual strength.

For cases where the non-uniform stresses do not exceed the peak strength of the soil anywhere along a potential failure surface, another mechanism will have to be proposed in order to be able to explain slope failures that have actually occurred in such cases. According to Skempton (1977), such a mechanism could probably be the presence of local stress concentrations at the discontinuities within the soil mass such as the fissures that are usually found in the highly O.C. plastic clays. Although the aforementioned mechanism is a necessary assumption for cases where the effective stresses after excavation do not exceed the peak strength anywhere behind a slope, that does not preclude it from contributing to the progressive failure mechanisms presented earlier in cases where the effective stresses after excavation exceed locally the peak strength of the clay.

Before this section is closed, it should be pointed out that the mechanism of the propagation of a shear surface in a fissured clay is clearly a subject deserving further

study. According to Bishop (1967), this mechanism may well prove to involve small scale stress concentrations around the end of the propagating surface of weakness and the interchange between different forms of energy. These include energy absorbed in forming the surface and released by relieving the stresses in the locally highly stressed material adjacent to it. Proneness to progressive failure may be directly associated with low tensile strength, in terms of effective stress, of the intact clay. Bishop has borrowed these concepts from the paper of Griffith (1921), "The Phenomena of Rupture and Flow in Solids."

As a closing remark, it should be mentioned that there are a number of factors which delay the full development of progressive failure. According to Bishop (1967) such factors are:

—The time lag, due to the low coefficient of swelling, in the readjustment of pore pressure resulting from (see also Skempton, 1977):

(a) the release of stress during the excavation of a slope; and

(b) due to the modification of ground water table resulting from the change in profile.

—Weathering, in relation to its effects on soil structure, with respect both to strength and to permeability (see also Bjerrum, 1966).

—The delayed release of strain energy due to time lag in the rebound curve with respect both to volume change and to shear deformation (see also Bjerrum, 1966). This would influence, for example, the spread of a crack of the Griffith type.

—The reduction in strength values, particularly at the peak, due to the rheological component of shear strength.

Consequently, although time effects are not the primary cause of the mechanism of progressive failure, as it has been described so far, the problem of progressive failure is inescapable of time.

3.5 "Fully Softened" and Critical State Strengths

As pointed out by Skempton (1970, 1977, 1978), the strength of stiff, fissured clays, as it is back-calculated from first-time slides, is neither the peak shear strength as measured by consolidated-drained triaxial tests, nor the residual strength as measured by various methods (ring shear apparatus, multiple reversal direct shear test, triaxial compression test on precut samples, etc.). He has estimated it to be closer to the "critical state" shear strength, or what he has called "fully softened" strength. As defined by Roscoe, Schofield and Wroth (1958), a saturated clay is at its critical state, in a drained test, if any further

increment in shear distortion will not result in any change in water content. For an ideal clay this occurs well after the peak and after this state is reached, the clay continues to deform under constant stress (which is the ultimate strength for this ideal clay) and at constant volume (Fig. 3.5.1). In particular, the critical state corresponds to the strength of a normally consolidated clay and, by definition (Roscoe, Schofield, Wrote, 1958), the water content at this state is equal to that attained ultimately by the overconsolidated clay due to dilatancy during shear. For real clays exhibiting sensitivity, bonding and preferred particle orientation, the behavior pattern is more complex and the determination (or even the definition) of critical state is very difficult. According to Schofield and Wroth (1968), the peak strength of a normally consolidated remolded clay occurs just before the critical state is reached. Skempton (1970) has suggested that the "fully softened" strength of an overconsolidated clay can be practically numerically approximated by the peak strength of that same clay after it has been remolded and reconsolidated (Fig. 3.5.2.). The above numerical approximation does not necessarily imply any physical correlation between the "fully softened" strength and the critical state or even the normally consolidated peak strength, although there might be one such correlation.

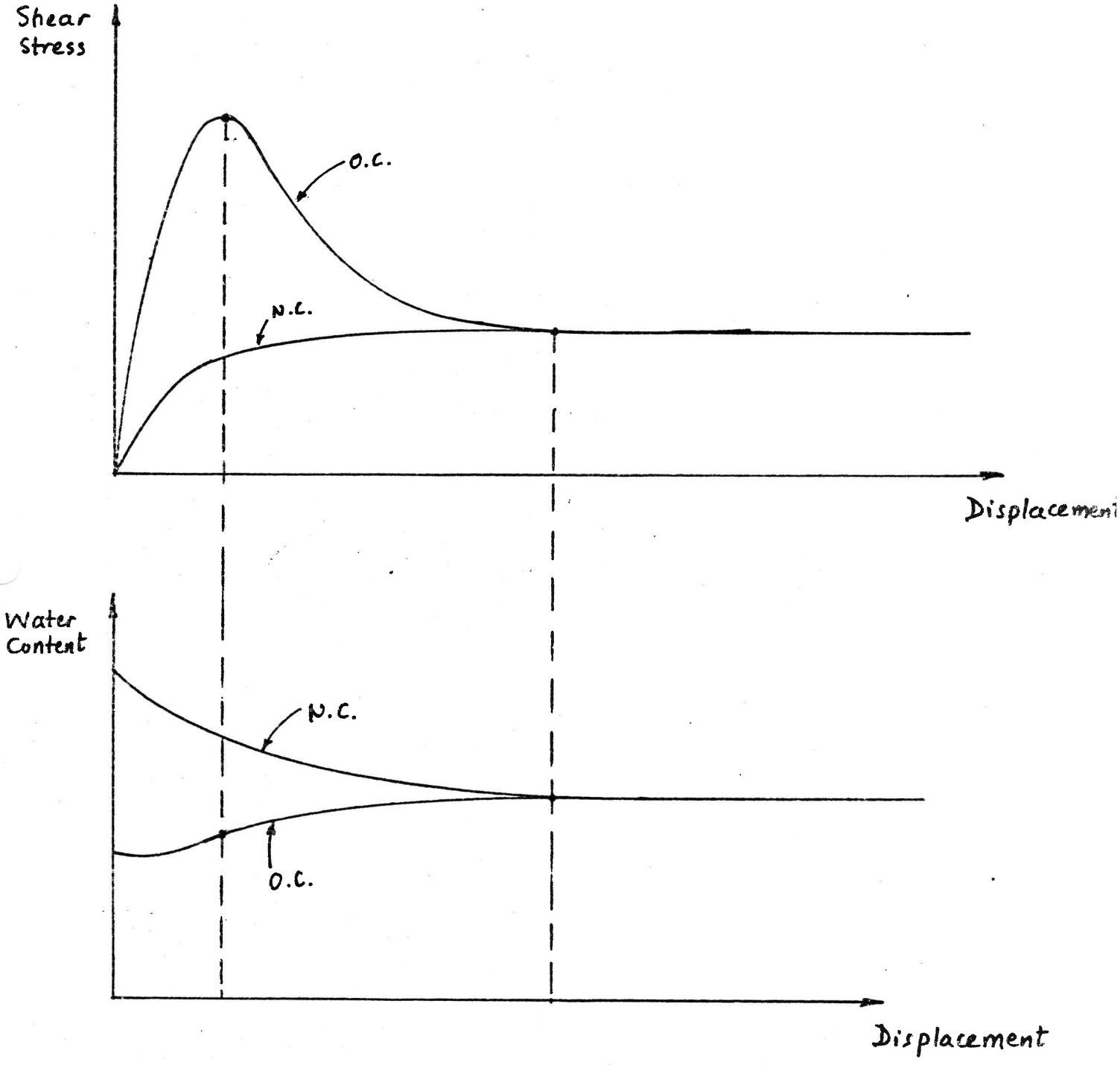


Fig. 3.5.1 Critical state in drained shear tests on ideal clay.

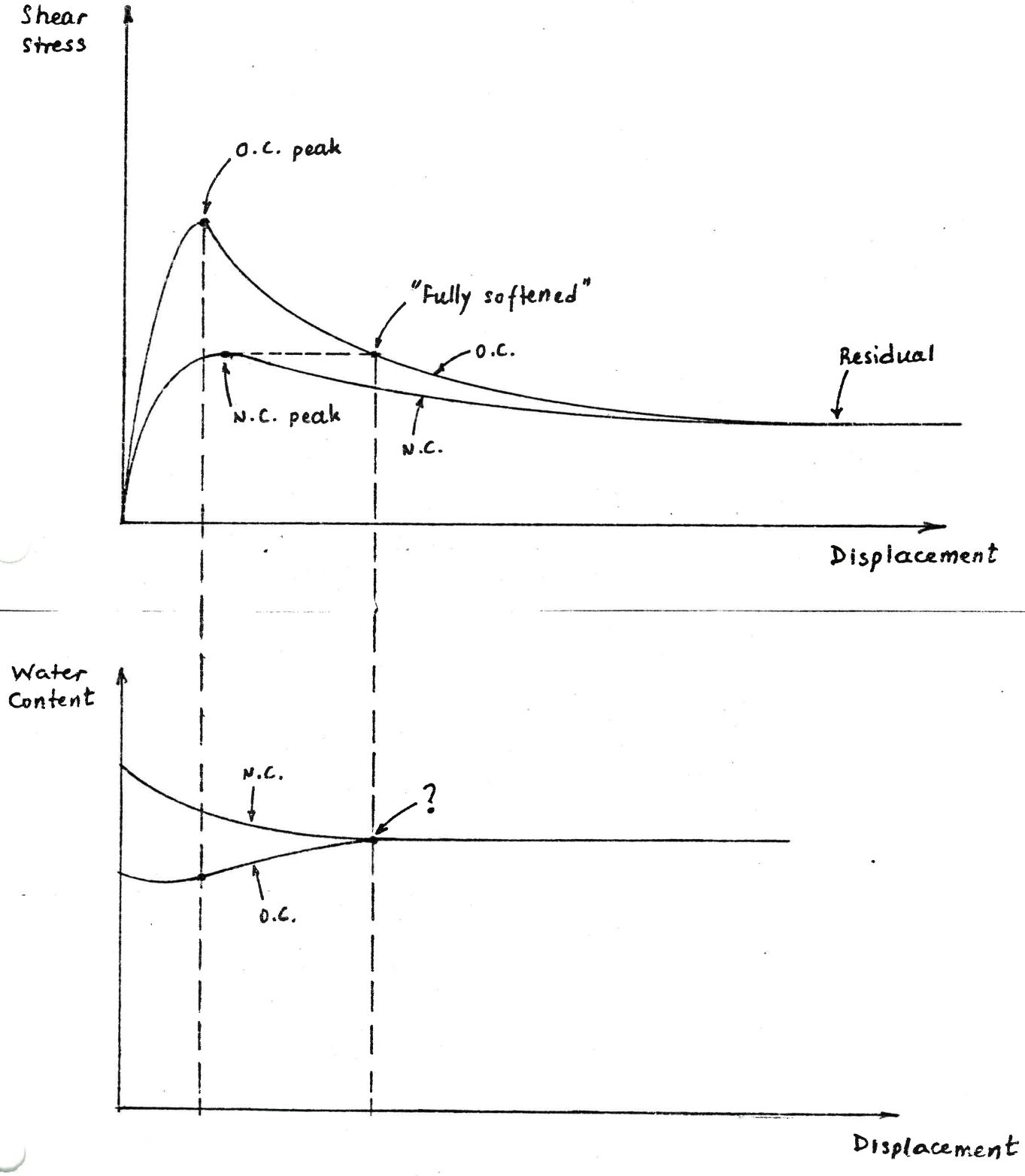


Fig. 3.5.2 Shear characteristics of real clays.

Skempton (1971) has proposed a possible mechanism for the development of the "fully softened" strength, in an attempt to correlate it to the normally consolidated peak strength of the remolded clay. He has suggested that the fissures can lead to softening of the clay mass and he refers to Terzaghi (1936), who has given an explanation for this process. Terzaghi has suggested that the lateral stress release component upon excavating a cutting could cause some fissures to open. In stiff clays, the strength is sufficient to allow a fissure to remain open at depth. Softening would then take place from the face of an open fissure, under zero effective stress. This would lead to further deformations, the opening of more fissures, etc. According to Skempton (1971), it follows (although Terzaghi did not draw this conclusion) that, unless a slip occurs, the end product of such a softening process must be a clay reduced essentially to its normally consolidated condition, for as deformation proceeds, fissures which once were open must sooner or later be closed (in order to transmit the overburden loads) and the clay which had softened under zero stress will be reconsolidated under the weight of overlying material. So, he concludes that the strength in the fully softened condition can be represented by the strength that the clay would have, under the same effective normal stress, if it were normally consolidated.

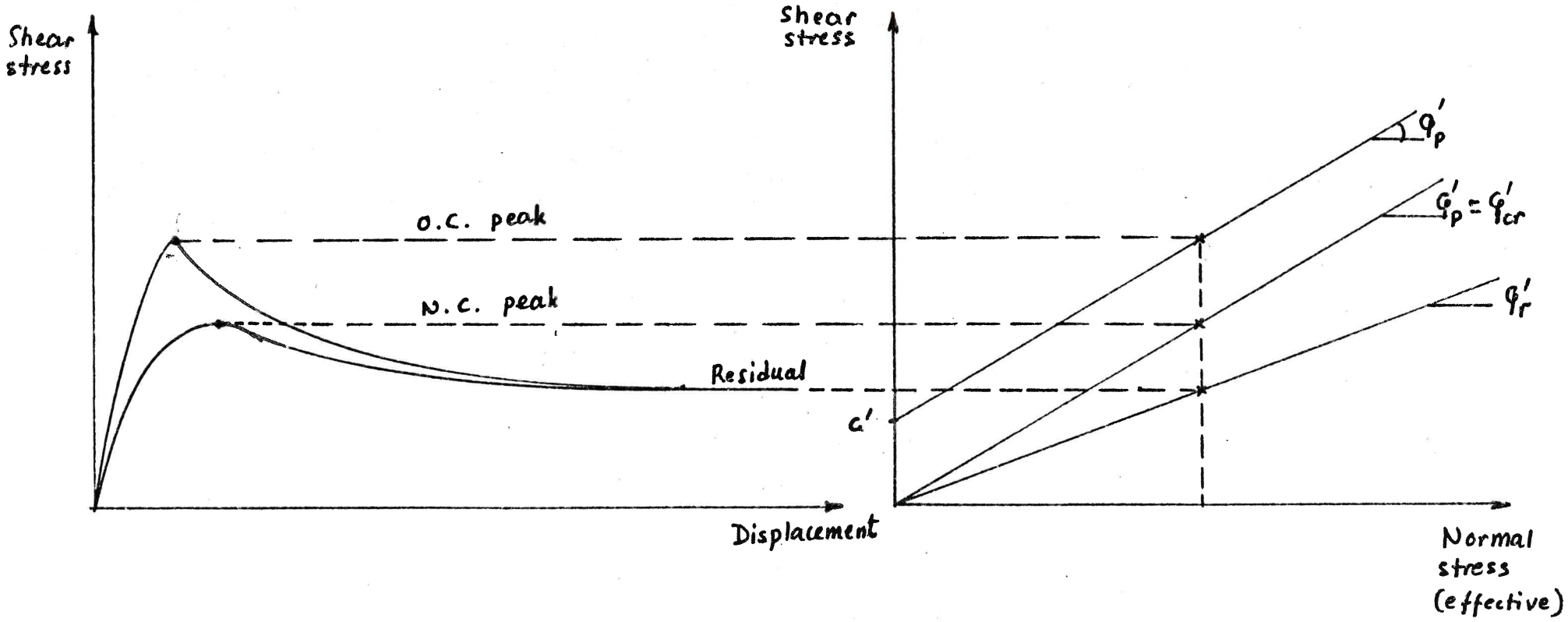


Fig. 3.5.3 Correlation of N.C. peak strength to O.C. peak and residual strengths.

Data from long-term, first-time slide backcalculation indicate a considerable decrease of the cohesion intercept, c', exhibited by the peak strength envelope, while φ' remains approximately the same. Chandler and Skempton (1974) give a possible explanation for that drop in c'. They have suggested that progressive failure permits the development of strains sufficiently large to allow full dilatancy, accompanied by water content increase in the shear zone, resulting in a "fully softened" condition (see also Fig. 3.5.3).

It should be pointed out, once again, that until a physical correlation is found between the strength of overconsolidated, stiff, fissured clays for first-time slides ("fully softened" strength) and the peak strength of the normally consolidated clay or the critical state strength, one should not make the generalized assumption that the operative strength for first-time slides in stiff, fissured clays and shales is the critical state or normally consolidated strength.

3.6 Summary

The peak strength of an overconsolidated, stiff, fissured clay depends on its geologic history (depositional environment, stress history, diagenesis, weathering, etc.) and on its structure (fissures, joints, slickensides, microscopic discontinuous shear planes, etc.).

The residual strength of a clay is the strength ultimately attained in a drained shear test, after a considerable amount of deformation. Shearing at the residual state is a constant volume process. The residual strength depends on the amount and composition of the clay, Atterberg limits, adsorbed cations for a given type of clay, salt concentration in the pore fluid and stress level. Residual strength controls the stability of slopes that have already slid in the past.

Progressive failure can lead to a considerable lowering of the average operative strength along a potential failure plane, for soils that exhibit a considerable and abrupt drop in strength from the peak to the residual. Other factors that promote progressive failure are:

—High lateral earth pressures (i.e., high K_o)

—High recoverable strain energy

—Fissures or other discontinuities in the clay mass.

Most overconsolidated, stiff, fissured clays exhibit a strength, in first-time slides, which has a value between the peak and the residual. This strength has been called "fully softened" strength and it has been hypothesized that due to dilatancy and increase of water content in the zone of shear, the clay softens and approaches the peak strength it would exhibit if it were normally consolidated. It has been suggested that the critical state or the normally

consolidated peak strength can be used as a good approximation of the "fully softened strength." Progressive failure may play an important role in the mechanism of softening.

4. APPROACH TO THE PROBLEM

4.1 General

So far, the slope stability problems in the Friars Formation have been described in Chapter 1, and some geological and geotechnical information about the Friars Formation have been given in Chapter 2. In Chapter 3 the concept of shear strength for stiff, fissured clays and shales and the factors it depends on, as related to the long-term stability of slopes in such soils was examined. Having formed this background about the Friars Formation in particular and about the stiff, fissured clays and shales in general (to which category Friars Formation belongs), we are now ready to examine an approach to the problem of stability of slopes not only in stiff, fissured clays and shales but in any kind of soil. This approach is the stress path method, which was first presented and subsequently improved and supplemented by case histories by Lambe (1967, 1969, 1973, 1979). The principles of this method are presented in the following Section 4.2. It was decided to adopt this method for laboratory testing and analysis and then compare the results obtained using this approach to those obtained by using conventional methods for laboratory testing and analysis. In this way, it was hoped to isolate any discrepancies between actual and predicted behavior, which may occur as a result of the method that has been

used to approach the problem, both analytically and in the laboratory.

After the principles of the stress path method will have been presented in this chapter, Chapter 5, and part of Chapter 6, will be devoted to the actual use of this method. The approach taken will be rather general so that, at the end, the conclusions drawn will be applicable not only for the case of the Friars Formation, but, in general, for any excavated slope in plastic, overconsolidated clays.

4.2 The "Stress Path" Approach

As suggested by Lambe (1967, 1969, 1973, 1979), a rational approach to force, deformation, stability and flow problems is the stress path method. Because soil properties and behavior are stress path dependent, it is important that the actual stress path is recognized and correctly followed in the laboratory, so that the results obtained represent the actual behavior of the soil under the given history and variation of stress. The stress path method employs the point where the shear stress has its maximum value, e.g., point A of Fig. 4.2.1 (a). The stress path is drawn on a p vs. q diagram where $p = \frac{\sigma_1 + \sigma_3}{2}$ and $q = \frac{\sigma_1 - \sigma_3}{2}$ (Fig. 4.2.1 (b)). Sometimes p and q are expressed in terms of σ_v and σ_h, the vertical and horizontal stresses respectively at a point in the ground. If the principal stress directions coincide

with the vertical and horizontal, then p and q are expressed as $p = \frac{\sigma_v + \sigma_h}{2}$, $q = \frac{\sigma_v - \sigma_h}{2}$ (Fig. 4.2.1 (c)). By convention, q has a positive value when $\sigma_v > \sigma_h$ and a negative value when $\sigma_h > \sigma_v$. In the case that the principal stress directions do not coincide with the vertical and horizontal, the stress path can still be used with p and q expressed as functions of σ_v and σ_h. In this case p and q are given by:

$$p = \frac{\sigma_v + \sigma_h}{2} \qquad \text{and} \qquad q = \sqrt{\left(\frac{\sigma_v - \sigma_h}{2}\right)^2 + \tau_{vh}^2} \ ,$$

where τ_{vh} is the shear stress on vertical and horizontal planes (Fig. 4.2.1 (d)). Notice that in the latter case it is not obvious what the sign of q should be, since the term $(\sigma_v - \sigma_h)$ is raised to the second power. According to the previously stated sign convention q will be taken negative when $\sigma_h > \sigma_v$. If only the magnitudes and directions of the principal stresses are known, then the above statement can be restated as follows (the following relationships are derived in Fig. 4.2.2):

$$p = \frac{\sigma_1 + \sigma_3}{2}$$

$$q = \frac{\sigma_1 - \sigma_3}{2} \quad , \text{ if } 0 \leq \theta \leq 45°$$

$$q = -\frac{\sigma_1 - \sigma_3}{2} \quad , \text{ if } 45° \leq \theta \leq 90°$$

where θ is the angle between σ_h and σ_1.

The stress path can be either drawn for effective stresses or for total stresses. In the former case, p and q

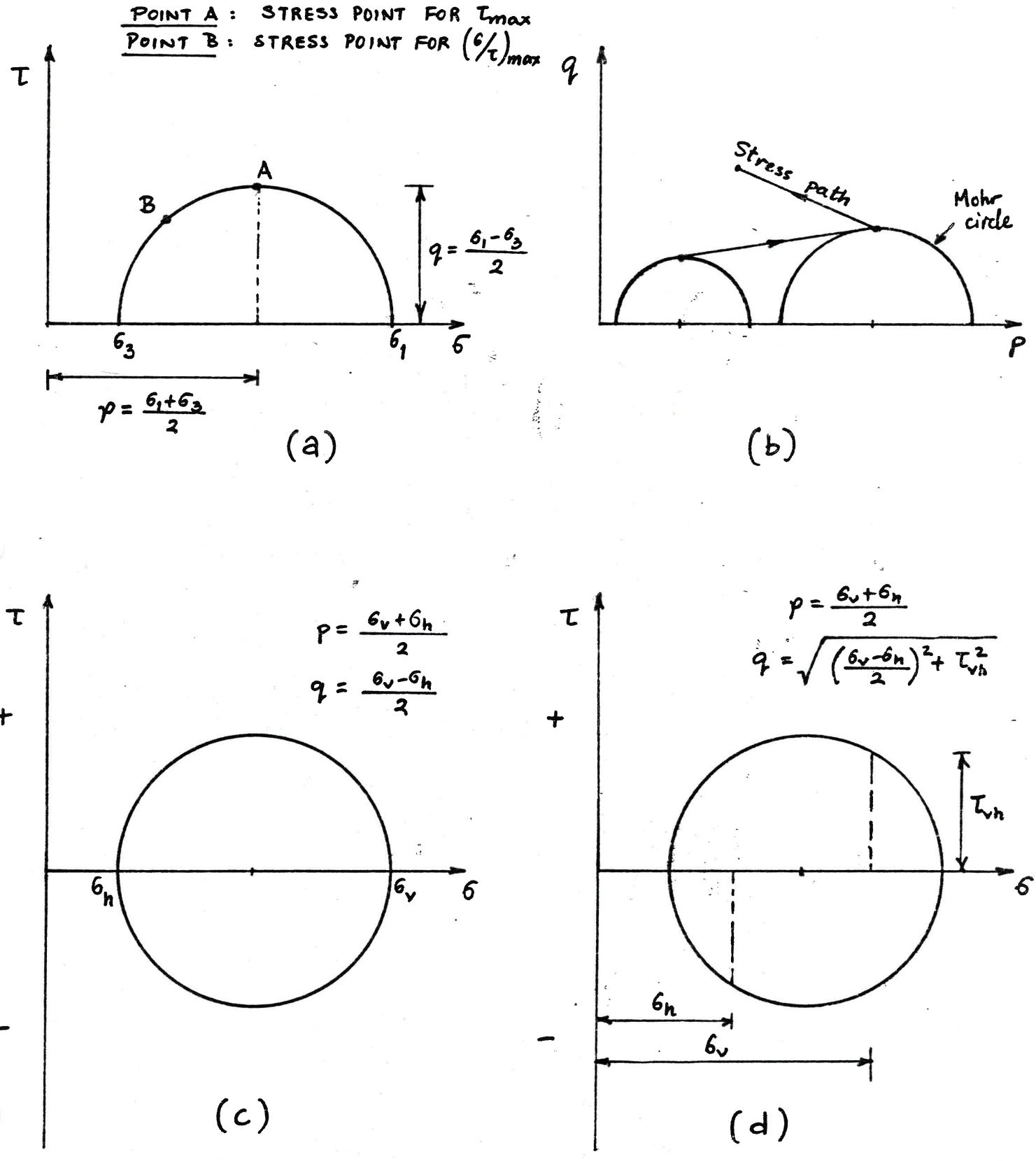
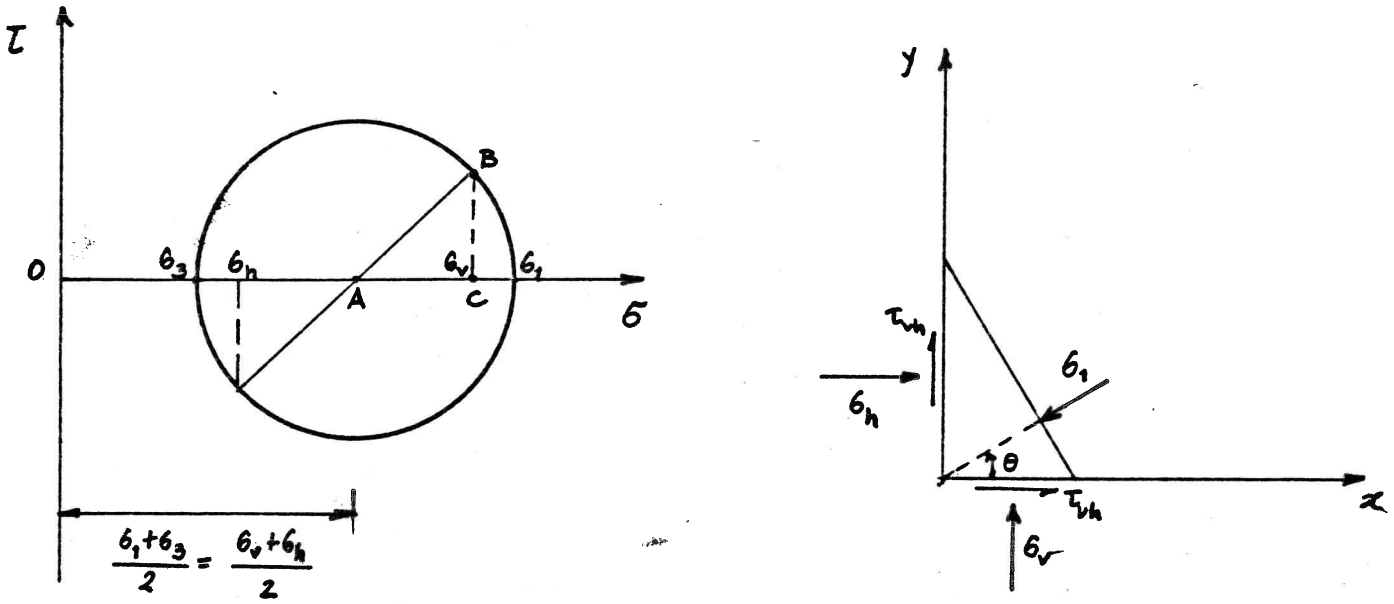


Fig. 4.2.1 Definition of stress path.



From fig. (a) above it is obvious that :

$$OA = \frac{\sigma_1+\sigma_3}{2} = \frac{\sigma_v+\sigma_h}{2} = p \quad (1)$$

From triangle ABC : $(AB)^2 = (AC)^2 + (BC)^2 \rightarrow$

$$\rightarrow \left(\frac{\sigma_1-\sigma_3}{2}\right)^2 = \left(\sigma_v - \frac{\sigma_v+\sigma_h}{2}\right)^2 + \tau_{vh}^2 = \left(\frac{\sigma_v-\sigma_h}{2}\right)^2 + \tau_{vh}^2 -$$

$$\rightarrow \frac{\sigma_1-\sigma_3}{2} = \sqrt{\left(\frac{\sigma_v-\sigma_h}{2}\right)^2 + \tau_{vh}^2} = q \quad (2)$$

If θ is the angle between the horizontal & the major principal stre direction , then from the theory of elasticity (refer also to fig. (b))

$$\sigma_h = \sigma_3 \sin^2\theta + \sigma_1 \cos^2\theta \quad (3)$$

$$\sigma_v = \sigma_3 \cos^2\theta + \sigma_1 \sin^2\theta \quad (4)$$

$$(3),(4) \rightarrow \sigma_v - \sigma_h = (\sigma_1-\sigma_3)\sin^2\theta - (\sigma_1-\sigma_3)\cos^2\theta = (\sigma_1-\sigma_3)(\sin^2\theta-\cos^2\theta) \rightarrow$$

$$\rightarrow \sigma_v - \sigma_h = -(\sigma_1-\sigma_3)\cos 2\theta \quad (5)$$

If $0^\circ \le \theta \le 45^\circ \rightarrow \cos 2\theta \ge 0 \rightarrow \sigma_v - \sigma_h \le 0 \rightarrow q \le 0$

If $45^\circ \le \theta \le 90^\circ \rightarrow \cos 2\theta \le 0 \rightarrow \sigma_v - \sigma_h \ge 0 \rightarrow q \ge 0$

Fig. 4.2.2

are:

$$\bar{p} = \frac{\sigma_1' + \sigma_3'}{2} \qquad \text{and} \qquad \bar{q} = \frac{\sigma_1' - \sigma_3'}{2} = \frac{\sigma_1 - \sigma_3}{2}$$

while in the latter case:

$$p = \frac{\sigma_1 + \sigma_3}{2} \qquad \text{and} \qquad q = \frac{\sigma_1 - \sigma_3}{2} \quad .$$

The stress path for the former case is called effective stress path (ESP) while for the latter it is called total stress path (TSP).

It should be mentioned that the stress path method ignores the intermediate principal stress σ_2 . This is justified by the fact that most conventional tests cannot control σ_2 independently of σ_1 and σ_3 and also because usually σ_2 has only a small effect on the strength and stress-strain behavior of soils (Lambe, 1979).

The stress path method consists basically of six steps:

1. Estimate the nature of the problem, i.e., select a "mechanism" for the problem in hand, based upon experience, publications on similar problems, etc.
2. Select one or more representative soil elements for study, based upon experience and available literature.
3. Estimate the stress history, state of stress before construction and variation of stress and strain during and after construction of the soil element(s) selected in step 2.

The above estimates are based upon:

—The geologic history of the site.

—Soil properties, determined by soil tests.

—In situ pore pressure measurements before, during and after construction.

—The known loads that are going to be applied by the structure on the ground.

—Some kind of analytical technique to determine the stress redistribution in the ground imposed by the known loads, during and after construction.

Using the aforementioned estimates, prepare the stress paths for the selected soil element(s).

4. Perform laboratory tests on soil samples, along the stress paths prepared in the previous step. The soil samples can be either undisturbed samples from locations close to the ones of the selected soil elements or they can be reconstituted samples. The latter are obtained by either remolding undisturbed samples or by resedimenting soil samples and then subjecting them to stresses along a stress path approximating that of the geologic history of the elements in the field. Notice that neither obtaining undisturbed samples nor reconstituting samples avoids disturbing the structure developed during the geologic history of the sample. Field tests can also be performed at this step, if one wishes to minimize disturbance, or to apply full scale loads.

5. Use the results of the stress path tests performed in the previous step to obtain soil parameters needed for predicting performance.
6. Use the soil parameters obtained in the previous step to predict performance (e.g., find the factor of safety in the case of a stability problem). However, if a more refined solution is desired, the results of step 6 can be used in step 1 for the selection of a more accurate "mechanism" for the problem and then proceed again through steps 2 - 6.

4.3 Summary

The stress path method consists of a systematic approach to elucidating and solving geotechnical engineering problems. The method organizes, states and extends principles of geotechnical engineering developed and applied over a number of years. Experimental evidence clearly shows that soil behavior depends very much on stress, orientation of stress on the soil sample, time, temperature, chemical factors, etc. The stress path method recognizes this important fact and attempts to test soils under conditions closely approximating field conditions. The method can be used to solve force, deformation, stability and flow problems. For stability problems in particular, the method consists of the following six steps:

1. Estimate location of the surface of minimum stability.
2. Select an average element or select several elements.
3. For selected element(s), determine stress paths for:
   (a) geological history, i.e., past; and
   (b) design life of structure, i.e., future.
4. On soil existing at or near selected elements in field situation, run tests along stress paths determined in step 3; orient samples for tests same as in the field.
5. Obtain strength or strength parameters.
6. Determine the factor of safety as the ratio of average strength to average shear stress along the surface of minimum stability determined in step 1. Obtain average shear stress using one or more of the following methods:
   —Force polygon.
   —Elastic analysis.
   —Finite element analysis.
   —Stress paths.

5. FINITE ELEMENT ANALYSIS OF THE STRESS CHANGES INDUCED BY AN EXCAVATION BEHIND A SLOPE

5.1 General

When a cut is made in a saturated clay deposit, total stress changes and reorientation of stresses occur behind the slope due to the unloading induced by excavation. As was explained earlier (Chapter 4), a knowledge of the magnitudes and orientations of the principal stresses after excavation are needed, in order to be able to apply the stress path method. From the methods that one can use in order to make an analysis of the stress changes induced by an excavation, and which were mentioned at the very end of Chapter 4, the finite element method has been chosen. For this purpose, a two-dimensional plane strain, finite element computer program, which assumes linearly elastic, isotropic materials, has been used. The analysis performed with this computer program, together with the assumptions that were made and the results obtained, are presented in Section 5.2.

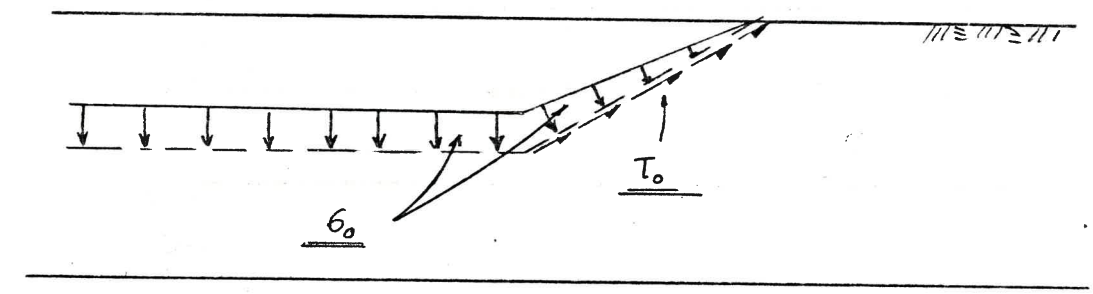
5.2 Presentation of the Analysis

In order to be able to make an analysis of the stress changes induced by an excavation behind a slope, it is first of all necessary to make an analytic simulation of the excavation. The excavation can be simulated to take place either in one step or in several smaller steps. Since it

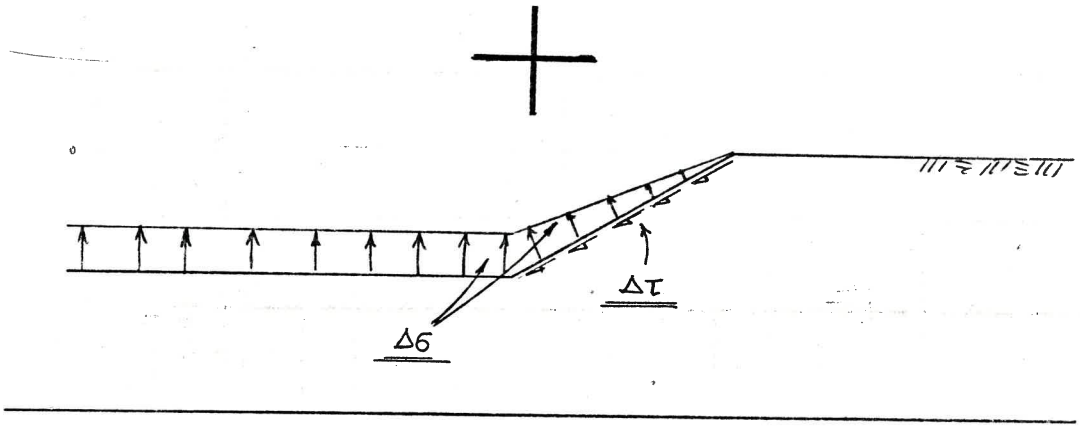
is assumed that the material is linearly elastic and isotropic, the principle of superposition is valid. Hence it is absolutely legal to substitute the actual stepped excavation by an imaginary one which is performed in only one step (Fig. 5.2.1). Notice that this would be true even for an elastoplastic material so long as the yield stress is not reached anywhere behind the slope. The latter statement, together with the fact that for low stress levels (up to about 70% of the peak strength), most soils, and especially the overconsolidated clays, behave within reason as linearly elastic materials, leads to the conclusion that this analysis will give a good approximation of the stress changes induced by excavations so long as the stresses do not approach the yield stress in any soil element.* The results of this analysis can be used as a guide in selecting the stress path along which we should test the samples in the laboratory. Another point to be made here is that the same modulus of elasticity E and Poisson's ratio ν has been assumed everywhere in the clay deposit. According to the theory of elasticity, this results in a stress analysis

---

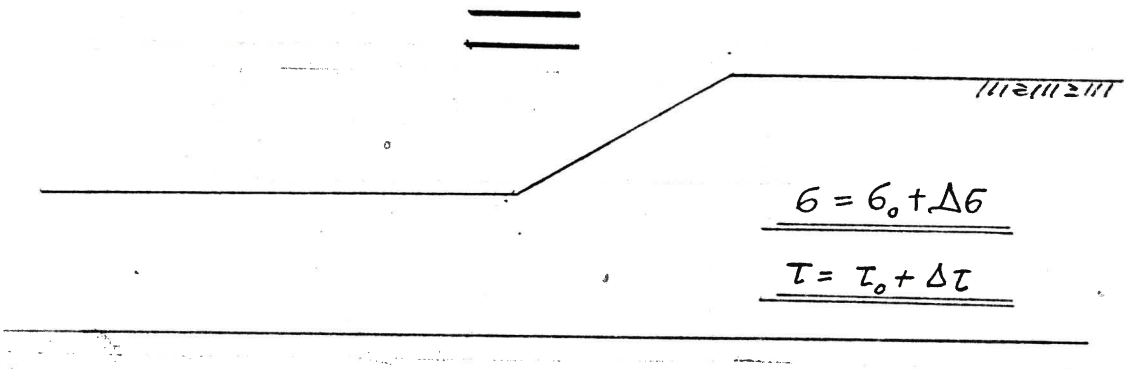
*As soon as local failure occurs somewhere behind the slope, there will be stress redistribution in all the unfailed soil elements, as it was described in more detail in Chapter 3 (Section 3.4), and the results of such an analysis will be no longer valid.



(a) Initial state of stress (before excavation)



(b) Stress change induced by excavation



(c) Final state of stress after excavation (stresses on surface are zero)

Fig. 5.2.1 Analytic simulation of excavation.

which is independent of what values of E and ν are used.

The analytic simulation of the excavation used for the finite element computer analysis is shown schematically in Fig. 5.2.1. Notice that the excavation has been simulated by applying normal and shear stresses along the bottom and the side of the cut equal in magnitude and opposite in direction to the normal and shear stresses that existed along these planes before excavation due to the geostatic stresses. This results in stress-free boundaries after the stress changes induced by excavation have been added to the initial stresses.

The program used is LSTRN-3, which is a two-dimensional, plane strain, finite element program. It assumes linearly elastic, isotropic materials and it can also handle bilinear materials (modulus of elasticity in tension $\neq$ modulus of elasticity in compression) as well as stress changes induced by temperature changes. The program was originally written by Wilson (1967) and it has subsequently been modified by others. A small modification in the subroutine "STRESS" (which calculates the stresses) of the most recent version of the program (Lysmer, 1971) was found necessary, so that both the stress changes and the final stresses and principal stress directions are given in the output. Another modification was made in the way data are input, so that the initial stresses are being input more easily.

Two slopes (1.5:1 and 3:1) have been analyzed for four different coefficients of total earth pressure at rest (K = 0.875,1.07,1.45,1.88). K can be related to K_o, the coefficient of effective earth pressure at rest, which is more often used.* According to the definitions of K and K_o:

$$K = \frac{\sigma_h}{\sigma_v} \quad (1), \qquad K_o = \frac{\sigma_h'}{\sigma_v'} \quad (2)$$

where σ_h, σ_h' are the total and effective horizontal stresses respectively and σ_v, σ_v' are the total and effective vertical stresses respectively. If γ is the total unit weight of the soil and u_z is the pore water pressure at depth z, then:

$$\sigma_v = \gamma z = \sigma_v' + u_z \quad (3)$$

$$\sigma_h = \sigma_h' + u_z \quad (4)$$

Combining equations (1), (2), (3), and (4) properly, we get:

$$K = \frac{\sigma_h}{\sigma_v} = \frac{\sigma_h' + u_z}{\sigma_v} = \frac{K_o \sigma_v' + u_z}{\sigma_v} = \frac{K_o(\sigma_v - u_z) + u_z}{\sigma_v} =$$
$$= K_o - K_o \frac{u_z}{\sigma_v} + \frac{u_z}{\sigma_v} \longrightarrow K = K_o + \frac{u_z}{\gamma z}(1 - K_o) \quad (5)$$

From the above expression, it can be seen that K is in general not equal to K_o. However, if the water table is deep enough, so that it does not affect the stability of the slope, then $u_z = 0$ and equation (5) reduces to $K = K_o$.

---

*The coefficient of effective earth pressure at rest is defined as the ratio of the effective horizontal stress over the effective vertical stress, for conditions of zero lateral strain.

Notice that for the special case where the water table is on the ground surface, then $u_z = \gamma_w z$, where γ_w is the unit weight of the water, and expression (5) becomes independent of depth:

$$K = K_o + \frac{\gamma_w}{\gamma}(1-K_o) \qquad (6)$$

However, it does depend on the unit weight of the soil.

The case where the water table does not enter the picture has been considered in the analysis. In this case $K = K_o$ and K_o can be readily obtained from published plots of K_o vs. PI (PI=plasticity index) for various overconsolidation ratios (OCR)* (Brooker and Ireland, 1965; see also Fig. 5.2.2). The four values of $K = K_o$ for which we have analyzed (K_o=0.875, 1.07, 1.45, 1.88) correspond to OCR = 2, 4, 8, 16 respectively. The plasticity index used (PI=40%) to derive these numbers was the one obtained from classification tests performed on the crushed, air-dried sample from the Friars Formation, as discussed in the section dealing with the preparation of the soil used for the tests.

Another assumption, inherent in the analysis, is that γ is constant everywhere in the slope, since we have normalized all stresses with respect to γH, where H is the height of the slope. This is not a bad assumption, as long

---

*The overconsolidation ratio (OCR) is defined as the ratio of the highest past effective overburden stress that has ever been applied on a soil element, over the present effective overburden stress on that element.

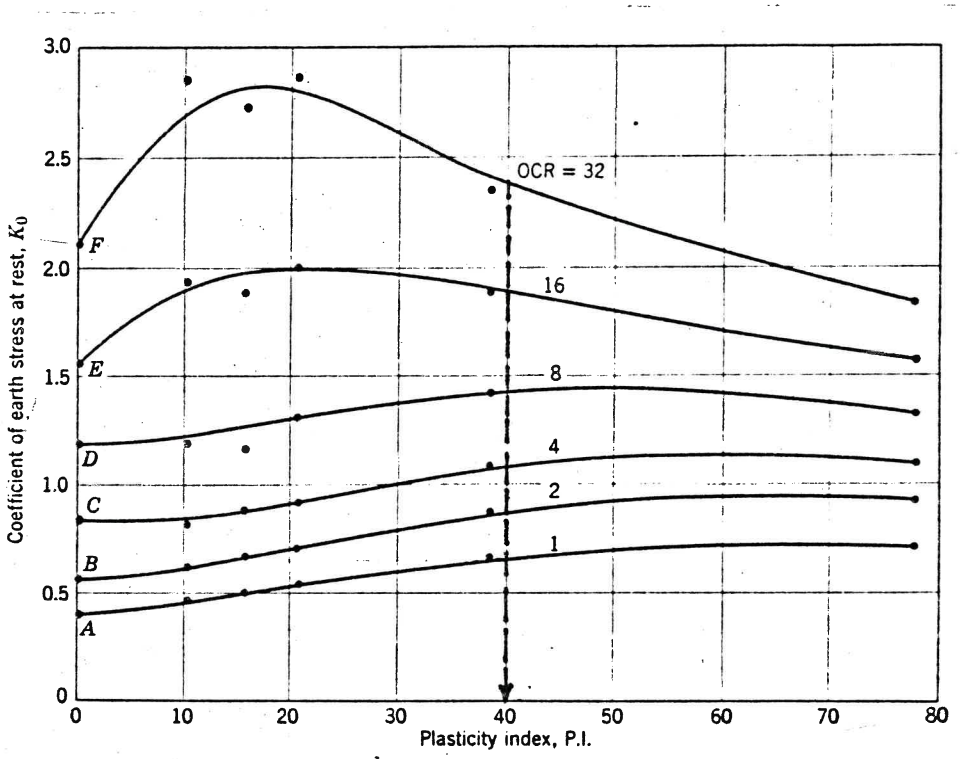


Fig. 5.2.2 K_o as a function of overconsolidation ratio and plasticity index (from Brooker and Ireland, 1965).

as the soil has approximately the same degree of saturation everywhere. It should be mentioned here that the results of this analysis can also be used for the special case where the water table is on the ground surface. In that case, K is computed from equation (6) and the answer is obtained by interpolation using the results of this analysis. The same holds if the soil under consideration has a PI different from 40%. The appropriate K_o is obtained from Fig. 5.2.2, given PI and OCR, K is computed using equation (6) (if the water table is on the ground surface), and K or K_o, whichever applies, is used to interpolate through the results presented here.

The dimensions of the sections analyzed for each of the two slopes are shown in Fig. 5.2.3. It was considered that a section extending horizontally 6H away from the crest of the slope and 3H away from the toe of the slope would be sufficient for analysis purposes, as the stress changes induced by the excavation that far would be very small and hence the lateral boundaries would not significantly affect the final state of stress after excavation. This assumption proved to be very good, as the stress changes close to the lateral boundaries obtained from the analysis have been found to be small and, in addition, the transition in stress orientation close to these boundaries is smooth. The position of the lower boundary which is assumed to be a harder layer of rock, does influence

the stresses in the slope region. In the present analysis, it has been taken to be at a depth H below the base of the excavation. The boundary conditions used in the analysis are also shown in Fig. 5.2.3. As it can be seen, the lower boundary is assumed to be fixed (no horizontal or vertical movements allowed), simulating full adhesion between bedrock and the softer clay layer above. The lateral boundaries are allowed to move vertically (zero reactions in the vertical direction) but not horizontally. Finally, the upper boundaries (ground surface after excavation) are allowed to move freely in any direction.

The finite element meshes used for the two slopes are also shown in Fig. 5.2.3. The number of elements used and their arrangement were selected in such a way that their size would be small close to the slope where the stress gradient is maximum and large away from the slope where the stress gradient is small. In addition, an effort was made to use as few elements as possible, without considerably affecting the accuracy of the results, in order to reduce computer time. A total of 147 elements for the 3:1 slope and 93 elements for the 1.5:1 slope have been used. Also, the bandwidth of the resulting stiffness matrix, on which actually the computer time depends, has been reduced to 11 for the 3:1 slope and to 10 for the 1.5:1 slope. The bandwidth is empirically found as the

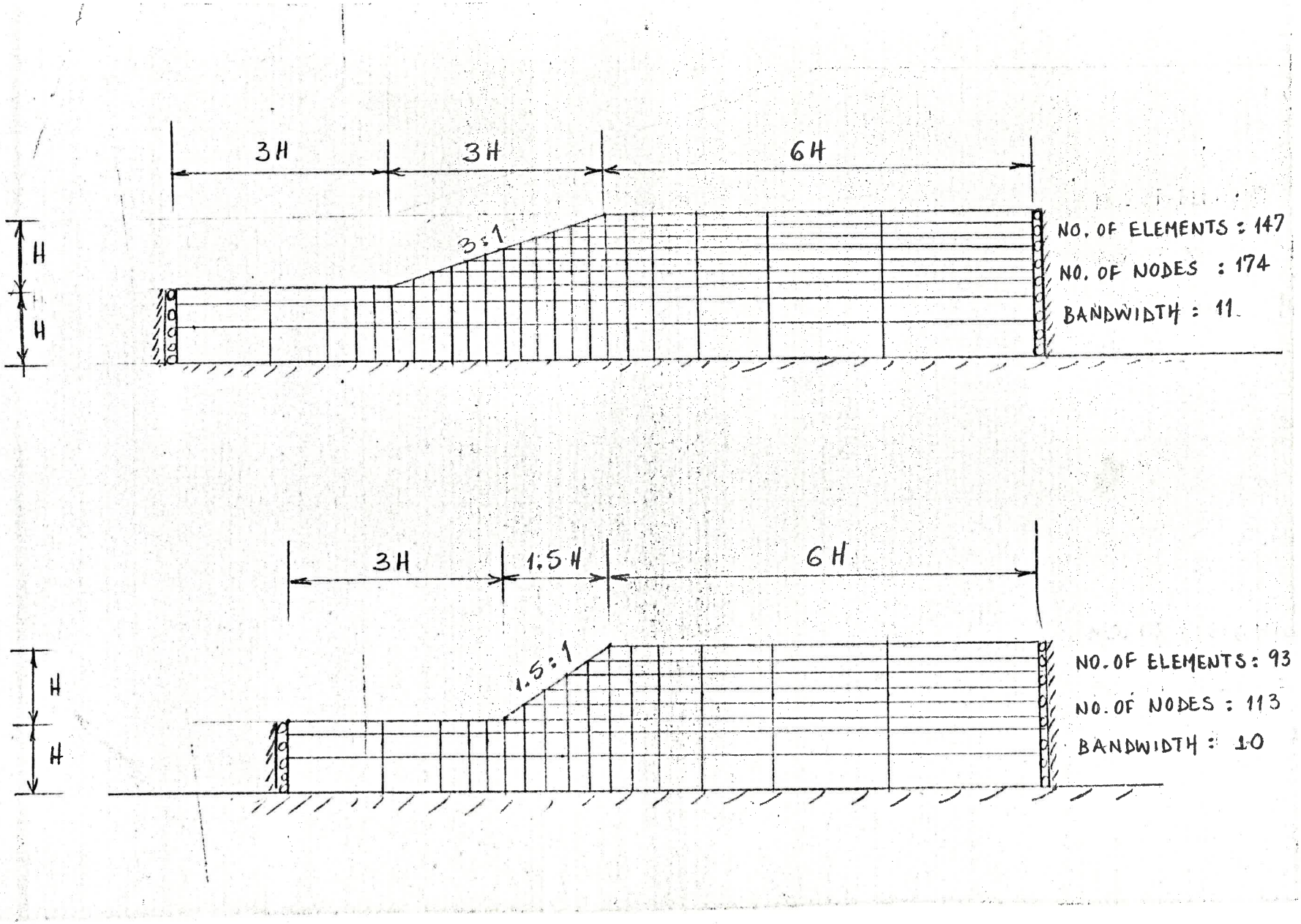


Fig. 5.2.3 Finite elements meshes and boundary conditions for the two slopes.

maximum difference between the numbers of any two nodes (belonging to the same element) of any one element of the mesh.

Due to program limitations, several loading assumptions had to be made for the slopes being analyzed. The basic limitation is that the program does not allow for any inclined stresses or non-uniform stress distributions to be applied on the sides of an element (i.e., only uniformly distributed normal stresses are allowed). However, concentrated forces of any direction are allowed on the nodes of an element (these forces are eventually analyzed in x and y directions). Fig. 5.2.4 shows the loading assumptions that had to be made. The continuous triangular normal stress distribution along the slope has been approximated by a number of uniform normal stress distributions, one for each element along the slope. The continuous triangular shear stress distribution along the slope has been approximated by a number of concentrated shear forces, one on each node along the slope. These shear forces have subsequently been analyzed into two components, one horizontal and one vertical. Fig. 5.2.5 shows the details of the approximation of the continuous shear stress distribution by concentrated nodal forces. Notice that the stresses have been normalized with respect to γH, and the lengths have been normalized with respect

to H, where γ is the unit weight of the soil (dry, saturated or buoyant depending on the case) and H is the height of the excavation.

The actual normal and shear stress distributions induced by the excavation along the side and the bottom of the cut are computed from the vertical and horizontal geostatic stresses σ_v and σ_h which existed there before excavation:

$$\sigma_v = \gamma z \quad \text{and} \quad \sigma_h = K\gamma z \tag{7}$$

where z is the depth from the crest of the slope. The details of these computations are shown in Fig. 5.2.6 from which we finally find that:

$$\frac{\sigma}{\gamma z} = \frac{1}{2}(1+K) + \frac{1}{2}(1-K)\cos 2\beta \tag{8}$$

$$\frac{\tau}{\gamma z} = -\frac{1}{2}(1-K)\sin 2\beta \tag{9}$$

where β is the angle between the side of the excavation and the horizontal. Using the above two relationships, the values of $\sigma/\gamma H$ and $\tau/\gamma H$ have been computed as a function of z/H for the two slopes and the various coefficients of earth pressure at rest K. These values are presented in Table 5.2.1. Tables 5.2.2 and 5.2.3 have been derived from Table 5.2.1 and give the values of $\sigma/\gamma H$ and $\tau/\gamma H$ at various normalized depths z/H. Notice that $\sigma/\gamma H$ has been computed at the midpoints between nodes and $\tau/\gamma H$ has been computed at the nodal points along the slope. This relates

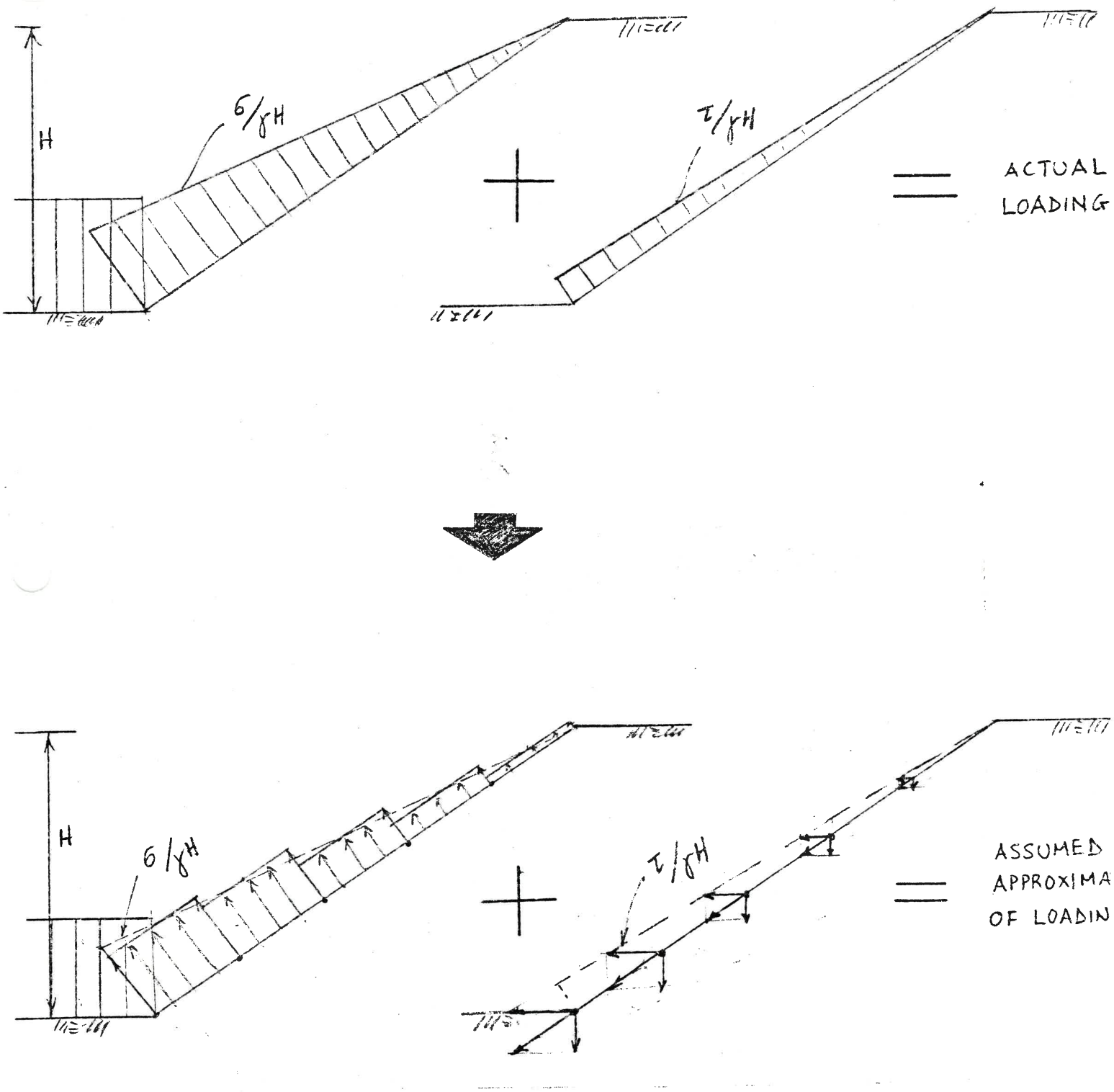
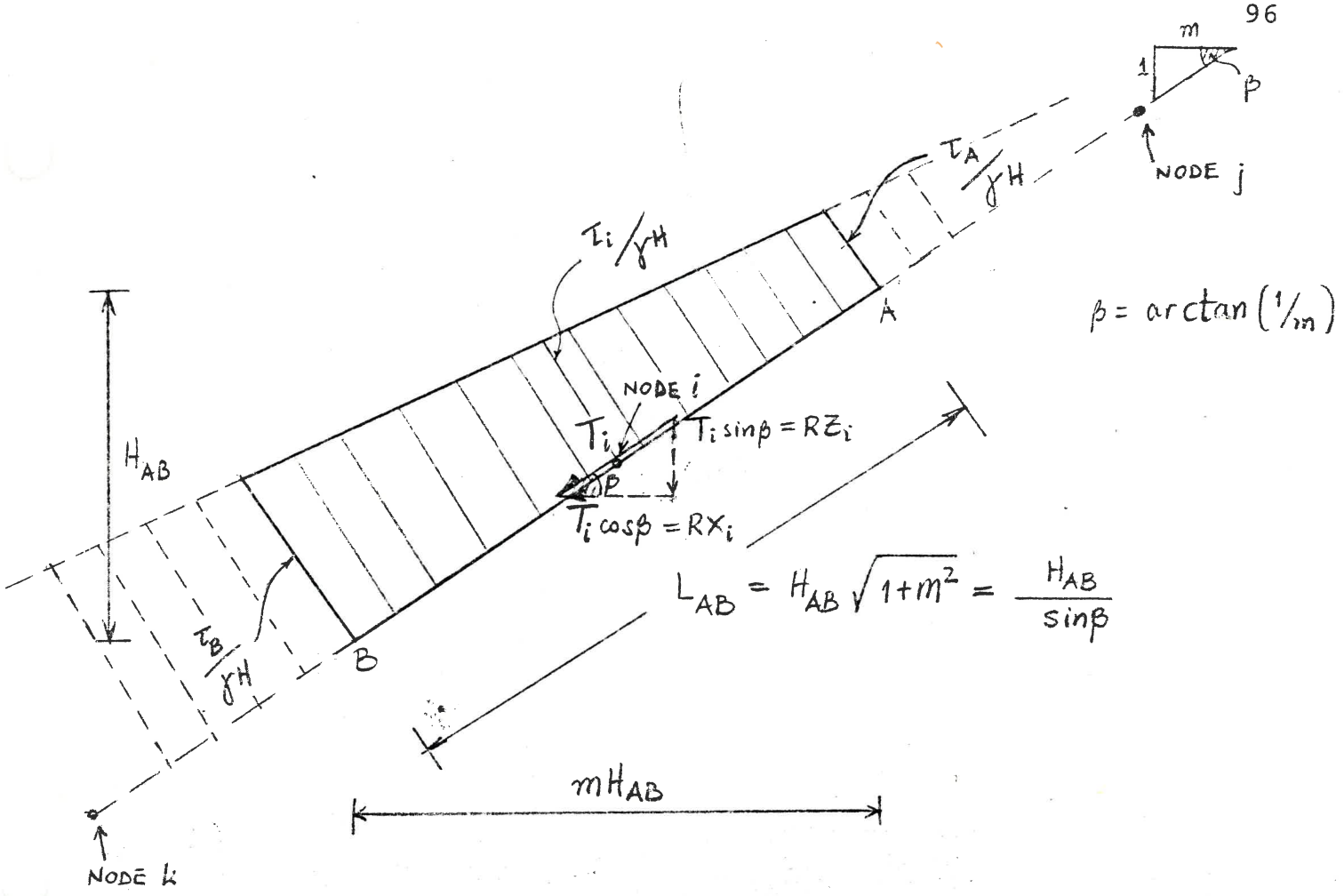


Fig. 5.2.4 Approximation of excavation induced loads.



$$T_i = \frac{\frac{\tau_A}{\gamma H} + \frac{\tau_B}{\gamma H}}{2} L_{AB} = \frac{\tau_A + \tau_B}{2\gamma H} H_{AB}\sqrt{1+m^2}$$

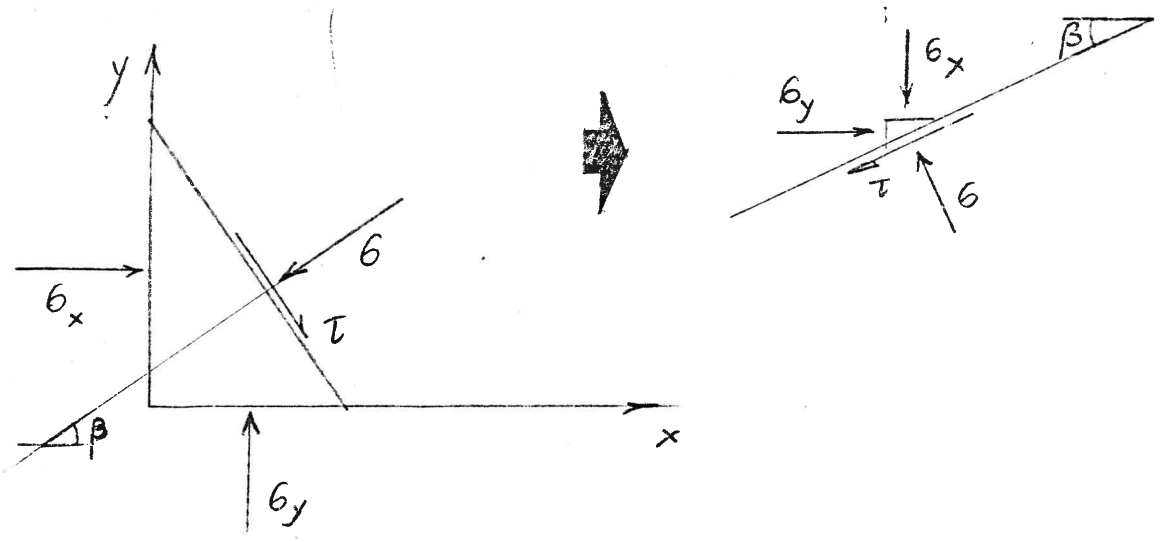
$$RX_i = T_i \cos\beta = \frac{\tau_A + \tau_B}{2\gamma H} H_{AB}\sqrt{1+m^2}\cos\beta =$$

$$= \frac{\tau_A + \tau_B}{2\gamma H} H_{AB} \frac{1}{\tan\beta} = \frac{\tau_A + \tau_B}{2\gamma H} m H_{AB}$$

$$\Rightarrow \boxed{RX_i = \frac{\tau_i}{\gamma H} m H_{AB}} \quad (1)$$

Similarly: $$\boxed{RZ_i = \frac{\tau_i}{\gamma H} H_{AB}} \quad (2)$$

Fig. 5.2.5 Approximation of continuous shear stress distribution by nodal forces.



$$\sigma = \sigma_x \cos^2\beta + \sigma_y \sin^2\beta = \frac{1}{2}(\sigma_x+\sigma_y) + \frac{1}{2}(\sigma_x-\sigma_y)\cos 2\beta$$
$$\tau = \frac{1}{2}(\sigma_y-\sigma_x)\sin 2\beta \qquad \Big\} \ (1)$$

$$\sigma_x = \gamma z$$
$$\sigma_y = k\gamma z \qquad \Big\} \ (2)$$

$$(1),(2) \rightarrow \quad \sigma = \frac{1}{2}(1+k)\gamma z + \frac{1}{2}(1-k)\gamma z \cos 2\beta \rightarrow$$

$$\rightarrow \boxed{\frac{\sigma}{\gamma z} = \frac{1}{2}(1+k) + \frac{1}{2}(1-k)\cos 2\beta}$$

$$(1),(2) \rightarrow \quad \tau = \frac{1}{2}(k-1)\gamma z \sin 2\beta \Rightarrow$$

$$\rightarrow \boxed{\frac{\tau}{\gamma z} = -\frac{1}{2}(1-k)\sin 2\beta}$$

Fig. 5.2.6 Normal and shear stress changes induced along the slope by the excavation.

Table 5.2.1

Geostatic Stresses Before Excavation

Along a Line Inclined to the Horizontal

		$\sigma/\gamma H$	$\tau/\gamma H$
$k = 0.875$ (OCR = 2)	SLOPE 3:1	$0.9875 \frac{z}{H}$	$-0.0375 \frac{z}{H}$
	SLOPE 1.5:1	$0.9615 \frac{z}{H}$	$-0.058 \frac{z}{H}$
$k = 1.07$ (OCR = 4)	SLOPE 3:1	$1.007 \frac{z}{H}$	$0.021 \frac{z}{H}$
	SLOPE 1.5:1	$1.0215 \frac{z}{H}$	$0.032 \frac{z}{H}$
$k = 1.45$ (OCR = 8)	SLOPE 3:1	$1.045 \frac{z}{H}$	$0.135 \frac{z}{H}$
	SLOPE 1.5:1	$1.1385 \frac{z}{H}$	$0.208 \frac{z}{H}$
$k = 1.88$ (OCR = 16)	SLOPE 3:1	$1.088 \frac{z}{H}$	$0.264 \frac{z}{H}$
	SLOPE 1.5:1	$1.271 \frac{z}{H}$	$0.406 \frac{z}{H}$

Table 5.2.2

Geostatic Stresses Before Excavation

Along a Line with Slope 1.5:1

z/H	$k = 0.875$		$k = 1.07$		$k = 1.45$		$k = 1.88$	
	$\sigma/\gamma H$	$\tau/\gamma H$	$\sigma/\gamma H$	$\tau/\gamma H$	$\sigma/\gamma H$	$\tau/\gamma H$	$\sigma/\gamma H$	$\tau/\gamma H$
0	0	0	0	0	0	0	0	0
0.1	.0962		.1022		.1139		.1271	
0.2		-.0116		.0064		.0416		.0812
0.3	.2885		.3065		.3416		.3813	
0.4		-.0232		.0128		.0832		.1624
0.5	.4808		.5108		.5693		.6355	
0.6		-.0348		.0192		.1248		.2436
0.7	.6731		.7151		.7970		.8897	
0.8		-.0464		.0256		.1664		.3248
0.9	.8654		.9194		1.0247		1.1439	
1.0		-.0580		.0320		.2080		.4060

Table 5.2.3

Geostatic Stresses Along a 3:1 Sloping Line Before Excavation

z/H	K = 0.875		K = 1.07		K = 1.45		K = 1.88	
	$\sigma/\gamma H$	$\tau/\gamma H$	$\sigma/\gamma H$	$\tau/\gamma H$	$\sigma/\gamma H$	$\tau/\gamma H$	$\sigma/\gamma H$	$\tau/\gamma H$
0.042	.0411		.0420		.0435		.0453	
0.083		-.0031		.0018		.0113		.0220
0.125	.1234		.1259		.1306		.1360	
0.167		-.0063		.0035		.0225		.0440
0.208	.2057		.2098		.2177		.2267	
0.250		-.0094		.0053		.0338		.0660
0.292	.2880		.2937		.3048		.3173	
0.333		-.0125		.0070		.0450		.0880
0.375	.3703		.3776		.3919		.4080	
0.417		-.0156		.0088		.0563		.1100
0.458	.4526		.4615		.4790		.4987	
0.500		-.0188		.0105		.0675		.1320
0.542	.5349		.5455		.5660		.5893	
0.583		-.0219		.0123		.0788		.1540
0.625	.6172		.6294		.6531		.6800	
0.667		-.0250		.0140		.0900		.1760
0.708	.6995		.7133		.7402		.7707	
0.750		-.0281		.0158		.1013		.1980
0.792	.7818		.7972		.8273		.8613	
0.833		-.0313		.0175		.1125		.2200
0.875	.8641		.8811		.9144		.9520	
0.917		-.0344		.0193		.1238		.2420
0.958	.9464		.9650		1.0015		1.0427	
1.000		-.0375		.0210		.1350		.2640

to the way the normal and shear stress distributions are approximated. The value of $\sigma/\gamma H$ at the midpoint between nodes is used as the value of the assumed uniform normal stress distribution between these two nodes. The value of $\tau/\gamma H$ at the nodal points is substituted into equations (1) and (2) of Fig. 5.2.5:

$$RX_i = \frac{\tau_i}{\gamma H} m H_{AB} \qquad (10)$$

$$RZ_i = \frac{\tau_i}{\gamma H} H_{AB} \qquad (11)$$

where the subscript i refers to node i, m is the slope of the excavation (m:1) and H_{AB} is the vertical distance between two consecutive nodes along the slope. From these expressions, the horizontal and vertical components of the approximated shear force T_i at node i are computed and are presented in normalized form in Tables 5.2.4 and 5.2.5. Notice that RX_i and RZ_i have originally been normalized with respect to γH and also that they represent forces per unit length of the slope (length perpendicular to the plane of the section we analyze). Hence the units of RX_i and RZ_i are $\frac{F/L}{F/L^2} = L$ and consequently the ratios RX_i/H and RZ_i/H, which are given in Tables 5.2.4 and 5.2.5, are pure numbers. The forces from these tables have been entered in the program as boundary nodal forces and they represent an approximation of the change in shear stress induced by the excavation along the side of the cut. The stresses $\sigma/\gamma H$ from Tables 5.2.2 and 5.2.3 have been entered

Table 5.2.4

Shear Forces Applied on the Nodes Along

The Slope--Slope M:1—H_{AB} = 0.2H, M = 1.5

NODE	Z/H	K = 0.875		K = 1.07		K = 1.45		K = 1.88	
		RX_i/H $\times 10^{+2}$	RZ_i/H $\times 10^{+2}$	RX_i/H $\times 10^{+2}$	RZ_i/H $\times 10^{+2}$	RX_i/H $\times 10^{+2}$	RZ_i/H $\times 10^{+2}$	RX_i/H $\times 10^{+2}$	RZ_i/H $\times 10^{+2}$
51	0	-0.044	-0.029	0.024	0.016	0.156	0.104	0.305	0.203
43	0.2	-0.348	-0.232	0.192	0.128	1.248	0.832	2.436	1.624
36	0.4	-0.696	-0.464	0.384	0.256	2.496	1.664	4.872	3.248
30	0.6	-1.044	-0.696	0.576	0.384	3.744	2.496	7.308	4.872
25	0.8	-1.392	-0.928	0.768	0.512	4.992	3.328	9.744	6.496
21	1.0	-0.827	-0.551	0.456	0.304	2.964	1.976	5.786	3.857

$$RX_i = \frac{\tau_i}{\gamma H} m H_{AB} \Rightarrow \frac{RX_i}{H} = \frac{\tau_i}{\gamma H} m \frac{H_{AB}}{H} \qquad (1)$$

$$RZ_i = \frac{\tau_i}{\gamma H} H_{AB} \Rightarrow \frac{RZ_i}{H} = \frac{\tau_i}{\gamma H} \frac{H_{AB}}{H} \qquad (2)$$

Values of $\tau_i/\gamma H$ are taken from table 5.2.2.

Node 51 : $\frac{\tau_{51}}{\gamma H} \Leftrightarrow \frac{\tau_{43}}{8\gamma H}$ (fictitious)

Node 21 : $\frac{\tau_{21}}{\gamma H} \Leftrightarrow \frac{3\tau_{21} + \tau_{25}}{8\gamma H}$ (ficticious)

} Substitutions to be made in the above formulas for nodes 51 & 21

Table 5.2.5

Shear Forces Applied on the Nodes Along the Slope

Slope M:1 — M = 3, H_{AB} = 0.083H

NODE	z/H	k = 0.875		k = 1.07		k = 1.45		k = 1.88	
		RX_i/H $\times 10^2$	RZ_i/H $\times 10^2$	RX_i/H $\times 10^2$	RZ_i/H $\times 10^2$	RX_i/H $\times 10^2$	RZ_i/H $\times 10^2$	RX_i/H $\times 10^2$	RZ_i/H $\times 10^2$
105	0	-0.010	-0.003	0.005	0.002	0.035	0.012	0.069	0.023
95	0.083	-0.078	-0.026	0.044	0.015	0.281	0.094	0.550	0.183
86	0.167	-0.156	-0.052	0.088	0.029	0.563	0.188	1.100	0.367
77	0.250	-0.234	-0.078	0.131	0.044	0.844	0.281	1.650	0.550
69	0.333	-0.313	-0.104	0.175	0.058	1.125	0.375	2.200	0.733
61	0.417	-0.391	-0.130	0.219	0.073	1.406	0.469	2.750	0.917
54	0.500	-0.469	-0.156	0.263	0.088	1.688	0.563	3.300	1.100
47	0.583	-0.547	-0.182	0.306	0.102	1.969	0.656	3.850	1.283
41	0.667	-0.625	-0.208	0.350	0.117	2.250	0.750	4.400	1.467
35	0.750	-0.703	-0.234	0.393	0.131	2.531	0.844	4.950	1.650
30	0.833	-0.781	-0.260	0.438	0.146	2.813	0.938	5.500	1.833
25	0.917	-0.859	-0.286	0.481	0.160	3.094	1.031	6.050	2.017
21	1.000	-0.459	-0.153	0.257	0.086	1.652	0.551	3.231	1.077

Use formulas (1) & (2) of fig. 5.2.5 to get RX_i/H and RZ_i/H.
Values of $\tau_i/\gamma H$ are taken from table 5.2.3.

Node 105 : $\frac{\tau_{105}}{\gamma H} \Leftrightarrow \frac{\tau_{95}}{8\gamma H}$ (fictitious)

Node 21 : $\frac{\tau_{21}}{\gamma H} \Leftrightarrow \frac{3\tau_{21} + \tau_{25}}{8\gamma H}$ (fictitious)

} Substitutions to be made in formulas (1) & (2) for nodes 105 & 21

in the program as boundary element pressures and they represent an approximation of the change in normal stress induced by the excavation along the side of the cut.

It should be mentioned here that Poisson's ratio was taken equal to $\nu = 0.45$ for the analysis. Poisson's ratio for soils primarily depends on the density of the soil and the level of deformation (Lambe and Whitman, 1969). The value of ν is small for small deformations, when the volume of the material decreases. However, for larger deformations ν increases and it can even become greater than 0.5 because of expansion of the material. The value selected ($\nu = 0.45$) is close to the ones usually used in Soil Mechanics for elastic analyses (Duncan and Dunlop, 1969; Lysmer, 1978). Fortunately, the value of ν usually has a relatively small effect upon engineering predictions. The modulus of elasticity used for our analysis is $E = 100\,\gamma H$ (it has been entered in the program as $E/\gamma H$). Actually it is not very important what E we choose since we are not interested in the deformations developing; a linearly elastic analysis can usually give good answers for stresses but very seldom can it give reliable answers for deformations, unless E is relatively constant in the range of stresses expected to develop and is reliably known.

The program initially computes the final horizontal and vertical stresses σ_x and σ_y as well as the final shear stress τ_{xy} on horizontal and vertical planes at the

center of each element and from these it computes the principal stresses σ_1 and σ_3, the major principal stress direction, given by the angle θ (which will be subsequently defined), and the maximum shear stress τ_{max}. Fig. 5.2.7 gives the equations used by the program in order to compute $\sigma_1, \sigma_3, \theta$ and τ_{max}. It also gives the sign conventions for $\sigma_x, \sigma_y, \tau_{xy}, \sigma, \tau$ and θ. The angle θ is the angle between the horizontal axis (x-axis) and the direction of σ_1. The value and sign of θ are determined as follows:

If we call $\delta = \tan^{-1}\left(\frac{2\tau_{xy}}{\sigma_x - \sigma_y}\right)$, then:

(i) If $(\sigma_x + \sigma_y) > 0$

$\theta = \frac{\delta}{2}$, if $\sigma_x \geq \sigma_y$

$\theta = \frac{\delta}{2} + \frac{\pi}{2}$, if $\sigma_x < \sigma_y$ & $\tau_{xy} \geq$

$\theta = \frac{\delta}{2} - \frac{\pi}{2}$, if $\sigma_x < \sigma_y$ & $\tau_{xy} <$

(The above sign conventions are given by R. Goodman in his lectures of Rock Mechanics, 1979).

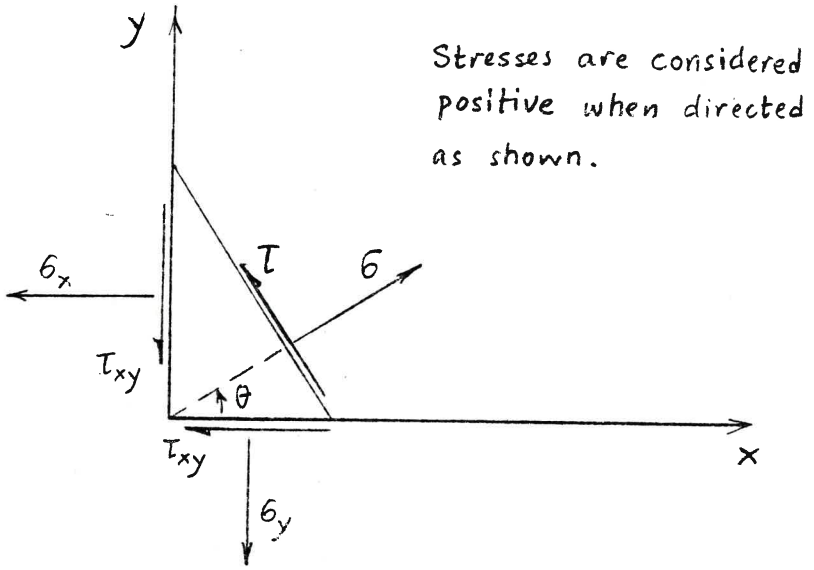
(ii) If $(\sigma_x + \sigma_y) \leq 0$

$\theta = \frac{\delta}{2}$, if $\sigma_x \leq \sigma_y$

$\theta = \frac{\delta}{2} + \frac{\pi}{2}$, if $\sigma_x \geq \sigma_y$ & $\tau_{xy} \leq$

$\theta = \frac{\delta}{2} - \frac{\pi}{2}$, if $\sigma_x \geq \sigma_y$ & $\tau_{xy} \geq$

(The latter sign conventions were developed for use in the present analysis in conjunction with the sign conventions for $\sigma_x + \sigma_y > 0$ given previously).



$$\sigma_1 = \frac{1}{2}(\sigma_x + \sigma_y) + \frac{1}{2}\sqrt{(\sigma_y - \sigma_x)^2 + 4\tau_{xy}^2} \qquad (1)$$

$$\sigma_3 = \frac{1}{2}(\sigma_x + \sigma_y) - \frac{1}{2}\sqrt{(\sigma_y - \sigma_x)^2 + 4\tau_{xy}^2} \qquad (2)$$

$$\tan 2\theta = \frac{2\tau_{xy}}{\sigma_x - \sigma_y} \qquad (3)$$

$$\tau_{max} = \frac{1}{2}\sqrt{(\sigma_y - \sigma_x)^2 + 4\tau_{xy}^2} = \frac{\sigma_1 - \sigma_3}{2} \qquad (4)$$

Fig. 5.2.7 Definitions and sign conventions for σ_1, σ_3, τ_{max}, and θ.

The program output gives the following:

—EL. NO.: Element number.

—X: x-coordinate of the center of the element.

—Y: y-coordinate of the center of the element.

—X-STRESS*: Horizontal normal stress at the center of the element expressed as a % of γH, i.e., $\frac{\sigma_h}{\gamma H} \times 100$.

—Y-STRESS*: Vertical normal stress at the center of the element expressed as a % of γH, i.e., $\frac{\sigma_v}{\gamma H} \times 100$.

—XY-STRESS*: Shear stress on vertical and horizontal planes at the center of the element expressed as a % of γH, i.e., $\frac{\tau_{xy}}{\gamma H} \times 100$.

—MAX-STRESS*: Major principal stress at the center of the element expressed as a % of γH, i.e., $\frac{\sigma_1}{\gamma H} \times 100$.

—MIN-STRESS*: Minor principal stress at the center of the element expressed as a % of γH, i.e., $\frac{\sigma_3}{\gamma H} \times 100$.

—ANGLE: Angle between the direction of σ_1 and the horizontal measured counterclockwise, i.e., the angle θ defined above.

—MAX-SHEAR STRESS: Maximum shear stress at the center of the element expressed as a % of γH, i.e., $\frac{\tau_{max}}{\gamma H} \times 100$.

---

*The first line in the output gives the stress change induced by the excavation, while the second line gives the final total stress after excavation. Also notice that all the stresses are total stresses.

The computer output from this analysis is presented in Appendix 1. In the following Figures 5.2.8 through 5.2.15, contours of the ratio $\tau_{max}/\gamma H$ have been plotted for both 3:1 and 1.5:1 slopes and all four coefficients of earth pressure at rest (K = 0.875, 1.07, 1.45, 1.88). The principal stress vectors after excavation for the aforementioned slopes and K values have been drawn in Fig. 5.2.16—5.2.23. Fig. 5.2.8—5.2.23 present only that part of the sections analyzed, which is of main interest for slope stability problems. These plots have actually been carried out to the boundaries of the sections analyzed in order to verify the assumption that the final state of stress after excavation is not seriously affected by the lateral boundary conditions.

An analysis similar to the above has been made by Duncan and Dunlop (1969). Some of the results of the present analysis were compared to theirs and a very good agreement was found for both values of $\tau_{max}/\gamma H$ and principal stress directions, despite the fact that a considerably smaller number of elements have been used in the present analysis (the sections analyzed here are of the same size as the ones analyzed by Duncan and Dunlop).

A different type of analysis that can be made in lieu of the one previously presented is to run the program for various H_p/H ratios, instead of various K values, where H_p is the equivalent height of soil which has precompressed

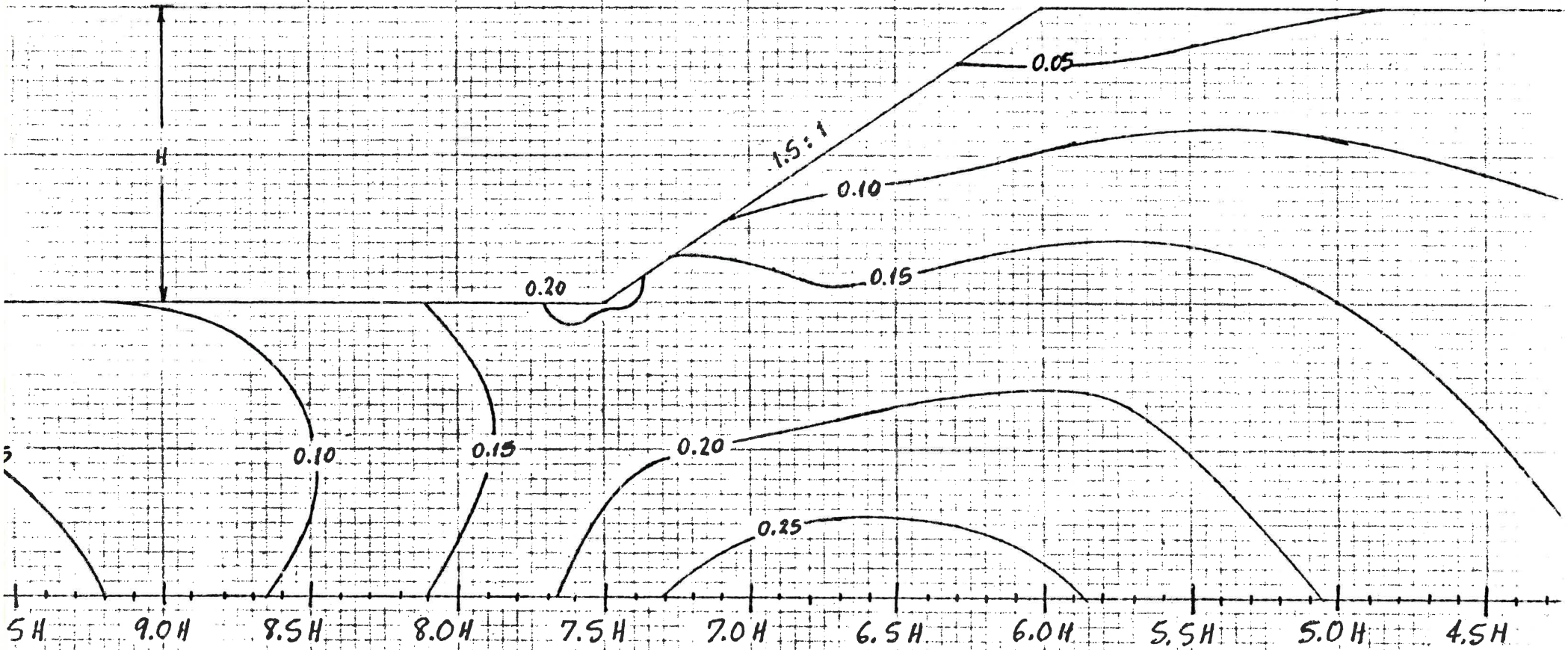


Fig. 5.2.8 Contours of $\tau_{max}/\gamma H$ for $K = 0.875$.

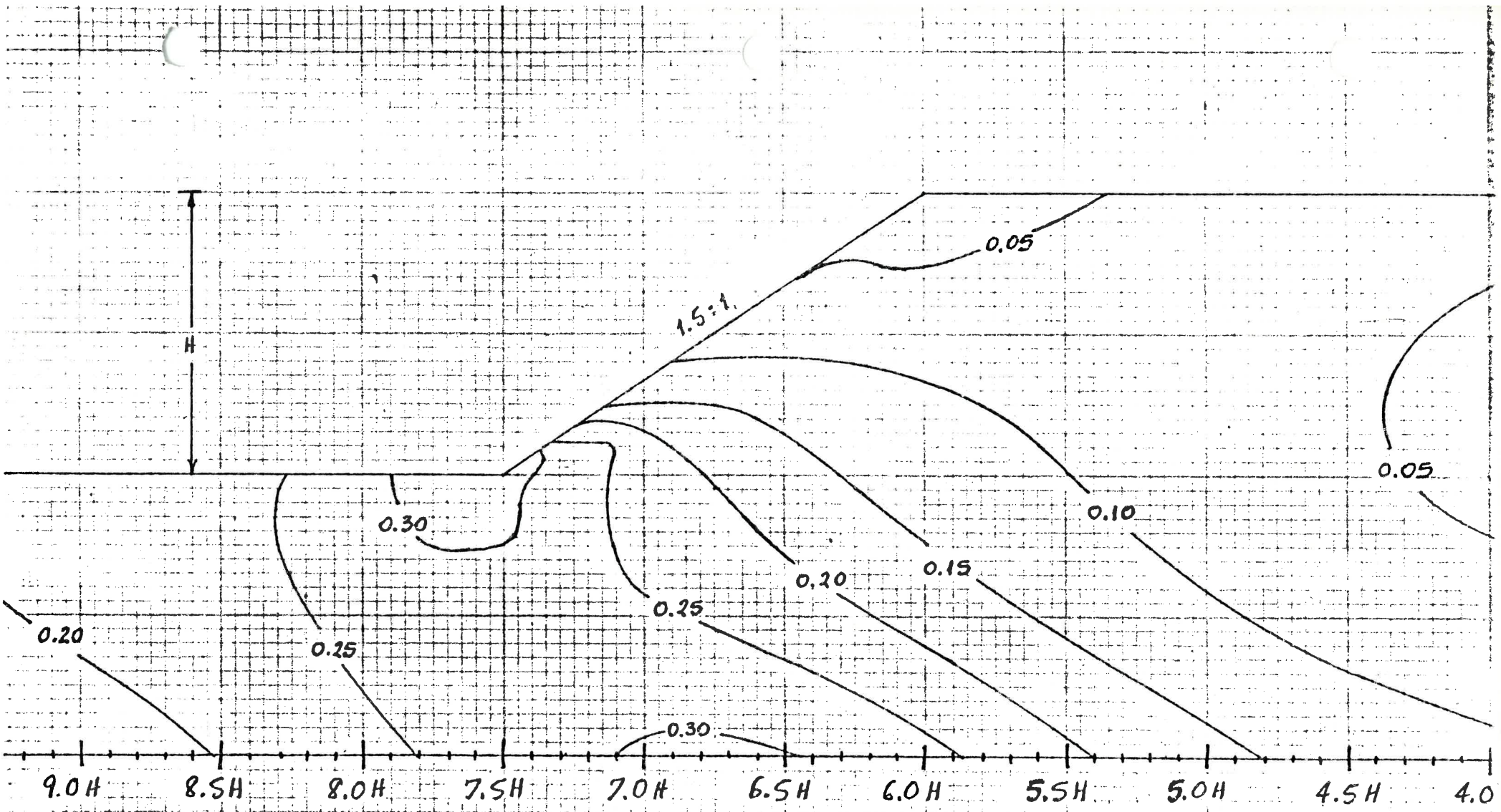


Fig. 5.2.9 Contours of $\tau_{max}/\gamma H$ for $K = 1.07$.

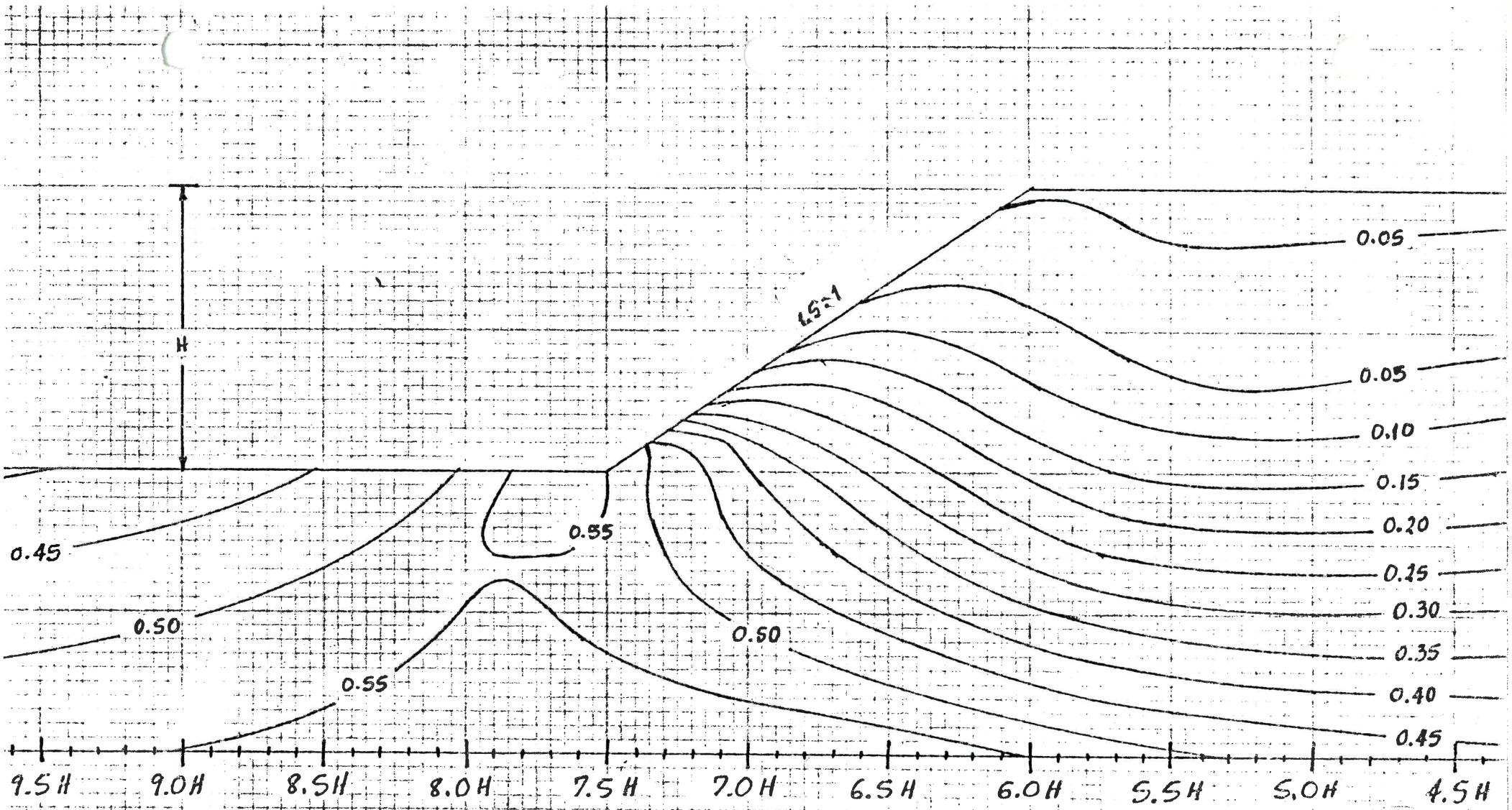


Fig. 5.2.10 Contours of $\tau_{max}/\gamma H$ for $K = 1.45$.

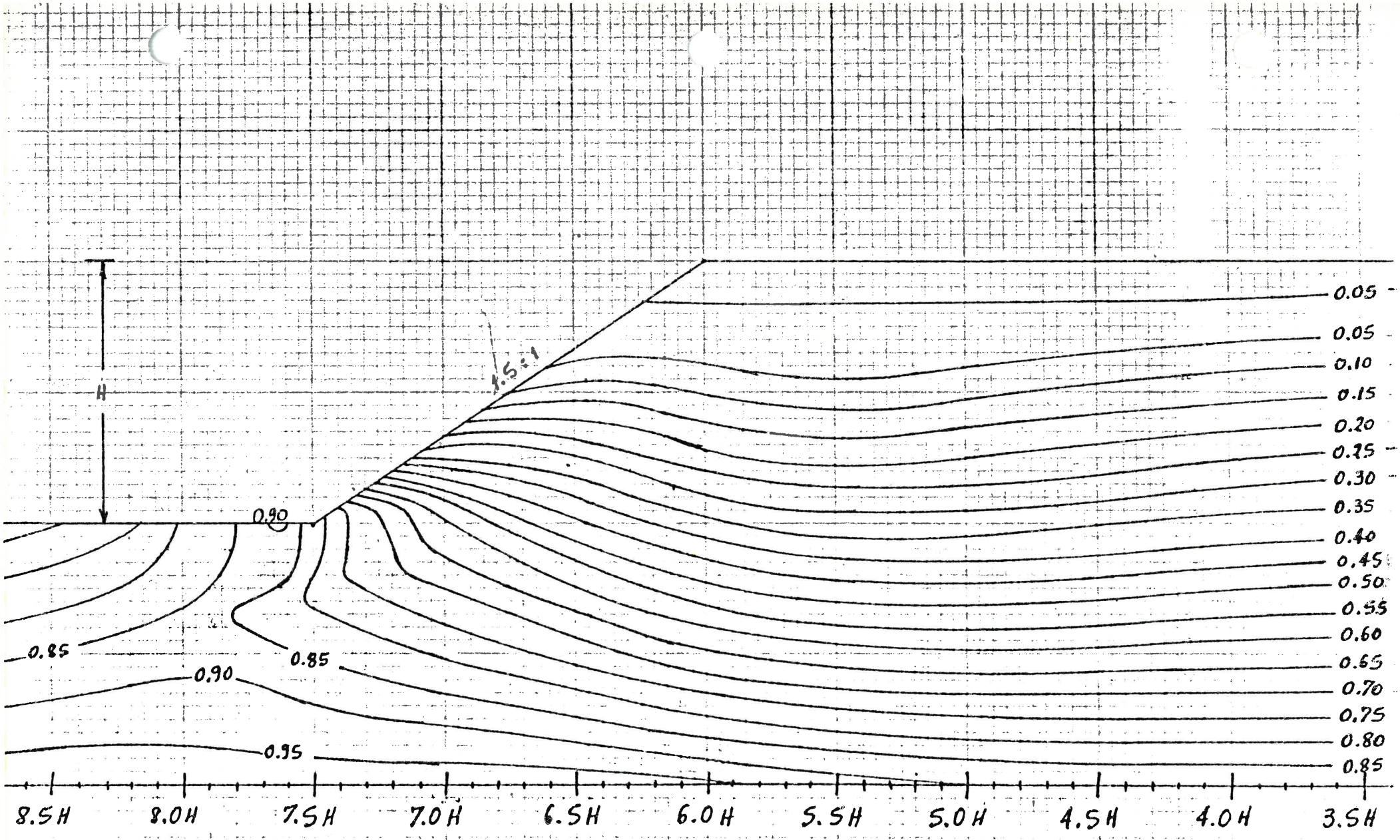


Fig. 5.2.11 Contours of $\tau_{max}/\gamma H$ for K = 1.88.

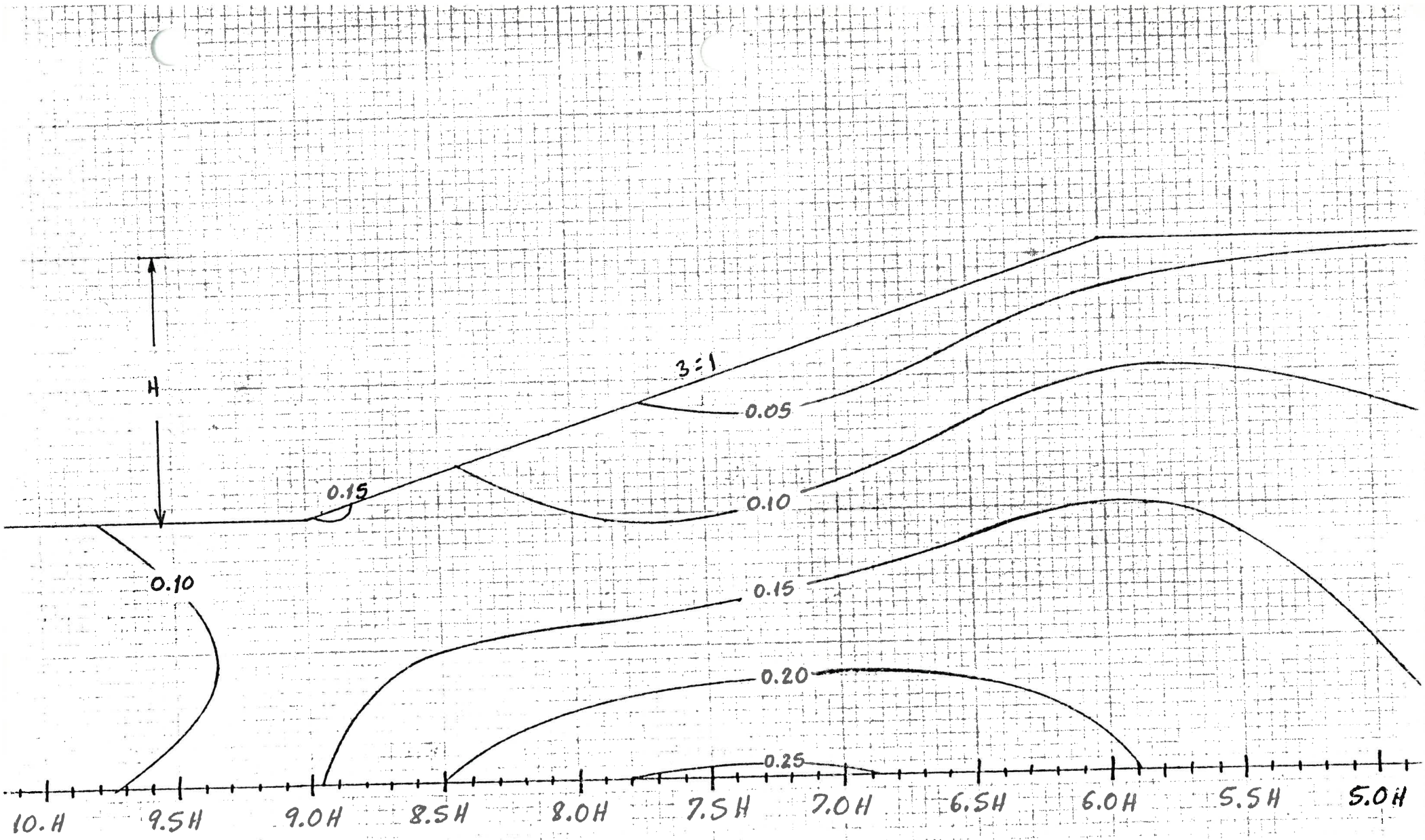


Fig. 5.2.12 Contours of $\tau_{max}/\gamma H$ for $K = 0.875$.

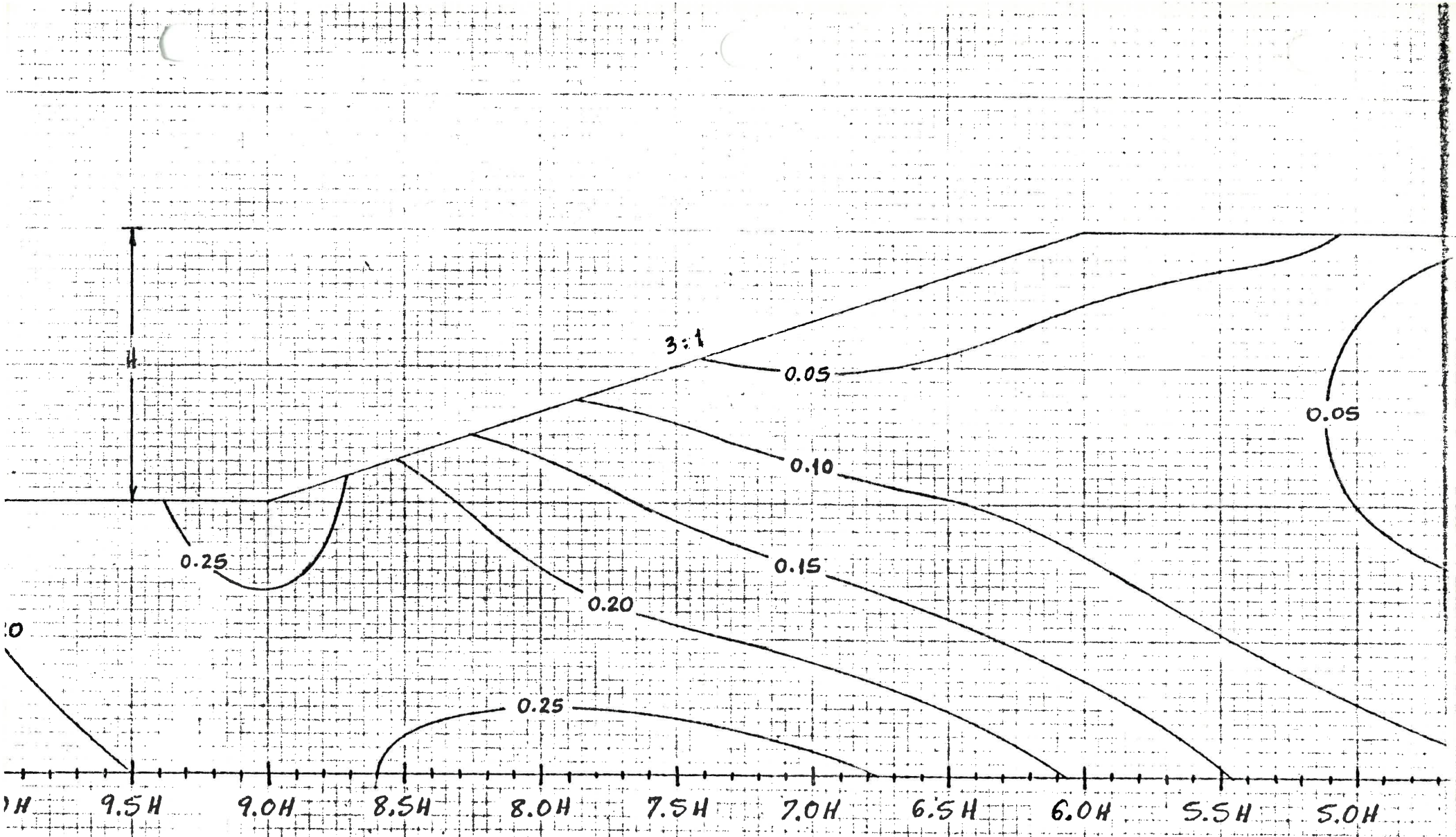


Fig. 5.2.13 Contours of $\tau_{max}/\gamma H$ for $K = 1.07$.

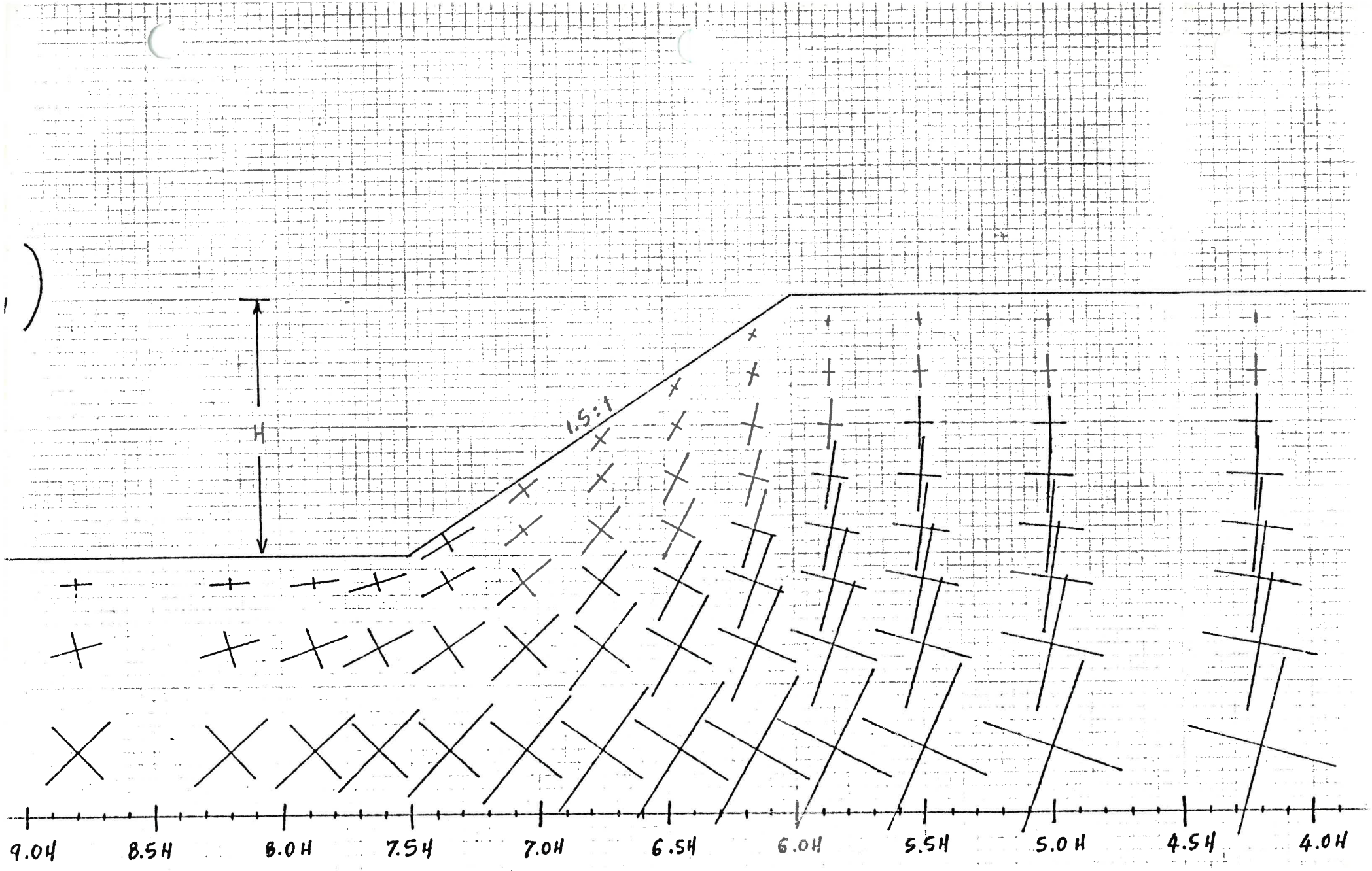


Fig. 5.2.16 Principal stress ratios for K = 0.875.

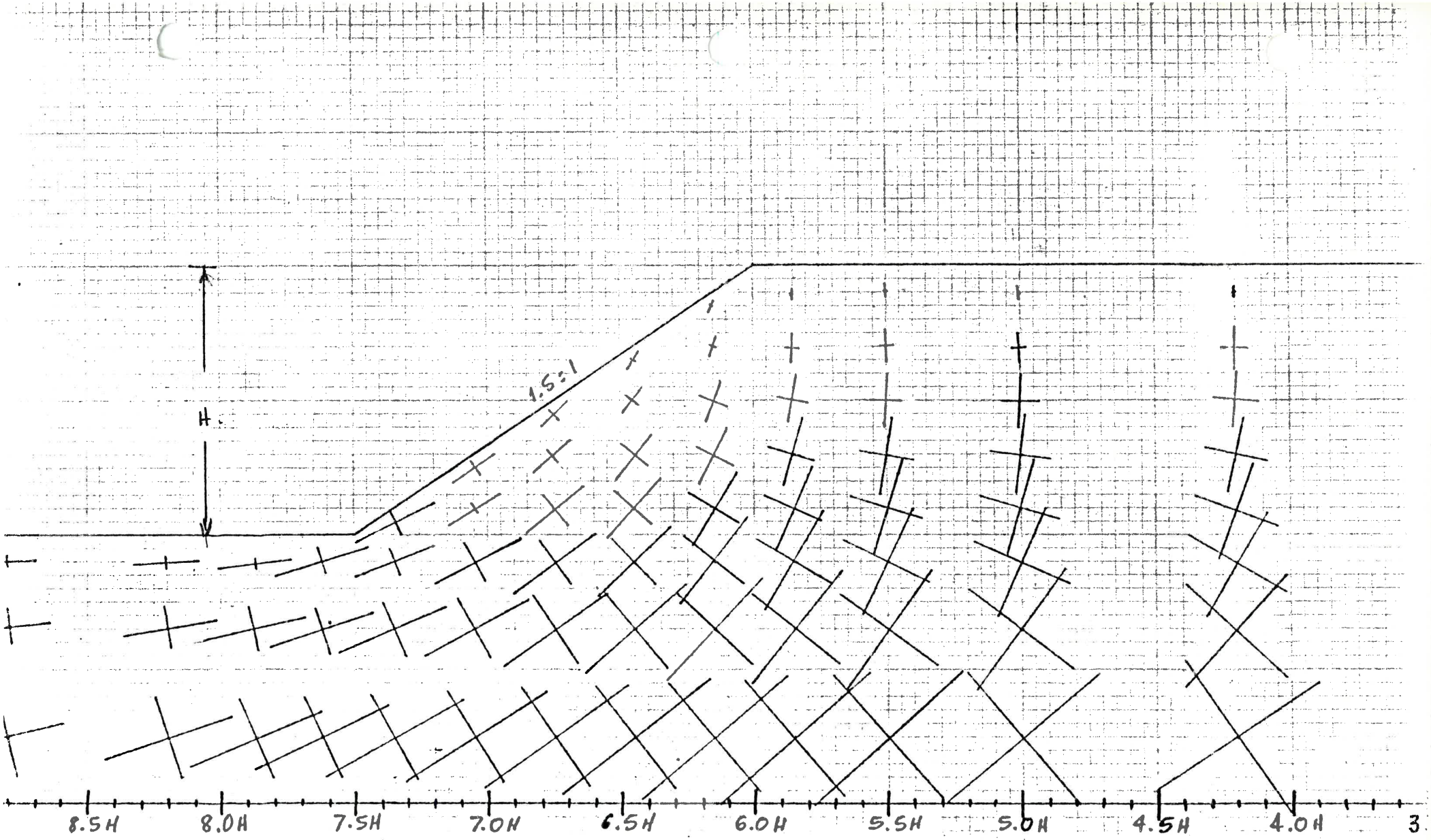


Fig. 5.2.17 Principal stress ratios for K = 1.07.

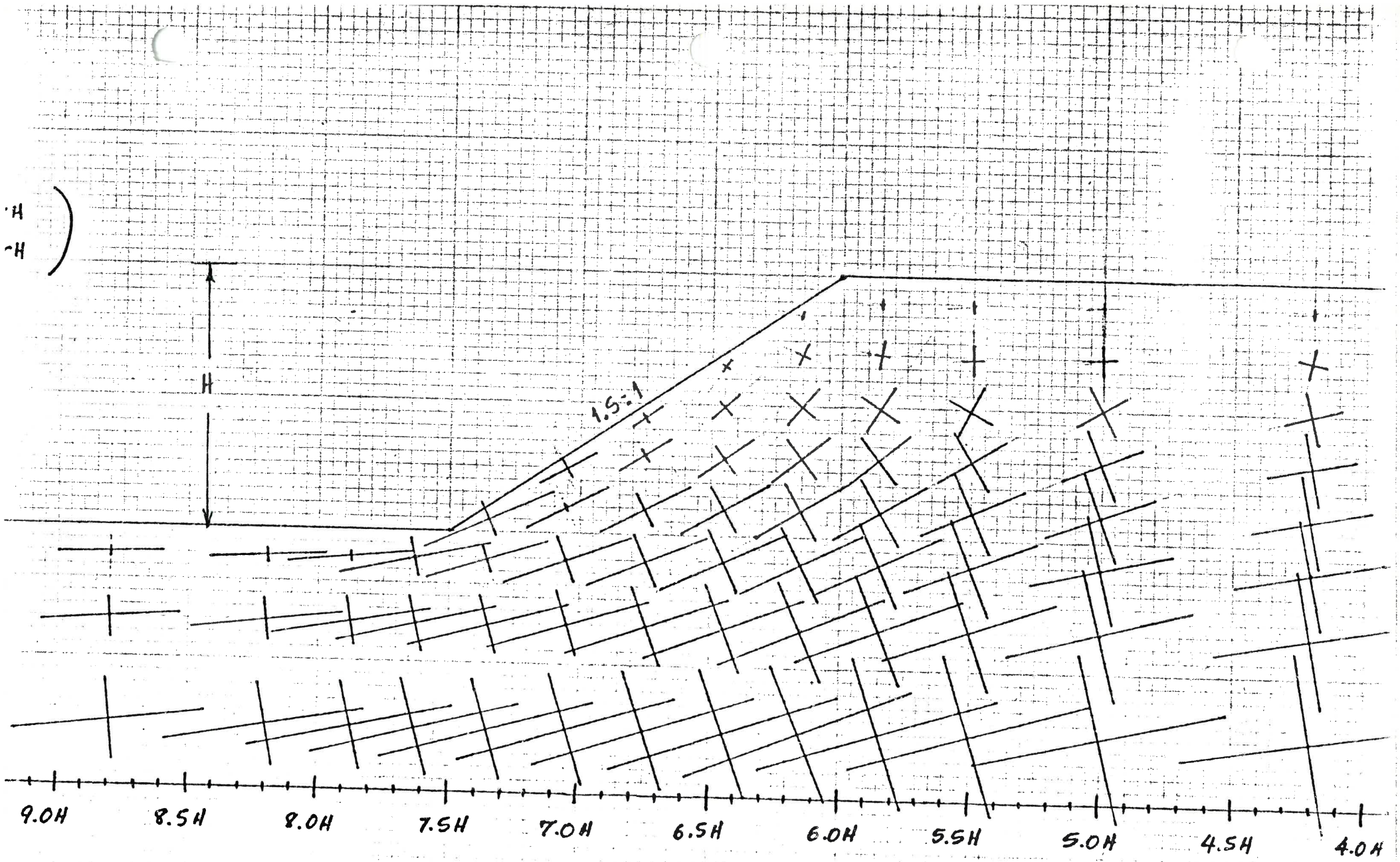


Fig. 5.2.18 Principal stress ratios for K = 1.45.

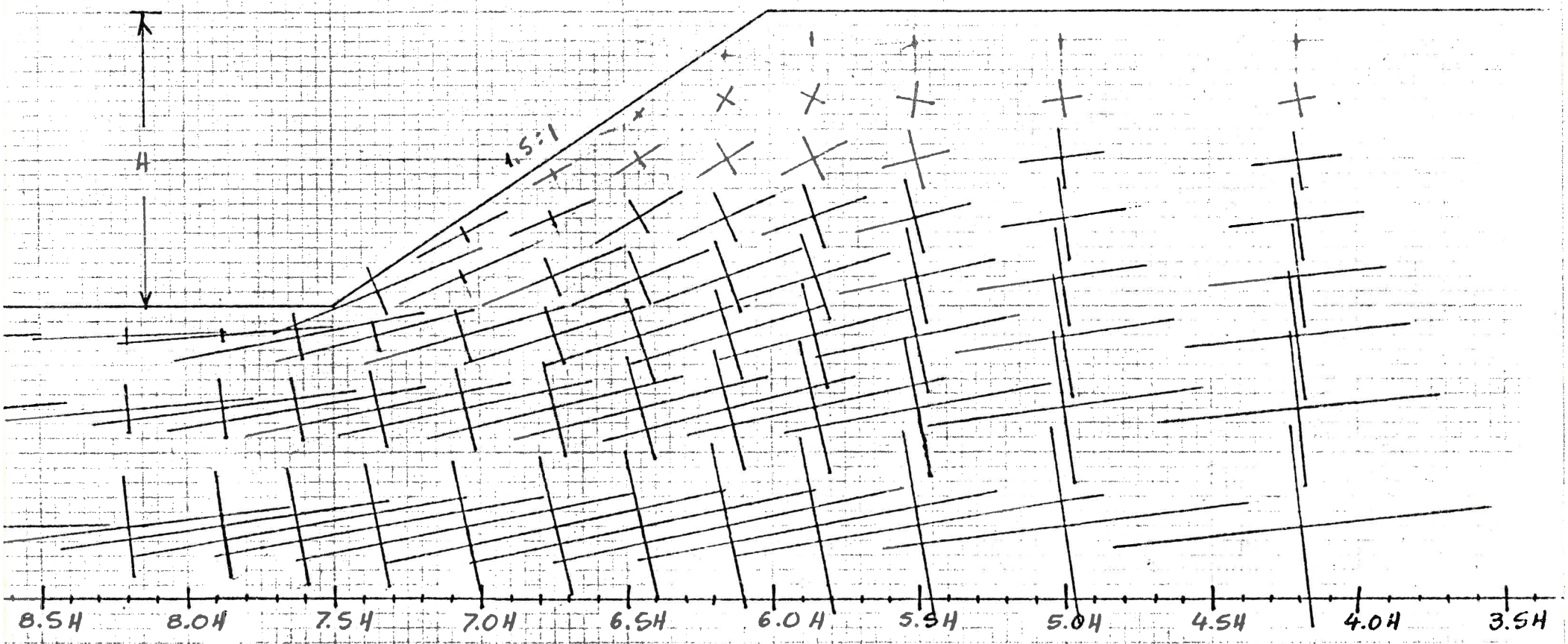


Fig. 5.2.19 Principal stress ratios for K = 1.88.

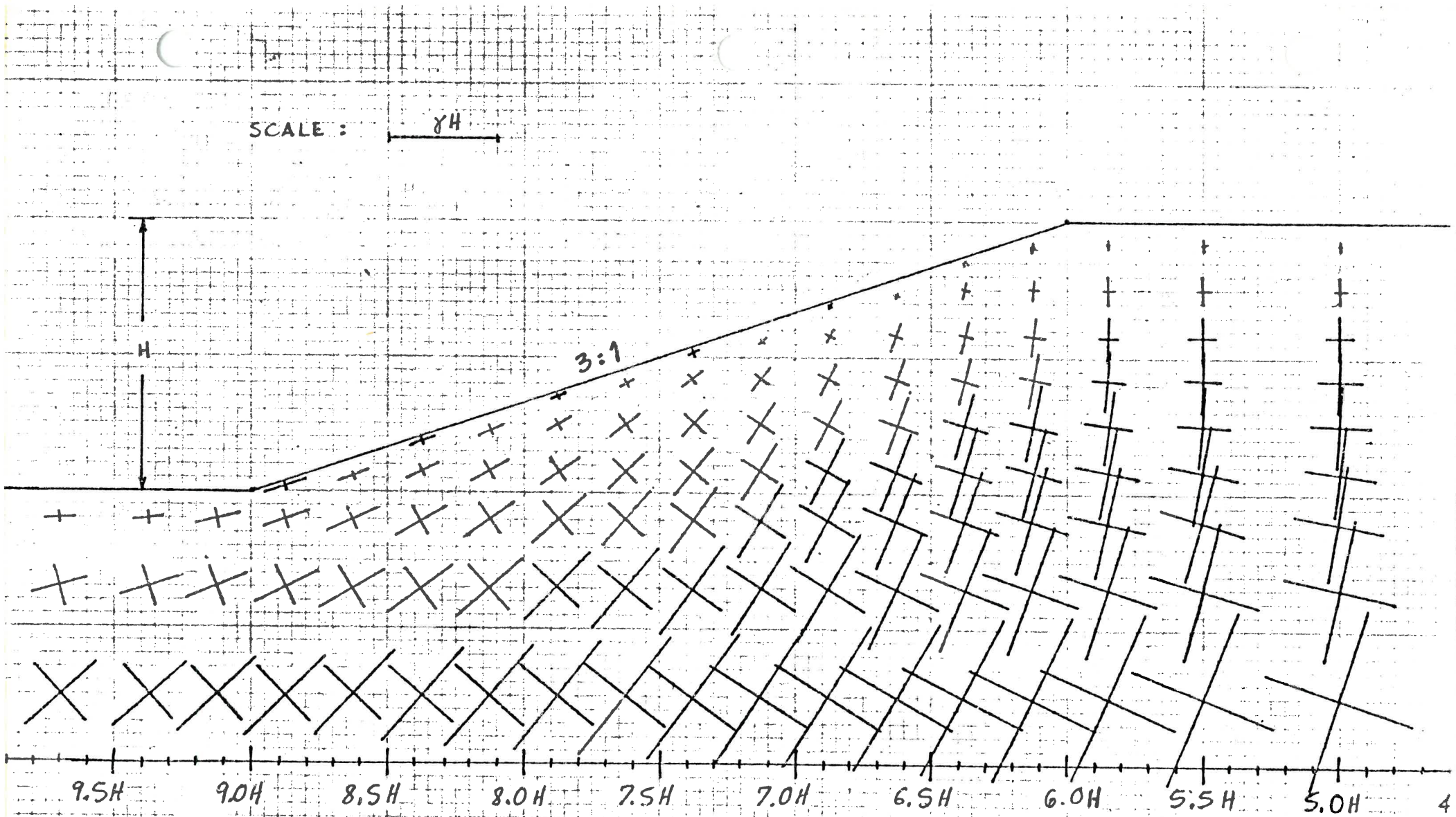


Fig. 5.2.20 Principal stress vectors for K = 0.875.

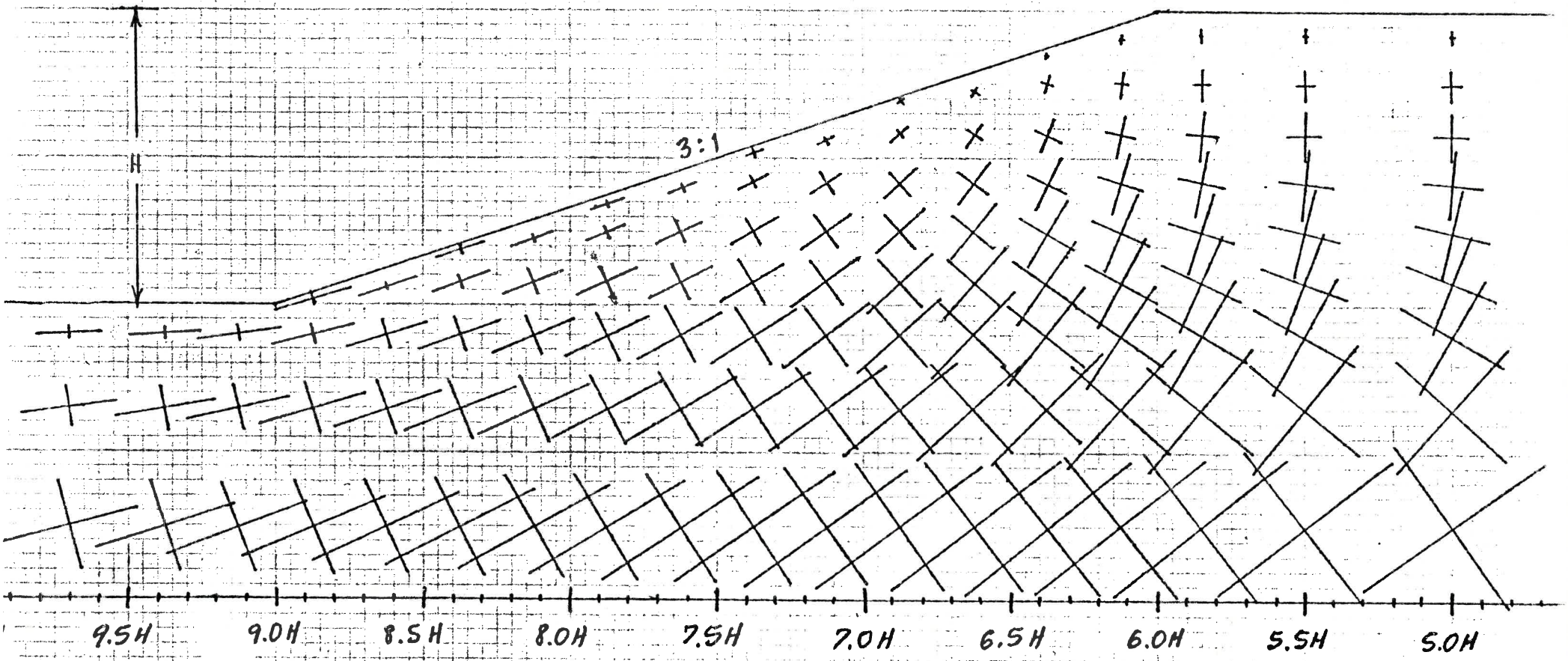


Fig. 5.2.21 Principal stress ratios for K = 1.07.

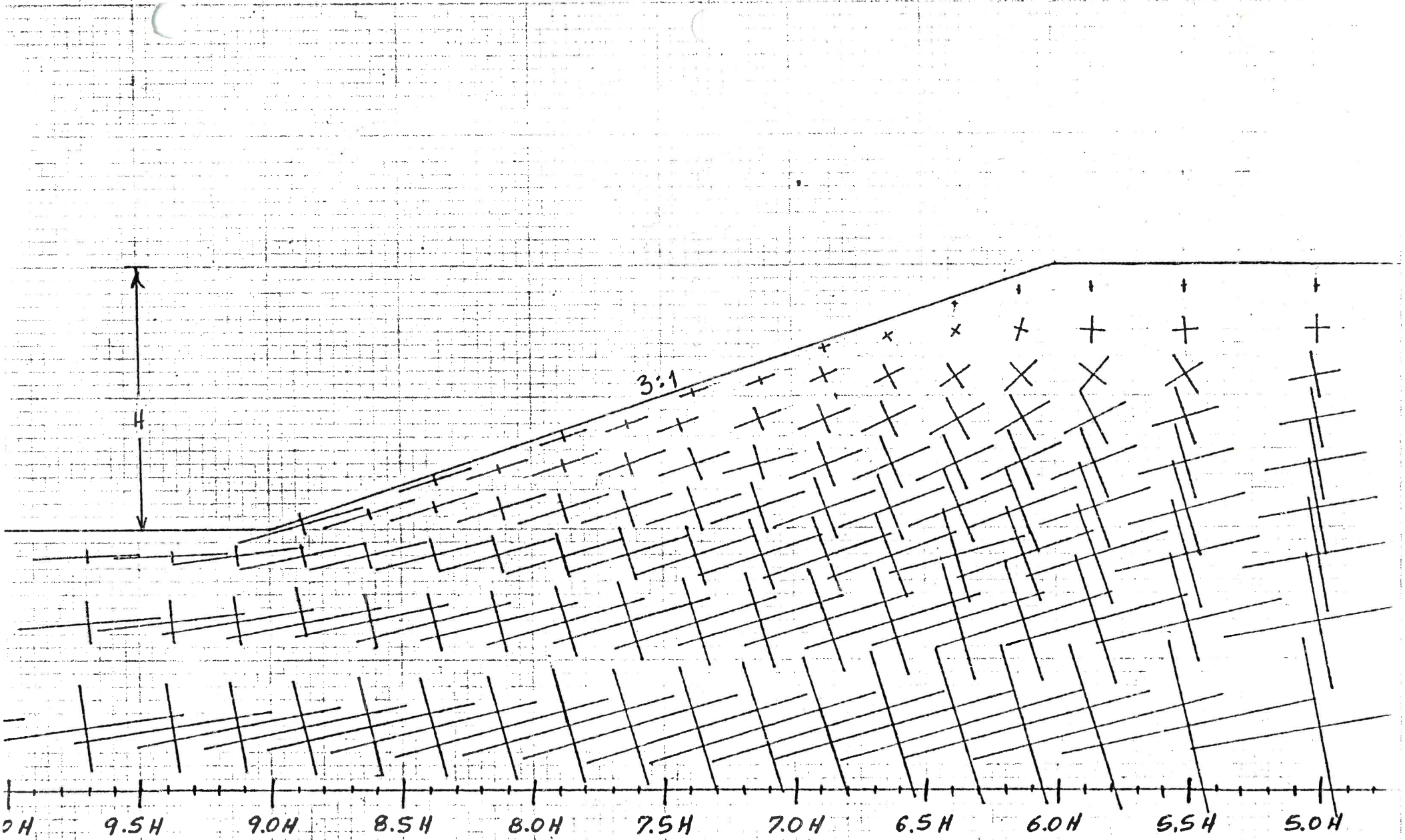


Fig. 5.2.22 Principal stress ratios for K = 1.45.

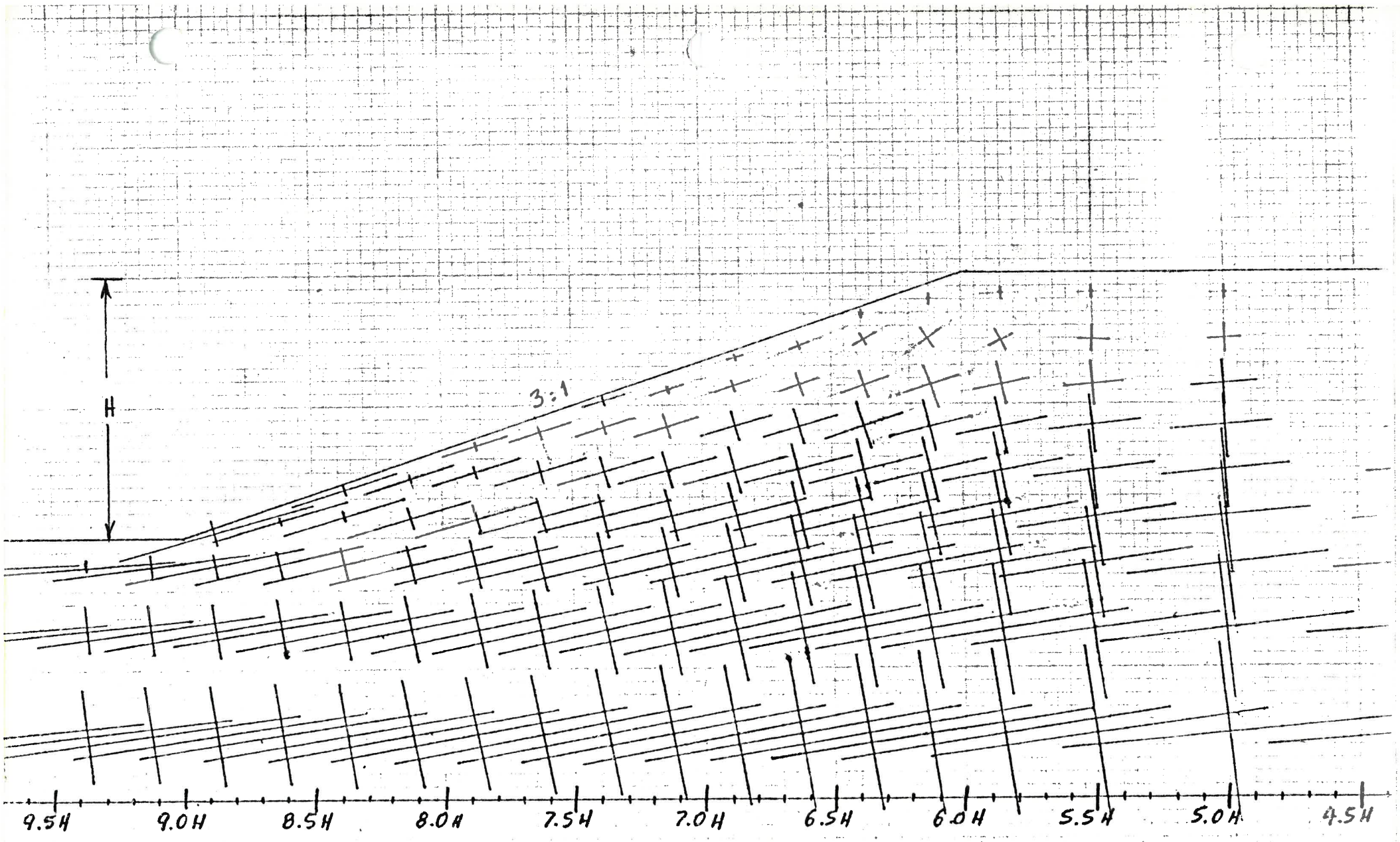


Fig. 5.2.23 Principal stress ratios for K = 1.88.

the site and H is the height of the excavation. Notice that if $\bar{p}_p$ is the precompression pressure (maximum past effective pressure that has been applied on the site), then $H_p = \bar{p}_p / \gamma$. By doing such an analysis, K does not have to be assumed the same at all depths, but it can decrease with depth, according to the overconsolidation ratio (OCR) existing at various depths. Assuming that the ground water table is very deep, OCR at depth z can be computed as follows:

$$OCR = \frac{\gamma(z+H_p)}{\gamma z} = 1 + \frac{H_p}{z} = 1 + \frac{H_p/H}{z/H} \qquad (12)$$

Hence, for a given H_p/H, the stresses before excavation at depth z are:

$$\sigma_v = \gamma z \qquad (13)$$

$$\sigma_h = K \gamma z \qquad (13a)$$

where K at depth z is a function of OCR. OCR at depth z can be computed from the expression given above and then, knowing OCR, $K=K_o$ can be obtained from the plots of Brooker and Ireland (1965) presented in Fig. 5.2.2. This way different values can be assigned to K at various depths, thus more closely approximating the actual initial state of stress at the site. Notice that if the clay is very highly overconsolidated, then H_p is much larger than all the values that z can take between 0 and 2H (which is the maximum depth for which we have analyzed) and consequently OCR will be

very large for the range between O and 2H. From the plots of Brooker and Ireland (Fig. 5.2.2) we see that K_o becomes relatively insensitive in changes of OCR, once OCR gets to be greater than 8.

We have made such an analysis, in addition to the one which assumes constant K_o with depth. The results of this analysis apply to the clay we have been using for our tests, as well as to all clays whose plasticity index is approximately equal to 40%. The way we have approached the problem is as follows:

—We first plot K_o vs. $\log_{10}(OCR)$, for PI=40%, from the data of Brooker and Ireland (1965). This plot is shown in Fig. 5.2.24.

—We then fit a curve through these points. The equation for the curve of Fig. 5.2.24 (corresponding to PI=40%) is:

$$K_o = 0.64 + 0.93\ [\log_{10}(OCR)]^{1.5} \qquad (14)$$

—Substituting OCR from equation (12) into equation (14) we get:

$$K_o = 0.64 + 0.93\ [\log_{10}(1 + \frac{H_p/H}{Z/H})]^{1.5} \qquad (15)$$

Equation (15) gives us K_o as a function of depth for a given ratio H_p/H.

—Assuming $K = K_o$, equation (15) is used in order to enter the initial stresses $\sigma_v = \gamma z$ and $\sigma_h = K\gamma z$ in the program. Actually, equation (15) has been

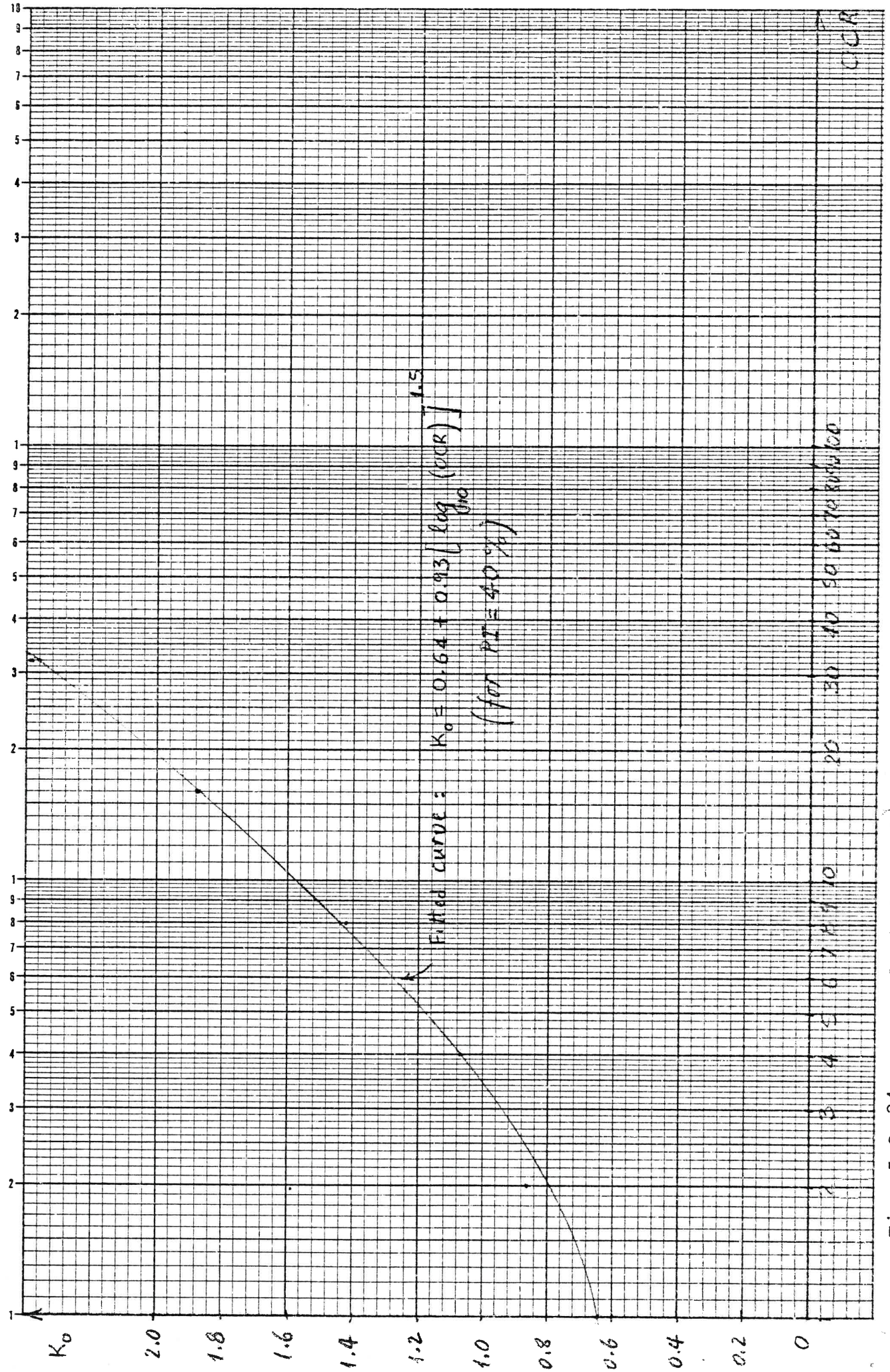


Fig. 5.2.24 K_o vs. $\log_{10}(OCR)$ for PI=40% (based on data from Brooker & Ireland, 1965).

plugged into the program and one needs only to specify in the input what H_p/H he is analyzing for. Depending on what depth an element is at (as defined by the y-coordinate of the center of the element), the program finds what is the K for that depth, by using equation (15). It subsequently finds the initial stresses σ_v and σ_h using equations (13) and (13a), where the depth z is the same as the y-coordinate of the center of the element. Using this newly defined K it is also found what are the normal and shear stress changes induced by the excavation along the bottom and the side of the cut.

Using this latter approach of variable K with depth, a 1.5:1 slope has been analyzed for six different preconsolidation pressure ratios H_p/H, namely:

H_p/H = 0.5, 1.0, 3.0, 7.0, 15.0, 31.0.

Table 5.2.6 gives $\sigma/\gamma H$ and $\tau/\gamma H$ before excavation as a function of depth ratio z/H along a plane with slope 1.5:1. Table 5.2.7 gives the shear forces RX_i/H and RZ_i/H applied on the nodes of the elements along a plane with slope 1.5:1, before excavation. In making Tables 5.2.6 and 5.2.7, the same procedure described earlier for Tables 5.2.2 and 5.2.4 has been followed. Fig. 5.2.25, 5.2.26, and 5.2.27 show the stress changes $\Delta\sigma/\gamma H$ and $\Delta\tau/\gamma H$ induced by the excavation along the side of the cut, for three different preconsolidation pressure ratios H_p/H, namely H_p/H = 0.5, 3.0, 31.0.

Table 5.2.6

Geostatic Stresses Before Excavation

Along a Line with Slope 1.5:1

z/H	$H_p/H = 0.5$		$H_p/H = 1.0$		$H_p/H = 3.0$		$H_p/H = 7.0$	
	$\sigma/\gamma H$	$\tau/\gamma H$	$\sigma/\gamma H$	$\tau/\gamma H$	$\sigma/\gamma H$	$\tau/\gamma H$	$\sigma/\gamma H$	$\tau/\gamma H$
0	0.0	0.0	0.0	0.0	0.0	0.0	0.0	0.0
0.1	0.1086	0.0128	0.1193	0.0290	0.1410	0.0616	0.1610	0.0915
0.2	0.2008	0.0012	0.2171	0.0257	0.2535	0.0802	0.2890	0.1334
0.3	0.2906	-0.0140	0.3104	0.0156	0.3580	0.0870	0.4069	0.1603
0.4	0.3796	-0.0306	0.4016	0.0024	0.4583	0.0874	0.5190	0.1784
0.5	0.4682	-0.0476	0.4918	-0.0123	0.5558	0.0837	0.6271	0.1907
0.6	0.5567	-0.0649	0.5813	-0.0281	0.6514	0.0771	0.7323	0.1985
0.7	0.6451	-0.0823	0.6704	-0.0444	0.7456	0.0684	0.8353	0.2030
0.8	0.7335	-0.0997	0.7592	-0.0612	0.8388	0.0582	0.9365	0.2048
0.9	0.8220	-0.1171	0.8479	-0.0781	0.9312	0.0468	1.0363	0.2044
1.0	0.9104	-0.1344	0.9365	-0.0953	1.0229	0.0344	1.1348	0.2022

Table 5.2.6 (continued)

Geostatic Stresses Before Excavation

Along a Line with Slope 1.5:1

z/H	$H_p/H = 15.0$		$H_p/H = 31.0$	
	$\sigma/\gamma H$	$\tau/\gamma H$	$\sigma/\gamma H$	$\tau/\gamma H$
0	0	0	0	0
0.1	0.1810	0.1214	0.2015	0.1523
0.2	0.3255	0.1882	0.3637	0.2456
0.3	0.4583	0.2375	0.5129	0.3194
0.4	0.5842	0.2763	0.6543	0.3814
0.5	0.7052	0.3078	0.7899	0.4349
0.6	0.8225	0.3338	0.9214	0.4820
0.7	0.9369	0.3554	1.0493	0.5240
0.8	1.0490	0.3735	1.1744	0.5616
0.9	1.1590	0.3885	1.2971	0.5956
1.0	1.2673	0.4010	1.4176	0.6265

Table 5.2.7

Shear Forces Applied on the Nodes Along the Slope—Slope M:1-H_{AB} = 0.2H, M=1.5

NODE	z/H	$H_p/H = 0.50$		$H_p/H = 1.0$		$H_p/H = 3.0$		$H_p/H = 7.0$	
		RX_i/H $\times 10^2$	RZ_i/H $\times 10^2$	RX_i/H $\times 10^2$	RZ_i/H $\times 10^2$	RX_i/H $\times 10^2$	RZ_i/H $\times 10^2$	RX_i/H $\times 10^2$	RZ_i/H $\times 10^2$
51	0	0.0046	0.0031	0.0964	0.0642	0.3007	0.2005	0.5004	0.3336
43	0.2	0.0366	0.0244	0.7709	0.5139	2.4060	1.6040	4.0032	2.6688
36	0.4	-0.9173	-0.6115	0.0732	0.0488	2.6213	1.7476	5.3534	3.5689
30	0.6	-1.9473	-1.2982	-0.8428	-0.5619	2.3127	1.5418	5.9552	3.9701
25	0.8	-2.9903	-1.9935	-1.8346	-1.2231	1.7467	1.1645	6.1444	4.0963
21	1.0	-1.8862	-1.2575	-1.3010	-0.8673	0.6049	0.4033	3.0430	2.0287

$$RX_i = \frac{\tau_i}{\gamma H} m H_{AB} \rightarrow \frac{RX_i}{H} = \frac{\tau_i}{\gamma H} m \frac{H_{AB}}{H} \qquad (1)$$

$$RZ_i = \frac{\tau_i}{\gamma H} H_{AB} \rightarrow \frac{RZ_i}{H} = \frac{\tau_i}{\gamma H} \frac{H_{AB}}{H} \qquad (2)$$

Node 51 : Instead of $\frac{\tau_{51}}{\gamma H}$, use $\frac{\tau_{43}}{8\gamma H}$ in expressions (1) & (2).

Node 21 : Instead of $\frac{\tau_{21}}{\gamma H}$, use $\frac{3\tau_{21} + \tau_{25}}{8\gamma H}$ in expressions (1) & (2).

Table 5.2.7 (continued)

Shear Forces Applied on the Nodes Along the Slope—Slope M:1-H_{AB} = 0.2H, M =1.5

NODE	Z/H	$H_P/H = 15.0$		$H_P/H = 31.0$	
		RX_i/H $\times 10^2$	RZ_i/H $\times 10^2$	RX_i/H $\times 10^2$	RZ_i/H $\times 10^2$
51	0	0.7058	0.4705	0.9209	0.6140
43	0.2	5.6460	3.7640	7.3675	4.9117
36	0.4	8.2888	5.5259	11.4413	7.6275
30	0.6	10.0135	6.6757	14.4609	9.6406
25	0.8	11.2035	7.4690	16.8482	11.2321
21	1.0	5.9116	3.9411	9.1537	6.1025

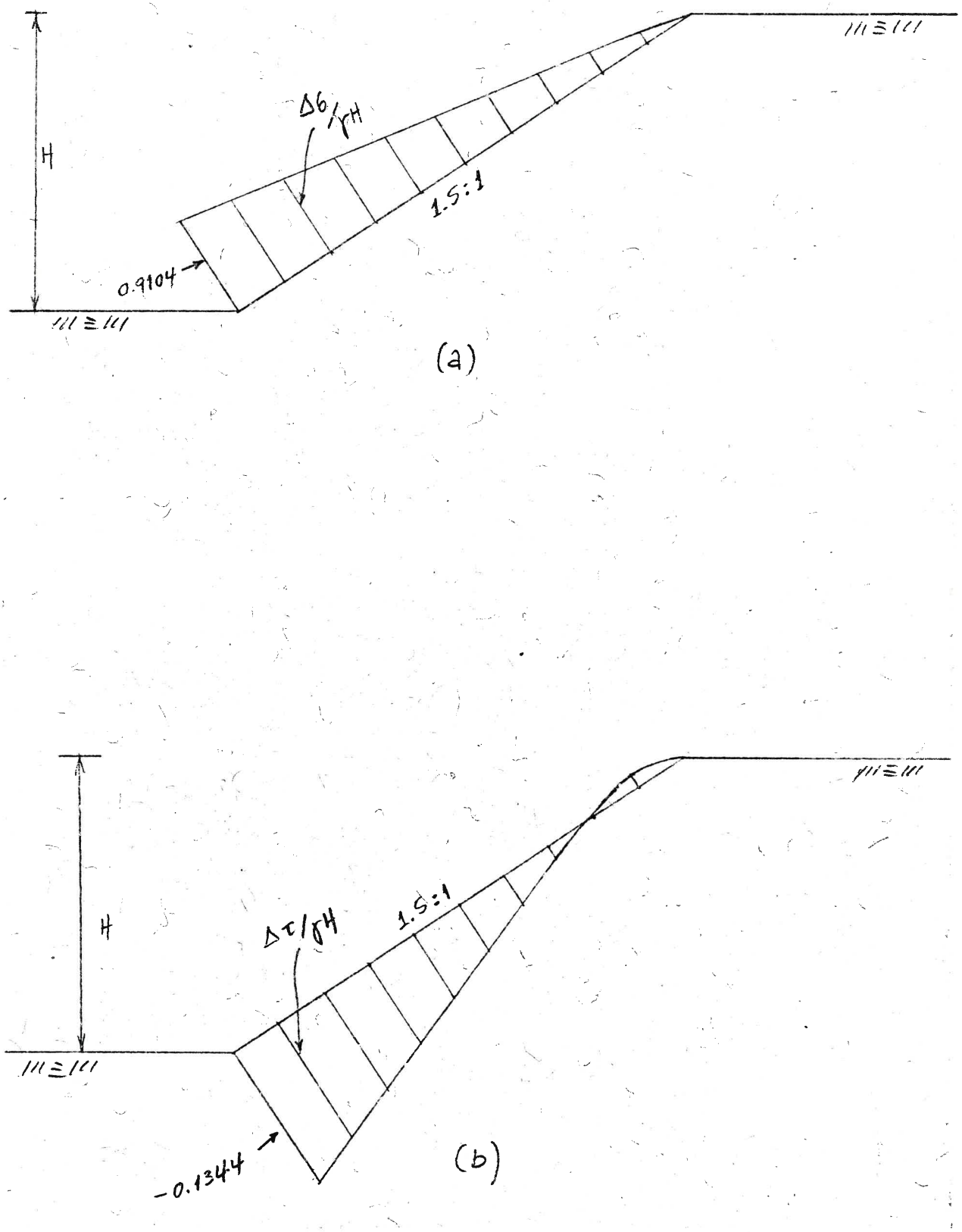


Fig. 5.2.25 Distribution of $\Delta\sigma/\gamma H$ and $\Delta\tau/\gamma H$ for $\frac{Hp}{H} = 0.5$.

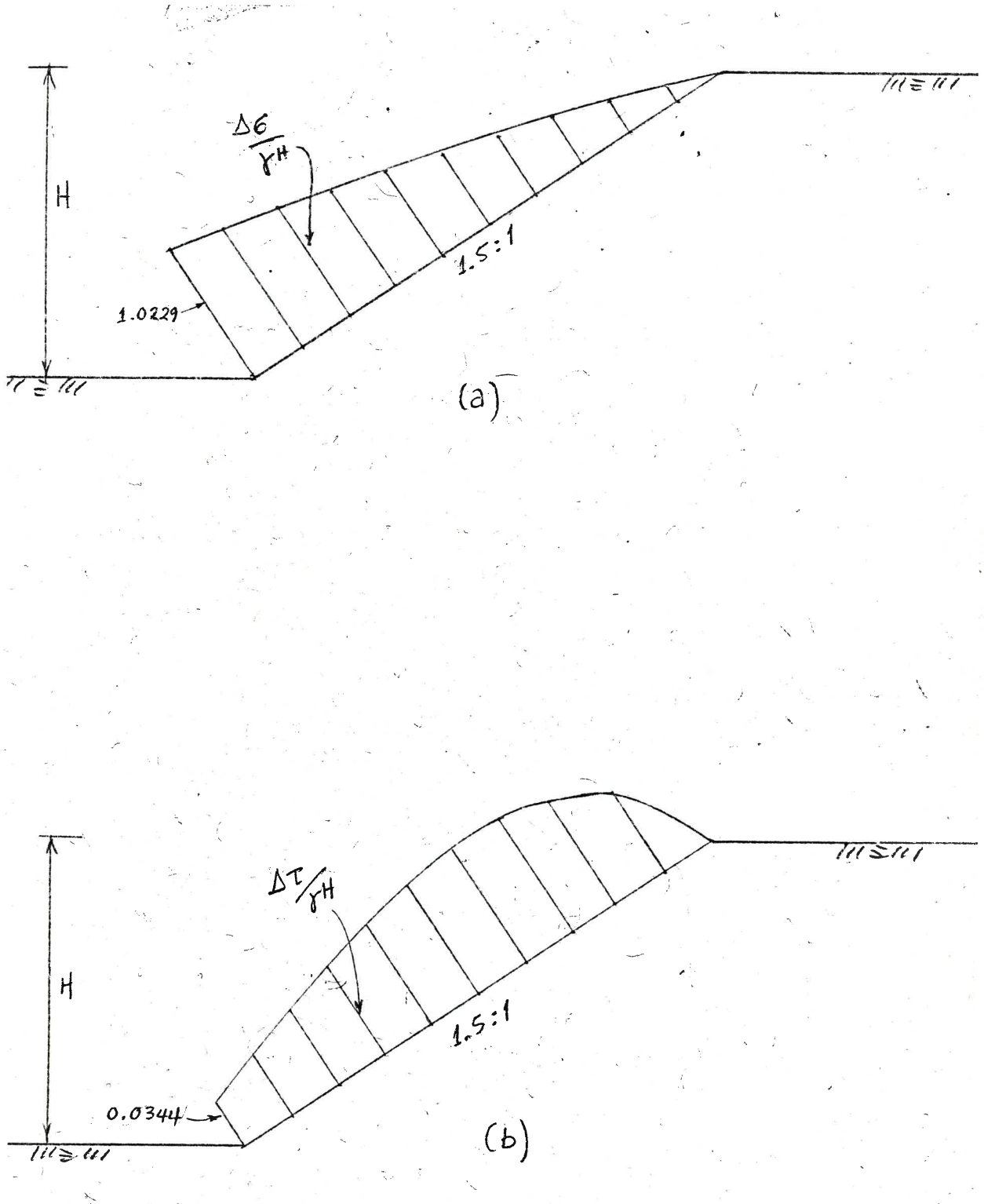


Fig. 5.2.26 Distributions of $\Delta\sigma/\gamma H$ and $\Delta\tau/\gamma H$ for $\frac{Hp}{H}$ = 3.0.

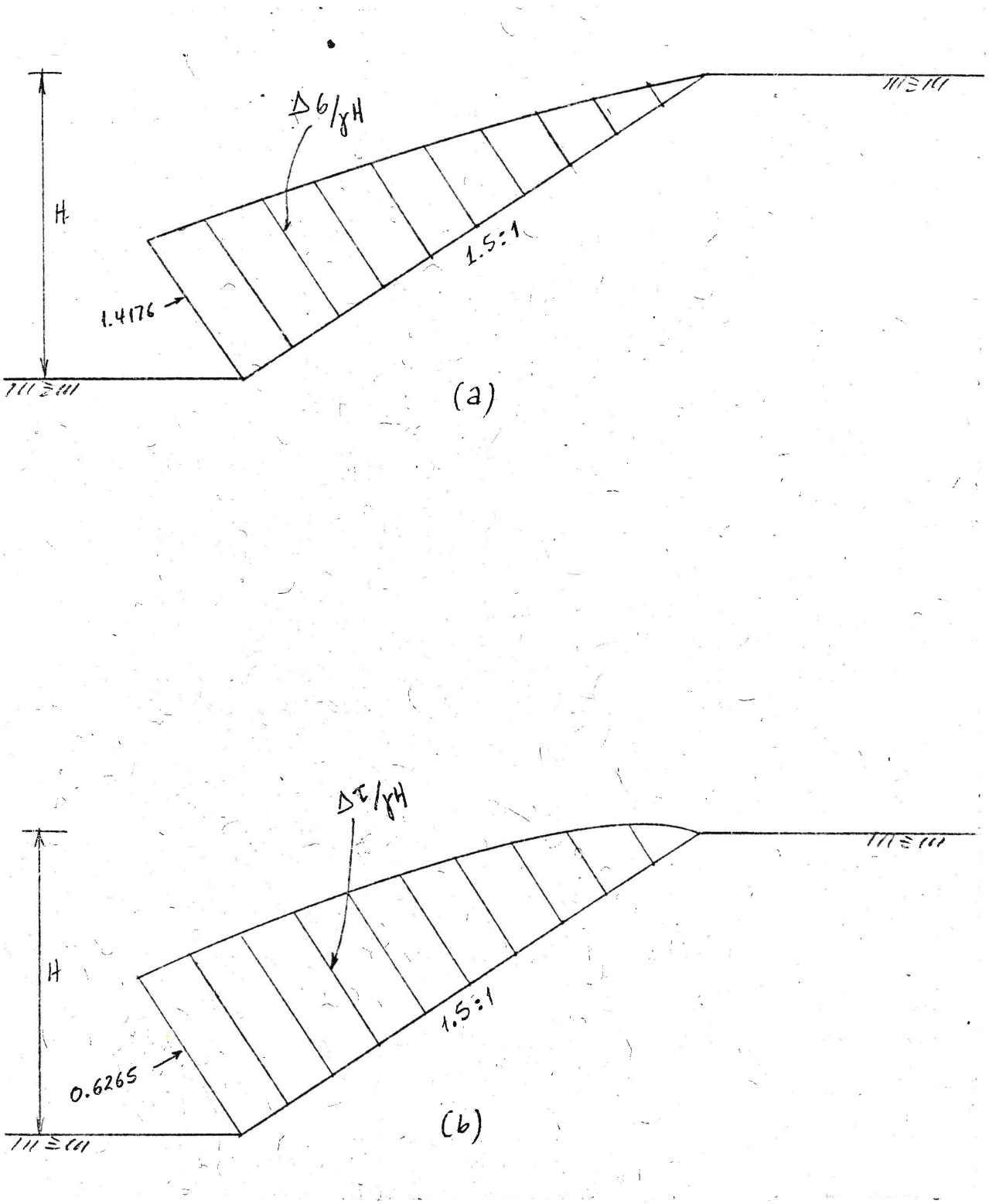


Fig. 5.2. 27 Distributions of $\Delta\sigma/\gamma H$ and $\Delta\tau/\gamma H$ for $\frac{Hp}{H}$ = 31.0.

Notice that the distribution of $\Delta\sigma/\gamma H$ with depth remains almost linear and triangular, as it was under the assumption of constant K. However, the distribution of $\Delta\tau/\gamma H$ with depth is no longer linear and it also changes sign for small preconsolidation pressure ratios (see for example Fig. 5.2.25). Notice also that as the preconsolidation pressure gets high (for example $H_p/H = 31$) the $\Delta\tau/\gamma H$ distribution tends to become triangular and linear, i.e., similar to the distribution of $\Delta\tau/\gamma H$ which is obtained by assuming the same value of K everywhere. This is consistent with the remark made earlier, namely that the assumption of constant K is not very bad in cases of high overconsolidation ratios, because the value of K_o becomes relatively insensitive for changes of OCR in the range of high OCR values.

By comparing the results of the two analyses it is found that both give reasonably close values for the magnitudes of the principal stresses after excavation, at a certain depth z, provided that the comparison is made for the appropriate values of K and H_p/H. By that it is meant that, if the depth of the element is z, then the appropriate K is the one corresponding to $OCR = \bar{p}_p/\gamma z$, while the appropriate H_p/H is: $H_p/H = (OCR-1)\cdot\frac{z}{H} = \left(\frac{\bar{p}_p}{\gamma z} - 1\right)$. However, the directions of the principal stresses in the K = constant analysis are not concentrated as much around $\theta = 45°$ as they are in the H_p/H = constant analysis.

5.3 Summary

A finite element analysis of the stress changes induced by an excavation behind a slope has been made and has been presented in this chapter. The analysis has been performed on a homogeneous, linearly elastic, isotropic material. The results are considered to be good for stress magnitudes and orientations so long as the stresses are lower than the peak. Two types of analysis have been performed:

—The coefficient of total earth pressure at rest, K, is assumed to be the same everywhere behind the slope.

—The preconsolidation pressure ratio, H_p/H, is assumed to be constant for a given site and K varies with depth according to an empirical relationship.

The results of the finite element analysis serve several purposes:

—They give a qualitative picture of the effect of OCR and cut slope on the magnitudes and directions of principal stresses after excavation.

—They help in the determination of the TSP for any soil element behind the excavated slope.

—They provide information about the stress distribution along any potential failure surface.

6. TESTING PROGRAM

6.1 General

As it was mentioned earlier (Chapter 4), one needs to run stress path tests on samples obtained from locations behind a slope corresponding to those which were selected in step 2 of the stress path method algorithm. It was noted in section 4.2 that one can either use undisturbed samples to run the stress path tests or reconstituted samples. It has been chosen to run the stress path tests on reconstituted samples from the Friars Formation basically for two reasons:

—Most of the samples that were available were bag camples. The only undisturbed sample available was a box sample from Rancho Bernardo, but that sample alone would not be enough to trim an adequate number of samples to run all the tests that had been planned for, especially considering the fact that the sample was very fissured and consequently an appreciable quantity of it would be spoiled just by trying to trim small vertical and inclined samples to run the stress path tests.

—It was desired to test samples which would be uniform and almost identical among them in all respects (composition, structure, void ratio, etc.), so that any differences in strength and behavior

obtained would not be attributed to any differences among the samples themselves.

As it will be explained in more detail in the next section, a serious disadvantage of the chosen approach was that it was impossible to reproduce the original sample in the laboratory, both in terms of preconsolidation pressure and in terms of structure. However, it was still possible to draw conclusions of general applicability since two different testing approaches were being compared. Of course, depending on what kind of samples one uses to compare the two approahces, the differences may be more or less pronounced. Such a study, where different kinds of samples are tested in conventional triaxial tests and stress path tests, would have as its objective to reveal the differences in strength and behavior occurring as a result of the testing approach for various types of soils. Such an extensive study was deemed outside the scope of this project and it was not pursued. Consequently, our conclusions apply to non-fissured, very plastic, lightly to medium overconsolidated clays.

The preparation of the reconstituted samples together with some classification tests that were performed are described in the following Section 6.2, while the stress path tests are described and their results are presented and discussed in Section 6.3.

Among other things, one of the objectives of this project was the measurement of the residual strength of the Friars Formation claystone. In order to select the type of test that should be used to measure the residual strength, all the methods available for such a measurement had to be compared. A critical presentation of the available testing techniques for measuring the residual strength in the laboratory is given in Section 6.4. Section 6.5 on the other hand deals in more detail with the particular testing technique we decided to use. In the same section the results of these tests are presented and discussed.

6.2 Sample Preparation

As it was mentioned in the previous paragraph, it was decided that the stress path tests would be run on reconstituted samples. However, a problem that was faced right from the beginning was the fact that the original sample was so stiff that remolding it was practically impossible. For this reason a different procedure was followed in preparing reconstituted samples. The original sample was first air-dried for several hours, until its water content dropped to about 10%, it was then broken down into small particles (Fig. 6.2.1) by crushing it through a series of crushers and it was subsequently mixed thoroughly with distilled water (Fig. 6.2.2) forming thus a slurry of 80% water content (Fig. 6.2.3) (the liquid limit

of the crushed soil was 63%). It should be mentioned here that air-drying the original sample resulted in an increase of both its liquid limit (LL) and its plasticity index (PI), while its plastic limit (PL) remained almost the same. The Atterberg limits of the original sample were:

LL = 52%, PL = 26%, PI = 26%,

while for the air-dried sample they were:

LL = 63%, PL = 25%, PI = 38%.

Similar observations on O.C. plastic clays have been made by Bjerrum (1966), who for example reports that the Atterberg limits of Little Belt Clay were changed from LL = 178%, PL = 46%, PI = 132% for the original moist sample, to LL = 205%, PL = 52%, PI = 156% for the air-dried sample. According to Bjerrum (1966), there are groups of particles bonded together so strongly that even the powerful agents of weathering have been unable to separate them. However, according to A. Casagrande (1949), if the sample is first dried in air and then soaked in water, an almost explosive disintegration occurs as a result of the capillary forces and this will cause a substantial increase in the liquid limit. Conversely, oven drying leads to a baking together of the particles leading to liquid limits smaller than the value determined on the untreated clay. It should be pointed out here that the PI that has been used in the calculations (e.g., for estimating K_o; see Chapter 5) was not the one corresponding to the original sample, but the

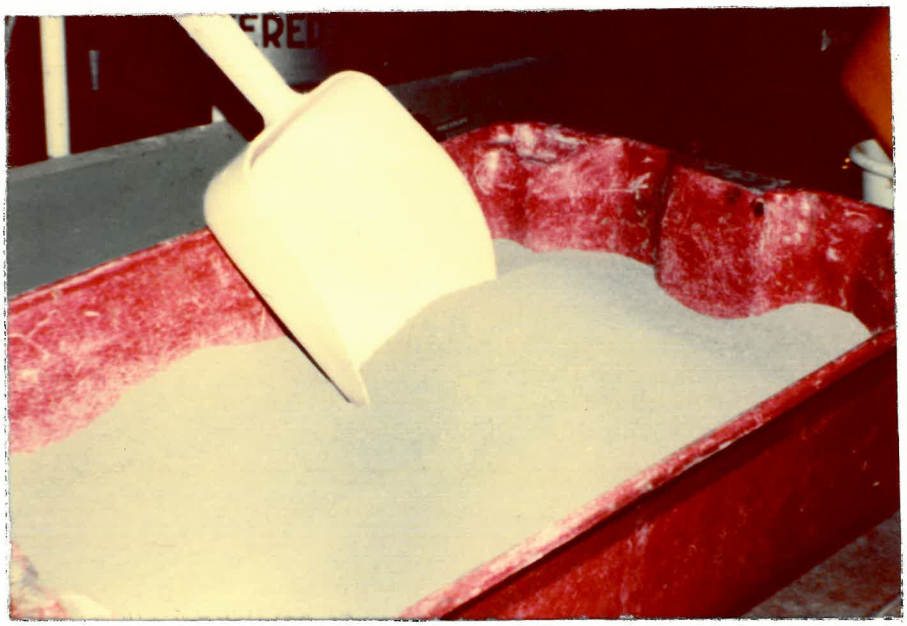


Fig. 6.2.1 Crushed sample, after air-drying.



Fig. 6.2.2 Mixing crushed soil with distilled water.

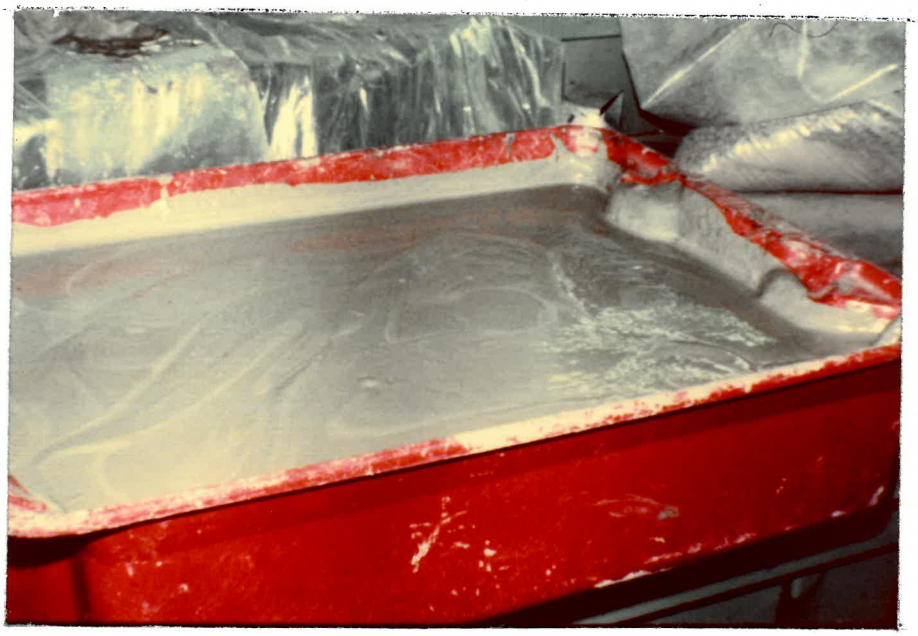


Fig. 6.2.3 Slurry of 80% water content (just before it was poured into the consolidation chamber).

one corresponding to the air-dried sample. In fact, the number has been rounded to 40% for calculation purposes.

After the slurry had been prepared, as described previously, it was poured into a stainless steel consolidation chamber 12 inches in diameter by 10 inches high (Fig. 6.2.4, 6.2.5, 6.2.6) and it was consolidated for 132 days under incrementally higher consolidation pressures: 0.25, 0.50, 1.00, 2.00, 4.00, 8.00 Kg/cm^2. The whole set up for the consolidation of the slurry is schematically shown in Fig. 6.2.7 (see also Fig. 6.2.8), while Fig. 6.2.9 gives a detail of the consolidation chamber. The pressure was applied by a piston which was forced upwards by air pressure, supplied through a pump. The pump was used in order to raise the house pressure from 7.04 Kg/cm^2 (100psi) to a maximum of 8 Kg/cm^2.

The purpose of making a slurry out of the original sample and consolidating it into the consolidation chamber has been to simulate the geologic history of the clay, i.e., deposition and subsequent consolidation under the overburden pressure. The simulation of the geologic history of the clay in the laboratory, however, is not perfect, because the clay has been consolidated in the field for thousands of years and has undergone a considerable amount of secondary compression. In addition, chemical alterations have taken place during that long period of time, as it was explained in Section 3.4. Notice that the slurry has

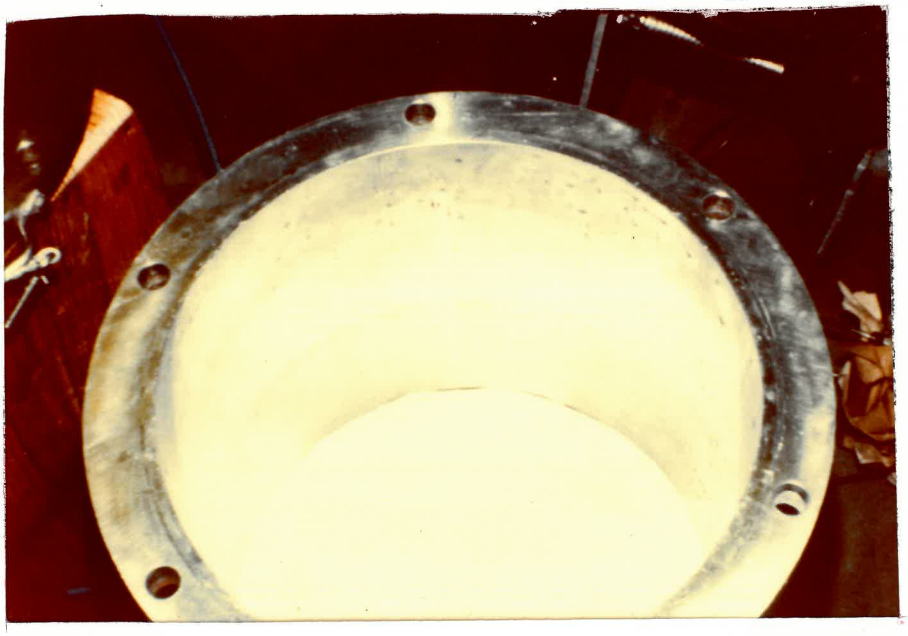


Fig. 6.2.4 Interior of consolidation chamber.



Fig. 6.2.5 Slurry already poured into consolidation chamber.

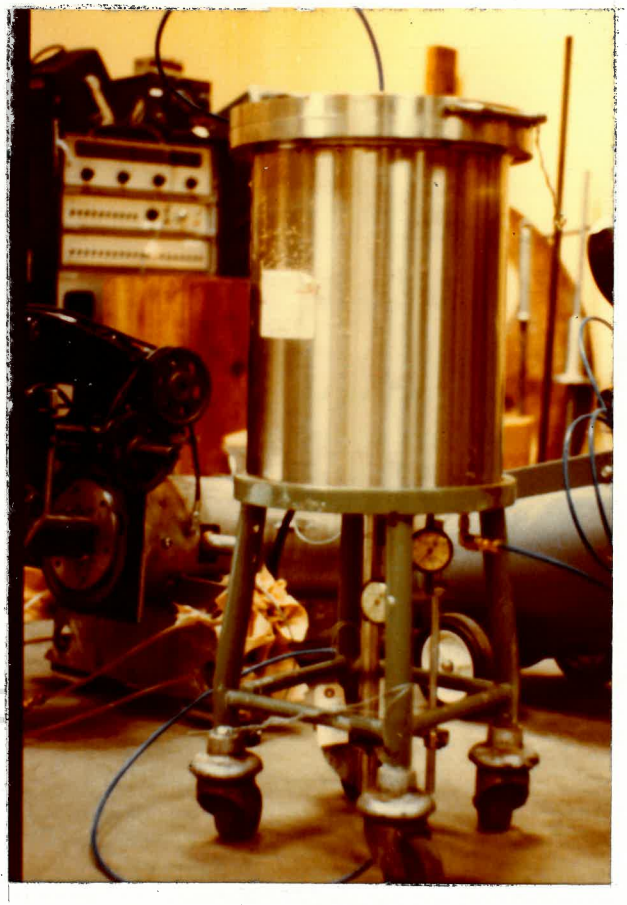


Fig. 6.2.6 Consolidation chamber.

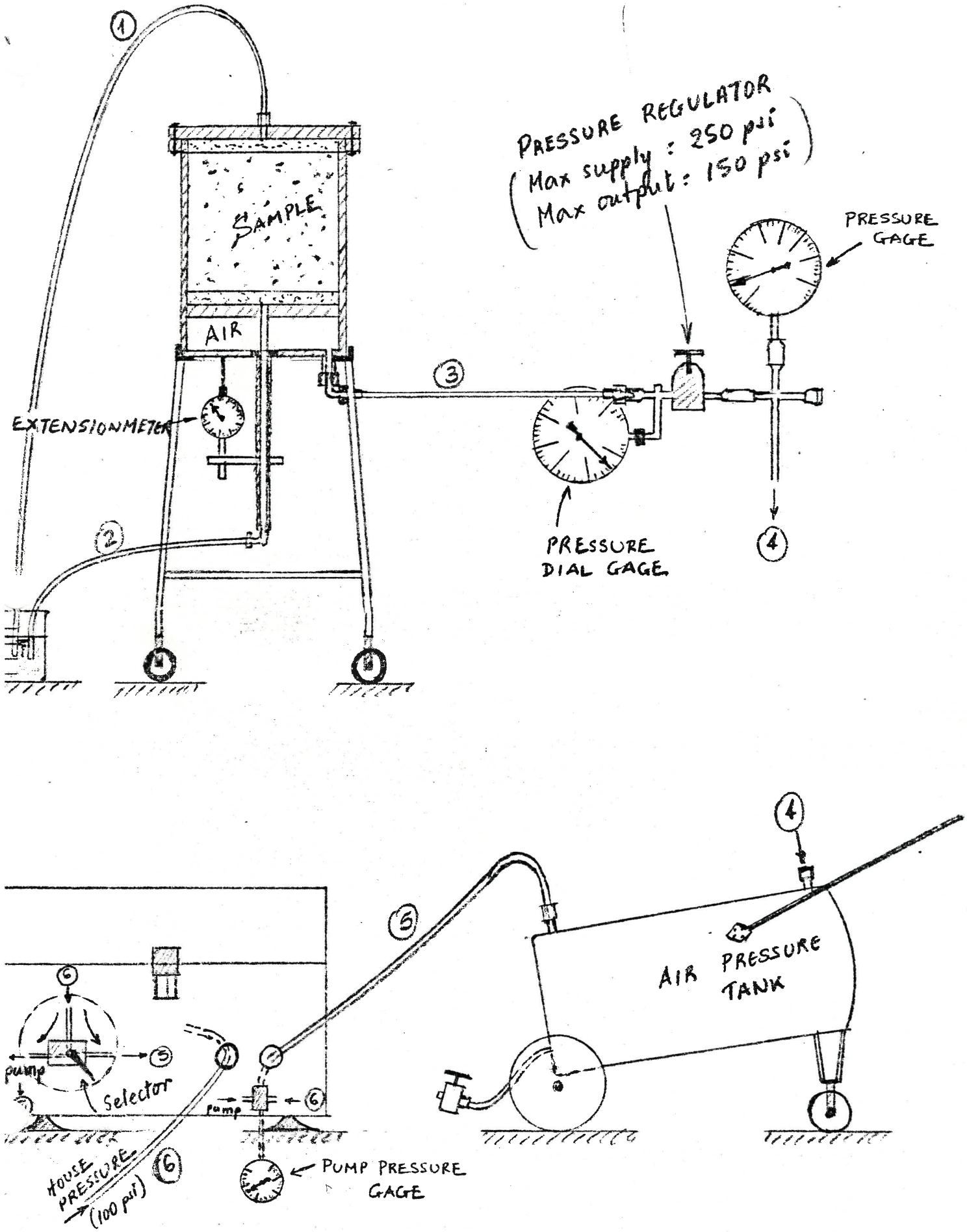


Fig. 6.2.7 Schematic representation of consolidation set up (not in scale)

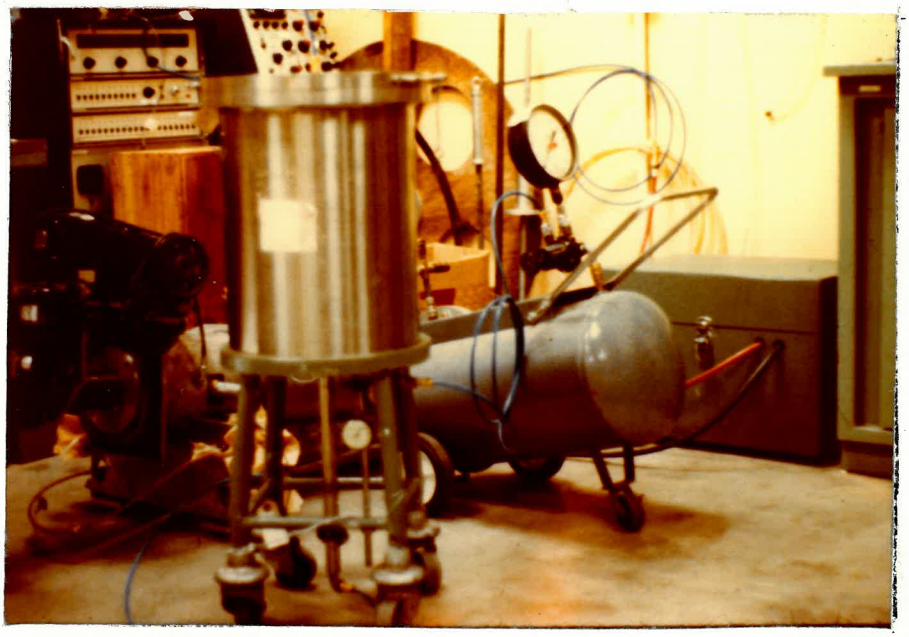


Fig. 6.2.8. Set up for the consolidation of the slurry.

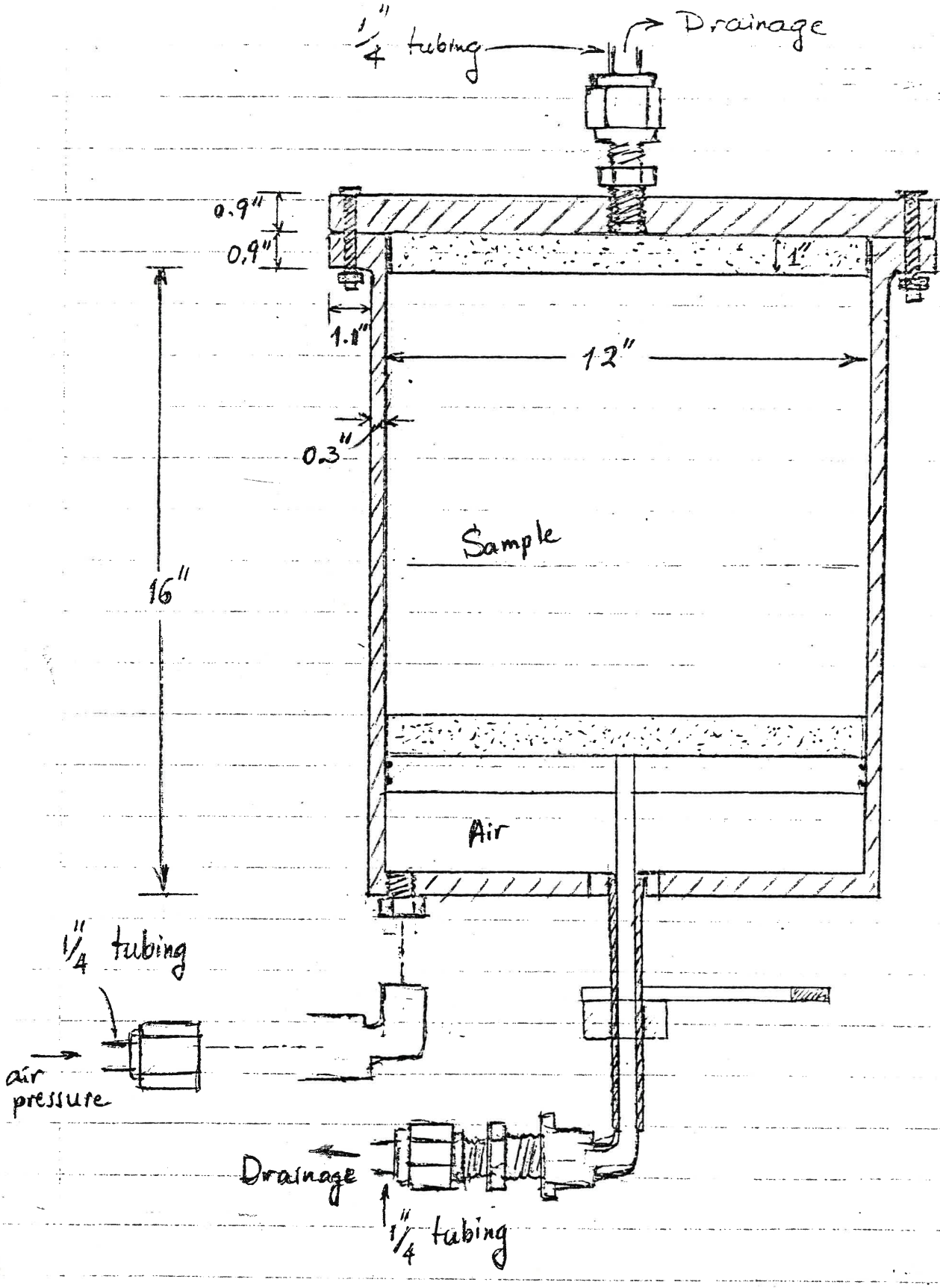


Fig. 6.2.9 Detail of consolidation chamber.

been consolidated for a quite long period of time, so that at least part of the secondary compression can take place.

At this stage of the preparation of the reconstituted samples, the problem was encountered that, due to several limitations of the apparatus, the application of as high consolidation pressures as the clay had felt in the field in its geologic history was not possible. Such limitations were:

—The air pressure regulator's maximum output was 150 psi (10.56 Kg/cm^2).

—The tubing could withstand a maximum of 200 psi (14.07 Kg/cm^2).

—The consolidation chamber had been designed for a maximum of approximately 12 Kg/cm^2.

Due to these limitations, we were forced to apply a maximum consolidation pressure of 8 Kg/cm^2, which is considerably lower than the effective preconsolidation pressure of the original sample. The latter has been estimated to be approximately 29 Kg/cm^2. This estimation was based on the e-logp curve (shown in Fig. 6.2.10), obtained from the consolidation of the slurry, and on the water content of the original sample. In the above, e is the void ratio of the sample at an effective consolidation pressure p. The estimation of the preconsolidation pressure was made as follows:

—The virgin compression part of the e-logp curve was first extended to the higher consolidation

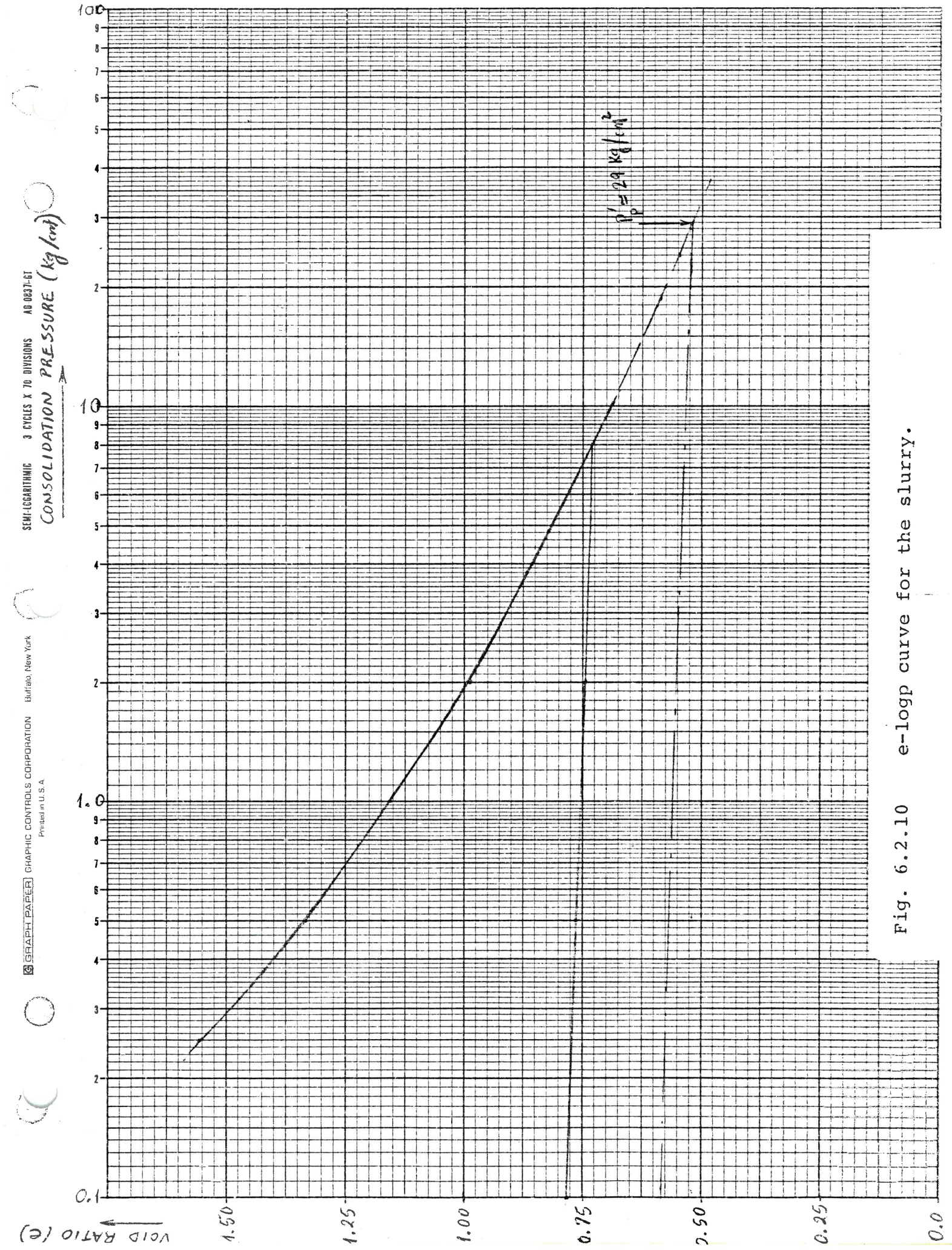


Fig. 6.2.10 e-logp curve for the slurry.

pressures (above 8 Kg/cm^2).

—Second, it was assumed that the original sample was saturated and that it came from a very shallow depth.

—Having the water content of the original sample (20.3%) and using the previous assumption, a point on the rebound curve of the original sample was obtained at the low consolidation pressures (it is reminded here that $e = wG_s$, for a saturated sample, where w is the water content of the sample and G_s is the specific gravity of the solids).

—Using the slope of the rebound curve (see Fig. 6.210), obtained by rebounding the slurry from 8 Kg/cm^2 to 0.10 Kg/cm^2, with 31 days, in 3 steps (8→2, 2→0.50, 0.50→0.10 Kg/cm^2), a rebound curve for the original sample was drawn, starting from the point at the low consolidation pressures, obtained as described above. The rebound curve for the original sample intersects the extension of the virgin compression curve at a point corresponding to a consolidation pressure of 29 Kg/cm^2. This has been taken as a first approximation of the preconsolidation pressure of the original sample.

It should be emphasized here that this is only a crude approximation, since the position of the virgin

compression curve depends substantially on the amount of secondary compression that has taken place and which is of course smaller in the consolidation process of the slurry than in the consolidation process of the clay deposit. In addition, the slopes of the rebound curves of the slurry and original sample are not necessarily the same. According to Bjerrum (1966) the slope of the rebound curve depends a lot on the diagenetic bonds that have been formed with time and the stronger the diagenetic bonds, the smaller the amount of swelling for the same decrease in effective consolidation pressure.

The settlement-log(time) curves both for the consolidation and the rebound phases of the slurry are presented in Appendix 1. Fig. 6.2.11 presents the c_v-logp curve, where c_v is the coefficient of consolidation of the sample at an effective consolidation pressure p.

It should be mentioned here that during the consolidation of the slurry, adhesion developed between the clay and the stainless steel sides of the consolidation chamber. This adhesion has been estimated to be in the order of 0.50 Kg/cm^2, because that was the pressure we had to apply on the piston in order to be able to force the sample out of the chamber. Following that, 0.50 Kg/cm^2 have been subtracted from the maximum preconsolidation pressure that has been applied on the slurry; thus the maximum preconsolidation pressure of the slurry is 7.50 Kg/cm^2.

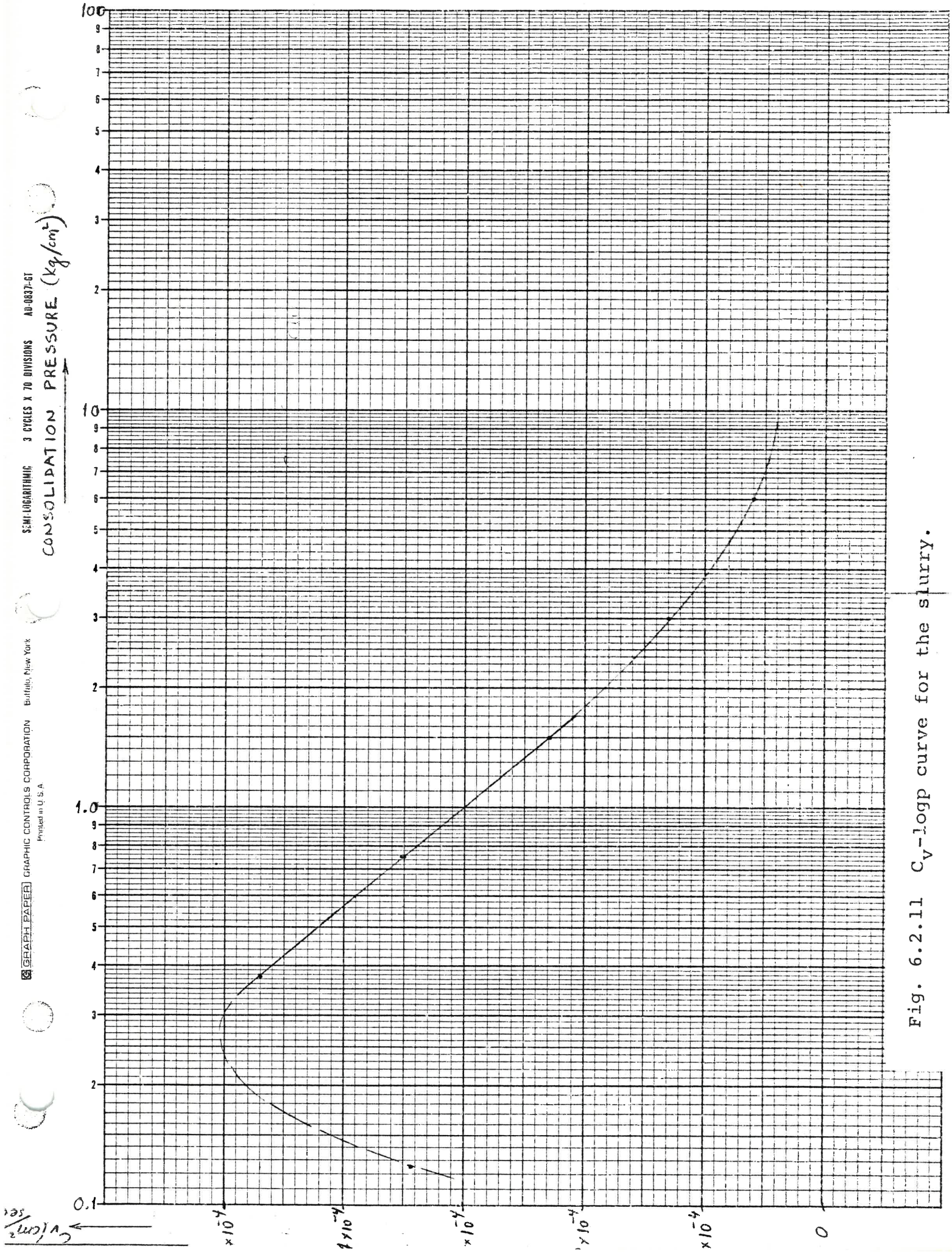


Fig. 6.2.11 C_v-logp curve for the slurry.

After the slurry had been consolidated and rebounded for a total of 163 days, it was forced out of the consolidation chamber (Fig. 6.2.12), it was weighed and finally it was covered with Saran plastic wrap (Fig. 6.2.13), sealed into a plastic bag and stored into the humid room, in order to be later used for the stress path tests on reconstituted samples (described in the next Section 6.3).

6.3 "Stress Path" Tests

Before describing the "stress path" tests, the way one can estimate a stress path based on the results of his stress analysis will be discussed. It will be actually shown how the stress paths have been estimated in the present case, based on the results of the finite element analysis performed, and which was described in Chapter 5. This section will be closed with a presentation and discussion of the results of the "stress path" tests which have been run on the reconstituted samples from the Friars Formation.

a. Estimating the Stress Path

In principle one can draw the total stress path (TSP) if he has performed a stepped analysis of the excavation and knows what the total stress changes induced by excavation at each step are. The stress path can thus be drawn for any point behind a slope, but usually this is done for one or more points selected along a potential



Fig. 6.2.12 Reconstituted sample immediately after rebound.



Fig. 6.2.13 Sealing reconstituted sample for storage in humid room.

failure surface, as it was explained in Chapter 4. If, however, a stepped analysis is not available, then one can only draw the TSP as a straight line connecting the points corresponding to the initial and the final states of stress. The initial state of stress is estimated from the geologic history of the site or from consolidation tests (by determining the preconsolidation pressure). The final state of stress is found from some kind of analysis as it was described in Chapter 4. Once the TSP has been drawn, one needs to make some kind of an assumption about the pore pressure changes that are going to develop, because of the stress changes induced by the excavation, in order to be able to draw the effective stress path (ESP). For a given change in total stresses $\Delta\sigma_1$ and $\Delta\sigma_3$, the pore pressure change induced, under undrained conditions, is:

$$\Delta u = B.\Delta\sigma_3 + \bar{A}\,(\Delta\sigma_1 - \Delta\sigma_3) \qquad (1)$$

where B and $\bar{A}$ are the pore pressure coefficients, first defined by Skempton (1954). B has a value close to 1 for saturated clays while $\bar{A}$ varies during deformation of a sample or of a soil element in the ground. The value of $\bar{A}$ at failure, denoted as $\bar{A}_f$ depends primarily on the OCR of the clay. In general the higher the OCR of the clay, the lower is $\bar{A}_f$; $\bar{A}_f$ can even become negative for highly O.C. clays. Since B can be estimated with some degree of accuracy, if the clay is not saturated, or it can be

assumed equal to 1, if the clay is saturated, drawing the ESP is dependent upon the assumption made about the value of $\bar{A}$. $\bar{A}$ is 0.33 for linearly elastic materials, while it varies for non-linear, non-elastic materials such as clays. A first estimation of $\bar{A}$ can be made using published data for various types of soils and various degrees of over-consolidation. Such a typical set of values is given in Table 6.3.1 (from Lambe and Whitman, 1969), for two different stress levels and various types of soil and OCR. Typical values for B, are also included in the same table, for various types of soil and rock and various degrees of saturation. Once an assumption about the value of $\bar{A}$ has been made, equation (1) can be used to find the pore pressure change Δu, corresponding to the principal total stress changes $\Delta\sigma_1$ and $\Delta\sigma_3$, induced by excavation.

It should be pointed out here that principal stress reorientation accompanies the excavation of a slope in a clay deposit, and in such a case the principal total stress changes will not in general be numerically the same as the changes in principal total stresses. Having estimated Δu from equation (1), the ESP for the stress changes induced by excavation can be drawn. If the change in pore pressures turns out to be negative (which is typically the case for O.C. clays), then the long-term equalization of pore pressures will lead to an increase of pore pressures with time. This part of the ESP will be horizontal

Table 6.3.1

Typical Values of Pore Pressure Parameters $\bar{A}$ and B.

(from Lambe & Whitman, 1969)

VALUES OF PARAMETER B

Material	$S(\%)$	B	Reference
Sandstone	100	0.286	
Granite	100	0.342	
Marble	100	0.550	Computed from
Concrete	100	0.582	compressibi-
Dense sand	100	0.9921	lities given by
Loose sand	100	0.9984	Skempton (1961)
London clay (OC)	100	0.9981	
Gosport clay (NC)	100	0.9998	
Vicksburg buckshot clay	100	0.9990	M.I.T.
Kawasaki clay	100	0.9988 to 0.9996	M.I.T.
Boulder clay	93	0.69	Measured by
	87	0.33	Skempton
	76	0.10	(1954)

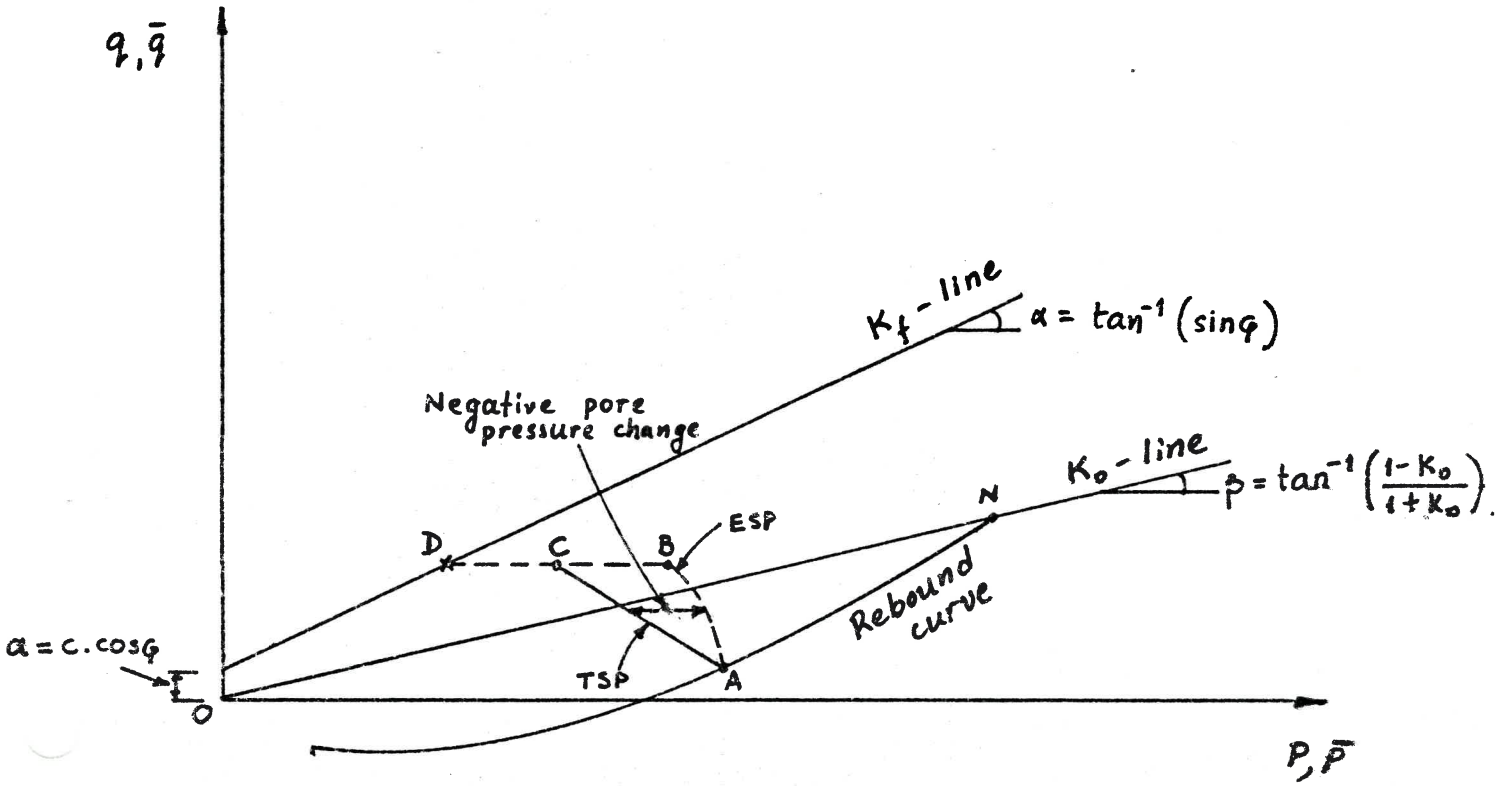
VALUES OF PARAMETER $\bar{A}$

Material ($S = 100\%$)	$\bar{A}$ (at failure)	Reference
Very loose fine sand	2 to 3	Typical
Sensitive clay	1.5 to 2.5	values
Normally consolidated clay	0.7 to 1.3	given by
Lightly overconsolidated clay	0.3 to 0.7	Bjerrum
Heavily overconsolidated clay	−0.5 to 0	

Material ($S = 100\%$)	$\bar{A}$ (for foundation settlement)	Reference
Very sensitive soft clays	>1	
Normally consolidated clays	½ to 1	From Skempton and Bjerrum (1957)
Overconsolidated clays	¼ to ½	
Heavily overconsolidated sandy clays	0 to ¼	

(parallel to the $\bar{p}$ axis), since pore pressure equalization takes place under constant shear stresses. A typical stress path both in terms of total stresses (TSP) and in terms of effective stresses (ESP) is shown in Fig. 6.3.1 for an O.C. clay. Notice that there is an additional portion of the ESP (CD), which corresponds to a raise of the ground water table (GWT). This is also a constant $\bar{q}$ process (assuming no significant change of the unit weight of the soil). Notice that the TSP is a point (point C) both for the pore pressure equalization and rise of GWT phases, since no change in total stresses occurs; only pore pressures change (again we assume no change in γ, otherwise the total stresses would have also changed; this is a good assumption if the soil is almost saturated, otherwise γ may be significantly increased by the processes of pore pressure equalization and rise of GWT).

The foregoing discussion refers to the estimation of the stress path from the time excavation is started until the slope fails or it comes to a long-term equilibrium. However, it is also necessary to estimate the stress path for the geologic history of the clay deposit, from the time it was first deposited until the time excavation was started. A consolidation test usually proves very helpful in estimating the preconsolidation pressure of the clay deposit at any depth. If the PI of the clay



Point A: Initial state of stress before excavation (no excess pore pressures assumed).

Point B: Final state of stress immediately after excavation, in terms of effective stresses.

Point C: Final state of stress immediately after excavation, in terms of total stresses; also final state of stress after pore pressure equalization (long-term), in terms both of effective & total stresses (no excess or static pore pressures assumed).

Point D: Failure after further increase of pore pressures beyond the point of pore pressure equalization (e.g. because of a raise in ground water table).

Fig. 6.3.1 Typical stress path for an excavated slope in an O.C. clay deposit.

is known, then one can use the Brooker and Ireland's results (see Fig. 5.2.2 in Chapter 5) to estimate K_o for various OCR. Having K_o as a function of OCR, then the stress path for the geologic history of the deposit can be drawn as follows (see also Fig. 6.3.1):

—Having K_o for OCR = 1, which corresponds to the time that the clay was normally consolidated (i.e., after the clay had been deposited and had been consolidated under the overburden pressure), line ON, which corresponds to the deposition history of the clay, can be drawn. This line has a slope equal to $\left(\frac{1-K_o}{1+K_o}\right)$ (where K_o corresponds to OCR = 1) and it can be readily drawn. Point N corresponds to the point of maximum preconsolidation pressure and it can be located on the $\bar{p}$ vs. $\bar{q}$ diagram once the effective preconsolidation pressure, $\bar{p}_p$, has been estimated ($\bar{p}_N = \frac{1+K_o}{2} \cdot p_p$, $\bar{q}_N = \frac{1-K_o}{2} \cdot \bar{p}_p$).

—The path NA, corresponding to rebound of the clay deposit as a consequence of vertical unloading (e.g., erosion, glacier retreat, etc.), can be estimated from the correlation of K_o to OCR. For any vertical consolidation pressure σ'_{vc} during rebound (because of erosion for example) OCR is defined as:

$$OCR = \frac{\bar{p}_p}{\sigma'_{vc}} \qquad (2)$$

Having OCR from (2), the estimated correlation between OCR and K_o is used to get K_o. Once K_o, which corresponds to the above σ'_{vc}, has been estimated, the point on the rebound stress path, corresponding to σ'_{vc}, is defined by:

$$\bar{p} = \frac{1+K_o}{2} \cdot \sigma'_{vc}, \quad \bar{q} = \frac{1-K_o}{2} \cdot \sigma'_{vc} \qquad (3)$$

The above calculations can be repeated for several effective consolidation pressures during rebound, until one gets to the present effective overburden pressure (before excavation is started).

—Having defined several points on the rebound stress path, curve NA can be drawn through these points.

Having described above the general guidelines on how to estimate the stress path for an element in the ground behind an excavated slope, the stress paths for the reconstituted samples that were prepared in the consolidation chamber can now be estimated. As far as the stress path for the geologic history is concerned, it is found from Fig. 5.2.2 that, for PI = 40% and OCR = 1, $K_o = 0.64$. Hence the slope of the K_o – line is: $\frac{1-K_o}{1+K_o} = \frac{1-0.64}{1+0.64} = 0.22$ or the angle β (see Fig. 6.3.1): $\beta = \tan^{-1}(0.22) = 12.4°$. Point N is determined from:

$$\bar{p}_N = \frac{1+K_o}{2} \cdot \bar{p}_p = \frac{1+0.64}{2} \times 7.5 = 6.15 \text{ Kg/cm}^2$$

$$\bar{q}_N = \frac{1-K_o}{2} \cdot \bar{p}_p = \frac{1-0.64}{2} \times 7.5 = 1.35 \text{ Kg/cm}^2$$

Thus line ON (K_o-line) is drawn, with an angle β = 12.4° to the horizontal, up to point N (6.15, 1.35), corresponding to the maximum consolidation pressure applied in the consolidation chamber (Fig. 6.3.3). Using again Fig. 5.2.2 for PI = 40%, several points on the rebound curve are found, as described previously. Thus the stress path NA for the unloading of the sample in the consolidation chamber (simulating the erosion process in the original clay deposit) is obtained (Fig. 6.3.3). This stress path is extended in the negative $\bar{q}$ range, which corresponds to values of K_o greater than one. It should be pointed out here that all stress paths have been drawn in terms of vertical and horizontal stresses, σ_v and σ_h. Thus, a negative $\bar{q}$ value means that the horizontal stress is higher than the vertical stress.

The part of the stress path corresponding to the geologic history of the clay deposit is common for all the reconstituted samples since they have all been prepared under the same stress conditions. Notice, however, that in an actual case, the preconsolidation pressure will depend on the depth of the sample and hence point N will be at different locations on the K_o-line depending on the depth of the sample. The part of the stress path corresponding to excavation of the slope and long-term equalization of pore pressures will be different for each sample, since the total stress changes induced by excavation vary from

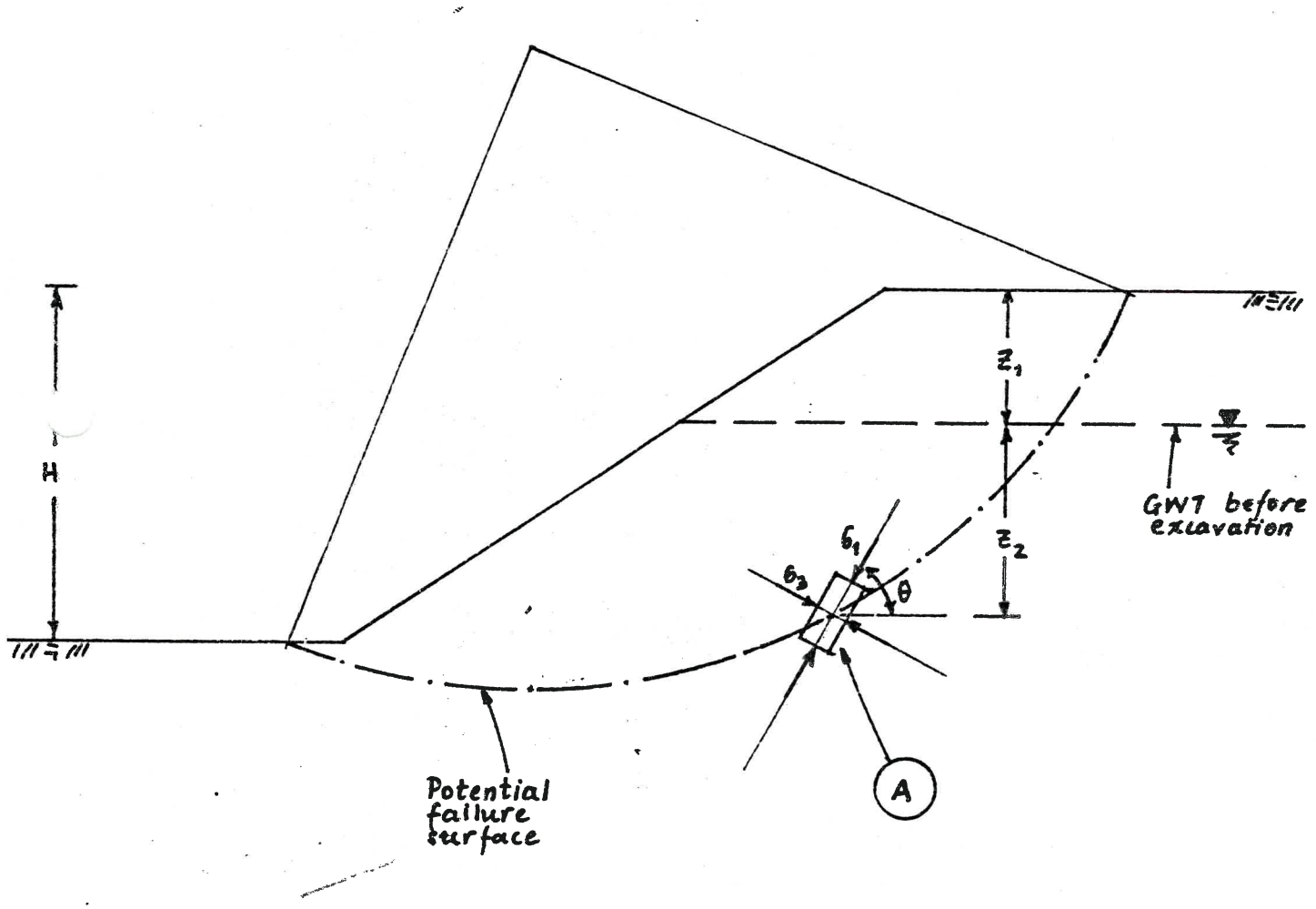


Fig. 6.3.2 Principal stress rotation behind an excavated slope--Definitions of various symbols.

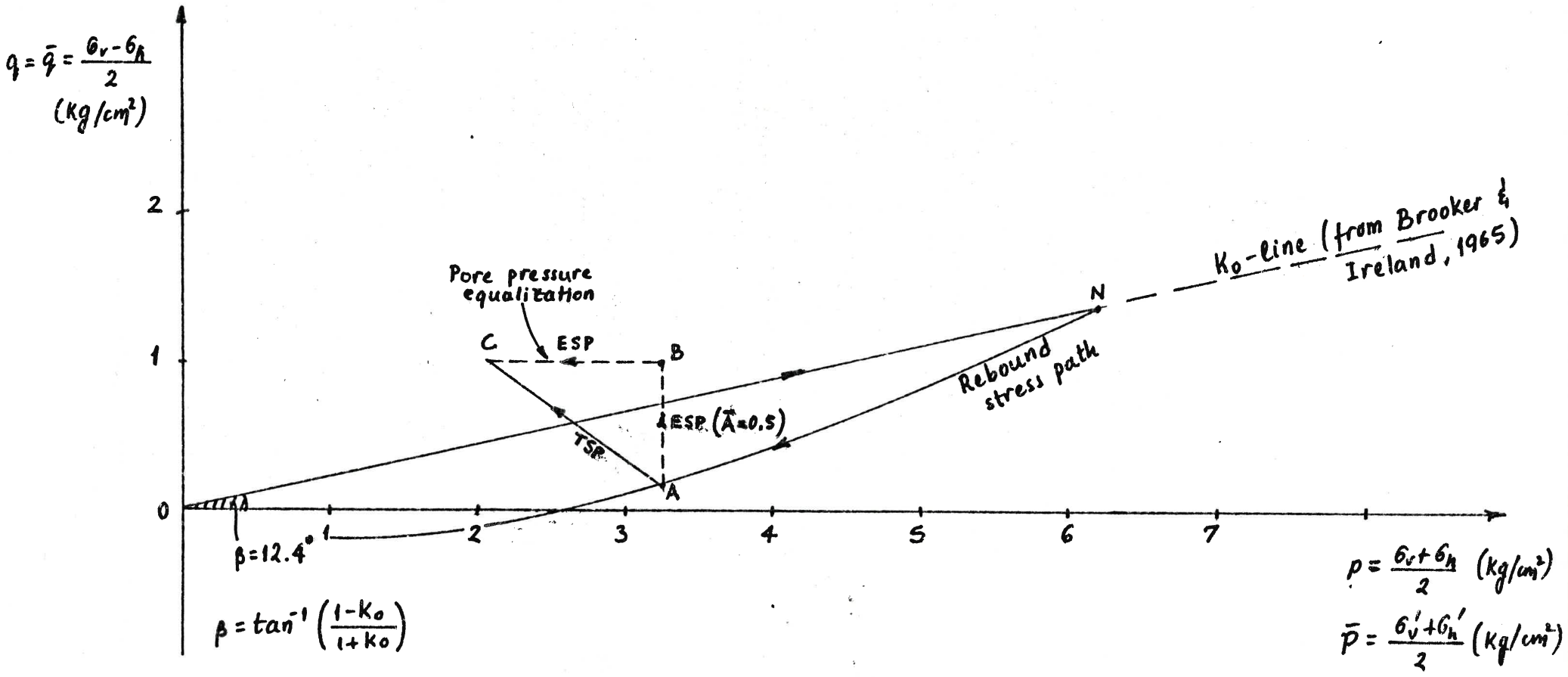


Fig. 6.3.3 Stress path for the consolidation history of the reconstituted samples (ONA). Typical estimated TSP and ESP during and after excavation (assumed $\bar{A}$ = 0.5).

element to element behind the slope. For each soil element, whose stress path is to be estimated, the following are done (see also Fig. 6.3.2, element A):

—Having the depth z of the element, its OCR is evaluated using the following expression:

$$OCR = \frac{\bar{P}_p}{\gamma_1 z_1 + \gamma_b z_2} \qquad (4)$$

where $\bar{P}_p$ is the effective preconsolidation pressure (=7.50 Kg/cm^2 in our case), γ_1 is the unit weight of the clay above GWT, γ_b is the boyant unit weight of the clay below GWT, z_1 is the depth of the GWT before excavation and z_2 is the depth of the element below GWT (Fig. 6.3.2).

—For the above OCR, K_o is found from Fig. 5.2.2 and then the effective vertical and horizontal stresses at element A before excavation are found, as:

$$\sigma'_v = \gamma_1 z_1 + \gamma_b z_2 \qquad (5)$$

$$\sigma'_h = K_o (\gamma_1 z_1 + \gamma_b z_2)$$

These are also the principal stresses at element A before excavation.

—From the results of the finite element analysis (Appendix 1), the magnitudes and directions of the final principal stresses after excavation are obtained, for the slope and K_o which are applicable in each case. Notice that if the slope, which is being analyzed, is different from 1.5:1 or 3:1, one

can interpolate or extrapolate between the results of these two analyses. The same applies for K_o, if it so happens that its value is different from the ones we have analyzed for. If one wanted to use the more accurate results of the H_p/H analysis, which was presented at the end of Section 5.2, then he would have to follow a slightly different approach. After he would have determined the initial principal stresses σ'_v and σ'_h before excavation, as described above, he would next find the ratio H_p/H corresponding to his case, as follows:

$$OCR = \frac{\bar{P}_p}{\sigma'_{vc}} = \frac{\gamma_1 H_p + \gamma_1 z_1 + \gamma_b z_2}{\gamma_1 z_1 + \gamma_b z_2} = \frac{\gamma_1 H_p}{\gamma_1 z_1 + \gamma_b z_2} + 1 = \frac{H_p/H}{\frac{\gamma_1}{\gamma_1}\cdot\frac{z_1}{H} + \frac{\gamma_b}{\gamma}\cdot\frac{z_2}{H}} +$$

$$\longrightarrow \frac{H_p}{H} = (OCR-1)\cdot\left(\frac{z_1}{H} + \frac{\gamma_b}{\gamma}\cdot\frac{z_2}{H}\right) \qquad (6)$$

Using the H_p/H found from (6), he would then interpolate or extrapolate between the results of the appropriate H_p/H from the finite element analysis (Appendix 1), in order to find what the magnitudes and directions of the final principal stresses (after excavation) will be.

Notice that the finite element solution applies to a clay deposit whose unit weight is the same everywhere. In addition, the analysis has been performed in terms of total stresses. The above two observations imply that an error is introduced if the unit weight above GWT, call it γ_1, is different

from the total unit weight below GWT, call it γ_2. However, if the numbers do not differ appreciably, then the error introduced is small and one can use an average for the whole slope, when working with total stresses.

This is practically achieved by using an equivalent γ, which is obtained as the weighted average of γ_1 and γ_2, as follows:

$$\gamma = \frac{\gamma_1 z_1 + \gamma_2 (H - z_1)}{H}$$

If however, the difference between γ_1 and γ_2 is significant, then a more sophisticated parametric analysis is necessary, unless one wants to run an analysis for specific values of γ_1, γ_2 and z_1, in which case LSTRN-3 can be easily used, even with a layered soil profile.

—Having the final principal stresses (in terms of total stresses) after excavation, the TSP can be drawn as a straight line connecting the points corresponding to the initial and final states of stress respectively (line AC in Fig. 6.3.1).

—In order to estimate the ESP an estimation of parameter $\bar{A}$ is needed, as explained earlier. The values given in Table 6.3.1 are used as a first approximation. Since the samples being tested are lightly to medium O.C., the following ranges for $\bar{A}$ are obtained:

$\bar{A}$ = 0.25 - 0.50, for low stress levels

$\bar{A}$ = 0.30 - 0.70, for high stress levels (close to failure)

From the above ranges, $\bar{A}$ = 0.50 is used as a first approximation throughout the test. Then from (1) we get:

$$\Delta u = B.\Delta\sigma_3 + \bar{A}\left(\Delta\sigma_1 - \Delta\sigma_3\right) = B.\Delta\sigma_3 + 0.50\left(\Delta\sigma_1 - \Delta\sigma_3\right)$$

Since the samples are saturated, B is very close to 1 and the above expression becomes:

$$\Delta u = \Delta\sigma_3 + 0.50\left(\Delta\sigma_1 - \Delta\sigma_3\right) \longrightarrow \Delta u = \frac{\Delta\sigma_1 + \Delta\sigma_3}{2} \quad (7)$$

For the case of no stress reorientation:

$$\Delta\bar{p} = \Delta\left(\frac{\sigma_1 + \sigma_3'}{2}\right) = \frac{\Delta\sigma_1' + \Delta\sigma_3'}{2} = \frac{\Delta\sigma_1 + \Delta\sigma_3}{2} - \Delta u \quad (8)$$

Combining (7) and (8):

$$\Delta\bar{p} = 0 \quad (9)$$

The above expression indicates that the ESP will be vertical (Fig. 6.3.3). Notice that in the case of stress reorientation we need to distinguish between the changes in principal stresses $\Delta(\sigma_1, \text{final}-\sigma_1, \text{initial})$ and $\Delta(\sigma_3, \text{final}-\sigma_3, \text{initial})$ and the principal stress changes $(\Delta\sigma)_1$ and $(\Delta\sigma)_3$ (designated here as $\Delta\sigma_1$ and $\Delta\sigma_3$). In order to apply equation (1), $\Delta\sigma_1$ and $\Delta\sigma_3$ need to be used and consequently (9) will be no longer valid for $\bar{A}$ = 0.50, if stress reorientation takes place.

After the stress paths have been estimated as described above, the stress path tests are performed,

as described in the next paragraph (b), following the estimated TSP and observing what the actual ESP is. From that, the value of $\bar{A}$ during the test can be back-calculated by solving (1) with respect to $\bar{A}$:

$$\bar{A} = \frac{\Delta u - B\Delta\sigma_3}{\Delta\sigma_1 - \Delta\sigma_3}$$

or for $B \simeq 1.00$:

$$\bar{A} = \frac{\Delta u - \Delta\sigma_3}{\Delta\sigma_1 - \Delta\sigma_3} \qquad (10)$$

The values of $\bar{A}$ given by (10) can be then used for subsequent tests in order to more accurately estimate the expected ESP.

b. Description of Apparatus and Testing Procedure

Since stress reorientation in the ground accompanies the excavation of a slope, a problem was faced right from the beginning, in performing triaxial "stress path" tests in the laboratory: namely, that rotation of principal stresses, other than 90°, in triaxial laboratory tests, is impossible. This is because it is not possible to apply shear stresses along the vertical and horizontal sides of a sample in the conventional triaxial apparatus; application of principal stresses in directions other than vertical and horizontal would require so. Hence a good approximation of the actual stress field would have to be found.

This led to the following dilemma:

—Should vertical samples be obtained from the consolidation chamber and be anisotropically consolidated in the triaxial cell under σ'_{1c} and σ'_{3c} corresponding to the estimated OCR of the soil elements, which are being simulated in the laboratory (i.e., $\sigma'_{1c} = \frac{\bar{p}_\rho}{OCR} = \gamma_1 z_1 + \gamma_b z_2$ and $\sigma'_{3c} = K_o \sigma'_{1c}$)? This alternative has the advantage that it brings the soil element (represented by the soil sample) to the correct state of stress before excavation, but as reorientation of principal stresses follows excavation, both normal and shear stresses would have to be applied on the sample in order for it to come to the correct state of stress after excavation. As explained previously, applying shear stresses on the sample is impossible. Hence only the normal stresses, corresponding to the vertical and horizontal directions after excavation, can be applied on the sample, this leading to the wrong final state of stress (see Fig. 6.3.4, 6.3.5).

—Alternatively, should inclined samples be obtained from the consolidation chamber, so that their axis is parallel to the major principal stress direction after excavation (Fig. 6.3.4) and consolidate them under the normal stresses they would have in that direction and the direction perpendicular to that

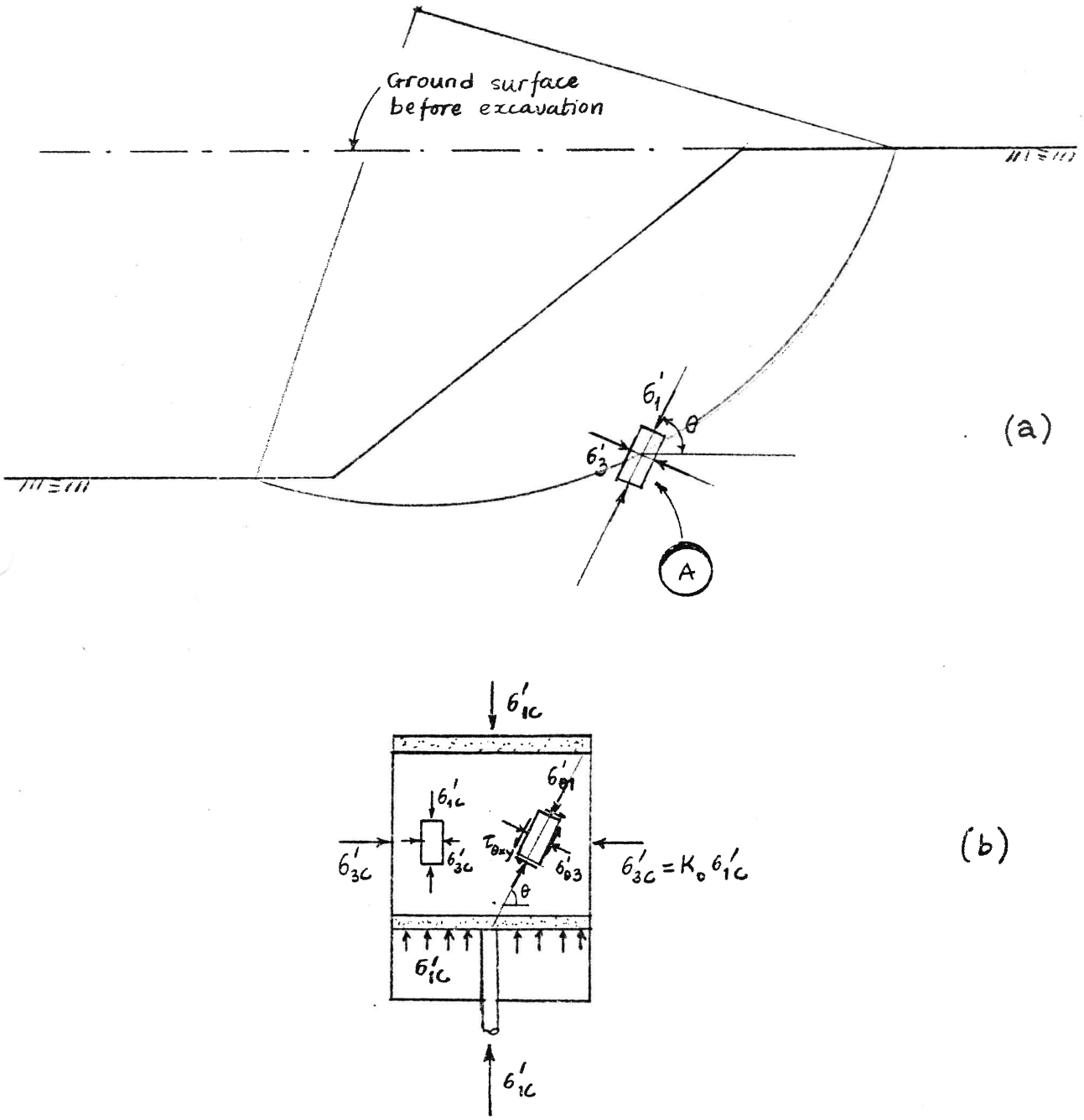


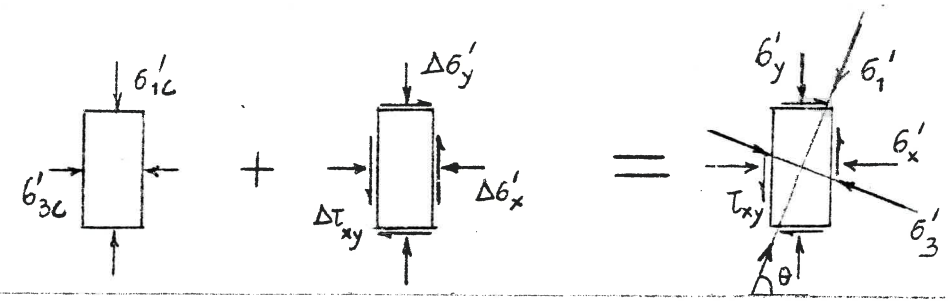
Fig. 6.3.4 (a) Principal stress rotation in the field, after excavation.

(b) State of stress in various directions in the consolidation chamber.

before excavation? From Fig. 6.3.4 (a) it is seen that the final principal stress directions are not in general vertical or horizontal, like the principal consolidation stress directions are. This means that there are shear stresses $\tau_{\theta xy}$ during consolidation in the directions forming angles θ and $(90° + \theta)$ with the horizontal, in addition to the normal stresses $\sigma'_{\theta 1}$ and $\sigma'_{\theta 3}$ (Fig. 6.3.4 (b)). Since $\tau_{\theta xy}$ cannot be applied in the triaxial apparatus, the sample will be under a wrong state of stress before excavation. However, since the direction of the axis of the sample coincides with the final major principal stress direction after excavation, applying the correct normal stress increments on the sides of the sample in the laboratory will result in the correct final state of stress (see also Fig. 6.3.6).

It was finally decided to follow the second alternative in performing triaxial "stress path" tests in the laboratory, basically for two reasons:

(i) It is believed that the omission of the shear stresses $\tau_{\theta xy}$ (see Fig. 6.3.6), in the reconsolidation phase of the test, will not significantly affect the structure of the sample, as compared to the structure that the sample would have in the consolidation chamber under the correct consolidation state of stress. This is because by the time we reconsolidate



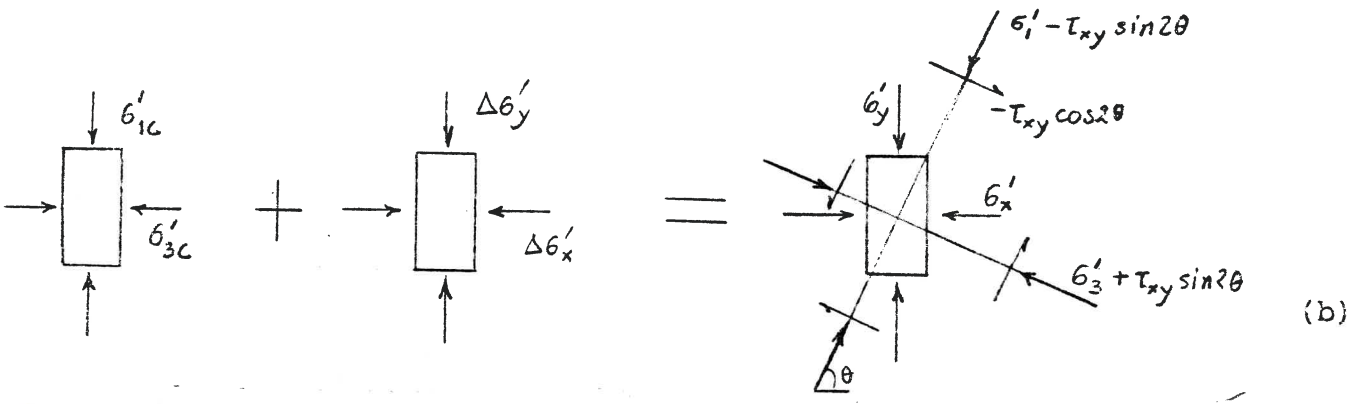
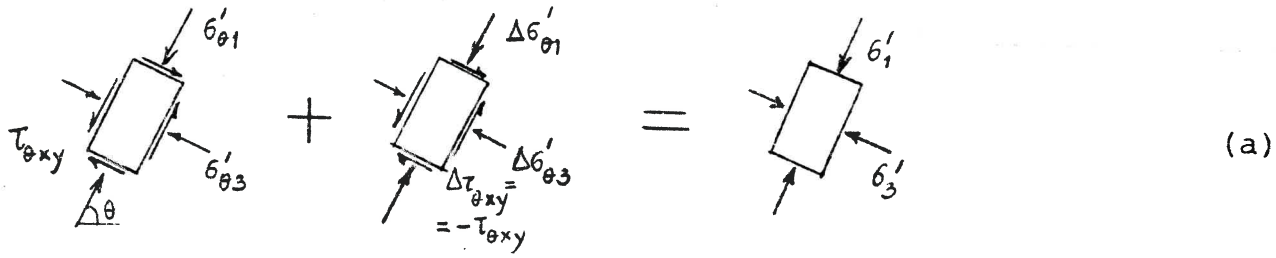


Fig. 6.3.5 (a) Actual initial & final stresses & stress changes in vertical direction.
(b) Initial & final stresses & stress changes in vertical direction, applied in the laboratory (first alternative).



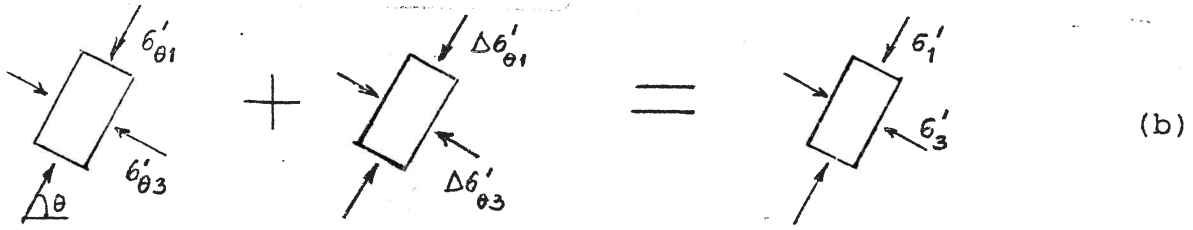


Fig. 6.3.6 (a) Actual initial & final stresses & stress changes in θ-direction.
(b) Initial & final stresses & stress changes in θ-direction, applied in the laboratory (second alternative).

the sample in the triaxial apparatus, it already has a structure which has been formed in the consolidation chamber during virgin compression and rebound, under the correct state of stress, and this structure is not very easily changed, unless we impose a drastically different stress field on the sample during reconsolidation.

(ii) It is more critical that the final state of stress, which could also be the state of stress close to failure, is simulated as correctly as possible in the laboratory. From this point of view the second alternative is more advantageous. Notice that none of the above two alternatives will exactly reproduce the actual ESP in the laboratory since the omission, in both cases of the shear stress changes along the sides of the sample in the undrained part of the test (simulating excavation), will result in pore pressure changes, which will be different from the actual.

After it had been decided on how to trim and test the samples in the laboratory, the following testing procedure was established:

—A critical failure surface was drawn for the excavated slope, by assuming some estimated strength parameters. In our case conventional isotropically consolidated, drained triaxial tests have been run and drained strength parameters c_d and φ_d have

been established. These strength parameters have been used in locating critical failure surfaces.

—Several representative soil elements were selected along this failure surface.

—The OCR was found for each element:

$$OCR = \frac{\bar{P}_p}{\gamma_1 z_1 + \gamma_b z_2}$$

—K_o was estimated by using Fig. 5.2.2, OCR (found above) and the PI of the sample (40% in our case). Alternatively, H_p/H was estimated from:

$$H_p/H = (OCR-1) \cdot \left(\frac{z_1}{H} + \frac{\gamma_b}{\gamma_1} \cdot \frac{z_2}{H}\right).$$

—Using the coordinates of the selected elements, it was found which of the elements of the finite element mesh were closest to each of the representative elements selected previously.

—Interpolation was made between the appropriate:

(i) K_o's (alternatively H_p/H's),

(ii) excavation side slopes,

(iii) elements,

from the results of the appropriate finite element analysis (K_o or H_p/H) (Appendix 1), by using the estimations of K_o (alternatively H_p/H) made earlier, the slope of the cut and the distances of the centers of the representative soil elements from the centers of their neighboring elements.

—From the interpolation made above θ, $\sigma_1/\gamma H$, $\sigma_3/\gamma H$ were found for each of the representative soil elements, where:

θ=angle between final major principal stress direction and horizontal,

$\sigma_1/\gamma H$ = normalized major principal stress after excavation,

$\sigma_3/\gamma H$ = normalized minor principal stress after excavation,

H = height of excavation,

γ = average unit weight of soil behind slope = $\frac{\gamma_1 z_1 + \gamma_2 (H - z_1)}{H}$

γ_1, γ_2, z_1 = as defined previously.

—The stresses, under which the samples will have to be anisotropically consolidated in the triaxial cell, were computed:

$$\sigma'_{\theta 1} = \sigma'_{vc} \sin^2\theta + \sigma'_{hc} \cos^2\theta = \sigma'_{vc} (\sin^2\theta + K_o \cos^2\theta)$$

$$\sigma'_{\theta 3} = \sigma'_{vc} \cos^2\theta + \sigma'_{hc} \sin^2\theta = \sigma'_{vc} (\cos^2\theta + K_o \sin^2\theta)$$

where $\sigma'_{vc} = \gamma_1 z_1 + \gamma_b z_2$.

—From the big reconstituted sample, prepared in the consolidation chamber, as many small cylindrical specimens as the representative soil elements selected in the beginning were cut and trimmed. The cylindrical specimens were 1.4 inches in diameter by 3.5 inches high. The axis of each of the specimens was inclined θ degrees to the horizontal, where θ was the angle

that was found earlier by interpolation, for each of the representative soil elements.

Then for each element the following were done:

—After the specimen had been weighed and its dimensions had been measured, it was placed on the triaxial apparatus and it was saturated by applying a back pressure u_b = 1.50 Kg/cm^2, for 24 hours. The back pressure was applied in three steps to avoid overconsolidation of the upper end of the specimen (the back pressure was applied from the bottom of the specimen). In each step, the cell pressure was maintained about 0.10 Kg/cm^2 higher than the back pressure in order to avoid "blow-up" of the membrane. The back pressure increments used were:

Step 1: u_b = 0.50 Kg/cm^2, σ_{cell} = 0.60 Kg/cm^2 (for two hours)

Step 2: u_b = 1.00 Kg/cm^2, σ_{cell} = 1.10 Kg/cm^2 (for two hours)

Step 3: u_b = 1.50 Kg/cm^2, σ_{cell} = 1.60 Kg/cm^2 (for 20 hours)

Notice that two membranes were used to seal the specimen in the triaxial cell, two O-rings on either end of the specimen to seal the membranes and a side filter paper drain which has been cut in 1/4 inch wide strips alternating with 1/4 inch open spaces. A thin layer of silicone grease was applied between inner and outer membranes. Each membrane was approximately 0.0018 inches thick. The filter paper drain used was Whatman's No. 54.

—After the end of saturation, the value of the pore pressure parameter B was checked in order to make sure that the sample was saturated. A B-value greater than 0.98 was considered satisfactory.

—The sample was consolidated anisotropically under:

$$\sigma_{\text{axial, consolidation}} = \sigma'_{\theta 1} + u_b = \sigma'_{vc}\left(\sin^2\theta + K_o\cos^2\theta\right) + u_b$$

$$\sigma_{\text{cell}} = \sigma'_{\theta 3} + u_b = \sigma'_{vc}\left(\sin^2\theta + K_o\cos^2\theta\right) + u_b$$

This was performed as follows:

First the cell pressure σ_{cell} was applied with the drainage valve closed.

Then the deviatoric consolidation stress was applied: $\sigma_{\text{axial, cons.}} - \sigma_{\text{cell}} = \sigma'_{\theta 1} - \sigma'_{\theta 3}$, with the drainage valve closed again. The sample was then left under these stresses for 5 minutes and the drainage valve was subsequently opened and the sample was left to consolidate for 24 hours. Readings of axial deformation and volume change were taken at time intervals increasing with time, the volume change vs. log(time) was plotted and t_{50}, the time required for 50% of primary consolidation to take place, was finally estimated from this plot.

—After consolidation was over, the drainage valve was closed and $\sigma'_{\theta 1}$ and $\sigma'_{\theta 3}$ were reduced to the final principal total stresses after excavation σ'_1 and σ'_3 respectively. This was done in several small steps.

The time interval between these steps was kept constant. The total time required for the undrained unloading (which simulates excavation) was chosen so that there was adequate pore pressure equalization within the sample. This depends on the magnitude of the coefficient of consolidation c_v, and on the type of drainage provided. Blight (1963) has suggested that for all-around drains and 95% pore pressure equalization, the time to failure, t_f, may be calculated from the equation:

$$t_f = 0.07\frac{D^2}{c_v}$$

where D is the diameter of the specimen (1.4 inches in our case) and c_v is the coefficient of consolidation of the specimen (ranging between 0.6×10^{-4} and 4.7×10^{-4} cm^2/sec in our case, depending on the consolidation pressure; see Fig. 6.2.11). D and c_v should be entered with compatible units in the above formula. Houston (1978) has suggested that c_v may be calculated from the following expression, for triaxial tests, provided the height to diameter ratio of the specimen is 2:

$$c_v = \frac{\pi D^2}{Kt_{50}}$$

where K is a constant depending on the type of drainage and t_{50} is the time for 50% of the primary consolidation to be completed. For the case of radial

and base drainage, Houston (1978) has suggested that K should be taken equal to 350. Substituting the equation for c_v into the one suggested by Blight for t_f, we get:

$$t_f = 7.8t_{50}$$

Notice that Blight (1963) has suggested that drained tests should be conducted at the same rate as undrained tests. The latter suggestion has been taken into account in deciding what the rate of loading should be in the conventional drained triaxial tests that have been run. The above expression has been used as a basis for estimating the duration of the undrained part of the "stress path" triaxial tests, by employing the value of t_{50} estimated in the consolidation part of the test. An allowance was made for the value of t_f since the height to diameter ratio in our case was 2.5 (H/D = 3.5/1.4 = 2.5). For our tests, t_{50} ranged between 900 sec and 2750 sec, which gave a range for t_f between $\frac{7.8 \times 900}{3600} \simeq 2$ hours and $\frac{7.8 \times 2750}{3600} \simeq 6$ hours. A duration of 8 hours was generally adopted for the undrained part of the test, except where the magnitude of the undrained unloading was quite high, in which case we used a 10 hour duration. The "stress path" tests were performed on a stress controlled triaxial apparatus (described later). The unloading was performed in steps and the time interval between steps

was taken to be 30 minutes. Since less creep is exhibited in lower stress levels, 70% of the final stresses were applied during the first 3 hours (3.5 hours for the 10-hour long undrained unloading) and the rest 30% was applied during the remaining 5 hours (6.5 hours for the 10-hour long undrained unloading). Pore pressure and axial deformation readings were taken at 29 minutes after the application of each loading.

—After the undrained unloading, the sample was left overnight with the drainage valve closed and with total stresses applied on it equal to the final total stresses (plus the back pressure) of the corresponding soil element after excavation.

—The next day, new pore pressure and axial deformation readings were taken, then the back pressure was set equal to the last pore pressure reading, and the drainage valve was opened. The back pressure was increased in small steps every 30 minutes. In order to ensure that there was enough time for adequate pore pressure equalization throughout the sample and also in order to minimize the uncertainty about the actual value of the pore pressure throughout the sample at any moment, the pore pressure increments were selected in such a way that: (a) the total duration of the pore pressure equalization phase was not less

than 8 hours and (b) the pore pressure increments were smaller than 0.05 Kg/cm^2. During this part of the test, the pore pressure was increased by as much as the negative pore pressure change induced by the undrained unloading. This phase simulates the long-term equalization of the negative pore pressure changes that are induced by the excavation around the slope. The pore pressure equalization phase was continued until the sample failed or until the pore pressure had been raised as high as the original back pressure (1.50 Kg/cm^2; pore pressure equalization completed; no excess pore pressures).

—If the sample did not fail in the previously described part of the test, the pore pressure was further increased at the same rate as before, until the sample failed. This part of the test simulates the case where the slope has come to an equilibrium, after equalization of the negative pore pressure changes, and then a rise of the GWT, due for example to heavy rainfalls, causes an increase of static pore pressures.

—Volume change and axial deformation measurements were made during the above two phases of the test, again at 29 minutes after each pore pressure increment.

—After the test was over, the triaxial cell was disassembled quickly, the sample was weighed, then it was sketched and finally it was placed in the oven

for a water content determination to be made. The increase in water content during the test was used as an independent check of the total volume change measured during the test with the volume change device.

Having described the test procedure above, a brief description of the apparatus used for the tests will be made. The triaxial cell used was the standard triaxial cell used in the University of California Soil Mechanics laboratories for 3.5 inches high by 1.4 diameter samples, with an older type of frictionless piston guide on it. A lucite cylinder formed the side of the cell, with a protective metal net around it. A 1/4 inch piston was used to apply the axial load on the sample. The axial load was applied on the piston by a loading frame which was hanging from a wire and it was balanced in position with the help of a fast pulley, through which the wire passed, and a counterweight hanging at the other end of the wire. The weights were applied on the frame with the help of a hanger, with a weight retainer at its end, hanging underneath the frame. The piston was sliding through a ball bearing bushing so as to minimize piston friction. The cell pressure was applied along the piston guide, so that an air-water interface was formed and no water leak occurred along the piston guide. The sample was seated on a lucite base

and porous stone. A lucite top cap was used for transfering the axial load from the piston on the sample. Drainage was provided through the base porous stone out to the volume change device by a drainage line (tubing) going through the lucite base. Axial deformation was measured with the help of a mechanical gage (accuracy 0.001 inches) rigidly connected through a rod, with the cell. The gage's moving part rested on the center of the top of the loading frame. A photograph of the triaxial cell and of the whole set up is shown in Fig. 6.3.7. The pore pressure and cell pressure measurements were made with the help of an electrical pressure transducer, which was connected on a full Wheatstone bridge and the unbalanced voltage of the bridge (corresponding to the pressure being measured) was read on a voltmeter. The pressure was obtained from the voltage measurement by having previously calibrated the pressure transducer against a HEISE mechanical pressure gage of high accuracy (0.01 Kg/cm^2).

A modification of the testing set up was necessary for the case where the horizontal consolidation pressure $\sigma'_{\theta 3}$ was higher than the vertical consolidation pressure $\sigma'_{\theta 1}$. For this to be achieved the piston had to be pulled up, since the cell pressure is applied on the sample in all directions (vertical and horizontal). In other words, a "negative" (directed upwards) deviatoric stress would have to be applied. This was achieved with the use of a piston

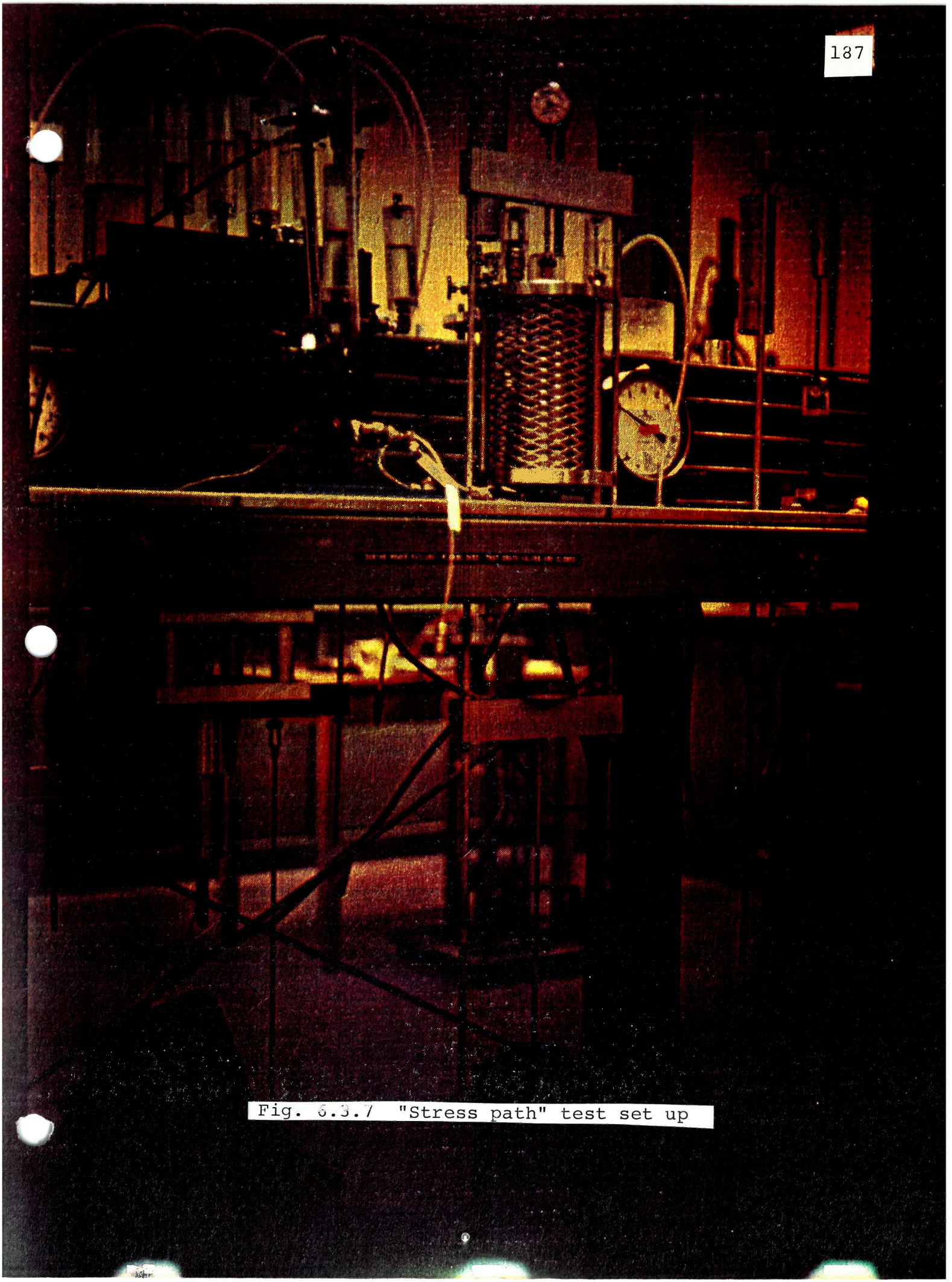


Fig. 6.3.7 "Stress path" test set up

threaded on the top cap and being pulled up by a wire connected on the top horizontal bar of the frame (Fig. 6.3.8 (a)). The counterweight, which was referred to before, was substituted by a hanger and weight retainer, so that the "negative" axial load could be applied on the piston (Fig. 6.3.8 (b)). As it can be seen from the picture of Fig. 6.3.8 (a), application of "positive" deviatoric stresses was also possible with the use of a flat-topped poston-wire connector, which the upper horizontal bar of the loading frame could sit on. A small change, in the way axial deformation was measured, had also to be made. The moving part of the gage was in this case indirectly connected to the piston, with the help of a small horizontal aluminum bar, which was fastened on the piston (Fig. 6.3.8 (a)).

The results of the "stress path" tests that have been run, following the previously presented procedure and using the apparatus described above, are presented and discussed in the following paragraph.

c. Results

An abbreviated name, descriptive of the type of the test, has been used for the "stress path" tests. They have been called ACUD tests, which stands for: Anisotropically Consolidated, unloaded under Undrained conditions and finally Drainage restablished for pore pressure equalization.

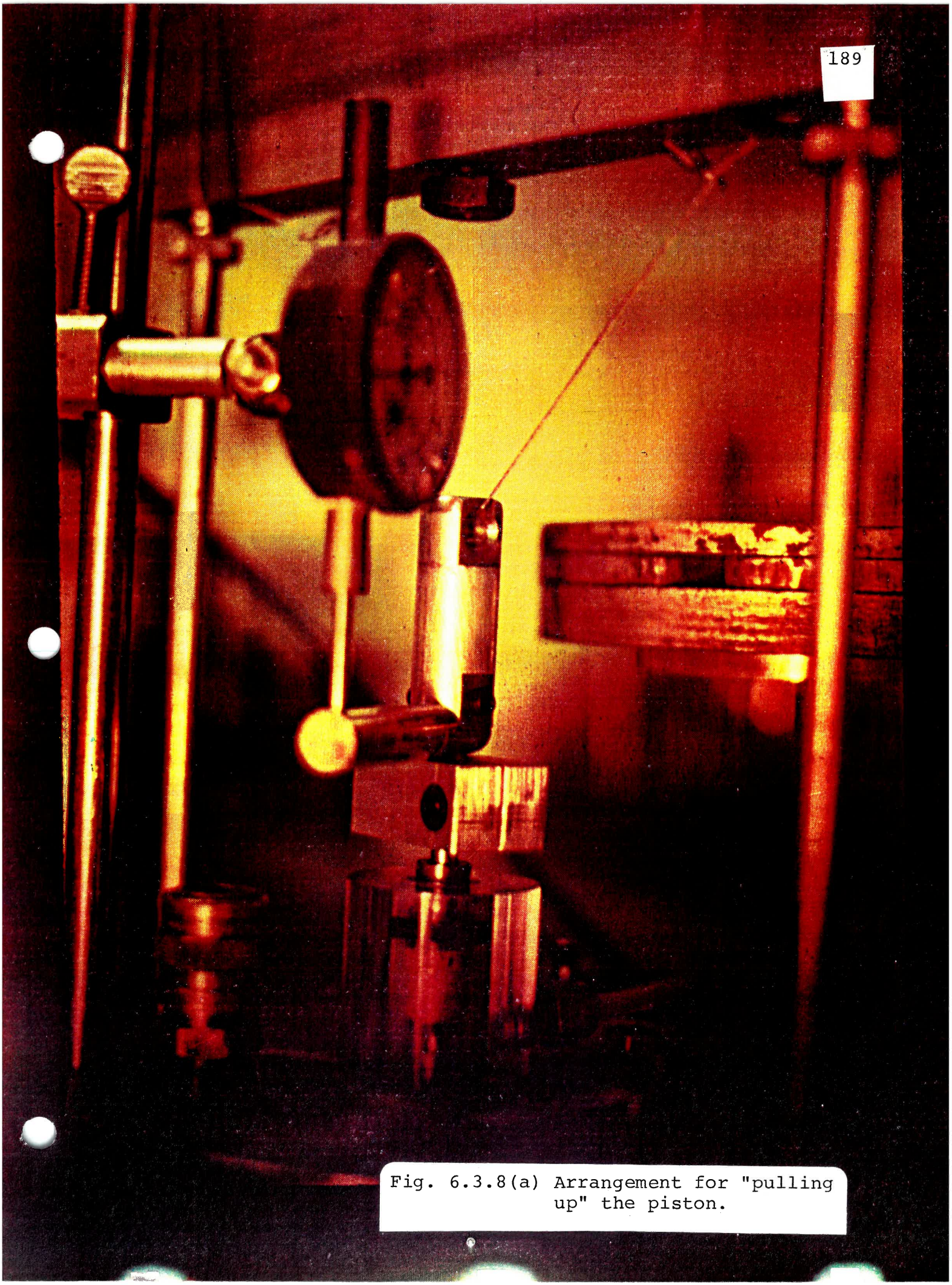


Fig. 6.3.8(a) Arrangement for "pulling up" the piston.

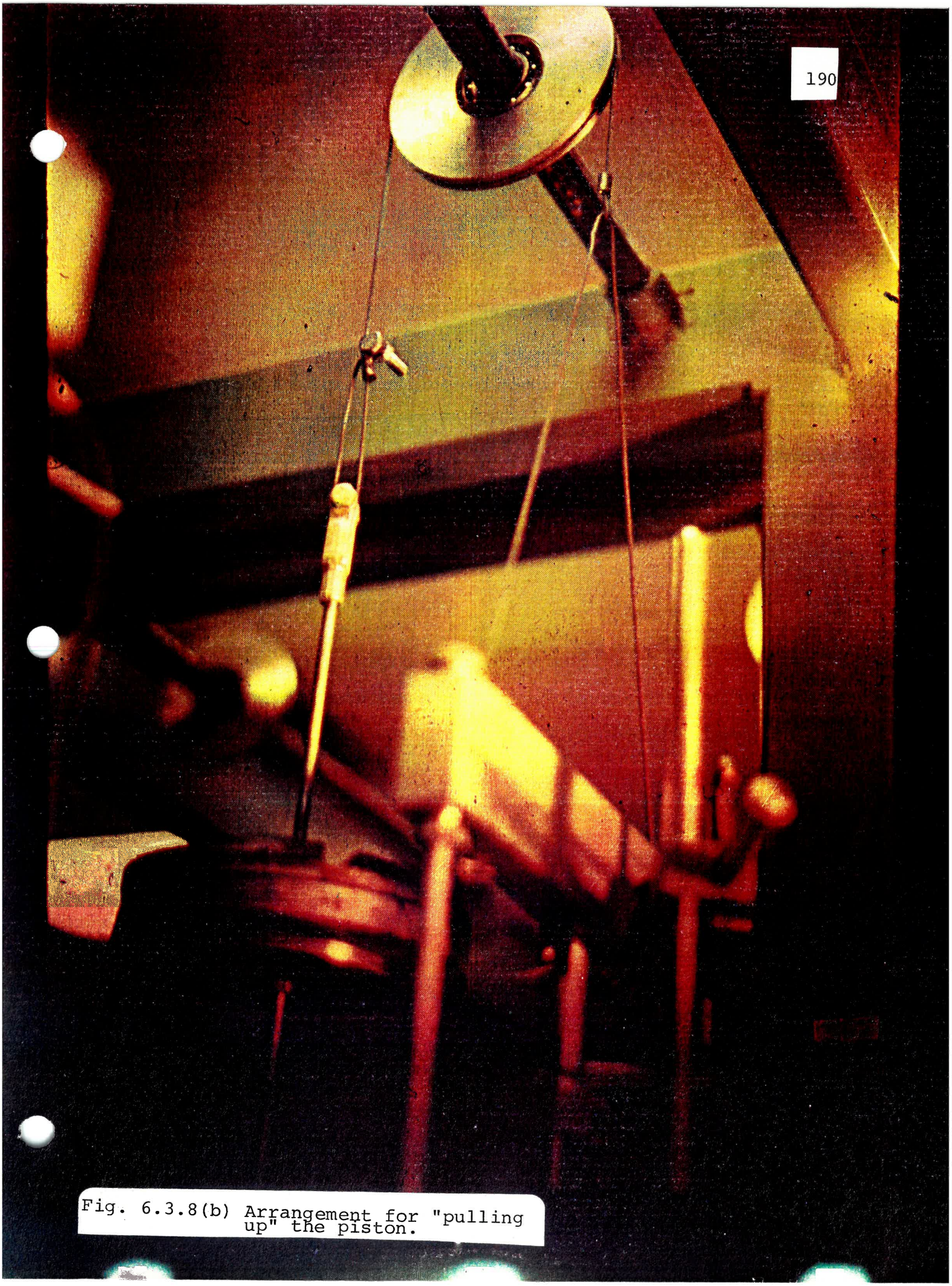


Fig. 6.3.8(b) Arrangement for "pulling up" the piston.

A total of six "stress path" tests were performed. Two of the samples tested had been trimmed with their axis vertical ($\theta = 90°$) (samples ACUD-6 and ACUD-8), two with their axis horizontal ($\theta = 0°$) (samples ACUD-5 and ACUD-7) and two with their axis inclined 50° to the horizontal ($\theta = 50°$; samples ACUD-4b and ACUD-9a). The total stress paths (TSP) and effective stress paths (ESP) are shown in the following Figures 6.3.9-6.3.14. Notice that there are two kinds of TSP drawn. The one is labelled TSP-u_b and it refers to the total stresses minus the back pressure that was applied during consolidation ($u_b = 1.50$ Kg/cm^2 for all of the tests performed). The other one is labelled TSP and it refers to the total stresses actually applied on the sample during the test.

As it can be seen from these figures, A has a value close to 0.50 for most of the tests, because the ESP is almost vertical. Notice, however, that sample ACUD-7 ($\theta = 0°$) significantly deviates from that rule. As a matter of fact, there are very small negative pore pressure changes during undrained unloading. Another thing to be noticed is that a jump rotation of principal stresses was imposed on that sample during testing. The horizontal stress was higher than the vertical stress during consolidation and at some point, during unloading, the vertical stress became higher than the horizontal. This principal stress jump rotation is believed to be responsible

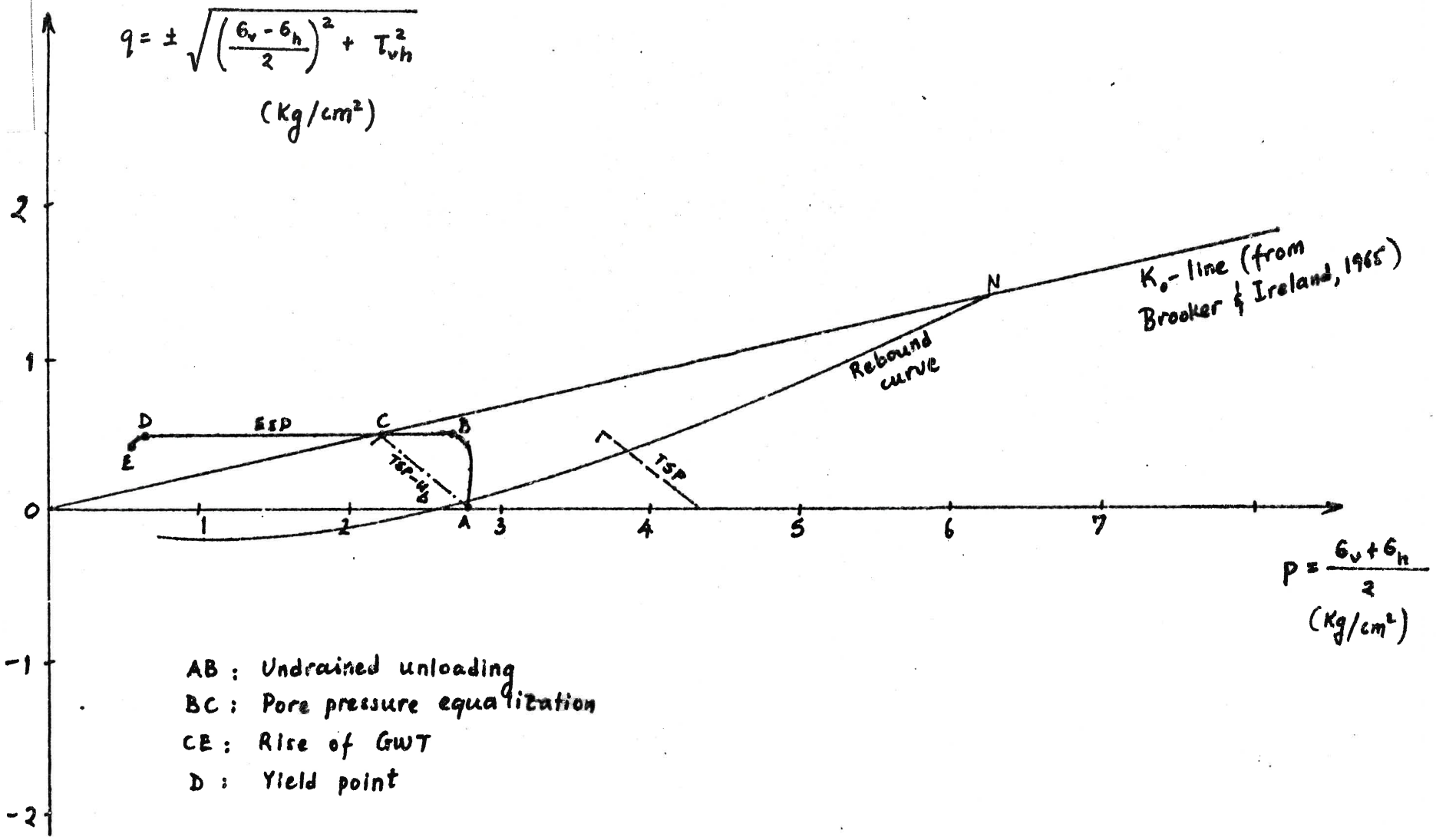


Fig. 6.3.9 Stress paths for sample ACUD-4b ($\theta = 50°$).

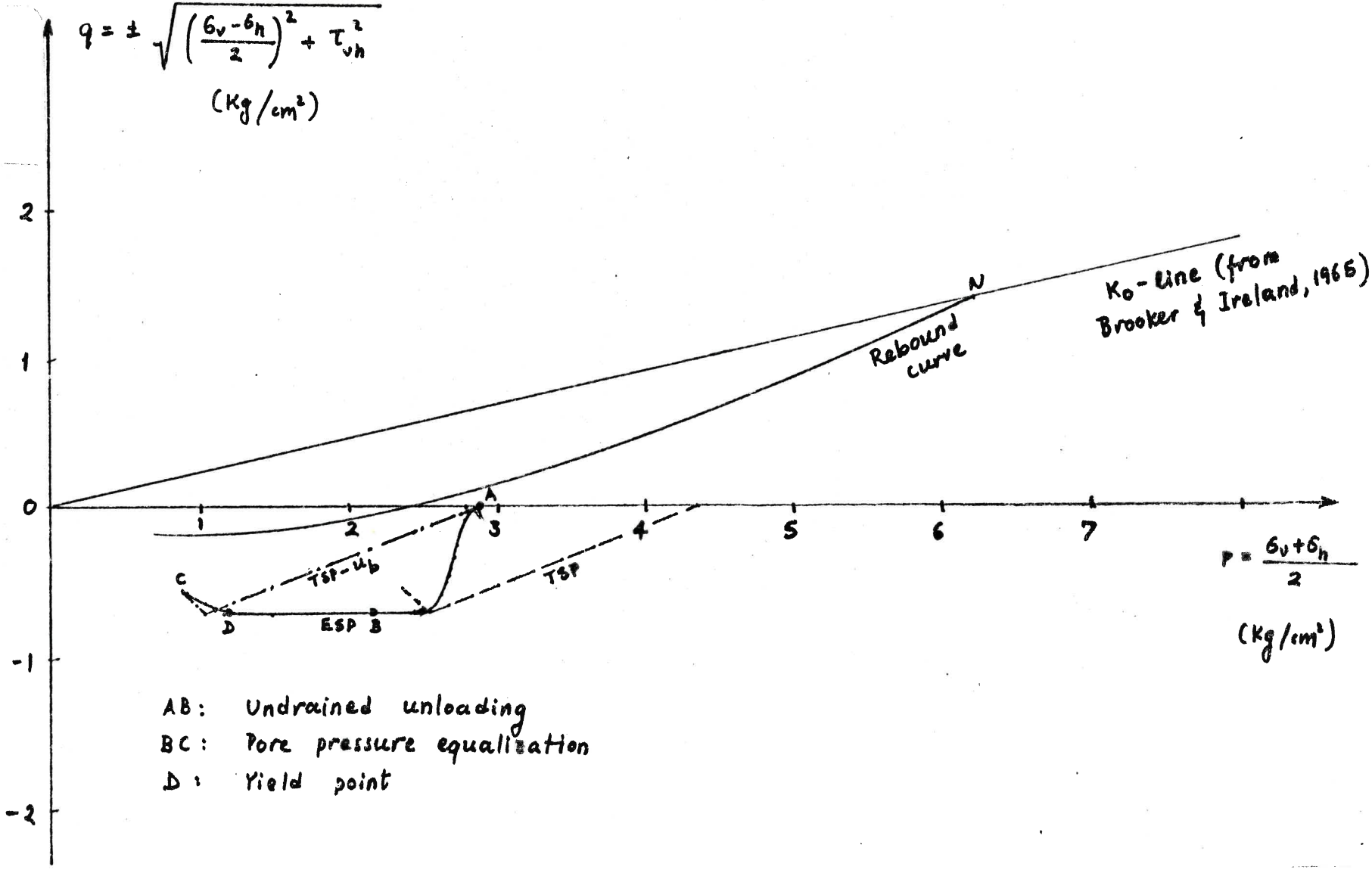


Fig. 6.3.10. Stress paths for sample ACUD-5 (θ=0°).

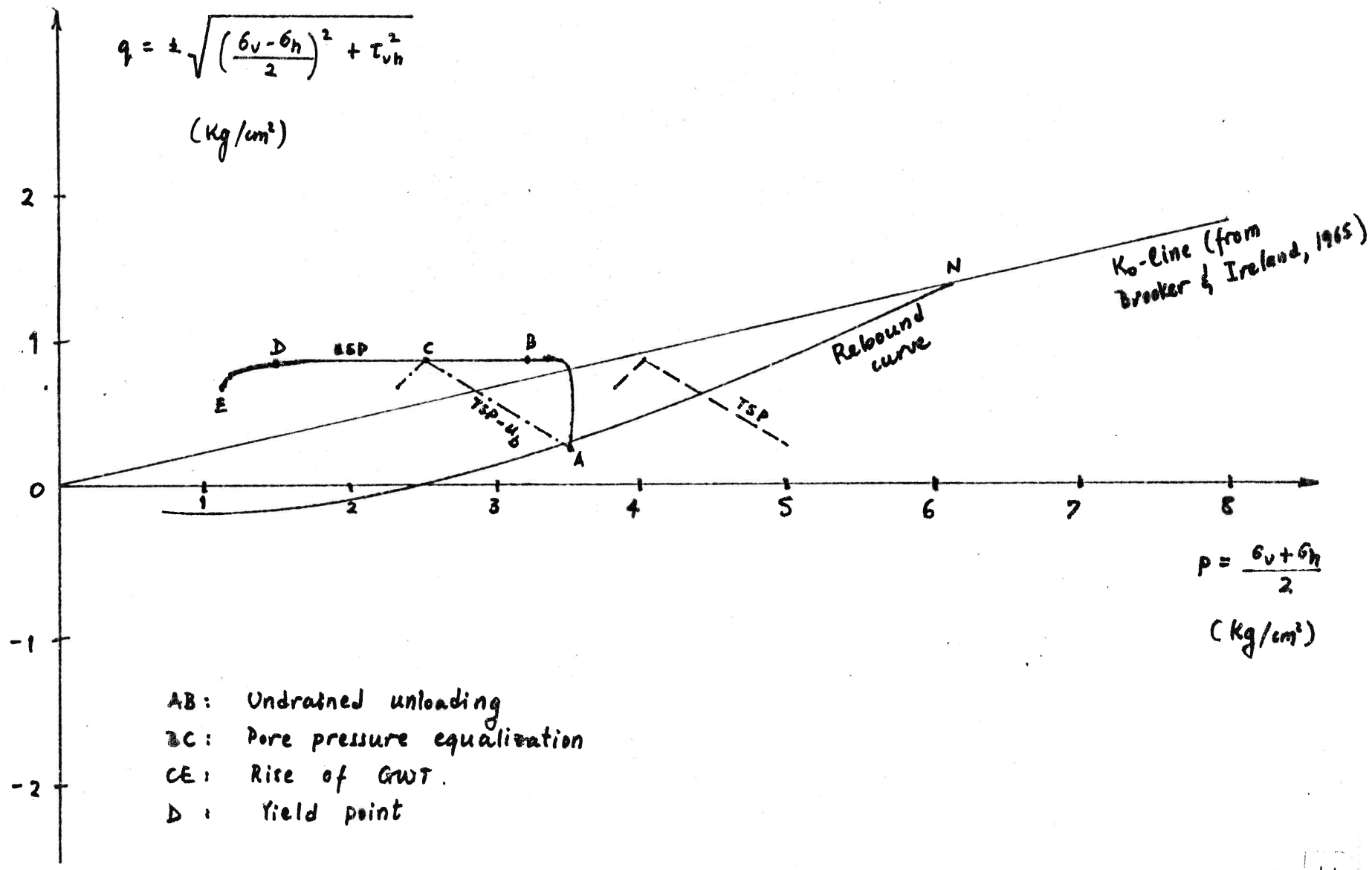


Fig. 6.3.11 Stress paths for sample ACUD-6 (θ=90°).

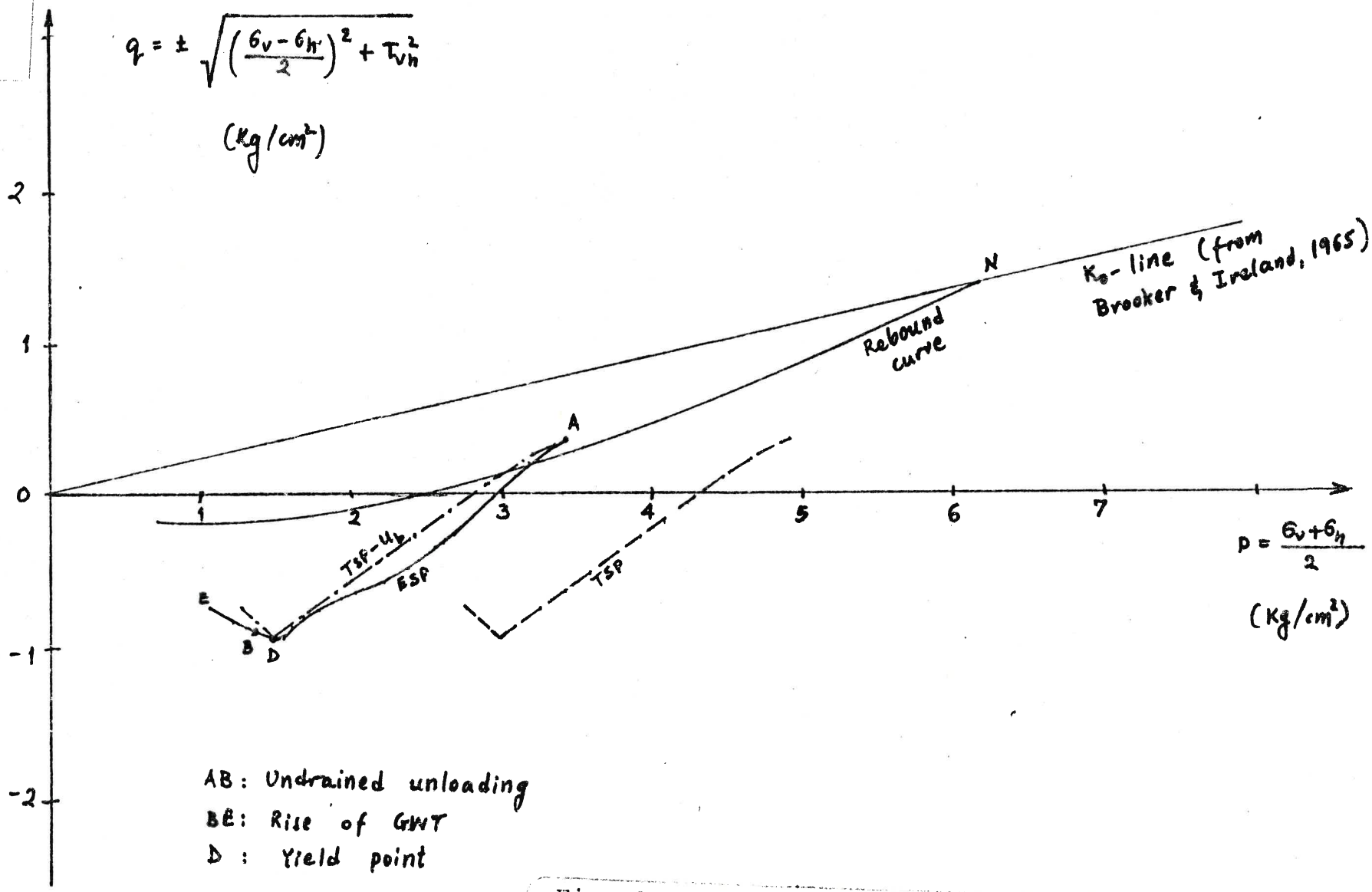


Fig. 6.3.12 Stress paths for sample ACUD-7 (θ=0°).

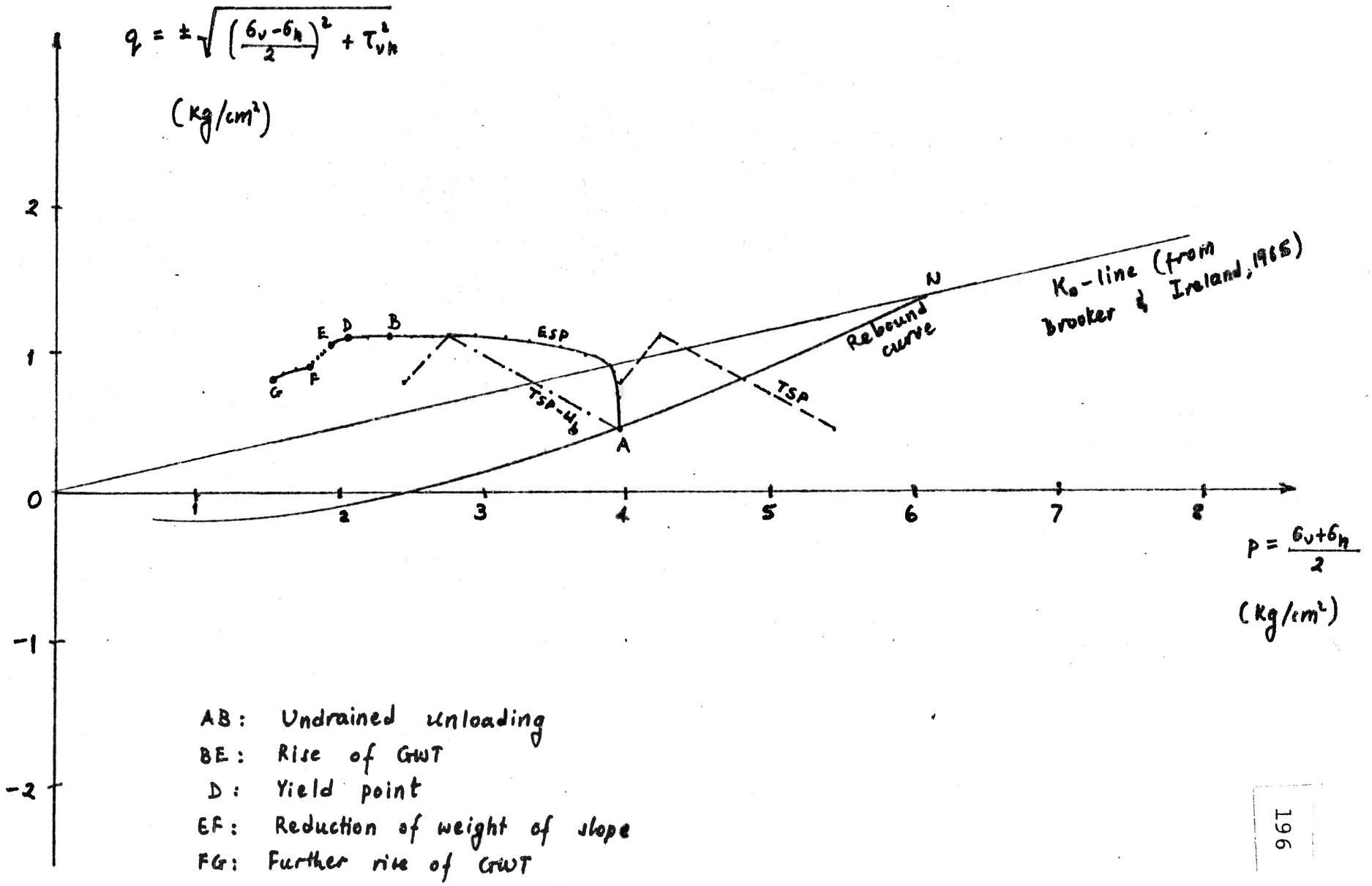
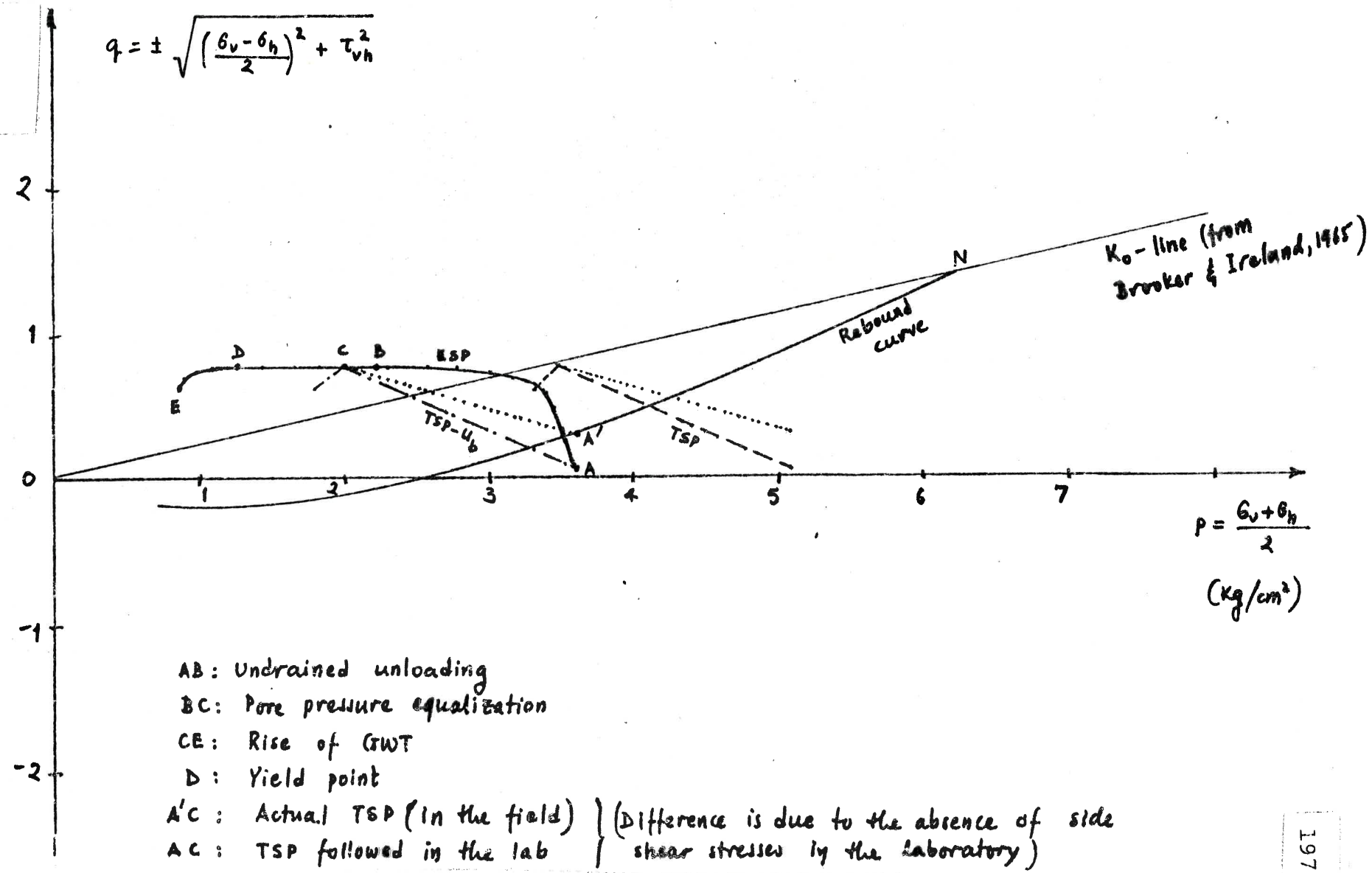


Fig. 6.3.13 Stress paths for sample ACUD-8 (θ=90°).



AB: Undrained unloading
BC: Pore pressure equalization
CE: Rise of GWT
D: Yield point
A'C: Actual TSP (in the field) } (Difference is due to the absence of side
AC: TSP followed in the lab } shear stresses by the laboratory)

Fig. 6.3.14 Stress paths for sample ACÜD-9a (ϑ=50°).

for the small negative pore pressure changes.

Failure can be defined in several ways, as for example:

—The point at which $(\sigma_1-\sigma_3)$ becomes maximum

—The point at which $\frac{\sigma_1'}{\sigma_3'}$ becomes maximum

—The point at which $\frac{\sigma_1-\sigma_3}{\sigma_1'+\sigma_3'}$ becomes maximum

In order to be able to make a meaningful comparison between the results of the conventional drained triaxial tests and the "stress path" tests, the same failure criterion would have to be used for both. Since failure is defined, in the consolidated-drained (CD) tests, at the point of $(\sigma_1-\sigma_3)_{max}$, the same criterion would have to be used for ACUD tests. Notice, however, that $(\sigma_1-\sigma_3)$ is maximum for every point along the ESP in the pore pressure equalization phase, as well as in the GWT rising phase. Thus, for ACUD tests, failure is defined as the point where $(\sigma_1-\sigma_3)$ starts to decrease from its maximum value. This point also coincides with the point where axial deformation starts to accelerate. This point has been denoted by letter D on the ESP plots and it has been called "yield point."

Notice that a phase of pore pressure increase beyond the point of pore pressure equalization (point C), was necessary for samples ACUD-4b, ACUD-6, ACUD-8, and ACUD-9a, in order to be led to failure. Samples ACUD-5 and ACUD-7

on the other hand failed at the end of the pore pressure equalization phase.

The total stress paths, along which the ACUD samples were tested, correspond to the TSP of representative soil elements selected from several slopes. The slopes analyzed were all 1.5:1 slopes and their height ranged from 13 to 37.5 meters. The geometries of the slopes analyzed are shown in Fig. 6.3.15 and 6.3.16. The locations of the samples behind the slopes are also shown on the same figures.

Fig. 6.3.17 presents all effective stress paths together on the same $\bar{p}$ vs. $\bar{q}$ plot. The virgin compression and rebound ESP are also shown on the same plot. Finally, the effective stress envelope, from the conventional consolidated-drained tests, has been drawn on the same plot, so that a comparison with the ACUD test results can be made. It will be noticed that the failure points, obtained from the ACUD tests, fall very close to the conventional effective stress envelope, except for the case of sample ACUD-7 ($\theta = 0°$) for which the point of failure is considerably higher than the envelope. However, the picture from the rest five ACUD tests is rather consistent and it leads to the following conclusions:

—The orientation of the samples does not seem to have any effect on the effective strength parameters.

—For lightly to medium O.C. clays it does not seem

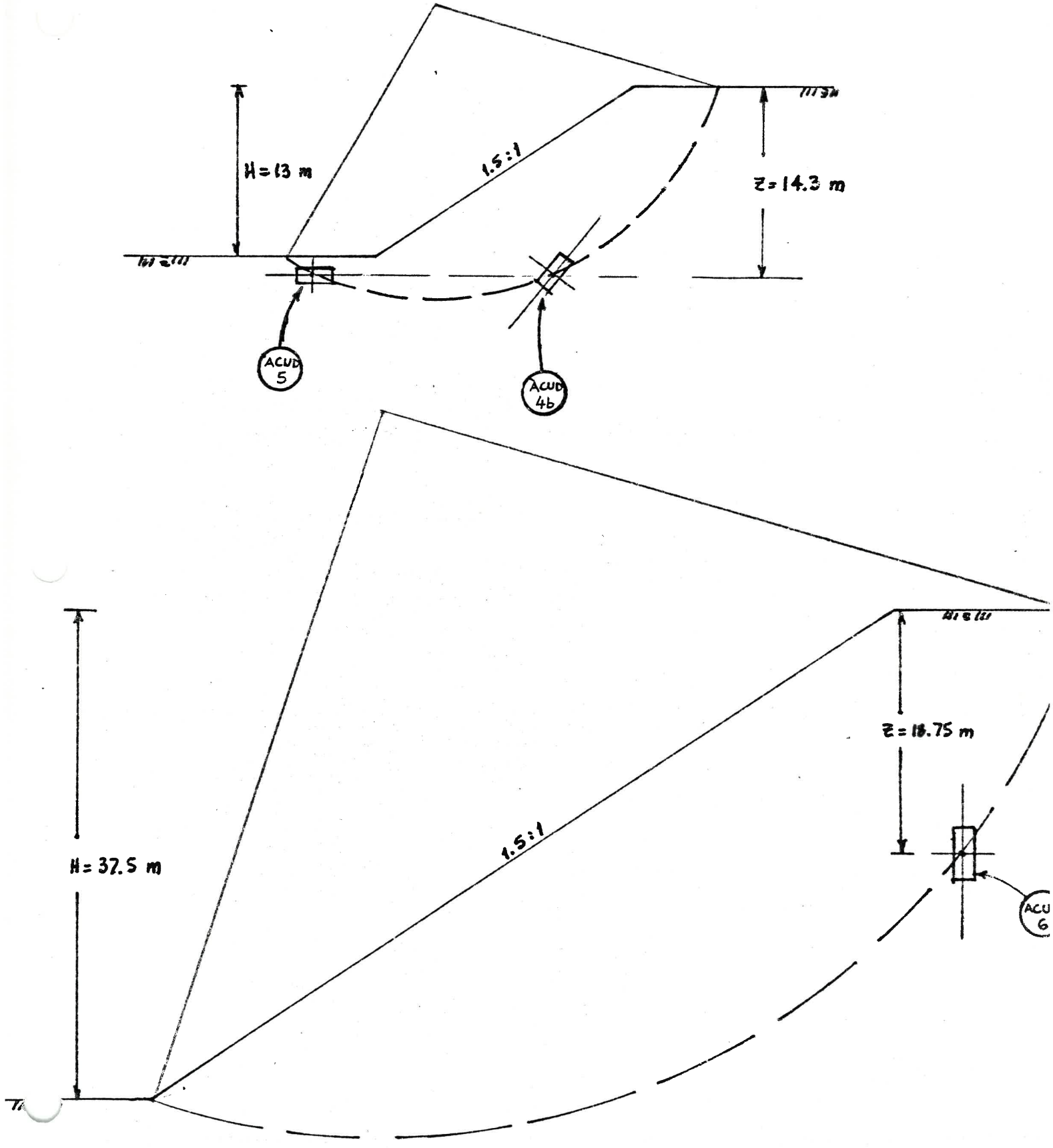
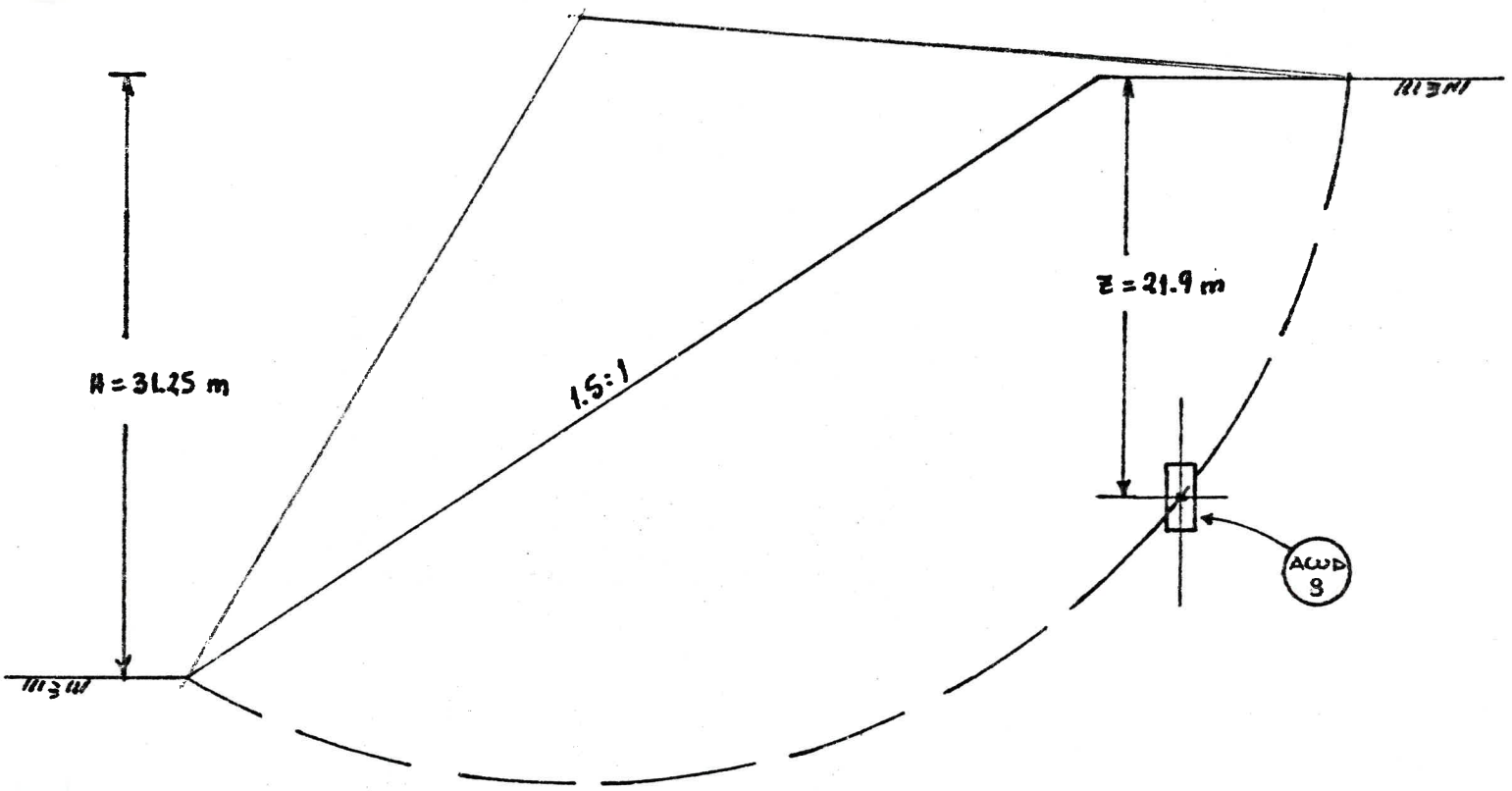


Fig. C.3.15 Geometries of slopes analyzed for ACUD tests



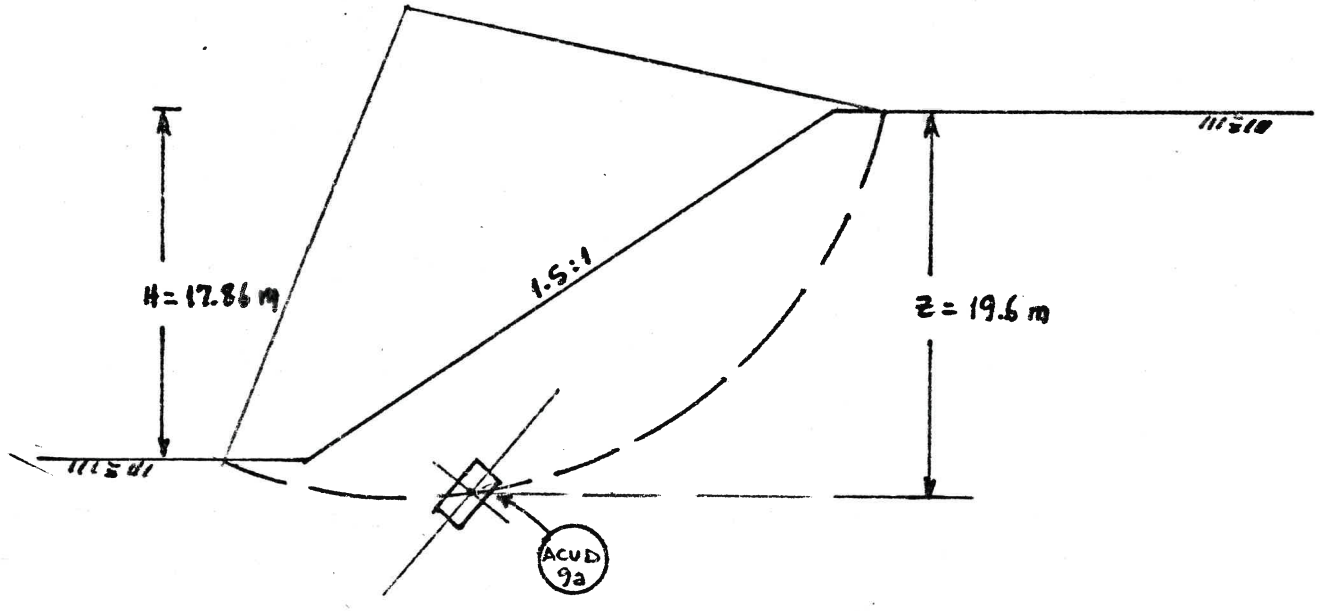


Fig. 6.3.16 Geometries of slopes analyzed for ACUD tests

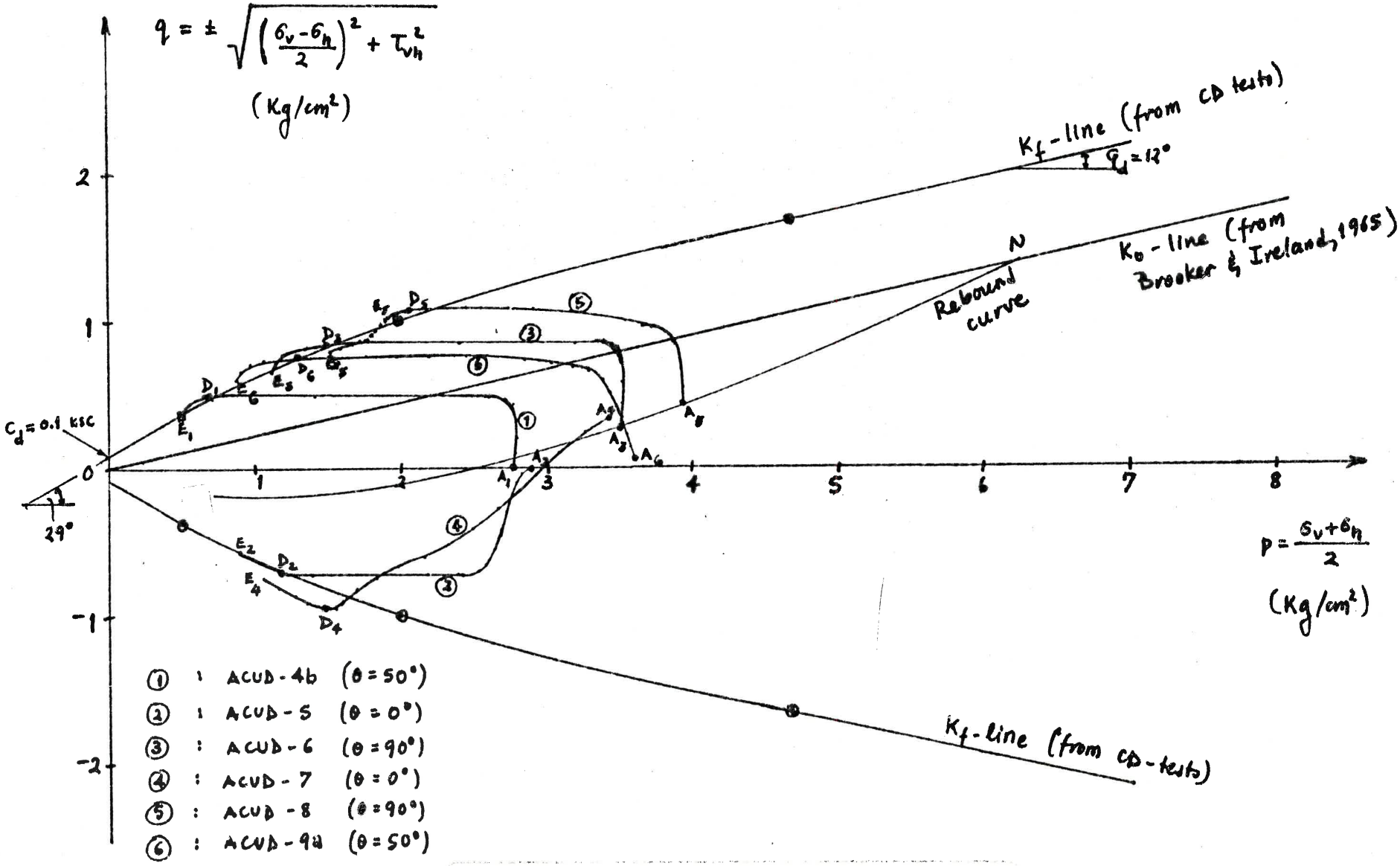


Fig. 6.3.17 Effective stress paths from all ACUD tests.

to exist any softening effect during pore pressure equalization, at least in the time scale of a laboratory test.

—The absence of fissures may also be responsible for the fact that no strength softening was observed.

—The development of negative pore pressure changes seems to depend a lot on stress reorientation.

6.4 Testing Techniques for Measuring the Residual Strength in the Laboratory

The various testing techniques that have been employed in the past for measuring the residual strength of soils (usually highly overconsolidated clays and shales) will be briefly discussed here and their relative advantages and disadvantages will be discussed.

a. Direct Shear Test

In this type of shear test the sample is forced to fail along a predetermined plane (horizontal). The shear "box" may be either round or square. A variety of shear "box" sizes are used, depending on the kind of soil to be tested (big samples are used for example when testing fissured clays in order to include the effect of the fissures on the strength of the clay). A normal force is applied on the failure plane and the shear stress required to fail the sample is taken as the shear strength of the

soil. That does not mean that the aforementioned normal and shear stress combination is the worst one for the sample (in other words, the pairs of values (σ, τ) at failure does not necessarily plot on the Mohr circle envelope). The direct shear test can be performed under drained or undrained conditions depending on the kind of field conditions that are being simulated. One problem inherent in the direct shear test is the uncontrolled rotation of principal stress axes during the test. The principal stress directions depend on the magnitude of the normal and shear stresses on the horizontal plane of failure as well as on the magnitude of the normal stress exerted by the shear box on the vertical sides of the specimen. The normal stress on the failure plane is the only one being controlled during the test (it is usually held constant), while the shear stress on the failure plane varies continuously and the normal stress on the vertical sides is unknown. Two moreproblems with this kind of test are the absence of complementary shear stresses along the vertical sides of the specimen (theoretically the specimen is not in moment equilibrium) and the non-uniformity of shear strains along a vertical profile. Although the state of stress of a soil element in the ground is very badly represented, this kind of test has the special advantage of inducing very high shear deformations along a relatively thin zone and subsequent particle orientation

parallel to the direction of shearing within this thin zone. These features are particularly desirable when the residual strength needs to be measured, since this strength develops after full particle orientation along the failure surface, as explained in more detail in the section dealing with the residual strength. The direct shear test has the additional advantages of simplicity both in sample preparation and test procedure, it requires relatively short testing time (short drainage path, relatively fast particle orientation along a thin zone) and the specimen can be readily wire-cut after consolidation, if desired (Danish Geotechnical Institute, 1964). The purpose of cutting the specimen is to help reach the residual strength sooner by breaking any bonds along the failure plane. Usually no peak is observed in such a case. Alternatively, the sample can be precut (cut before it is placed into the shear "box") and then consolidated (DeBeer, 1967). A small peak is usually observed in such a case because of bonds forming along the failure plane during consolidation. Precutting the specimen (before conslidation) can of course be done with other types of tests, too. It has been found that cutting the specimen gives in general a lower residual strength (De Beer, 1967; Bishop et al., 1971). A problem of the direct shear test, directly related to residual strength measurements, is the limited shear displacement that can be tolerated with this kind

of apparatus, relatively to the displacement usually required for the strength to drop to the residual. The multiple reversal direct shear test, which is described next, and its various modifications are usually used in an attempt to overcome this problem.

b. Multiple Reversal Direct Shear Test

This test is very similar to the one previously described, the only difference being the continuous back and forth shearing of the specimen in order to attain large total shear displacements. The disadvantages of this kind of shear test are the complicated stress conditions across the sample (as discussed under the direct shear test), and that the soil may be squeezed out between the two halves of the shear box during the later stages of the test (Chattopadhyay, 1972), limiting thus the number of reversals. Another serious disadvantage is that the small back and forth displacements may not be equivalent to a test with a displacement of the same total magnitude always in the same direction. The latter has been confirmed among others by Bishop (Bishop, Green, Garga, Andresen, Brown, 1971), who compared the results of multiple reversal direct shear tests and ring shear apparatus tests (described next) and found discrepancies in many cases. These discrepancies may be due to the fact that full particle orientation along the failure plane cannot

be attained in the multiple reversal direct shear test, because the direction of shearing is reversed before the particles have fully oriented themselves parallel to the failure plane; reversing the direction of shearing will results in a rotation of the particles in the opposite direction than before and this will go on with the particles rotating back and forth and never really getting fully oriented. This problem can be possibly overcome by shearing the specimen always in the same direction. This can be achieved by lifting the sample at the end of each one-directional shearing, putting it back in place, reconsolidating it and finally by shearing it again in the same direction. This procedure is of course more time-consuming than the multiple reversal direct shear test, since the consolidation phase will have to be repeated in each cycle.

c. Ring Shear Apparatus Test

The new ring shear apparatus was developed by Bishop and his colleagues (Bishop et al., 1971) and it is an improvement of earlier attempts by other investigators. It consists of a ring shear "box" the lower part of which rotates relative to the upper, thus shearing an annularly shaped sample. A cylindrical sample is obtained from a clay block, an inner core is then removed from it and a sample 0.75 inches thick, 4 inches in inner diameter and

6 inches in outer diameter is finally obtained. The top and bottom of the sample are clatched on annular porous ceramics with the help of radial fins, which protrude into the sample. The sample can thus be sheared in one direction by rotation of the lower ring for as large shear deformations as desired.

The obvious advantage of this kind of apparatus is the unlimited shearing of the sample in only one direction, so that the residual strength of the soil can finally be attained. However, it fails to satisfy the criteria of simplicity of construction and operation and in addition it has the disadvantages of local concentrations of strains and uncertainty about the directions of the principal stresses as the test proceeds (the last two are also disadvantages of the other types of shear tests described earlier, but they are not very important in residual strength measurements). Another disadvantage is the variation in strain produced across the sample, due to the variable linear displacement of the outer and inner edges, for a given angular rotation. However, this becomes insignificant after the residual strength has been reached everywhere across the sample. Squeezing out of the sample between the two halves of the ring may occur at very large deformations (which can also be the case in the multiple reversal direct shear apparatus, as described previously). This can be avoided by performing

the initial part of the test slowly leaving a small gap between the upper and lower parts of the ring, then proceed faster closing at the same time the gap to avoid any loss of the sample and then perform the last part of the test slowly and with the gap again slightly open (Bishop et al., 1971). The purpose of the fast part of the test is to form a failure plane so that the residual strength can more easily be attained in the last, slower, part of the test. Finally, it may be difficult to prepare specimens for use in the ring shear apparatus with stiff, fissured clays.

Bishop (1971) has compared the results of the ring shear apparatus, for the residual strength of the Brown London clay, with those obtained using other testing techniques and he found that the latter gave a residual friction angle 2° - 6° higher than that obtained using the ring shear apparatus.

d. Triaxial Test

Drained triaxial tests can be used for measurement of the residual strength. However, they suffer from the serious disadvantage that in many cases the deformation necessary to reach the residual strength state cannot be obtained in the triaxial compression apparatus, except possibly in the case of very brittle clays. According to Chandler (1966) this difficulty can be overcome by precutting

the sample along a plane forming an angle $\alpha = 45° + \varphi_r'/2$ with the horizontal, where φ_r' is the expected residual friction angle. Test results suggest that measured values of φ_r' are not much influenced by small inaccuracies in the choice of the inclination of the shear plane. Chandler (1966) has also developed corrections for the effects of the change in the cross-sectional area and the restraint of the rubber membrane, which become critical at large axial displacements. The horizontal movements of the upper half of the specimen, above the precut plane, can be facilitated by using two top caps separated by small stainless steel balls. An advantage of the triaxial compression test on precut specimens is the fact that the test can be performed in multiple stages by reconsolidating and reshearing the specimens at higher cell pressures, once the residual strength has been reached, in order to define several points on the residual strength envelope (Chandler, 1966; Symons, 1967). Another advantage is the fact that the stresses applied on the sample are more easily controlled and more accurately known than in any of the previously described shear tests.

Good agreement has been found between results obtained from direct shear tests and triaxial tests on precut samples. However, the values are usually somewhat higher compared to those obtained from ring shear tests (Bishop et al., 1971), which suggests that even artificial

polishing of slip surfaces by a spatula or glass plate does not establish maximum particle orientation.

e. Direct Shear Test Using Composite Specimens

This testing method was developed by Kanji (1974, 1977) and it is based on direct shear testing of composite samples of clay soil and hard surfaces (polished rock, metal, etc.) in the conventional direct shear apparatus. The soil is remolded at the liquid limit, it is then consolidated between two hard surfaces and it is finally sheared.

The main advantage of this testing method is the small displacement (in the order of 1 cm) required to affect particle orientation and bring the soil to its residual strength. This happens because during shear there are no particles projecting across the shear plane and catching on each other and also because the hard, smooth surface provides a fixed plane to guide the alignment of particles (Mitchell, 1976).

A disadvantage of this kind of test is the interference of granural particles as the silt or sand contents increase, which makes the orientation of the clay particles difficult, resulting in higher residual shear strengths. Also, it is not clear whether the residual friction angle, as measured, corresponds to that for soil alone or to the friction angle between soil and rock. Notice that the

friction angle between clay particles and hard surfaces may not be the same as the friction angle between the clay particles themselves.

6.5 Residual Strength Measurements

From the testing techniques available for measuring the residual strength, we finally selected the triaxial test on precut samples, because the stresses are more easily controlled in such a test and also because it was hoped that multistage tests could be performed. The samples used for the tests were reconstituted samples. We decided to use reconstituted samples instead of the original samples because residual strength is independent of sample disturbance and remolding, and it only depends on the composition and pore water chemistry of the sample. However, reconstituting the samples may have caused some change in the pore water chemistry. Using reconstituted samples had, nevertheless, the extra advantage of relatively easy trimming, precutting and in general handling of the sample.

In the following paragraph the apparatus and testing techniques adopted for residual strength measurements are described first, followed by a presentation and discussion of the results.

a. Description of Apparatus and Testing Procedure

The triaxial cell used for the residual strength measurement tests (which are briefly called CDR tests by abbreviation of Consolidated, Drained, Residual strength measurement test) was very similar to the one used for the "stress path" tests. The basic difference was the top cap arrangement for the CDR tests, which consisted of two caps with stainless steel balls in between. The lower of the two top caps was on top of the sample and its upper surface was flat so that the stainless steel balls could easily slide on it. A lucite steel ball retainer kept the eight balls in position. A schematic representation of this set up is shown in Fig. 6.5.1. With the use of such an arrangement there was practically no constraint in the horizontal movement of the upper half of the specimen. The CDR tests were performed in a strain controlled loading apparatus. This apparatus had the advantage that it used a very stiff load cell, instead of a considerably more flexible proving ring, for measuring the load. This had the advantage that there was very little strain energy stored into the load cell during loading, so that accurate post peak measurements could be made (because of the very small strain energy release after the peak). Strain gages mounted on the load cell made it possible to measure accurately the applied load, even for the very small deformations of the stiff load

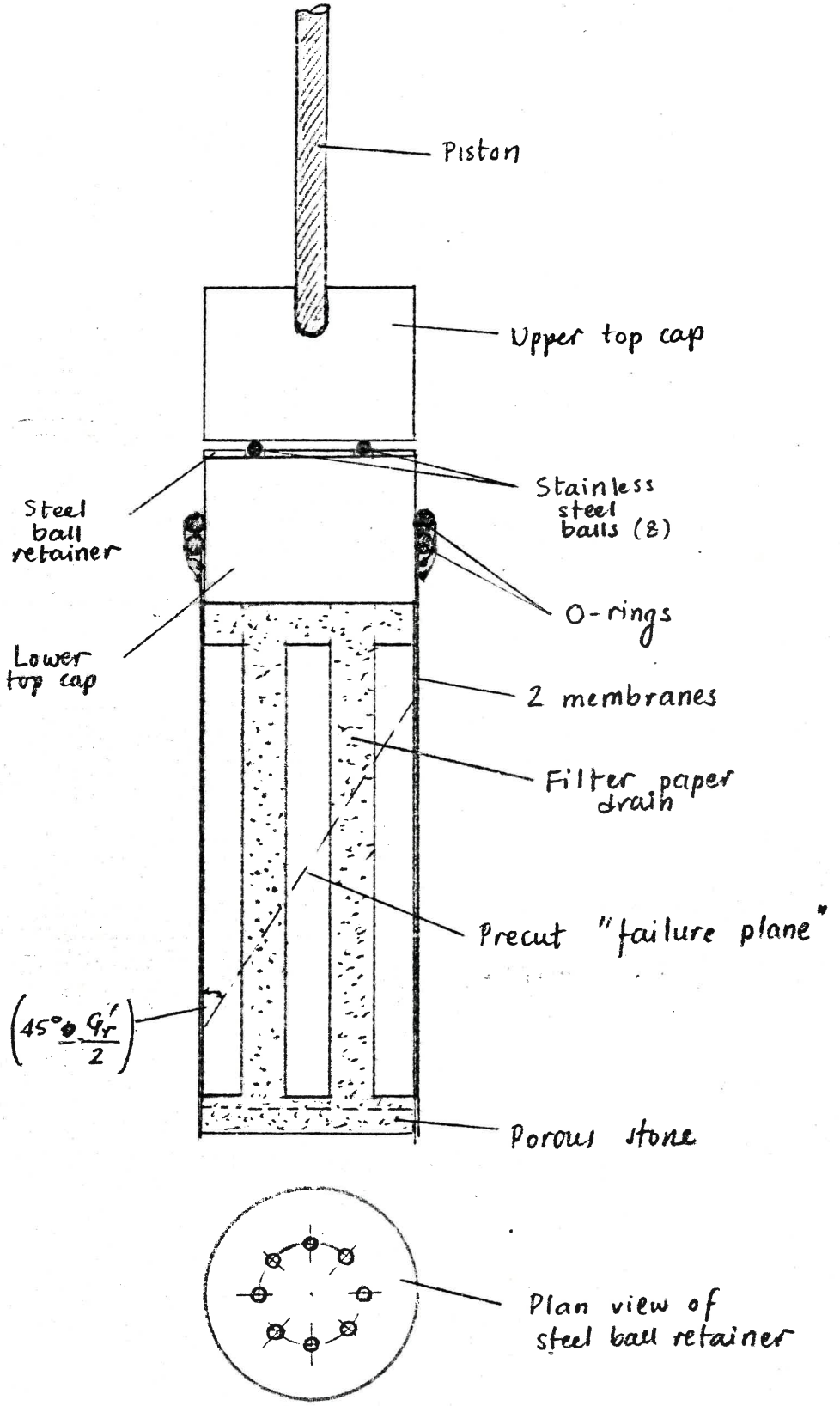


Fig. 6.5.1 Schematic representation of CDR test set up.

cell diaphragm. The load cell was connected to the same full Wheatstone bridge arrangement, described in Section 6.3. The rate of advancement of the piston was controlled by the flow of oil through a micrometer valve. By controlling the opening of the valve, the rate of advancement could be controlled. This rate remained fairly constant throughout the test.

The testing procedure adopted for the CDR tests was the following:

—The specimen was cut from the big reconstituted sample, with its axis vertical.

—After it had been trimmed down to a cylindrically shaped specimen (1.4 inches in diameter by 3.5 inches high), it was cut in two pieces in such a way that an artificial "failure plane" was formed (Fig. 6.5.2). This plane formed an angle $\alpha = 45° + \frac{\varphi'_r}{2}$ with the horizontal, where φ'_r is the estimated residual angle of internal friction. An angle α equal to 50° (accuracy for α : ± 1°) was used for the tests of this investigation (which corresponds to $\varphi'_r = 10°$). Notice that small inaccuracies in the selection of φ'_r do not affect the value of the measured residual strength.

—The artificial "failure plane" was then "polished" with a spatula. The spatula was moved always in the same direction, which coincided with the direction

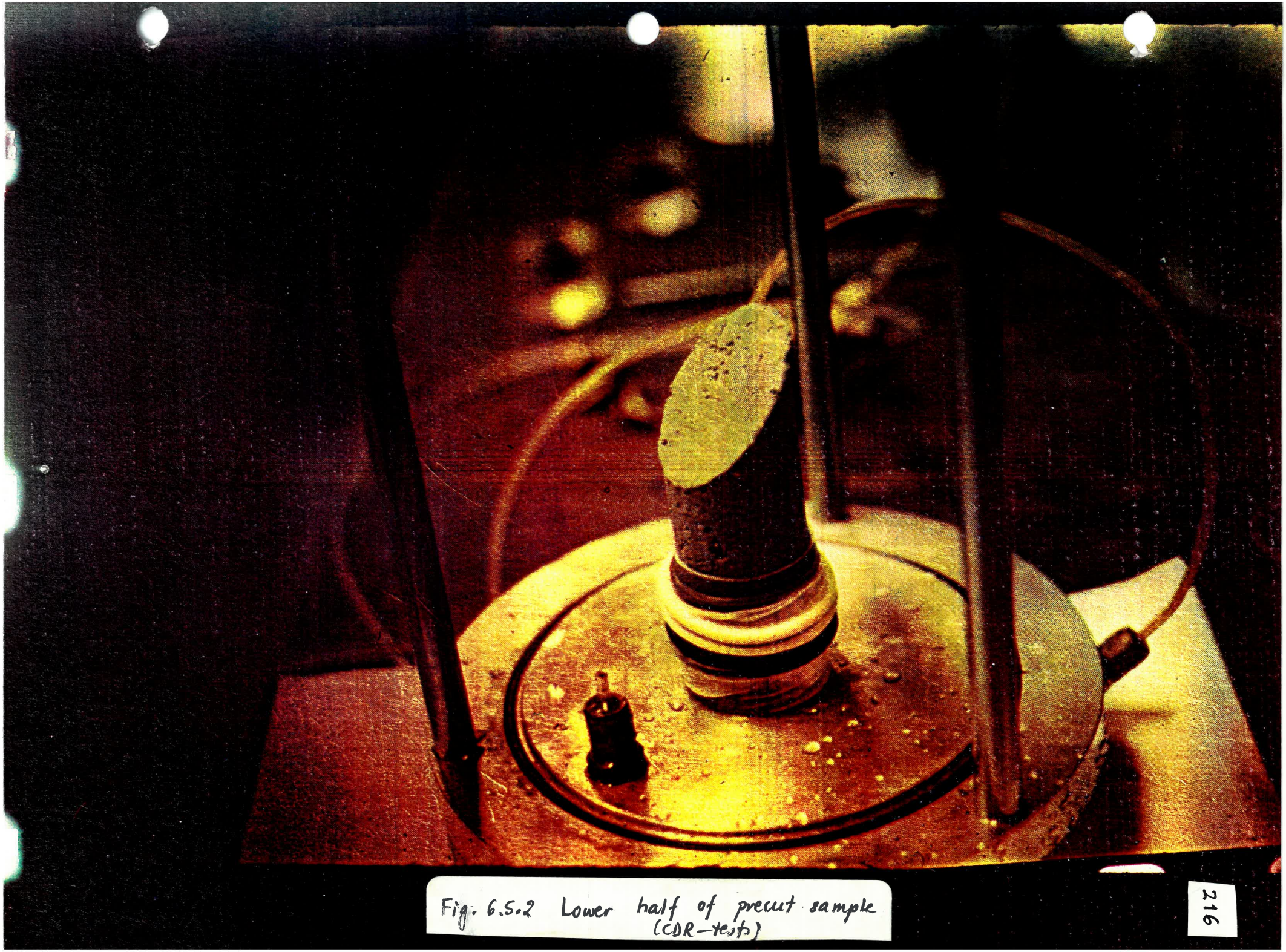


Fig. 6.5.2 Lower half of precut sample (CDR—tests)

of relative movement of the one half of the specimen relative to the other, during the test.

—After polishing the "failure plane," the two pieces were put together again, the sample was placed into the triaxial cell and the cell was assembled, as described for the "stress path" tests. Special care was taken at this stage to properly center the stainless steel balls.

—The specimen was saturated in the triaxial cell for 24 hours, by raising the back pressure to 1.50 Kg/cm^2 and the cell pressure to 1.60 Kg/cm^2 in three steps (same as for the "stress path" tests).

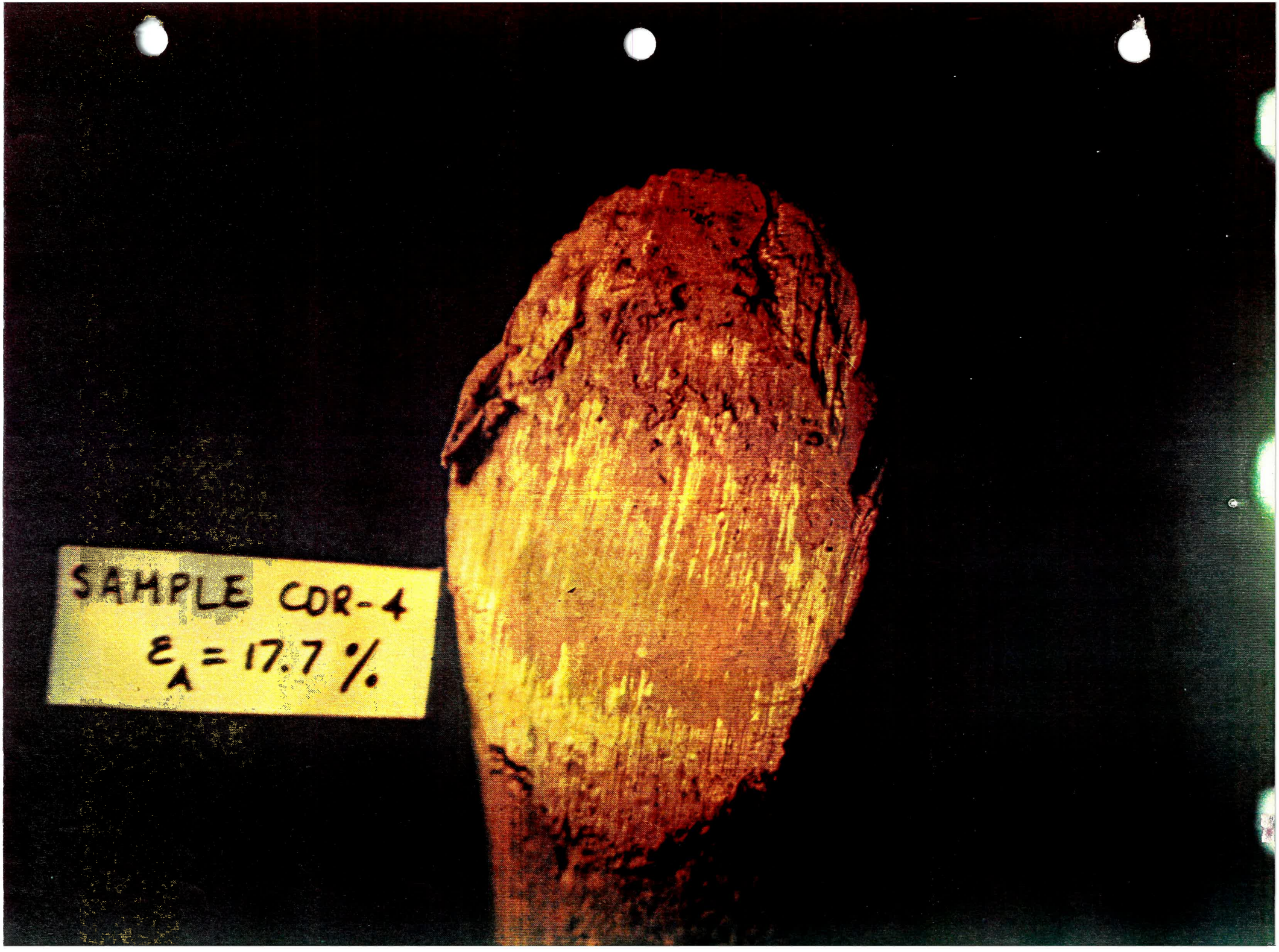
—The specimen was then isotropically consolidated for 24 hours under the desired effective consolidation pressure. Consolidation pressures equal to 1.00, 2.00, and 3.00 Kg/cm^2 were used.

—After consolidation was over, the advancement of the piston was started. A rate of advancement approximately equal to 0.00019 inches/minute was used throughout the test, for all CDR tests. This rate was considered to be sufficiently slow, so that any excess pore pressures would dissipate. Measurements of axial load, axial deformation and volume change were made at regular intervals. The tests were usually stopped when the axial strain reached 17%-20%.

There was one test which was continued out to an axial strain of 32%, but it was decided to establish 20% as a maximum strain, since eccentricities became rather pronounced after 20% and the membranes were overstressed, to a point that they could potentially fail. The loading part of the test usually lasted for 2 to 2.5 days.

—After the test was over the cell was disassembled and the upper half of the specimen was forced in the same direction that it had been moving during the test, until the two pieces were separated. Measurements of the major and minor axes of the "failure plane" and of the true area of contact at the end of the test were made. These measurements were used in the corrections for filter and membrane effects and true area of contact, as described in Appendix 3. The configuration of the true area of contact was very clear on the "failure plane," because material was squeezed out from the area of contact during the test, and was deposited on the rest of the "failure plane."

—Some of the specimens were stored in the humid room, in order to be later tested again (if for example the residual strength state had not been attained during the first run).


SAMPLE COR-4
ε_A = 17.7 %

b. Results

A total of 11 triaxial residual strength tests (CDR tests) were performed. Two of these were performed in the load controlled apparatus (described under the "stress path" tests), and the rest 9 in the strain controlled apparatus (described in the previous paragraph). Using the load controlled apparatus it was very difficult to get any meaningful results for the post peak behavior of the clay. In addition it was practically impossible to maintain a relatively slow and constant rate of axial deformation with the load controlled apparatus. For these reasons the strain controlled apparatus was adopted for testing after the first two tests. The nine CDR tests were performed under three different effective consolidation pressures. Five tests were performed under $\sigma'_{3c} = 2.00\ kg/cm^2$, three tests were performed under $\sigma'_{3c} = 3.00\ kg/cm^2$ and one test was performed under $\sigma'_{3c} = 1.00\ kg/cm^2$. From the five tests performed under $\sigma'_{3c} = 2.00\ kg/cm^2$, four tests were performed on the same sample (sample CDR-2a) so that the number of runs, required for perfect particle orientation to be attained, could be found. The load vs. displacement curves for these four runs are shown in Fig. 6.5.3. From that figure it can be seen that repeated loadings result in a drop in strength. From the same figure it will be noticed that runs 1 and 4 exhibit a very irregular

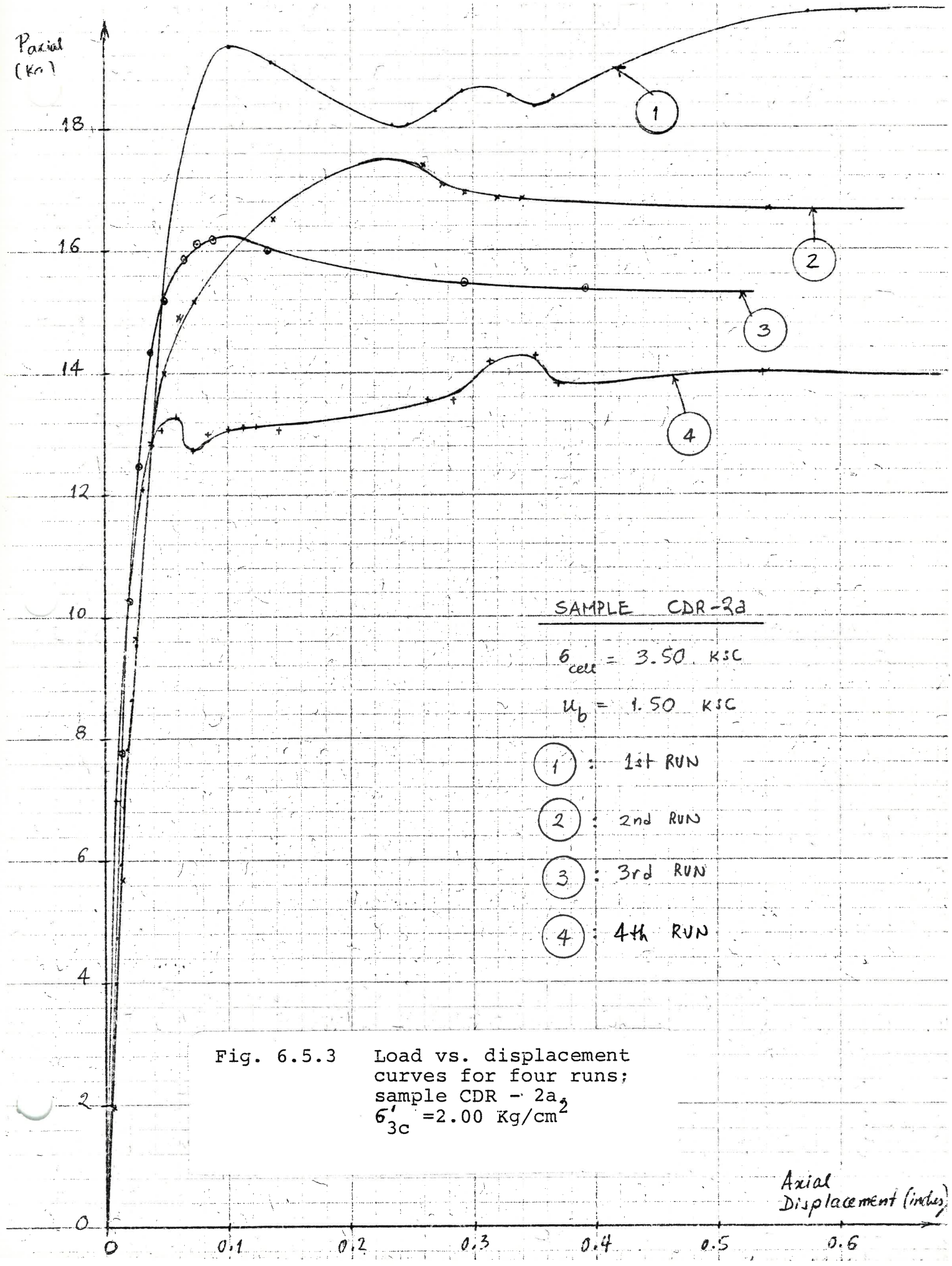


Fig. 6.5.3 Load vs. displacement curves for four runs; sample CDR - 2a, σ'_{3c} =2.00 Kg/cm^2

load-displacement curve, while run 2 exhibits a rather unusual load-displacement curve. In addition the strengths corresponding to these load-displacement curves are higher than expected. Careful consideration of the forces acting on the specimen during the test, as well as of the way each component of the test set up functions, revealed the following mechanism as being responsible for these inconsistencies (see also Fig. 6.5.4):

The thickness of the steel ball retainer (made of lucite) was slightly less than the diameter of the stainless steel balls. In the beginning of the test, no horizontal movement of the upper half of the specimen had taken place and consequently no eccentricities existed (Fig. 6.5.4 (a)). As the test proceeded and the upper half of the specimen started moving to the left, the axial load became eccentric, the eccentricity being e/2, where e is the horizontal distance between the axis of the piston and the axis of the upper half of the specimen (Fig. 6.5.4 (b)). Due to this eccentricity the upper half of the specimen tended to rotate clockwise. Since the piston was not rigidly connected to the upper of the two top caps, a small rotation was allowed and it did take place. This led to a situation like the one shown in Fig. 6.5.4 (c), i.e., the ball retainer was sandwiched between the two top caps and a

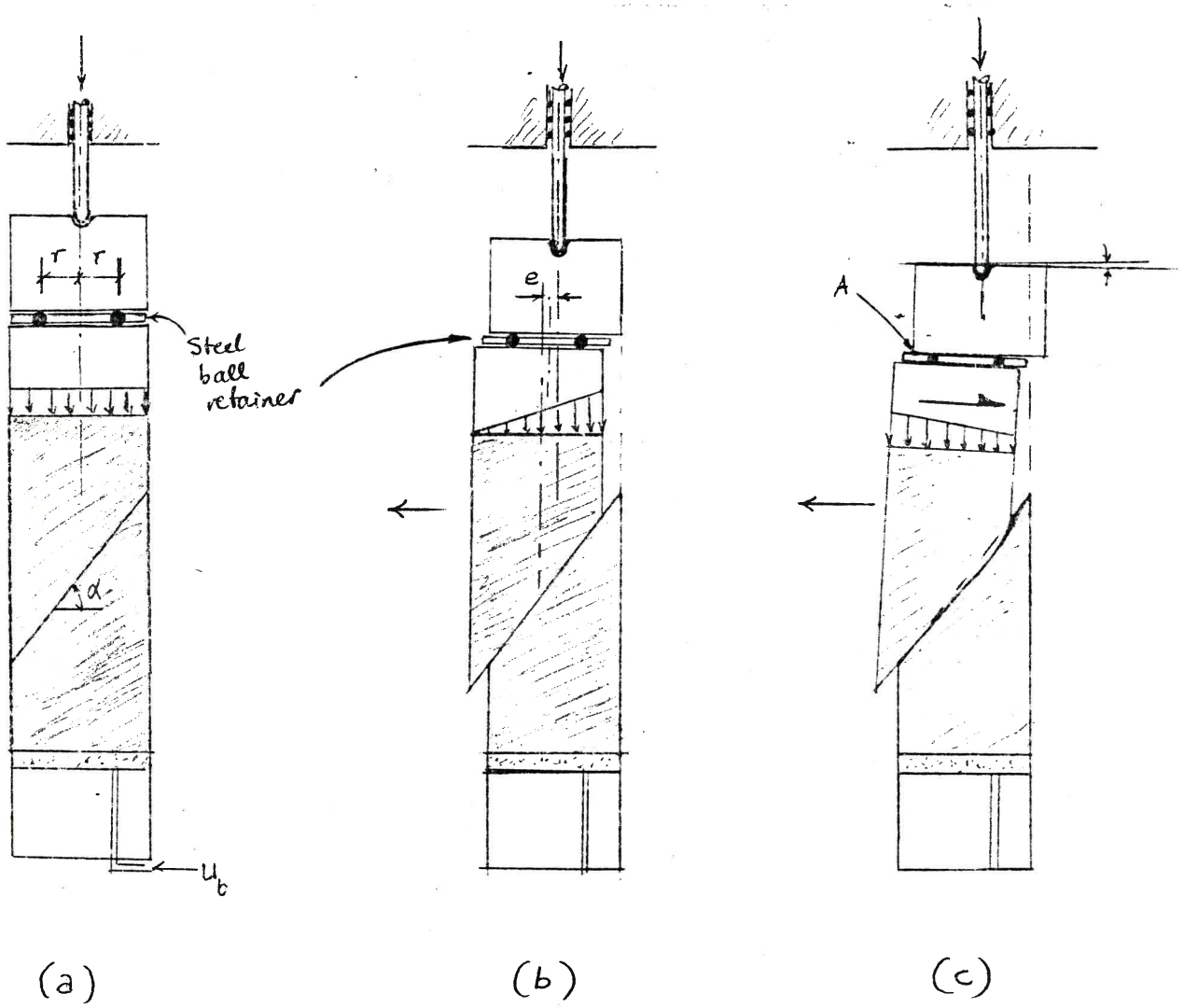


Fig. 6.5.4 Schematic representation of mechanism leading to application of horizontal forces on the top of the specimen.

contact point was formed at point A. Further horizontal movement of the upper half of the specimen caused a frictional horizontal force to develop at point A. By considering the force equilibrium of the upper half of the specimen (see Appendix 3), it is found that this horizontal force contributes to the strength of the specimen and this results in an apparently higher strength. The irregularities in the load-displacement curves are believed to be caused by a stick-slip type of frictional sliding of the two top caps on the ball retainer. Having realized what caused the apparent inconsistencies in the CDR test results, the lucite retainer was trimmed down to half its original thickness. This way no contact could be formed between the upper top cap and the ball retainer, as the rotation of the upper top cap, allowed by the piston-cap connection,was very small and inadequate for a contact to be formed. Three tests (CDR-4, CDR-5, CDR-6) were performed using this new ball retainer, and the results confirmed the above mechanism, as the load-displacement curves became smooth, consistent and gave considerably lower strengths. The three tests were performed for three different effective consolidation pressures, and the load-displacement and volume change-displacement curves from these tests are plotted in Fig. 6.5.5. For reasons of comparison, the load-displacement curves for two pairs of samples (CDR-2a and

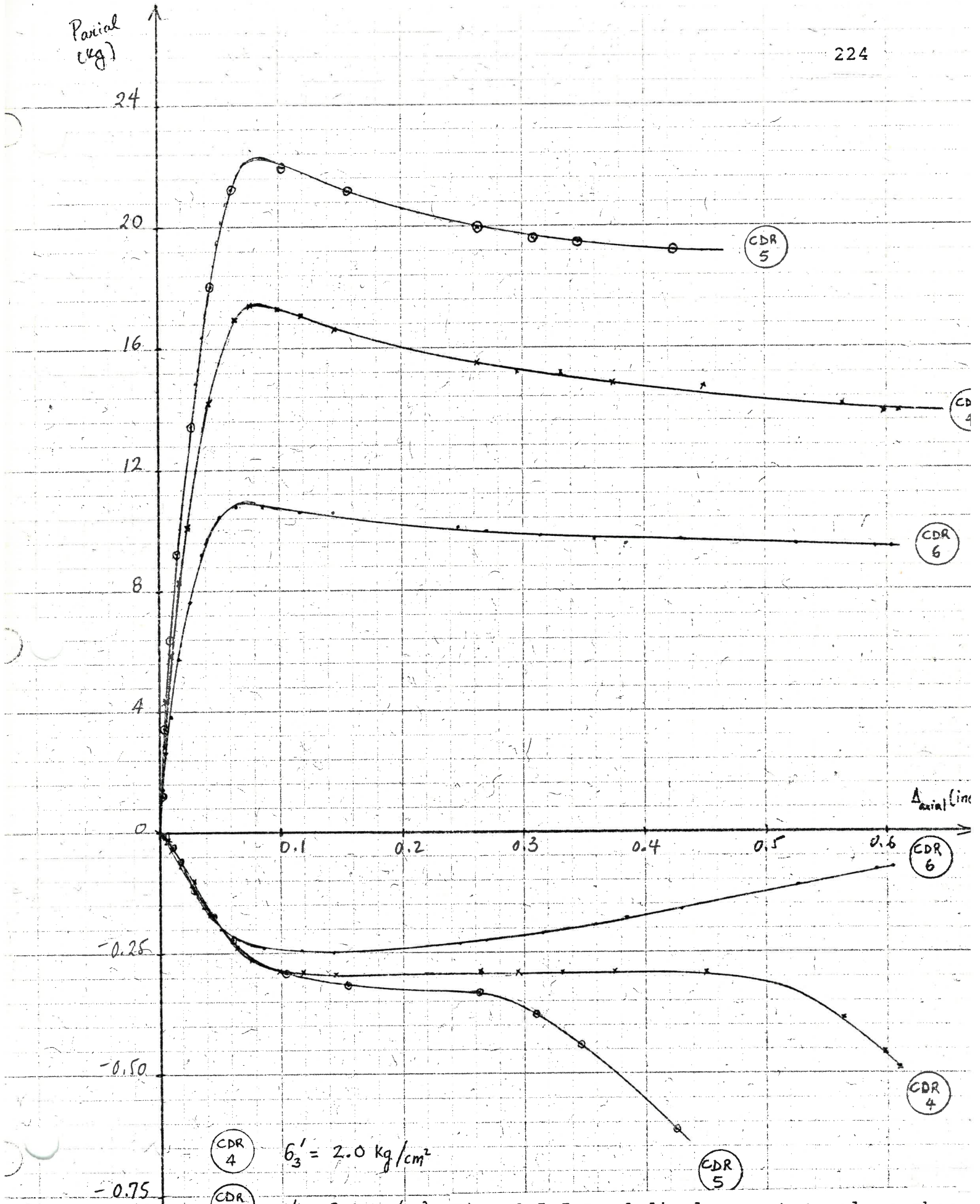


Fig. 6.5.5 Load-displacement & volume chang
displacement curves for samples CDR-4, CDR-
CDR-6; trimmed steel ball retainer used.

CDR-4; CDR-3 & CDR-5), which have been tested under the same effective consolidation pressures (2.00 Kg/cm^2 and 3.00 Kg/cm^2 respectively) but with different steel ball retainers (samples CDR-2a and CDR-3 have been tested with the untrimmed ball retainer while the other two samples have been tested with the trimmed ball retainer), have been plotted in Fig. 6.5.6 and 6.5.7. Using the correct curves in conjunction with the equivalent uncorrected ones, an approximate method of correction of the old curves was developed. This method is presented in Appendix 3.

There were some more corrections that had to be applied on the results of the CDR tests in order to be able to translate the measured loads in stresses. The corrections were necessary so that the effect of the filter paper drain and of the two membranes could be taken into account. For samples failing along a single failure plane, as was the case in these tests, the restraint of the membrane becomes critical. In order to be able to take these effects into account, several tests were run on precut samples, on the failure plane of which two pieces of membrane, with a thin layer of silicone grease in between, were placed. Since the silicone grease is a viscoelastic material, its resistance to shearing depends on the rate of shearing.

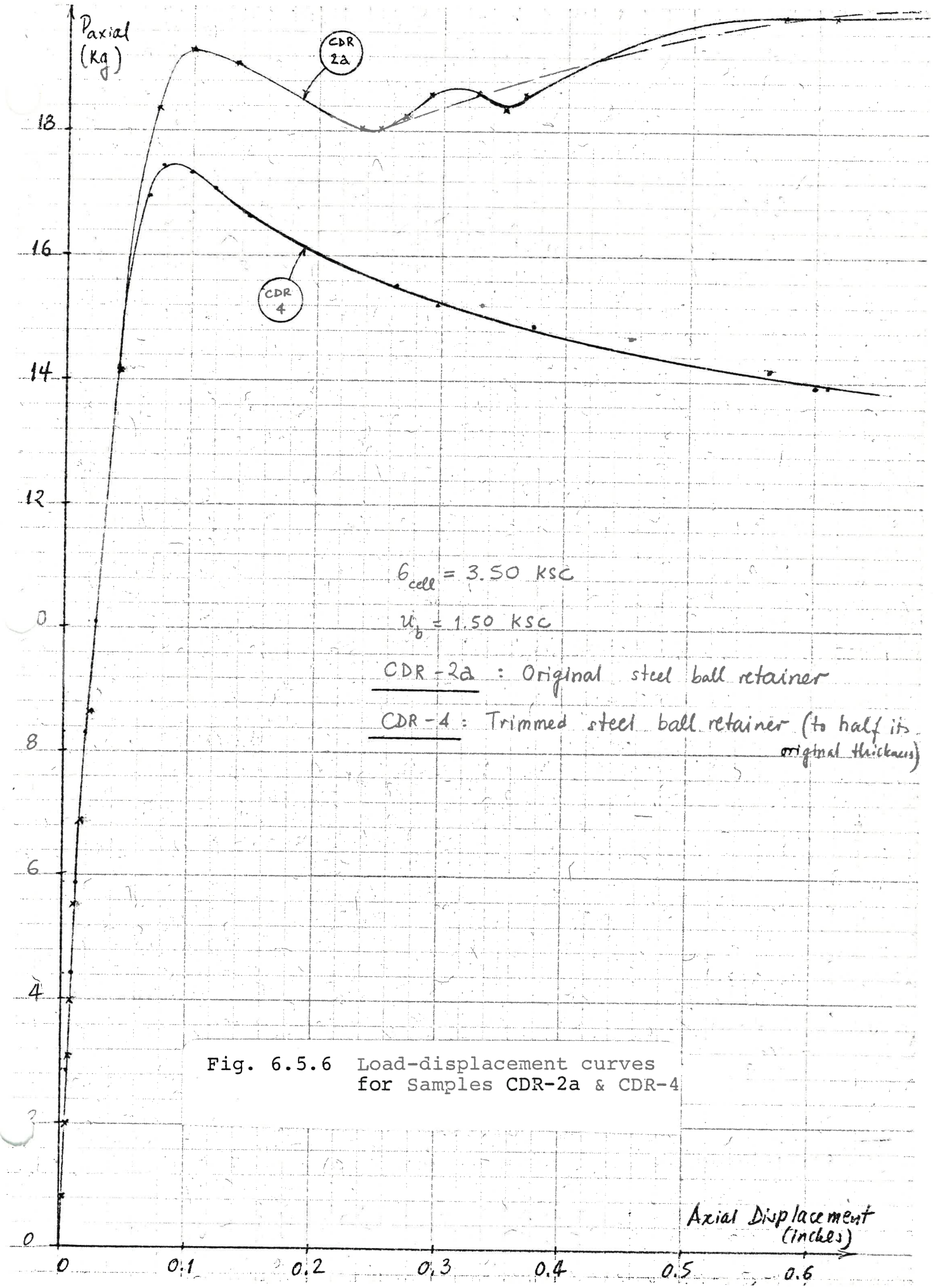


Fig. 6.5.6 Load-displacement curves for Samples CDR-2a & CDR-4

$\sigma_{cell} = 4.50$ KSC

$\sigma_b = 1.50$ KSC

CDR-3_1 : Sample CDR-3 ; 1st loading } Original steel ball retainer

CDR-3_2 : Sample CDR-3 ; 2nd loading }

CDR-5 : Trimmed steel ball retainer (to half its original thickness

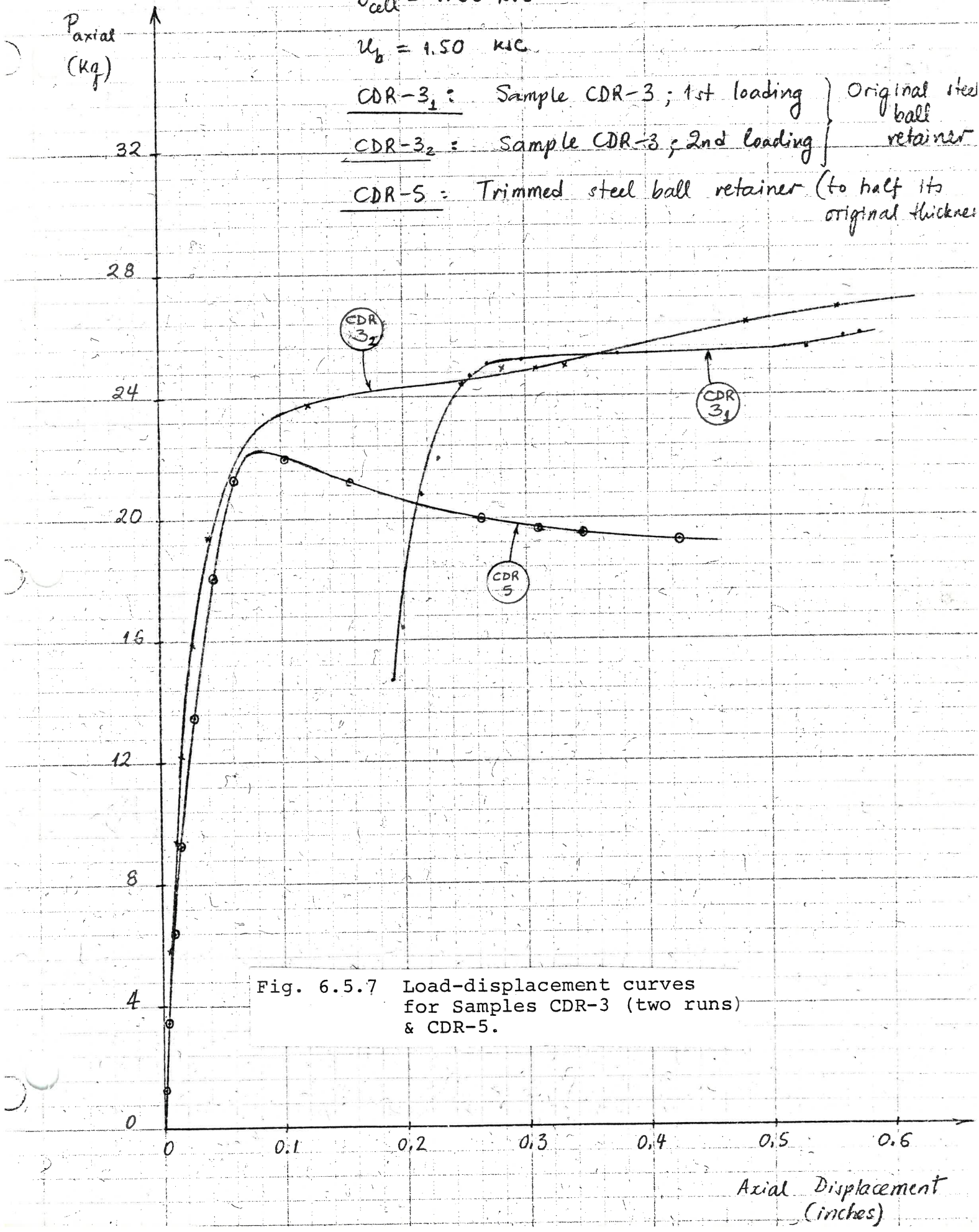


Fig. 6.5.7 Load-displacement curves for Samples CDR-3 (two runs) & CDR-5.

By using a constant rate of piston advancement, the constant resistance of the grease could be isolated and the remaining resistance was attributed to the filter and the two membranes. The results of these correction tests are presented in Appendix 3. These results were not in general very consistent, but they all had the same trend and in addition they approximately agreed with the results of other investigators (Chandler, 1966). This apparent inconsistency is believed to be due to the fact that the membrane was sliding on the "lubricated" failure plane at the higher displacements.

Another correction had also to be made for the true area of contact. The latter can be expressed as a function of the axial displacement ΔH, the inclination of the precut plane, α, and the radius of the sample, r, as follows (see also Fig. 6.5.8):

$$A_c^{plan} = 2r^2 \cos^{-1}\left(\frac{x}{r}\right) - 2x\sqrt{r^2 - x^2} \qquad (1)$$

where A_c^{plan} is the horizontal projection of the true area of contact, A_c, and $x = \frac{\Delta H . \cot\alpha}{2}$ (2)

Since the measured ΔH was not totally attributed to rigid sliding of the one half of the specimen on the other, but there was also some axial deformation taking place, an alternative formula was developed for A_c^{plan} (for a derivation of this formula, see Appendix 3):

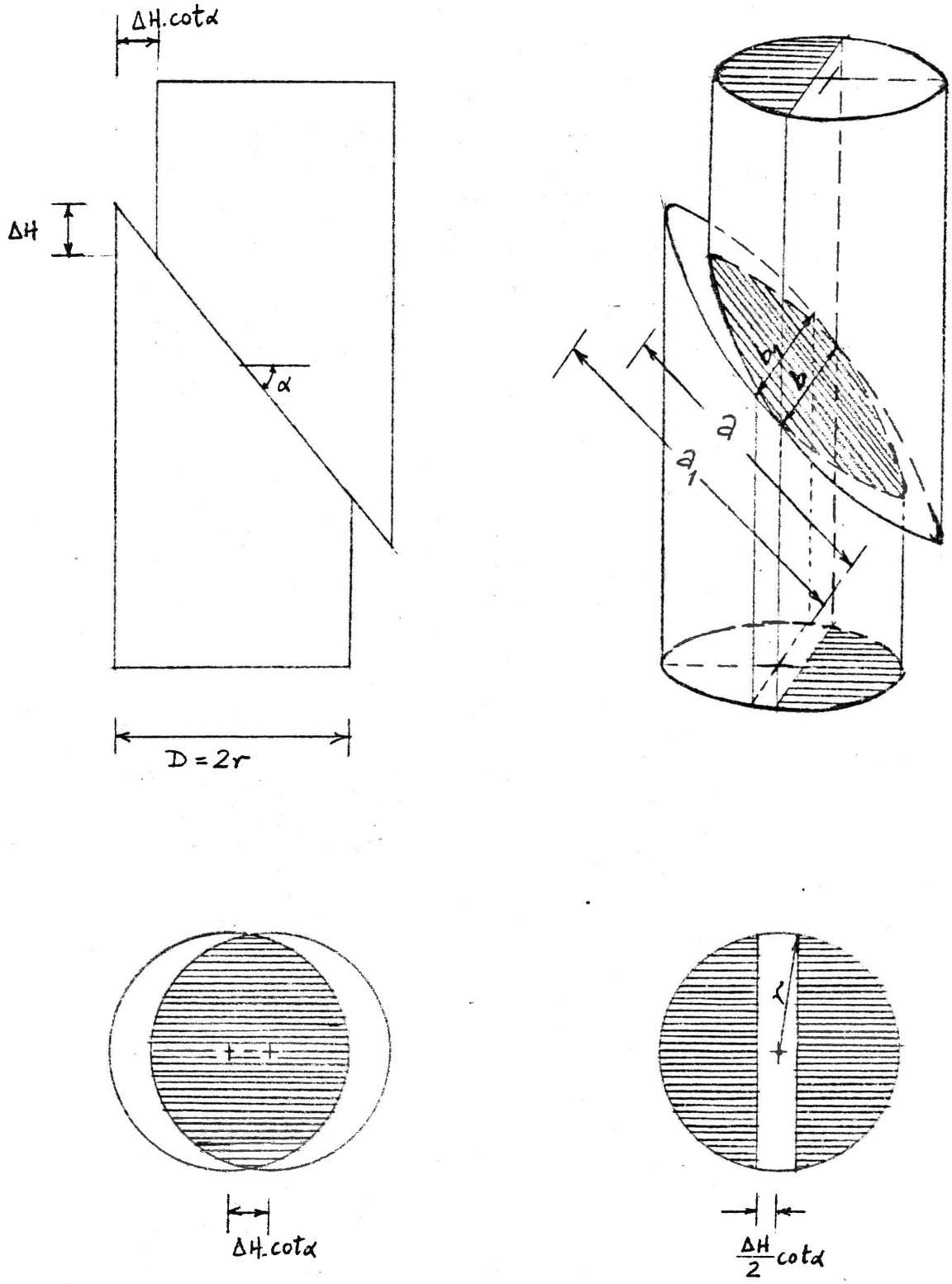


Fig. 6.5.8 True area of contact in CDR tests.

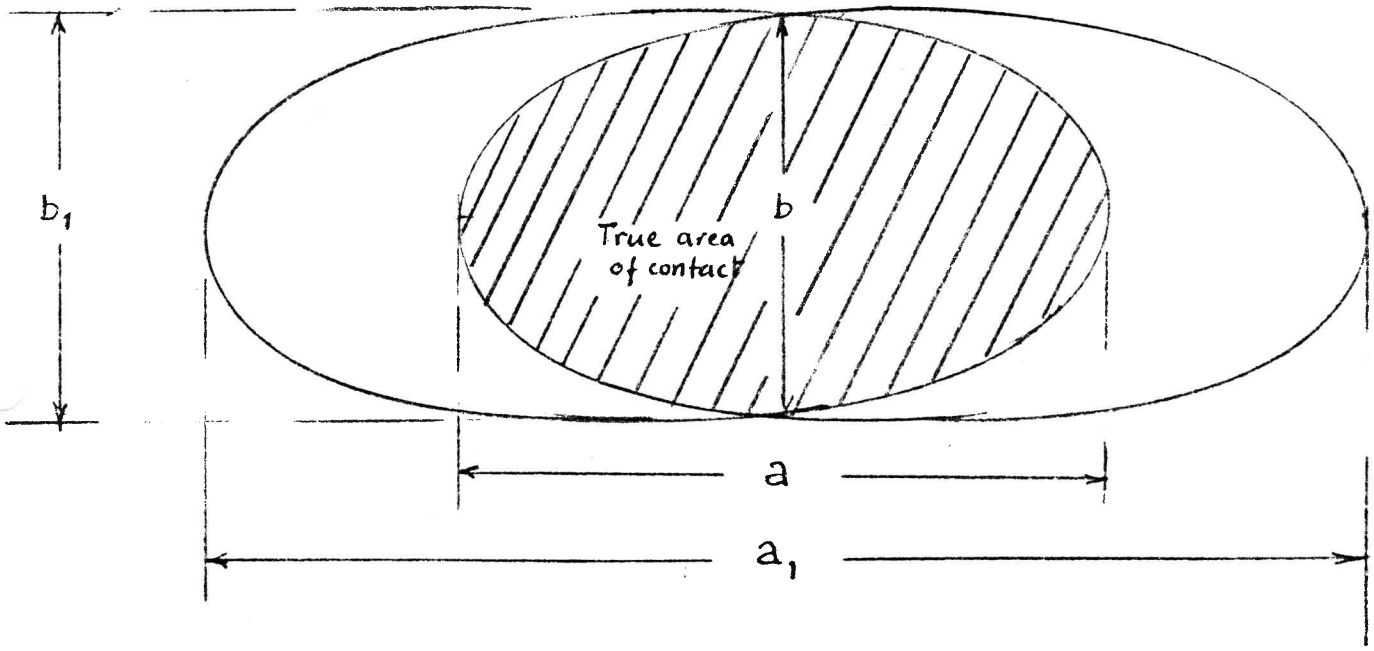


Fig. 6.5.9 Definition of a, b, a_1, b_1.

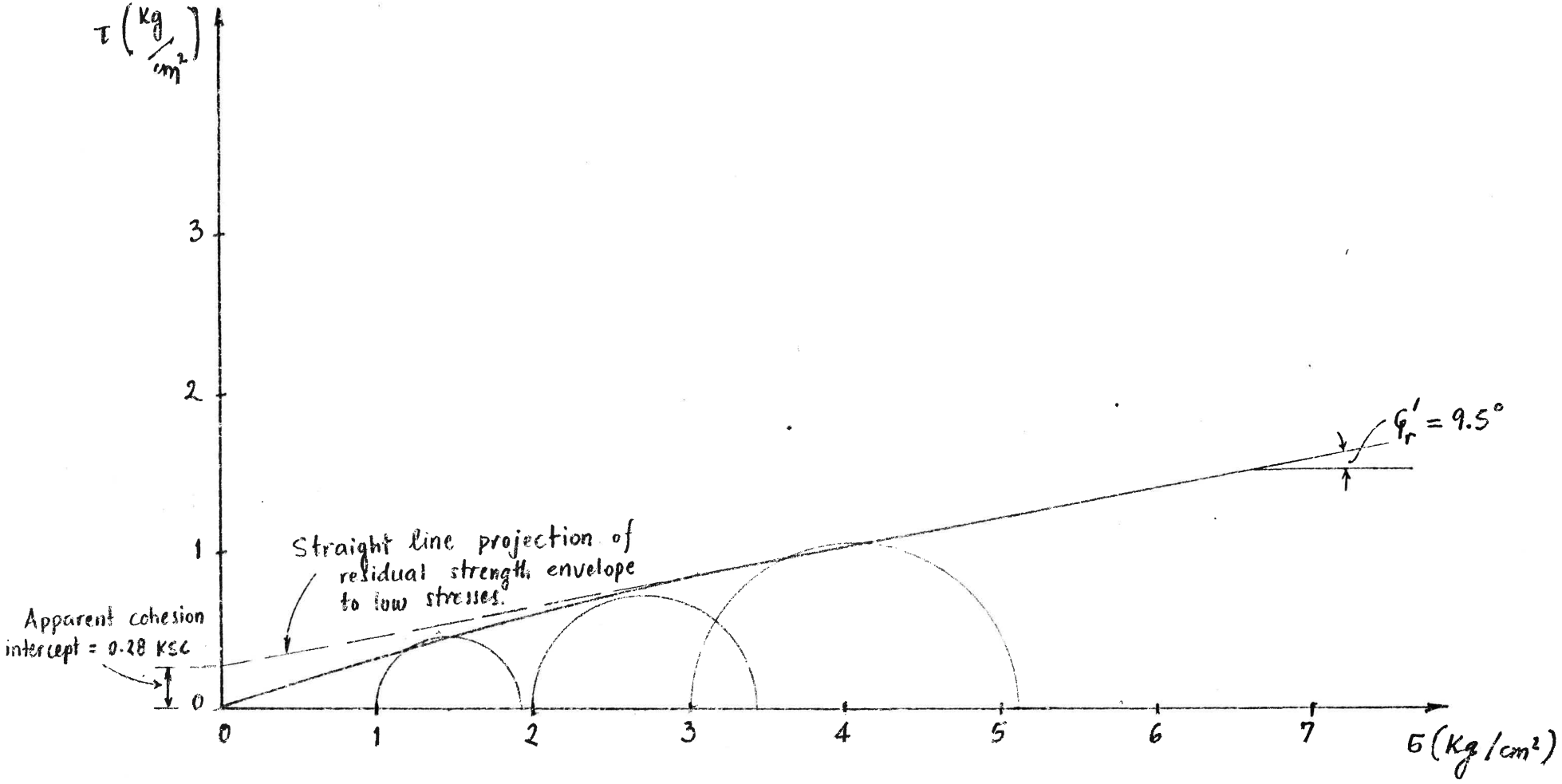


Fig. 6.5.10 Mohr's envelope for the residual strength of samples from the Friars Formation.

$$A_c^{plan} = \left[a_1^2 \cos^{-1}\left(1 - \frac{a}{a_1}\right) - (a_1 - a)\sqrt{a(2a_1 - a)} \right] \frac{\cos^2\alpha}{2} \qquad (3)$$

where the definition of a, b, a_1, b_1 is given in Fig. 6.5.9. As it was mentioned in the previous paragraph, a, b, a_1 and b_1 were measured after the test and from that the true area of contact at the end of the test could be found.

Using all the previously described corrections (which are also presented in Appendix 3), three Mohr circles were defined for the residual state of stress and the envelope shown in Fig. 6.5.10 was drawn through these points. Notice that the envelope is slightly curved at the lower stresses. This is consistent with the point made in Section 3.3, namely that the residual strength is stress dependent at low stress levels (its value decreases with stress at low stress levels, until it finally becomes constant at higher stress levels).

6.6 Summary

Using the results of the finite element analysis, one can make an estimation of the stress path that an element of soil behind a slope will follow after excavation.

There does not seem to exist any softening effect, due to pore pressure equalization, for lightly to medium O.C. nonfissured clays, at least in the time scale of a laboratory test.

The effect of sample orientation on the drained strength seems to be minor. Stress reorientation affects mainly the magnitude of the developing pore pressures, under undrained conditions.

There are several tests which can be used for residual strength measurements, such as:

—Direct shear test

—Multiple reversal direct shear test

—Ring shear apparatus test

—Triaxial test

—Direct shear test using composite specimens

Residual strength measurements can be made in the laboratory, by testing precut samples in the triaxial test apparatus. Good results can be obtained but the test is rather an involved one in terms of the many and significant corrections that have to be made.

7. CONCLUSIONS AND RECOMMENDATIONS

From the results of the investigation previously described, the following conclusions may be drawn:

1. Residual strength controls the stability of slopes in stiff, fissured clays and shales, in places where a continuous failure surface has already been formed. This continuous failure surface could be the result of a previous landslide or tectonic movements. Also, the residual strength may control the stability of slopes in cases where a progressive failure mechanism takes place. Hence, it is recommended that the residual strength be used in design where "bedding plane faults" exist in the Friars Formation. From the results of previous investigations, which are supported from the results of this investigation, a residual friction angle between 6° and 10° can be used in most cases for design in the Friars Formation (where shear zones seem to exist).
2. The residual friction angle can be measured with reasonable accuracy in the laboratory, by testing precut samples in the triaxial test apparatus. The results of this investigation show that small inaccuracies in the selection of the angle at which the sample should be precut ($\alpha = 45° + \varphi_r'/2$), do not affect the measurement of the residual friction angle.

The major difficulty in such a kind of test are the corrections for the effects of filter paper drain and membranes as well as the correction for the actual area of contact on the failure plane. Corrections for the effect of filter paper drain and of two membranes were developed. By comparing these results with the results of other investigators it is concluded that one can obtain corrections for the effects of filter and membrane with reasonable accuracy, by using published correction curves, so long as the latter are accompanied by the thickness of the membranes and the dimensions of the specimens used.

The use of two top caps with stainless steel balls in between enables the development of very high axial strains without imposing any restraint in the movement of the upper part of the specimen in the horizontal direction. It is, however, recommended that the maximum strains to be used should not exceed 17%-20%. At least four runs are required for full orientation of clay particles to be obtained and the strength to drop to the residual. However, two runs are recommended for most practical purposes.

3. Progressive failure can lead to a significant lowering of the average operative strength along a potential failure surface. Factors promoting progressive failure are:

•Considerable and fast drop in strength after the peak.

•High values of K_o (i.e., high OCR, high lateral earth pressures compared to the overburden pressure).

•High degree of fissuring.

•High degree of weathering.

•Steep and high slopes.

Progressive failure seems to be responsible for failures of slopes in the Friars Formation, in places where no "bedding plane faults" seem to exist. The fact that many slopes have failed 3-10 years after excavation shows that there is ample time for progressive failure to develop.

The only method available at the time, for progressive failure to be taken into account, is the finite element method applied for a strain softening material. However, such a method would be expensive and difficult to perform on a routine basis. Consequently, either or both of the following are recommended for the design of slopes in the Friars Formation, in places where no "bedding plane faults" have been found to exist:

•Perform once and for all several finite element analyses for various heights and slopes of excavation for a strain softening material, by approximating the stress-strain curve of samples from the Friars Formation by three linear portions. Then the average operative strength along a critical failure surface, at the point

of limiting equilibrium, can be found and thus empirical design strength parameters can be established for various slope geometries. Interpolation between the results of such an analysis can be later made.

•Back-calculate the average operative strength from slopes that have failed in places where no "bedding plane faults" existed, and establish thus average design strength parameters.

4. The surface cracks, which are filled with water during the rainy period, can potentially lower the factor of safety of a slope for two reasons:

•There is practically no strength along the open cracks.

•The water filling the cracks creates a pressure head, which contributes to the driving forces.

Since surface cracks exist, in many cases, in the Friars Formation, they should be taken into account in design.

5. The stress path method can be used in order to find the factor of safety at any point behind an excavated slope. This is achieved by making an analysis of the stress changes induced by excavation and by then testing properly orientated samples, from behind the slope, along the stress paths estimated using the results of the stress analysis. The method is especially recommended for soils which exhibit pronounced strength anisotropy. It can also help reveal points where

failure is more likely to occur.

6. Softening does not seem to accompany pore pressure equalization for lightly to medium overconsolidated, non-fissured clays, at least in the time scale of a laboratory test.

7. Strength anisotropy, as a result of sample orientation, in terms of drained effective strength parameters, does not seem to exist. Reorientation of stresses, however, under undrained conditions, affects the magnitude of the developing pore pressures.

8. The results of a plane strain finite element analysis have been presented in this report. These results show the effect of the degree of overconsolidation and of the slope of excavation on the magnitudes and orientations of the principal stresses after excavation. The results have been presented in normalized form for two slopes and for various degrees of overconsolidation (expressed either by K or by H_p/H), so that they can be used for a variety of soils, OCR, heights of excavation, or slopes of excavation.

8. REFERENCES

1. de Beer, E. (1967)
"Shear characteristics of the 'Boom Clay'," Proc. Geot. Conf., Oslo, Vol. I., p. 83-88.

2. Bishop, A. W. (1967)
"Progressive failure with special reference to the mechanism causing it," Proc. Geot. Conf., Oslo, Vol. II, p. 142-150.

3. Bishop, A. W. (1971)
"The influence of progressive failure on the choice of the method of stability analysis," Geotechnique 21, p. 168-172.

4. Bishop, A. W., Green, G. E., Garga, V.K., Andresen, A., Brown, J. D. (1971)
"A new ring shear apparatus and its application to the measurement of residual strength," Geotechnique 21, No. 4, pp. 273-323.

5. Bjerrum, L. (1966)
"Progressive failure in slopes of overconsolidated plastic clay and clay shales," 3rd Terzaghi lecture, Journal S.M.F.D., Vol. 92, No. SM5, September 1966.

6. Blight, G. E. (1963)
"The effect of non-uniform pore pressure on laboratory measurements of the shear strength of soils," Proc. ASTM/NRC Symposium on Laboratory Shear Testing of Soil, Ottawa, 1963.

7. Blight, G. E. (1967)
"Observations on the shear testing of indurated fissured clays," Proc. Geot. Conf., Oslo (1967), Vol. I, p. 97-102.

8. Brooker, E. W., Ireland, O. H. (1965)
"Earth pressures at rest related to stress history," Canadian Geotechnical Journal, Vol. 2, No. 1, p. 1-15.

9. Brown, C. B., King, I. P. (1966)
"Automatic embankment analysis: Equilibrium and instability conditions," Geotechnique, Vol. 16, No. 3, p. 209-219.

10. Chandler, R. J. (1966)
"The measurement of residual strength in triaxial compression," Geotechnique 16, p. 181-186.

11. Chandler, R. J., Skempton, A. W. (1974)
"The design of permanent cutting slopes in stiff-fissured clays," Geotechnique 24, No. 4, p. 457-466.

12. Chattopadhyay, P. K. (1972)
"Residual shear strength of some pure clay minerals," Ph.D. thesis, University of Alberta, Edmonton, Canada.

13. Deere, D., Lawton, C., Caldwell, D., Platis, A. (1973)
"Compositional analysis of Friars Formation and Ardath Shale—San Diego," Term paper for class CE 273—Soil Behavior, U. C. Berkeley.

14. Duncan, J. M. (1965)
"The effect of principal stresses on the shear strength

of saurated clay," Ph.D. thesis, submitted at U. C. Berkeley.

15. Duncan, J. M., Dunlop, P. (1966)
"Slopes in stiff-fissured clays and shales," Journal S.M.F.D., Vol. 92, No. SM2, March 1969, p. 467-492.

16. Duncan, J.M. (1978)
Class notes from the lectures in course CE 270B—Advanced Soil Mechanics and Foundation Engineering, U. C. Berkeley.

17. Dunlop, P., Duncan, J.M. (1970)
"Development of failure around excavated slopes," Journal S.M.F.D., Vol. 96, March 1970, p. 471-493.

18. Gibson, R. E., Henkel, D. J. (1954)
"Influence of duration of tests at constant rate of strain on measured 'drained' strength," Geotechnique 4, No. 1, p. 6-15.

19. Goodman, R. E. (1979)
Class notes from the courses in Rock Mechanics, U. C. Berkeley.

20. Houston, W. (1978)
Notes from course CE 270L—Advanced Soil Mechanics Laboratory, U. C. Berkeley.

21. Kanjii, M. A. (1974)
"The relationship between drained friction angles and Atterberg limits of natural soils," Geotechnique 24, p. 671-674.

22. Kanjii, M. A. (1974)
"Unconventional laboratory tests for the determination of the shear strength of soil-rock contacts," Proc. 3rd Congr. Int. Soc. Rock Mech., Denver, CO., Vol. IIA (1974).

23. Kanjii, M. A., Wolle, C. M. (1977)
"Residual strength—New testing and microstructure," 9th Int. Conf. Soil Mech. & Found. Eng., Tokyo, 1979, p. 153-154.

24. Kenney, T. C. (1967)
"The influence of mineral composition on the residual strength of natural soils," Geotech. Conf., Oslo, on shear strength properties of natural soils and rocks, Proc. Vol. I, p. 123-129.

25. Kenney, T. C. (1977)
"Residual strength of mineral mixtures," 9th Inter. Conf. S.M.and F.E.—Tokyo, p. 155-160.

26. Lambe, T. W. (1967)
"Stress path method," J.S.M. and F.D., ASCE, SM6, p. 309-331.

27. Lambe, T. W. (1969)
"Soil mechanics," John Wiley & Sons, N. Y.

28. Lambe, T. W. (1973)
"Predictions in soil engineering," 13th Rankine Lecture Geotechnique, Vol. 23, No. 2, p. 149-202.

28a. Lambe, T.W. (1951)
"Soil testing for engineers", John Wiley & Sons, N.Y.

29. Lambe, T. W. (1979)
"Applications of stress path method," Lecture given at the University of California, Berkeley, in March 1979.

30. Lambe, T. W., Marr, W. A. (1979)
"Stress path method: Second edition," Journal of the Geotechnical Engineering Division, ASCE, Vol. 105, No. GT6, p. 727-738.

31. Lo, K. Y., Lee, C. F. (1973)
"Stress analysis and slope stability in strain-softening materials," Geotechnique, Vol. 23.

32. Lo, K. Y., Lee, C. F. (1973)
"Analysis of progressive failure in clay slopes," 7th Int. Conf. SMFE, Moscow (1973), Vol. 4:3, p. 314-315.

33. Lysmer, J. (1978)
Class notes from the course, "Theoretical Soil Mechanics," U. C. Berkeley.

34. Mitchell, J. K. (1976)
"Fundamentals of soil behavior," John Wiley & Sons, N.Y.

35. Morgenstern, N. R. (1967)
"Shear strength of stiff clay," Proc. Geot. Conf., Oslo, (1967), Vol. 2, p. 59-69.

36. Pickney, C. J., Lee, L. J.
"The influence of bedding plane faults on the evaluation of

landslides in western San Diego county, California," Woodward-Clyde Consultants.

37. Poulos, H. G., Davis, E. H. (1974) "Elastic solutions for soil and rock mechanics," John Wiley & Sons, N. Y.

38. Roscoe, K. H., Schofield, A. N., Wroth, E. P. (1958) "On the yielding of soils," Geotechnique, Vol. 8, No. 1, p. 22-53.

39. Skempton, A. W. (1954) "The pore pressure coefficients A and B," Geotechnique, Vol. 9, p. 143-147.

40. Skempton, A. W. (1964) "Long-term stability of clay slopes," 4th Rankine Lecture, Geotechnique, Vol. 14, p. 77-102.

41. Skempton, A. W. (1966) "Some observations on tectonic shear zones," Proc. 1st Congr. Inst. Soc. of Rock Mech., Lisbon, (1968) Vol. I, p. 329-335.

42. Skempton, A. W. (1970) "First-time slides in O.C. clays," Geotechnique 20, p. 320-324.

43. Skempton, A. W. (1977) "Slope stability of cuttings in Brown London clay," 9th Int. Conf. in Soil Mech. and Foundation Eng., Tokyo.

44. Skempton, A. W. (1978)
"The stability of clay slopes and cuts," Special lectures given at the University of California, Berkeley, for the geotechnical group of the Dept. of Civil Eng., Nov. 1978.

45. Symons, I. F. (1967)
Free discussion on the "shear strength of stiff clays," Prog. of the Geot. Cong., Oslo, (1967), Vol. II.

46. Voight, B. (1973)
"Correlation between Atterberg plasticity limits and residual strength of natural soils," Geotechnique, Vol. 23, p. 265-267.

47. Ward, P. L. (1967)
Panel discussion on "shear strength of stiff clay," Proc. Geot. Conf., Oslo, (1967), Vol. 2, p. 140-141.

48. Williams, A. A. B., Jennings, J. E. (1977)
"The in situ shear behavior of fissured soils," 9th Int. Conf. S. M. and F. E., Tokyo, 1977, p. 169-176.

49. Woodward-Clyde Consultants (1979)
"Preliminary partial draft--Friars Formation generic study--San Diego, California," Woodward-Clyde Consultants.

9. LIST OF SYMBOLS AND ABBREVIATIONS

English Letters

A = Area

= Pore pressure parameter

$\bar{A}$ = Pore pressure parameter

ACUD = Anisotropically Consolidated-Undrained unloading triaxial test with subsequent p. p. equalization under drained conditions (stress path test—inclined samples)

A_c = Contact area

$\bar{A}_f$ = $\bar{A}$ at failure

A_o = Initial area

a = Intercept on q-axis in p vs. q diagrams

= Major axis of true area of contact between upper and lower halves of precut samples (triaxial residual strength tests)

a_1 = Major axis of artificial failure plane in triaxial residual strength tests

B = Pore pressure parameter

b = Minor axis of true area of contact between upper and lower halves of precut samples (triaxial residual strength tests)

b_1 = Minor axis of artificial "failure plane" in triaxial residual strength tests

C_c = Compression index

CD = Consolidated-Drained triaxial test

CDR = Consolidated-Drained triaxial test for residual strength determination (precut samples)

c = Cohesion

c' = Cohesion intercept based on effective stresses

c_v = Coefficient of consolidation

D = Diameter of a specimen

D_o = Initial diameter

d_s = Volume or height change corresponding to 0% degree of consolidation

d_{50} = Volume or height change corresponding to 50% degree of consolidation

d_{100} = Volume or height change corresponding to 100% degree of consolidation

E = Young's modulus of elasticity

ESP = Effective stress path

e = Void ratio

F.E. = Finite element

FS = Factor of safety

G_s = Specific gravity of solids

GWT = Ground water table

H = Height of an excavated slope or height of a specimen

H_o = Initial height of a sample

K = Coefficient of total earth pressure at rest

k = Permeability

K_o = Coefficient of effective earth pressure at rest

L = Length of a potential failure surface behind a slope

LL = Liquid Limit

NC = Normally consolidated

OC = Overconsolidated

OCR = Overconsolidation ratio

$p = \frac{\sigma_v + \sigma_h}{2}$ or $\frac{\sigma_1 + \sigma_3}{2}$

PI = Plasticity Index

PL = Plastic limit

$q = \frac{\sigma_v - \sigma_h}{2}$ or $\frac{\sigma_1 - \sigma_3}{2}$

r = Radius of a specimen

T = Time factor (consolidation)

TSP = Total stress path

TSP-u_b = Total stress path minus the static pore pressure (or back pressure in triaxial tests)

t = Time

t_f = Time elapsed from the beginning of a "strength" test to failure

t_{50} = Time corresponding to 50% degree of consolidation

U = Average degree of consolidation

u = Pore water pressure

u_b = Back pressure

u_z = Pore water pressure at depth z

V = Volume

V_o = Initial volume of a sample

w = Water content

Z = Depth in the ground measured from the surface

Z_1 = Depth of ground water table below ground surface

Z_2 = Depth of a soil element measured from elevation of ground water table

Greek Letters

α = Angle between the failure plane of a sample and the horizontal

= Angle between K_f - line and horizontal in p vs. q diagrams

β = Angle between K_o-line and horizontal in $\bar{p}$ vs. $\bar{q}$ diagrams

γ = Unit weight

γ_b = Boyant unit weight of soil

γ_w = Unit weight of water

γ_1 = Unit weight of soil above ground water table

γ_2 = Total unit weight of soil below ground water table

Δ = Denotes change of a quantity when used before of it (e.g., ΔV = volume change; $\Delta\sigma$ = stress change, etc.)

ε = Strain

ε_A = Axial strain

ε_v = Volumetric strain

θ = Angle between σ_1 and horizontal, measured counterclockwise

η = Shear stress level

ν = Poisson's ratio

σ = Normal stress

σ_v = Vertical stress)
) Principal stresses in the ground
σ_h = Horizontal stress) before excavation

σ_x = Normal stress in x-direction

σ_y = Normal stress in y-direction

$\sigma_{\theta 1}$ = Normal stress in θ-direction at a point before excavation; θ-direction is the direction of the major principal stress at a particular point after excavation

$\sigma_{\theta 3}$ = Normal stress in (90+θ)-direction at a point before excavation; (90+θ)-direction is the direction of the minor principal stress at a particular point after excavation

σ_1 = Major principal stress

σ_3 = Minor principal stress

τ = Shear stress

τ_{max} = Maximum shear stress

τ_{xy} = Shear stress in x and y-directions

$\tau_{\theta xy}$ = Shear stress in final principal stress directions at a point before excavation; final principal stress directions are the principal stress directions at a particular point after excavation

φ = Friction angle

φ' = Effective friction angle

φ_d = Drained friction angle (obtained from drained tests)

φ'_r or φ'_{res} = Residual friction angle